

STUDY OF STRUCTURAL BEHAVIOR OF GEOPOLYMER CONCRETE TO CHECK THE APPLICABILITY OF EUROCODE 2

AN EXPERIMENTAL INVESTIGATION



MASTERS THESIS

ANJALI SHAH



NOVEMBER 2021

EVALUATION OF SCIENTIFIC RESEARCH FOR
STUDY OF STRUCTURAL BEHAVIOUR OF GEOPOLYMER TO
CHECK THE APPLICABILITY OF EUROCODE 2 FOR GPC

Masters Graduation Thesis

For the partial fulfilment of the Master of Science degree-Track Structural Engineering
in Civil Engineering and Geo-Sciences at Delft University of Technology

by

Anjali SHAH

(5071380)



Graduation Committee

Thesis Committee:

Committee Chair

Dr. ir. Yuguang Yang,
Technische Universiteit Delft
Department of Engineering Structures, Concrete structures

Daily supervisor and Company Supervisor

Dr. ir. Herbert Van Der Ham,
Technische Universiteit Delft
Department of Engineering Structures, Concrete structures
Lead Civil Engineer at Boskalis Nederlands

Committee Member

Dr. G. (Guang) Ye,
Technische Universiteit Delft
Department of Materials, Mechanics, Management and Design
Materials and Environment

Masters student

Anjali Shah
Technische Universiteit Delft
Structural Engineering, Track specialisation- Concrete Structures

An electronic version of this thesis is available at
<http://repository.tudelft.nl/>.



CONTENTS

Summary	vii
Acknowledgements	xi
List of Figures	xii
List of Tables	xv
1 Introduction	1
1.1 Project Description	1
1.2 Research Gap and Motivation	2
1.3 Research objectives, Research questions and sub-questions	3
1.4 Scope of the thesis	4
1.5 Thesis outline	5
2 Literature Review	6
2.1 Geopolymer Concrete.	7
2.1.1 Background	7
2.1.2 Applications and advantages of GPC.	8
2.1.3 Challenges and limitations of GPC.	8
2.1.4 Components used in Geopolymer concrete	9
2.1.5 Mechanical properties	10
2.1.6 Structural behaviour of GPC concrete	11
2.1.7 Existing/Available codes in practice	12
2.1.8 Observed performance in real constructions.	13
2.2 Structural behaviour and Eurocode formulations:	16
2.2.1 Possible failure modes in normal RC beams:	16
2.2.2 Material parameters	17
2.2.3 Shear.	18
2.2.4 Crack Width Control	22
2.2.5 Bending moment	24
2.3 Experiments	26
3 Methodology	27
3.1 Research plan	28
3.2 Experimental part.	29
3.2.1 samples used	29
3.2.2 Tests for mechanical properties	30
3.2.3 Casting and curing of beams:	30
3.2.4 Classification of the beams:	30
3.2.5 Experimental setup and instrumentation	35

3.2.6	LVDTS positioning	37
3.3	Post experimental part	40
3.3.1	Analytical calculations	40
3.3.2	Post processing of results	41
4	Results & discussions	43
4.1	Material Behaviour	44
4.1.1	Compressive Strength	44
4.1.2	Split Tensile Strength.	49
4.2	Beam Results	53
4.2.1	Crack patterns visualisation & Failure modes:	53
4.2.2	Shear capacity	62
4.2.3	Bending capacity.	69
4.2.4	Crack behaviour	77
5	Conclusions and Recommendations	83
5.1	Conclusions.	84
5.1.1	Failure modes	84
5.1.2	Material properties	84
5.1.3	Shear.	84
5.1.4	Bending	84
5.1.5	Crack.	85
5.2	Discussion regarding research questions	85
5.3	Limitations	87
5.4	Scope for future research	87
A	Appendix	93
A.1	Experiments	93
A.2	Analytical calculations	98
A.2.1	Compressive strength and tensile strength measured values.	99
A.2.2	Compressive strength estimation using EC clause 3.1.2 (6).	100
A.2.3	Relation between compressive strength and splitting tensile strength 101	
A.2.4	Calculation of surface factor (α) and distance factor (β)	102
A.2.5	Shear and crack calculations:	103
A.2.6	Bending moment and $M - \kappa$ diagrams:	111
A.2.7	Bending moment calculations:.	112
A.3	Eurocode Tables	122
A.4	Load-Deflection diagrams of all beams	124
A.5	Experimental $M - \kappa$ diagrams	132
A.6	Beam pictures at failure.	139
A.7	Individual beam pictures at every load step.	144

SUMMARY

Global climate change has been a huge matter of concern today. While there are several factors that contribute to greenhouse gases, adversely affecting the planet, CO₂ emission is one of them. It is said that 8% of total carbon dioxide emission is caused due to the production of Ordinary portland cement used for concrete in construction [30]. The construction industry highly relies upon concrete as a major and widely used construction material. Solutions to reduce the production of Portland cement without having to entirely remove concrete as a building material has been an important discussion. A possible solution is to replace the Portland cement in concrete with industrial by-products further activating the binder with alkali activators producing a green concrete called 'Geopolymer concrete' (GPC) which would reduce CO₂ emission.

The biggest challenge yet is that, designing any structure, a standard validated code/regulation is required and GPC doesn't have a standard code of practice. All the concrete codes till now are formulated taking the parameters for Ordinary Portland cement concrete. This lack of design models specifically formulated for GPC restricts contractors and engineers to use GPC in structures. This is why GPC has not gained much acceptance in practice. This gives the main motivation towards carrying out this research giving the main research question of this thesis as: **"Upto what extent can Eurocode 2 be applied for Geopolymer concrete"**.

This research was done in collaboration with Boskalis. A bridge (KW15-N69) has been constructed using geopolymer concrete in North Brabant province of the Netherlands. To make the bridge sustainable and circular, the GPC used contained no cement and aggregates were fully replaced by thermally recycled asphalt aggregates. For design of the bridge, Eurocode 2 for concrete structures was used and additionally regulations by dutch ministry of transport and infrastructure was followed. As discussed earlier that since EC2 has not been validated for GPC, an additional test program was planned to check how safe are the beams that would be used in the bridge. This was intended to be done at Stevin II laboratory in TU Delft.

To answer the research question and to test the beams for construction, an experimental investigation to study the behaviour of GPC concrete beams with respect to design models in Eurocode 2 was done. A total of 24 beams (representing different components of the bridge) were casted which was designed in accordance to EC2 regulations. An experimental program was setup for four point bending tests with an aim to study shear and bending behaviour of these beams. LVDTs were attached to all of the beams to measure the crack openings during the experiment. 12 beams (without shear reinforcement) were designed to fail in shear and 12 of them to fail in flexure which was an assumption made prior to the experiment. These beams varied in parameters like concrete strength

class, depth, amount of reinforcement and distance between loads and supports. Mechanical behaviour of GPC like compressive strength, tensile strength and elastic modulus were tested over time in commercial laboratory and the data obtained were used for this research. Eurocode models for shear, bending, crack were used to calculate and predict the results and further was compared to the obtained data from the experiments.

The failure modes of these beams were observed as predicted from EC2 calculations. Ultimate force at failure for the beams that failed in shear resulted to be more than analytically calculated shear capacity ($V_{Rd,c}$). Primarily, all the calculations were made using mean values and later using design values. Test to prediction ratios of all these beams were more than 1. Different influencing parameters were further studied using experimental results. The main influencing factors of shear capacity of normal cement concrete are reinforcement ratio, effective depth and a/d ratio. These factors were seen to have a similar effect on shear capacity of GPC beams tested here. In addition to these comparisons, some data of OPC reinforced concrete beams from past research whose parameters were close to the range of GPC beams used here were taken to compare the ultimate shear capacity and found to be similar.

Secondly, bending capacity was checked. Ultimate moment capacities of beams that failed in bending were also more than the predicted ones. Moment at every stages - cracking moment (M_{cr}), yielding moment (M_y), ultimate moment (M_u) were compared to the analytically obtained values. Furthermore, the factors effecting these capacities were studied.

The predicted load at which first crack would occur was close to the actual crack that was observed in the experiment. Cracking moment calculated using the experimental results was observed to be close to the predicted cracking moment. The maximum crack spacing and crack width calculated using EC2 equations were compared. Crack width was measured by the LVDTs and using crack measuring card at certain load steps. For most of the beams, crack spacing noted in the experiments were less than the calculated ones.

Additionally, the expressions given by Eurocode 2 to estimate the compressive strength over time and to calculate tensile strength using f_{ck} were analysed for Geopolymer concrete. Comparing the estimated and measured values, although the values were close, it is still uncertain if these formula can be used to estimate the strength development of GPC.

Lastly, this research concludes that Eurocode 2 models for shear and bending are conservative for GPC. While this gives a positive indication towards the applicability of Eurocode 2 for Geopolymer concrete, the design models were not validated in this research. The results obtained here can be added to expand the database to further study and validate the models to be able to use GPC for construction freely. To verify that Eurocode 2 models are "safe" for the type of GPC utilized here, more statistical analysis is required. Only two GPC mixtures are employed in this study and every type of GPC can vary in proportions affecting the overall behavior. As a result, calculating design value from experimental data using a probabilistic approach employing Eurocode 1990:2002, which

covers all model uncertainties, would be the best way to demonstrate the safety. Using all the results obtained from experiments, GPC was considered safe to use for this bridge and the construction was completed in July this year, which is said to be the first prestressed Geopolymer concrete bridge in the Netherlands.

Green building is not about buildings, it is about people.

-Sandy Wiggins

ACKNOWLEDGEMENTS

This thesis is a result of 8 months of research- the final phase of my Masters degree. I am very thankful to many people who have supported and helped me in this journey. I would like to take this opportunity to thank each one of them.

Firstly, I would like to thank my thesis committee members who helped me a lot with their valuable feedback and suggestions throughout my research. I was very fortunate to have got the opportunity to work on my thesis with really talented, kind and helpful people. I would like to thank Herbert, my daily supervisor and company supervisor for firstly, providing me an opportunity to work on this really interesting project with Boskalis. Him taking time out of his busy schedule for weekly meetings, checking my progress, answering and explaining even my smallest doubts, guiding me, showing me correct approach so that I am on the right track, everything really helped me. It would have never been possible without him. I got to learn a lot from him during this period. I could not have asked for a better mentor, thanks!

Many thanks to my chair Yuguang Yang for his valuable suggestions, making all the study materials available, suggesting new ideas, helping me whenever I got stuck. It was an honour to work with him. His knowledge in this field and critical thinking towards the problems was really inspiring.

Further, I owe my sincere gratitude to Dr. Guang Ye from whom I learnt a lot about Geopolymer concrete as a building material. Dr. Ye has been my mentor since my internship time. I am grateful that I could work with him on my thesis as well. His questions and suggestions in monthly meetings has helped me improve my work a lot.

For making it possible to carry out all the experiments safely, successfully and on time, I would like to thank Albert and Jakub. Thank you for all the help and a proper guidance throughout. Lab work was never boring because of them. I enjoyed working with them.

I am really thankful to all of my friends here in TU Delft and friends back home. It was a challenging journey and I wouldn't have made it this far without them. Much love!

I would like to thank my parents for their constant support, never ending encouragement and of course the financial support. Thank you Papa, for everything, for always pushing me and most importantly for believing in me. I am who I am because you are who you are and you have always let me be what I wanted to be. Lastly, my dearest and nearest Rishi and Sneha, love you so much! Thank you for always being there.

*Anjali Shah
Delft, November 2021*

LIST OF FIGURES

1.1	Site and the bridge picture after construction of KW15 (Boskalis)	1
1.2	3D plan of KW15 (boskalis)	2
1.3	Structural detailed drawing of KW15 (Bosaklis)	2
1.4	A Summary of all the chapters	5
2.1	Advantages of Geopolymer concrete [21]	8
2.2	Load deflection curve OPC vs GPC beam [25]	11
2.3	Global change Institute (GCI), Australia (top) and Geopolymer concrete beam being positioned at the site during construction [29]	13
2.4	Load deflection curve of the GPC used for GCI [27]	14
2.5	Brisbane West Wellcamp Airport construction site [12]	14
2.6	Flexure failure mode[34]	16
2.7	Shear failure mode: a)Shear compression failure b)Flexure shear failure[11]	16
2.8	Normal distribution curve for compressive strength[31]	17
2.9	truss model used to calculate shear capacities for beams with shear reinforcement present [35]	20
2.10	Shear transfer mechanisms	21
2.11	Different phases of crack of concrete	24
3.1	Cube specimen prepared (Jansen and Sqape laboratory)	29
3.2	Casting of GPC beams at Valkenswaard (Boskalis)	30
3.3	Designed test setup	35
3.4	Actual test setup in the lab with a beam	36
3.5	LVDTs positions and dimensions of beams 10, 11, 16, 17, 18 (all dimensions are in mm)	38
3.6	Picture after placing the LVDTs in one of the beams (front part)	38
3.7	Picture after placing the LVDTs in one of the beams (bottom part)	39
3.8	Measurement of cracks using concrete crack width ruler	39
4.1	Development of compressive strength with time	45
4.2	Strength development over time for RAMAC C33/43 taking "s"=0.2 (Eurocode 2 estimation vs measured)	46
4.3	Strength development over time for RAMAC C28/35-2 taking "s"=0.2 (Eurocode 2 estimation vs measured)	46
4.4	Strength development over time for RAMAC C33/43 taking "s"=0.25 (Eurocode 2 estimation vs measured)	47
4.5	Strength development over time for RAMAC C33/43 taking "s"=0.38 (Eurocode 2 estimation vs measured)	48

4.6	Development of split tensile strength with time	50
4.7	Comparison of split tensile strength over time (Calculated from cylinder compressive strength vs average split tensile strength measured in the lab)	50
4.8	Ratio between splitting tensile strength and compressive strength (RAMAC C33/43)	52
4.9	Ratio between splitting tensile strength and compressive strength (RAMAC C28/35-2)	52
4.10	Crack propagation in beam 3	55
4.11	Load deflection curves of beam 3 showing the cracking (F_{cr}), yielding (F_y) and ultimate load (F_u)	56
4.12	Load deflection curves of beam group 1-2-3-13-14-15	56
4.13	Crack propagation in beam 8	57
4.14	Load deflection curves of beam 8 showing the cracking (F_{cr}), yielding (F_y) and ultimate load (F_u)	58
4.15	Load deflection curves of beam group 7-8-9	58
4.16	Crack propagation in beam 22	59
4.17	Load deflection curves of beam 22 showing the cracking (F_{cr}), yielding (F_y) and ultimate load (F_u)	59
4.18	Load deflection curves of beams 22, 23, 24	60
4.19	Shear capacity of Beam group 7, 8, 9 (experimental vs analytical)	63
4.20	Shear capacity of Beam group 22, 23, 24 (experimental vs analytical)	63
4.21	Shear resistance comparison (Experimental vs analytical) according to shear-span ratio	64
4.22	Influence of compressive strength on shear capacity- beams 7, 8, 9	65
4.23	Influence of compressive strength on shear capacity- beams 22, 23, 24	65
4.24	Graphical Comparison of prediction of EC2 with experimental results	66
4.25	Influence of a/d on $\left(\frac{V_{exp}}{V_{pre}}\right)_{EC2}$	68
4.26	Influence of effective depth on $\left(\frac{V_{exp}}{V_{pre}}\right)_{EC2}$	68
4.27	Influence of reinforcement on $\left(\frac{V_{exp}}{V_{pre}}\right)_{EC2}$	68
4.28	Ultimate moment - Experimental vs Analytical (beams 1, 2, 3, 13, 14, 15)	69
4.29	Ultimate moment comparison - Experimental vs Analytical (beams 4, 5, 6)	70
4.30	Ultimate moment comparison - Experimental vs Analytical (beams 16, 17, 18)	70
4.31	$M - \kappa$ diagram of beams 1, 2, 3, 13, 14, 15 (experimental vs calculated); distance between loads for these beams = 1000 mm	71
4.32	$M - \kappa$ diagram of beams 4, 5, 6, 16, 17, 18 (experimental vs calculated); distance between loads for beams 4, 5, 6 = 300 mm and for beams 16, 17, 18 = 500 mm	71
4.33	Flexure behaviour with varying compressive strength and reinforcement ratio	73
4.34	Behaviour with varying reinforcement ratio	74
4.35	Comparison of prediction of EC2 with experimental results	75
4.36	Influence of amount of tensile reinforcement on $\left(\frac{M_{u,exp}}{M_{pre}}\right)_{EC2}$	76

4.37 Crack spacing of beam 1 for reference	77
4.38 Crack spacing (Experimental vs prediction)	78
4.39 Influence of bar diameter of tension zone on $\left(\frac{S_{r,max}(exp)}{S_{r,max}(pre)}\right)_{EC2}$	79
4.40 Influence of effective reinforcement on $\left(\frac{S_{r,max}(exp)}{S_{r,max}(pre)}\right)_{EC2}$	79
4.41 Comparison of calculated crack width and LVDT measured crack width- Beam 1 (top) and Beam 2 (bottom)	80
4.42 Comparison of calculated crack width and LVDT measured crack width- Beam 4 (top) and Beam 5 (bottom)	81
4.43 Crack width comparison for beam 1	82
4.44 Crack width comparison for beam 3	82
A.1 LVDTs positions and dimensions of beams 10, 11, 16, 17, 18	93
A.2 LVDTs positions and dimensions of beams 4,5, 6, 7, 8, 9, 12, 22, 23, 24	94
A.3 LVDTs positions and dimensions of beam 19 (3-point loading)	94
A.4 LVDTs positions and dimensions of beam 20, 21 (3-point loading)	95
A.5 LVDTs positions and dimensions of beam 1, 2, 3, 13, 14, 15	95
A.6 Strength development with time curve for RAMAC C33/43 used to approx- imate the compressive strength value according to the experiment date . .	97
A.7 Strength development with time curve for RAMAC C28/35 used to approx- imate the compressive strength value according to the experiment date . .	97
A.8 Four point beam [28]	111

LIST OF TABLES

3.1	Classification of beams according to depth, reinforcement layout and strength class	31
3.2	The components in the structure and respective beam representative . . .	32
3.3	Reinforcement layout in all the beams	33
3.4	Classification of beams according to the distance between loads and supports	34
3.5	LVDTs used in each beam and their aim	37
3.6	An overview of all the formulae used to make analytical predictions	40
4.1	Overview of measured compressive strength values according to time (Tests done in Jansen and Sqapec laboratory)	44
4.2	EC calculated vs measured (experimental) compressive strength over time for both RAMAC C33/43 and RAMAC C28/35-2	47
4.3	Overview of measure Splitting tensile strength according to age (Tests done in Jansen and Sqapec laboratory)	49
4.4	calculated vs measured split tensile strength over time for both RAMAC C33/43 and RAMAC C28/35-2	51
4.5	General overview of results of all the beams showing the loads at different stages and respective failure modes	53
4.6	failure mode comparison with some past research database ([4])	60
4.7	Summary of results of beams failed in shear (Predicted and Experimental)	62
4.8	Comparison showing decrease in shear capacity due to decrease in reinforcement in tensile zone	64
4.9	Comparison of ultimate shear force and test prediction ratios for GPC beams with that of normal cement concrete from past database [4]	67
4.10	Summary of results of beams failed in bending (Predicted and experimental)	69
4.11	Summary of predicted and experimental results for each phases	72
4.12	Comparison between EC2 and calculated values	75
4.13	Measured and calculated maximum crack spacing of all the beams	77
A.1	Dates of when the beams were casted and tested	96

1

INTRODUCTION

1.1. PROJECT DESCRIPTION

This research is carried out in collaboration with Boskalis. The idea of this research is motivated by a project of a sustainable and fully circular bicycle bridge (no use of Portland cement and aggregates partially replaced with recycled aggregates) recently constructed near Eindhoven, Netherlands.

This project is one of Boskalis's remarkable works- the post-tensioned bicycle bridge KW15 shown in figure 1.1. Since the idea was to use Geopolymer concrete for this particular bridge, various mixes were tested, and the results were analysed as per requirements of the bridge construction. According to the structural calculations, there were certain criteria to be fulfilled in terms of structural stability, strength, environmental safety and service life. The superstructure of this bridge was intended to be fully post tensioned concrete solid slab (no cracks in SLS and no cracks in ULS), supported by a substructure of reinforced concrete abutments. The approach slabs were made of reinforced concrete as well.



Figure 1.1: Site and the bridge picture after construction of KW15 (Boskalis)

Coming to the design aspect, the current design of this bridge is based on Eurocode 2 for regular concrete and ROK 1.4 (additional regulations by the Dutch Ministry of Transport and Infrastructure). Because the bridge would be build making use of geopolymer concrete, an additional experimental program has been set up to prove the structural safety and durability, since the bridge should have a lifetime of 100 years. Several tests were performed in TU Delft and obtained results were then processed to construct the bridge and draw conclusions required for the research. Figure 1.2 shows a 3D representation of the bridge which was to be built and figure 1.3 shows a detailed structural drawing of the bridge.

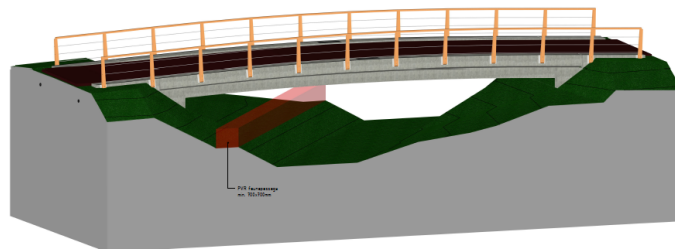


Figure 1.2: 3D plan of KW15 (boskalis)

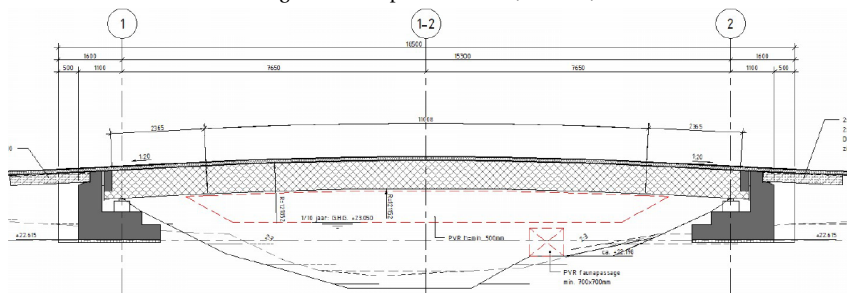


Figure 1.3: Structural detailed drawing of KW15 (Bosaklis)

Other companies contributing in this project for the Geopolymer concrete production part are SQAPE and AJansen BV, the concrete contractor for this project. Together the companies carry out different experiments and research to optimize the use of geopolymer concrete and make it better for all applications.

1.2. RESEACH GAP AND MOTIVATION

The growing concern about climate change and CO2 emissions has escalated a number of research in Geopolymer concrete. The benefit of using GPC has been discussed better in the literature review section (2) of this document. Designing any structure a standard code is used in engineering practice. And almost all the standard codes (for concrete structures) were formulated for conventional cement concrete (produced using OPC). This is one of the main reasons that GPC has not gained much acceptance in practice. Several research regarding the study of general property of GPC as a material has been

done and are still being done. But on the structural point of view, engineers tend to look for the structural behavior and how it can be used safely. The structural aspects like shear, bending, cracks behavior has also been experimented and studied in the past but a standard code of practice has not been formulated as such or there are no any modification done in the existing codes and design models which would give a freedom to use GPC in structures or provide a safety assurance. Therefore, this research will act as one of the pioneer studies to investigate the overall structural behaviour of geopolymer concrete beams with respect to standard codes which should help design engineers up to some extent to execute and design structures using GPC in future.

1.3. RESEARCH OBJECTIVES, RESEARCH QUESTIONS AND SUB-QUESTIONS

The main objectives of this thesis are as follows:-

- To study the structural behaviour of Geopolymer concrete from the experiments.
- To analyse the correlation between experimental findings and current Eurocode prediction methods for reinforced Portland cement concrete structural members to check the accuracy of Eurocode.
- To identify the main influencing factors from experimental observations.
- To observe the similarities and differences in overall behaviour of GPC and normal cement concrete within the scope of the research.

Some research has been done in the past about the use of Geopolymer concrete and how it is different in structural aspect from that of Portland cement concrete. It has been concluded that the strength development of GPC varies from that of cement concrete but eventually it is possible to achieve a similar strength which is one of the facts that can be taken into account to draw a line between GPC and OPC concrete and also can provide a reason that both of them can be used for similar application. Some more conclusions drawn from past researches which are discussed in the literature review section (2). In this research, the main focus will be the cracking behavior, bending behavior and shear behavior the beam as a part of the bridge. Also, the research consisting of both structural and material aspect, the beam composition and that as a whole in regard to the how it behaves as a material, its properties are also to be studied which is important to answer some questions. For designing concrete structures, Eurocode 2 (en.1992.1.1.2004) is used and this design code was formulated for normal cement concrete; it does not give a valid safety proof for the usage of GPC which gives **THE MAIN RESEARCH QUESTION** as,

"Upto what extent can Eurocode 2 be applicable for Geopolymer concrete structures"

Although there is one main question, it requires few more questions to be explained to

draw conclusion and to answer the main research question. This will be derived from the experimental results and past research and studies making comparisons depending on the conditions. Some relevant and useful sub questions that are important to be answered are given below:

1. What are the observed mechanical behaviour like tensile, compressive strength, etc. of the concrete mix used here? Can EC2 estimations for calculating these properties according to time formulated for normal cement concrete be used for GPC as well?
2. How do the failure of the beams look like? Are the crack initiation, crack propagation, crack pattern any different from that of normal concrete? If yes, in what way?
3. How accurately does the analytical models by EC2 predict the experimental results?
4. Are the critical parameters influencing mechanisms in normal concrete influential for GPC as well?
5. Is it safe to use GPC over normal cement concrete for similar application? Is there a way to prove the overall safety? How?

1.4. SCOPE OF THE THESIS

- Evaluation is done comparing between the predicted values (from Eurocode models) and the obtained experimental values to prove that Eurocode can be used for Geopolymer concrete as well. These comparisons in general will include the resistance of bending and shear and crack width control.
- Further, possible influencing parameters is discussed for each model (shear/ bending/ crack) given by EC2 to check how much variation would those result for GPC beams used with respect to normal concrete which is done using the available experimental data. However, since all the parameters is not studied in detail; firstly because of a limited time for this research, evaluating them in detail to give a concrete conclusion would take a long time and secondly because of lack in variation of the parameters to compare with each other.
- Time dependent effects in GPC are out of scope of this thesis.
- Prestressing component will be disregarded from analytical calculations using EC models for this research. Although it is an important area to study and the bridge construction itself used prestressing, the experimental beams did not have prestressing and thus was not possible to study this part.

1.5. THESIS OUTLINE

<u>Chapter 1</u> Introduction	<ul style="list-style-type: none">•chapter 1 gives the introduction of this thesis project highlighting background and motivation behind this research. The research question, and derived sub questions, goals and objectives have been covered in this chapter.
<u>Chapter 2</u> Literature Review	<ul style="list-style-type: none">•Chapter 2 is about the Literature review which covers a general survey about Geopolymer concrete structural behaviour. Furthermore, EC models formulated for normal cement concrete are briefly introduced along with important and affecting parameters. Relevant information from past researches needed to compare and analyse this research has been studied and written.
<u>Chapter 3</u> Methodology	<ul style="list-style-type: none">•Chapter 3 covers a step by step methods and approach adopted for this research. Detailed description about all the experiments carried out and the whole research plan has been discussed.
<u>Chapter 4</u> Results and discussions	<ul style="list-style-type: none">•Chapter 4 provides an overview of all the results and observations obtained from the experiments carried out in Stevin II laboratory as well as some from the company laboratory. Comparisons are made to derive conclusions and answer the research questions.
<u>Chapter 5</u> Conclusions and recommendations	<ul style="list-style-type: none">•Chapter 5 is about conclusions and recommendations. This chapter includes summarizing the conclusions from the observations, comparisons and analysis done in chapter 4. Furthermore, answers of the research questions is discussed. Lastly, research limitations are mentioned and future research recommendations are suggested.
Appendix	<ul style="list-style-type: none">•Appendix includes all the calculations done required for this research. All experimental pictures and graphs are attached in this section.

Figure 1.4: A Summary of all the chapters

2

LITERATURE REVIEW

This chapter consists of study done during the research that were relevant for this thesis.

2.1. GEOPOLYMER CONCRETE

CO₂ emission has become one of the major causes of global warming according to US Environmental protection agency. According to BBC climate change statistics [30], 8% of the total emission of CO₂ is due to the production of Portland cement. And since the construction industry highly relies upon concrete as the major and widely used construction material, moreover the demand for concrete will never stop as it is hugely used by construction industry. Concrete is used in such large amounts because it is, simply, a remarkably good building material; not just for basic road construction [38]. Because an important fact that it leaves a carbon footprint cannot be ignored as well, since it is then not sustainable which will lead to continuation of the existing environmental problems because of carbon emission.

One of the possible solutions of this problem is suggested to replace ordinary Portland cement (major contributor of CO₂ emission) with precursors made of industrial by-products such as fly ash and blast furnace slag activated by alkali solutions. This technology is referred to as alkali activation or under certain conditions geopolymerization, and the concrete – geopolymer concrete. Huge research has been done and is still being done to study the specialties of geopolymer concrete as a new construction's material in terms of strength, durability, and sustainability. However, it is still rarely used in real-world constructions due to lack of data about mechanical properties of geopolymer concrete. The authorities demand equivalent performance in Eurocode design methods (design by testing) for bringing this into industrial application.

2.1.1. BACKGROUND

Geopolymer concrete which is also known as Alkali activated concrete (AAM) comes from 'geopolymer' binders which is said to be first invented by Joseph Davidovits to describe inorganic polymers based on alumino-silicates that can be formed by the reaction of pozzolanic chemicals or alumino-silicate source materials with very alkaline solutions [17]. Geopolymer binders are environmentally friendly polymers that have the potential to replace cement in the construction sector. Fly ash (FA), granulated blast furnace slag (GBFS), rice husk ash, and red mud are all examples of waste materials that can be used to make geopolymer binders. [14]. The geopolymerization reactions are the reaction processes in geopolymer binders that primarily involve three processes: the first is the dissolving process, in which the alkali solution dissolves the aluminosilicate precursors to liberate the aluminum and silicon species in the combination. Geopolymerization process is the reaction that occurs in geopolymer binders. It includes three processes- dissolution, condensation and hardening.

2.1.2. APPLICATIONS AND ADVANTAGES OF GPC

The applications of Geopolymer concrete are no different than that of Portland cement concrete. Geopolymer concrete has been used for the construction of different structures like water tanks, pavements and roads, walls, bridges[27].

ENVIRONMENTAL BENEFITS

There is a growing demand for innovative materials with low CO₂ emissions that can be used for a variety of applications and a potential material to use in construction industry can be GPC. There are multiple benefits of using GPC over normal cement concrete from environmental point of view.

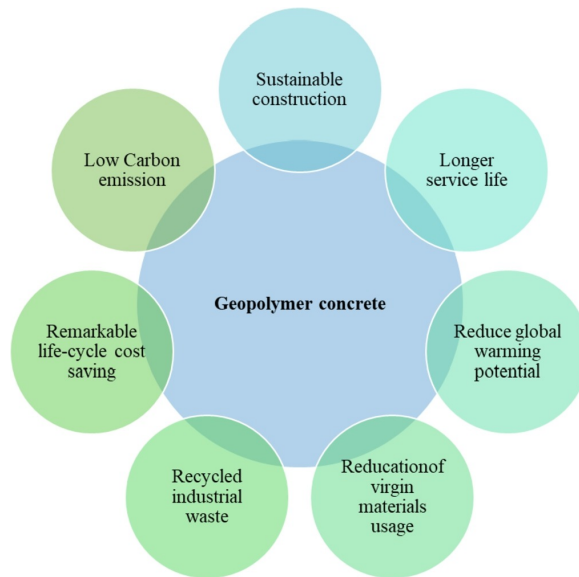


Figure 2.1: Advantages of Geopolymer concrete [21]

2.1.3. CHALLENGES AND LIMITATIONS OF GPC

Some building owners, concrete suppliers, and finishers have been reluctant to replace cement with fly ash on steel-trowelled floors because of the increased risks associated with the fly ash like its tendency to effloresce along with concerns about freeze/thaw performance, Increase of salt scaling, etc.[39]

Despite the fact that GPC is good for sustainability and reduction of Global warming, it is still not used in practice. Although many tests and researches have been carried out, it still faces challenges. One of the most significant obstacles is the lack of standards that should be developed by a global committee. Institutional difficulties and a lack of specifications or standards will restrict the adaption of such new materials[15]. This is one of the main motivations behind this research.

2.1.4. COMPONENTS USED IN GEOPOLYMER CONCRETE

Like in ordinary portland cement concrete, Geopolymer binder (Geopolymer cement) needs aggregates to form Geopolymer concrete. Additionally, alkali activator is needed for reaction to set and harden the concrete. This geopolymer cement is composed of industrial byproducts from steel industries, thermal power plant, etc., like blast furnace slag, fly ash, rice husk ash, metakaolin etc. Geopolymer concrete can be composed of varying proportions in regard to FA, GGBS,

FLY ASH (FA)

Fly ash is a byproduct of pulverized coal combustion in electric power plants. Mineral impurities in coal fuse in suspension during burning and float out of the combustion chamber with the exhaust gases. The melted material cools and forms into spherical glassy particles known as fly ash as it rises. Although the fine powder resembles portland cement, it is chemically distinct[41]. Depending on the physical and chemical properties, all fly ashes display cementitious properties in different degrees. Generally, there are two types of Fly ash commonly known as Type F and Type C. Type F fly ash is mostly used for geopolymer binders. The use of type C fly ash for geopolymerisation has received little attention, because of its rapid setting qualities[17]

BLAST FURNACE SLAG (BFS)

Blast furnace slag is a non-metallic byproduct obtained from the production of hot metal. During production process, iron ore converted to iron sinks to the furnace's bottom leaving materials on the top known as slag. The quenching procedure of slag improves cementitious qualities and generates granules that resemble coarse sand particles. which further refined is called Ground Grnulated blast furnace slag [18].

ALKALI ACTIVATORS

One of the important components used in GPC is alkali activator. It helps in the activation process while hydration of the binder. The activators are often added as a solution to the mixture, but they can also be added as a solid, blended or integrated with the slag and/or ash. Alkali hydroxides and silicates are the most commonly used activators. However, both in slags and fly ash, the type of the activators plays a critical role in the activation process [19]. Most commonly used activators in GPC are sodium silicate (Na_2SiO_3) and sodium hydroxide (NaOH).

AGGREGATES

Aggregates used in concrete can be of different types. Commonly used aggregates are natural gravel and sand from river, seabed, etc. Due to growing concern about circularity, recycled aggregates have also started being used. Using recycles aggregates instead of natural aggregates could reduce the need to use raw natural resources. In regard of using recycled aggregates for GPC, some research have been done to study the influence. In an experimental study about mechanical and durability properties of GPC with recycled aggregates (RCA) by Faiz Uddin et al. [16], replacing natural aggregates with RCA partially showed a decrease in compressive, tensile strength.

For this project, the GPC mix used **thermally recycled asphalt aggregate (TRI)**. To produce TRI, the process can be described as a thermal process in which tar containing asphalt is cleaned in to fine and coarse granulates. Therefore bitumen and Tar-containing products are evaporated during the process at about 600 - 650 degrees Celsius. The aggregates/granulates are suitable for use in Concrete production.

But this type of aggregate has not been used in practice much and hardly any research or experiments have been performed to study its influence in concrete mechanical or structural behaviour.

2.1.5. MECHANICAL PROPERTIES

COMPRESSIVE STRENGTH

Compressive strength of the concrete is one of the most important and useful properties of a concrete. For all the other behaviour of concrete, compressive strength is the first base parameter to be considered. This factor is needed for almost all other verifications in standard codes as well which makes it more important to study and analyse. In short, directly, or indirectly the behaviour and capacities are primarily dependent on concrete compressive strength. In some studies done earlier, it has been observed that GPC has a compressive strength comparable to that of OPC concrete. Mustafa et al. [10] concluded that the fly ash-based geopolymer concrete produced higher compressive strength compared to OPC concrete at 1, 7 and 28 days.

However, the development of compressive strength on itself depends on several factors such as chemical composition, water binder ratio, curing conditions, strength development over time, aggregate binder ratio, type of aggregate used etc.[8]. And thus a general conclusion cannot be given as every mixes can be different in proportion.

TENSILE STRENGTH

Tensile strength of Geopolymer concrete is seen less than the compressive strength, similar to that of normal OPC concrete. In a research done by Zhu Pan et al.[9] to compare the properties between GPC and OPC, it was concluded that GPC showed higher tensile strength than that of OPC. However, it can again vary depending on the type of GPC used. Different research carried out had varying parameters and gave different conclusions. Many research concluded a correlation of tensile strength to compressive strength in GPC which is seen in OPC concrete too. In an experimental study for mechanical properties of GPC by Azad et al. [24], after performing number of tests, it was concluded that the relation between compressive and tensile strength could be influenced by number of factors like varying amount of components used, curing temperature.

2.1.6. STRUCTURAL BEHAVIOUR OF GPC CONCRETE

Some experimental investigations and research have been done to study the structural behaviour of GPC. Some studies done in the past indicate a similar structural behaviour of GPC and conventional concrete. Sumajouw et al. (2006) concluded from his experimental research on GPC columns that the crack patterns, modes of failure, mid-span deflection, the effect of longitudinal reinforcement, concrete compressive strength, load-eccentricity were similar to that of observed in conventional OPC concrete [37]. To analyse the structural behaviour of fly ash Geopolymer concrete, in another study by Sumajouw [36], the flexural behaviour and strength of reinforced GPC beams were concluded to be similar to that of OPC concrete beams. Similar conclusion about failure modes was drawn in Sarker's comparative experimental study [13] where both reinforced OPC concrete and GPC beams showed a similar behaviour.

Yost [43], from his experimental observations from testing alkali activated fly ash concrete (AAFAC) concluded that the shear mechanism is identical to that of ordinary portland cement concrete. However, for flexure, the failure was observed to be more brittle. In terms of performance, both the OPC and AAFAC behaved in a similar way.

In one recent experimental research [25], flexural behaviour of GPC (with flyash, GG-BFS, and cement) was studied comparing it with OPC concrete beams. It was concluded that the load carrying capacity was 10% higher in GPC beams. The observed crack width was also wider in OPC concrete beams and beam deflection was higher too. The load deflection curve obtained from the experiment for both the samples (OPC & GPC) has been shown in figure 2.2

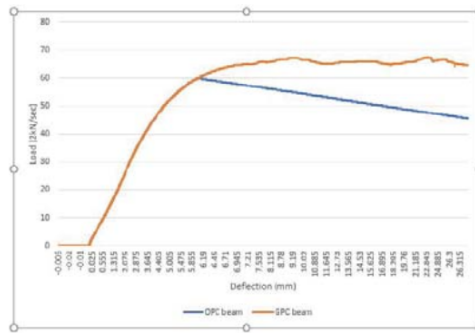


Figure 2.2: Load deflection curve OPC vs GPC beam [25]

2.1.7. EXISTING/AVAILABLE CODES IN PRACTICE

- **Australian AS 3600:2018 for concrete structures and American Concrete Institute Building Code**

A study by Sumajouw et al. (2006) experimented and came to a conclusion that the design provisions contained in the Australian Standard for Concrete Structures AS3600 and the American Concrete Institute Building Code ACI318-02 are applicable to reinforced geopolymer concrete columns.[37]. The deflection and load capacity predicted using Australian standard AS3600 and American Concrete Institute Building Code ACI 318-02 did agree with the obtained results in experiments. In an experimental research done by Ee Hui Chang, a comparison between experimental results and prediction for shear strength using American Concrete Institute Building Code ACI 318-08 and Australian Standard for Concrete Structures AS3600-05 was done [5]. He concluded that the verification procedure and calculations used to calculate and predict the shear strength can be applicable and are safe for GPC. He tested several beams to study the behaviour of GPC with respect to different parameters. Additionally, it was observed that shear capacity in GPC increased with the increase in reinforcement ratio which is similar to normal cement concrete as well.

From another experimental study by Yost [43], it was concluded that flexure members for alkali activated fly ash concrete could be designed using the same models formulated for that of OPC concrete. Sarker from his comparative study about GPC beams design, arrived to the conclusion that the current Australian code and ACI are conservative in designing the shear and flexure failures of Geopolymer concrete beams suggesting that the current current practices and procedures can be used conservatively for design of Geopolymer concrete structural members [13].

- **Eurocode en.1992.1.1.2004**

In an investigation about properties and structural design relation for new concretes by R. K. Dhir et al.[3], EC2 equations for predicting the shear strength of reinforced concrete beams were used to predict that for concrete produced partially replacing portland cement (PC) with fly ash (FA) and Ground granulated blast furnace slag (GGBS), it was concluded that EC2 equations to predict the shear strength was valid for the concrete beams used.

A discussion from a paper [6] of comparative study between American code for structural concrete, ACI and Eurocode 2 for study of flexure design, it was concluded that both the codes show a significant difference in the safety theory. However, this did not seem to have a large effect on calculating the flexure strength. It was also observed that EC2 regulations are more conservative in this regard.

2.1.8. OBSERVED PERFORMANCE IN REAL CONSTRUCTIONS

1. Queensland's University GCI:

The University of Queensland's Global Change Institute (GCI), in Australia is said to be the world's first building successfully constructed using GPC. It consists of comprises 3 suspended geopolymer concrete floors with 33 precast panels, shown in figure 2.3 which are made from slag/fly ash-based geopolymer concrete[42]. The Global Change Institute (GCI) is a University of Queensland organisation researching global sustainability issues including resource security, ecosystem health, population growth and climate change[29]. The idea was to make it sustainable and the motivation behind that was to achieve Australia's first Living Building Challenge compliance which is an international rating system. It was initially thought to make use of Timber-Composite Concrete (TCC) but later, the benefits of replacing the GPC with normal concrete in TCC was realised.

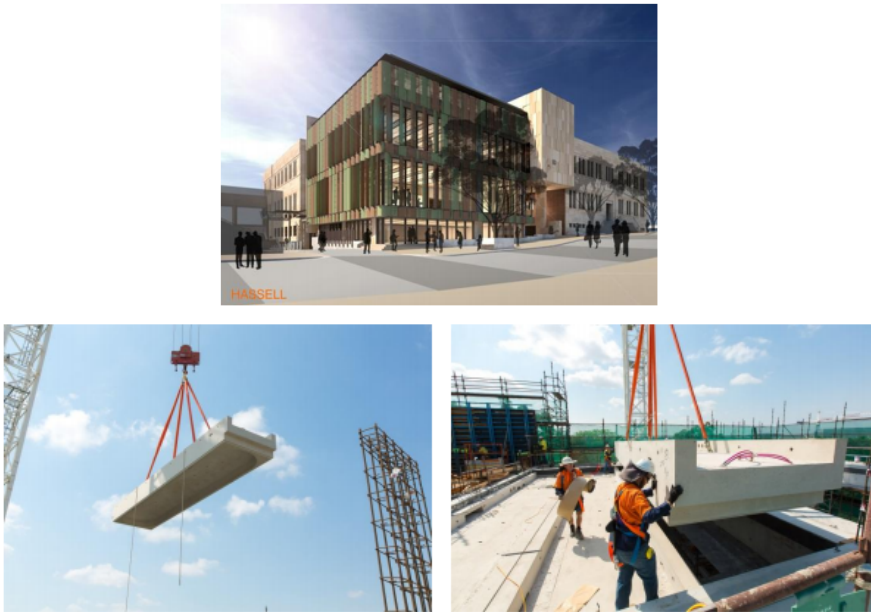


Figure 2.3: Global change Institute (GCI), Australia (top) and Geopolymer concrete beam being positioned at the site during construction [29]

As for the design procedure, primarily to check the material properties, compressive strength, flexure strength, tensile strength, density, elastic modulus, shrinkage creep, stress-strain, chloride and sulphate content, alkali aggregate reaction etc. tests were carried out. Secondly, for the structural verifications, they relied on Australian standard code for concrete structures- AS 3600. A load test was done to study the midspan deflection behaviour which can be seen in figure 2.4 which was predicted to be 3mm but resulted in 2.85 mm.

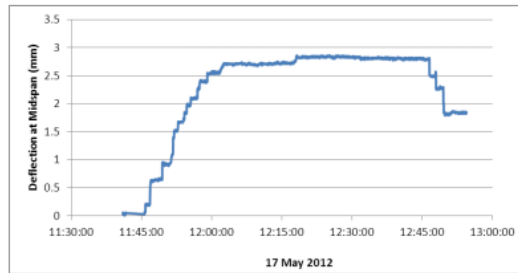


Figure 2.4: Load deflection curve of the GPC used for GCI [27]

It was found that the structural property held with the design basis for reinforced concrete structures provided in AS 3600. After multiple tests and investigation for this project, it was concluded that as long as necessary verifications are done (which in this project was all fulfilled) for the necessary structural performance, structures can be designed using GPC.

2. Brisbane West Wellcamp Airport:

Brisbane West Wellcamp Airport (BWWA) constructed in November 2014, which is another successfully constructed structural pavement using Geopolymer concrete of approximately $40,000 m^3$ is said to be the largest project in the world using GPC[12]. Prior the actual construction, a trial construction for a private apron was done 6 months before to check the mix design's suitability for the actual project. The concrete specification and requirements for flexure strength and shrinkage given by engineers according to standard codes were verified for that mix design. The trial phase was successful and eventually the main apron was constructed.



Figure 2.5: Brisbane West Wellcamp Airport construction site [12]

The rapid and successful execution of this project gives an example that GPC can be a great alternative for OPC with many benefits- both sustainable and structural. In the BWWA report. It serves as an encouragement and confidence for future engineers for designing, producing and using this kind of concrete. However, since this project was not executed using standard code that would give a structural verification but just on the basis of lab tests and trial construction, a challenge still remains. Also, there are not any old structures to give a practical verification and information about the durability of GPC.

2.2. STRUCTURAL BEHAVIOUR AND EUROCODE FORMULATIONS:

2.2.1. POSSIBLE FAILURE MODES IN NORMAL RC BEAMS:

A reinforced concrete beam can fail in two different ways commonly known as shear and flexure. In simple terms, if a beam has less shear capacity it fails in shear whereas flexure failure occurs when the load exceeds the bending capacity of the beam. Furthermore, shear failure can be categorised as: **Diagonal tension failure**, **shear compression failure** and **splitting shear** (true shear) failure.[11][33]

Flexure Failure

This kind of failure starts from tension zone of the beam. The vertical cracks are initiated due to yielding of steel reinforcement. Crack slowly propagates upwards leading to crushing of concrete in compression zone. This failure shows ductile behaviour. The amount of deflection is more in this failure.

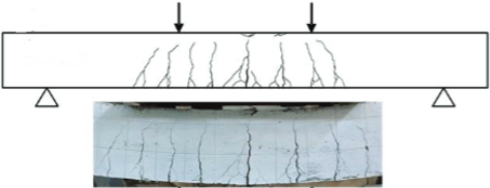


Figure 2.6: Flexure failure mode[34]

Shear compression failure	Flexure shear/Diagonal tension failure
---------------------------	--

This failure occurs when a critical diagonal crack leads to crushing of concrete in compression zone. In some cases, this crushing and failing might lead to propagation of another splitting crack of concrete strut as shown in the figure below.

This failure mode originates from flexure shear crack at the bottom. The crack grows diagonally with increment of load towards the loading area of top fibre of the beam, shown in the figure as critical inclined crack.

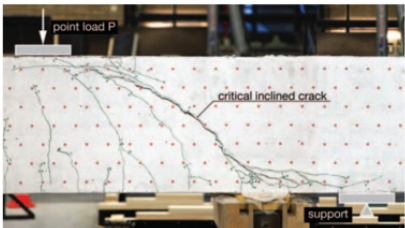
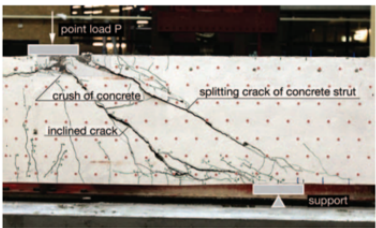


Figure 2.7: Shear failure mode: a)Shear compression failure b)Flexure shear failure[11]

A DETAILED LOOK AT EUROCODE EN.1992.1.1

In this section, a detailed look at the Eurocode EN 1992-1-1:2004 aspects to calculate and design will be done- the ones to be analysed within this research.

2.2.2. MATERIAL PARAMETERS

Concrete class/Strength:

Concrete strength for any concrete is decided based on compressive tests carried out for cylindrical and cube specimens after 28 days of casting. According to EN 206 "Concrete specification, performance, production and conformity", compressive strength is defined by characteristic value f_{ck} below which not more than 5% of the test results fall. In the curve, probability variability for compressive strength is shown to understand the explanation. Concrete class for example, if is C35/45, indicates that the cylinder and cube characteristic strengths are 35 MPa and 45 MPa respectively. Eurocode (Table 3.1) gives an approximation to calculate the mean compressive strength as $f_{cm} = f_{ck} + 8$ where, f_{ck} is the characteristic cylinder compressive strength.

Additionally, EC clause 3.1.2(6) suggests a prediction of strength development of concrete according to the age. Formulated in accordance with EN 12390, the expression to estimate compressive strength at various ages is given as,

$$f_{cm}(t) = \beta_{cc}(t) f_{cm}$$

where,

$$\beta_{cc}(t) = \exp \left\{ s \left[1 - \left(\frac{28}{t} \right)^{\frac{1}{2}} \right] \right\}$$

Here, "s" is a coefficient which depends on the type of cement used classified as:

0.20 for Class R (rapid hardening); cement of strength classes CEM 42,5R, CEM 52,5N and CEM 52,5R

0.25 for Class N (normal hardening); cement of strength classes CEM 42,5N and CEM 32,5R

0.38 for Class S (slow hardening); cement of strength class CEM 32,5N.

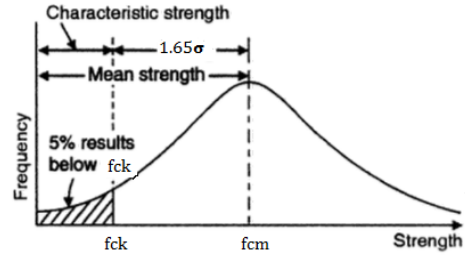


Figure 2.8: Normal distribution curve for compressive strength[31]

Tensile strength of concrete:

To calculate the tensile strength of concrete, there is no direct test to identify the value; first split tensile strength test is carried out which gives the value of splitting tensile strength, $f_{ct,sp}$ and using that, Eurocode provides an approximate value to calculate the axial tensile strength and then the tensile strength using the relation:

$$f_{ctm} = 0.9 f_{ct,sp}$$

According to EC (Table 3.1)A.3, tensile strength,

$$f_{ctm} = 0.30 * f_{ck}^{2/3} \quad \text{for } (\leq C50/60).$$

2.2.3. SHEAR

Eurocode gives some general procedure for the verification of shear capacity in concrete for the following:

$V_{Rd,c}$, the design shear resistance of the member without shear reinforcement. This expression gives the shear capacity of the concrete when shear force is less than the concrete capacity.

$V_{Rd,s}$, the design value of the shear force which can be sustained by the yielding shear reinforcement. When $V_{Rd,c}$ is less than the shear force, then there is a need to add stirrups in the concrete to take that shear force and increase the resistance; the resistance then is determined by $V_{Rd,s}$.

$V_{Rd,max}$, the design value of the maximum shear force which can be sustained by the member, limited by crushing of the compression struts.

**Other components for shear verification of inclined chords are out of the scope of this research.*

Members not requiring design shear reinforcement:

The design shear resistance of the member without shear reinforcement, $V_{Rd,c}$ is given as,

$$V_{Rd,c} = [C_{Rd,c} k (100 \rho_l f_{ck})^{1/3} + k_1 \sigma_{cp}] b_w d > (v_{min} + k_1 \sigma_{cp}) b_w d$$

where:

$V_{Rd,c}$ is the design value of the shear force capacity.

f_{ck} is the characteristic compressive strength of concrete.

A_{sl} is the area of the tensile reinforcement, which extends

$$k = 1 + \sqrt{\frac{200}{d}} \leq 2$$

$$\rho_l = \frac{A_{sl}}{b_w d} \leq 0.02$$

b_w is the smallest width of the cross section in the tensile area.

σ_{cp} is the axial stress caused by loading or prestressing: $\sigma_{cp} = \frac{N_{Ed}}{A_c} \leq 0.2 f_{cd}$

A_c is the cross-sectional area of the concrete.

f_{cd} is the design cylinder compressive strength of the concrete.

N_{Ed} is the axial force due to loading or prestressing ($N_{Ed} > 0$ for compression);

$$v_{min} = 0.035 k^{\frac{3}{2}} f_{ck}^{\frac{1}{2}}$$

The expression provides particulars about variables that influence the shear capacity that would be calculated using this formula. Firstly, compressive strength of concrete is one of the important parameters is a base for all other behaviours of concrete as well. Longitudinal reinforcement ratio, size of the beam (width & effective depth), k factor (size effect), k_1 and $C_{Rd,c}$ factor also play role in providing resistance to shear in concrete according to the formula. However, it has been observed from experiments that tensile strength has more effect than compressive strength[2]. To calculate the tensile strength, code gives a general rule of compressive strength to the power 2/3. It shows that shear strength increases as the reinforcement ratio increases. Another variable known to have a significant effect on capacity is the size effect (k). The Dutch Annex of EN 1992-1-1 uses recommended values: $C_{Rd,c} = 0.18/\gamma_c = 0.12$ and $k_1 = 0.15$. However, the factor $C_{Rd,c}$ was decided for design shear resistance in Eurocode 2 but to have a better prediction of mean value of shear resistance, Regan replaced this factor with $C_{Rm,c} = 0.15$ and was later used by König and Fischer to evaluate where value 0.163 for $C_{Rm,c}$ was found to be better fitting [11].

Members requiring design shear reinforcement

**Only the part for members with vertical shear reinforcement will be analysed as among the beams experimented, the ones with shear reinforcement were only vertical shear reinforcement. Members with inclined shear reinforcement is out of the scope of this research*

The resistance of the member with shear reinforcement (for vertical shear reinforcement) V_{Rd} is the smaller value of:

$$V_{Rd,s} = \frac{A_{sw}}{S} z f_{ywd} \cot \theta$$

and

$$V_{Rd,max} = \alpha_{cw} b_w v_1 f_{cd} / (\cot \theta + \tan \theta)$$

where:

A_{sw} is the cross sectional area of the shear reinforcement.

S is the spacing of the stirrups

f_{ywd} is the design yield strength of the shear reinforcement

v_1 is a strength reduction factor for concrete cracked in shear

α_{cw} is a coefficient taking account of the state of the stress in the compression chord

θ is the angle made by compressive strut with the beam axis

z is the inner lever arm, for a member with constant depth, corresponding to the

bending moment in the element under consideration. In the shear analysis of reinforced concrete without axial force, the approximate value $z = 0.9d$ may normally be used.

The recommended limits for $\cot\theta$ given in national annex are $1 \leq \cot\theta \leq 2.5$

In case of beam without shear reinforcement, the imposed load leads to bending causing flexural cracks slowly developing into a shear crack eventually leading to failure.

But by adding the shear reinforcement in the beam, an inclined crack does not lead to a failure but introduces a new load transfer mechanism which is explained and derived using a truss model. This truss has to carry design shear force. In the figure below, α denotes inclination of the tensile ties and θ denotes the compression struts. The shear carried by these tensile ties and compressive strut derived using this truss model are denoted by $V_{Rd,s}$ and $V_{Rd,max}$ respectively. When θ is taken as 45 degrees ($\cot\theta = 1$), the shear capacity is underestimated. Eurocode 2 then follows another approach where it is assumed that shear reinforcement carries all the shear force taking value of θ between $\cot^{-1} 0.4$ and $\cot^{-1} 2.5$. It can only go below this angle if there are constraints and different geometrical detailing. [2][35]

From the $V_{Rd,s}$ formula, it can be said that the capacity can be increased simply by increasing the amount of reinforcement. But the capacity of strut rather varies according to the strength and not the shear reinforcement.

It is evident that the amount of shear reinforcement, compressive strength of concrete, yield strength of reinforcement, strut angle and size of the beam influences the overall shear capacity of beams with shear reinforcement.

The truss model used to derive these capacities according to forces can be seen in the figure below

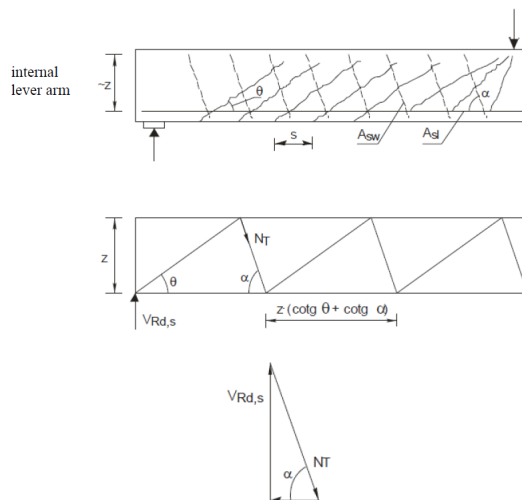


Figure 2.9: truss model used to calculate shear capacities for beams with shear reinforcement present [35]

MECHANISM OF SHEAR TRANSFER IN CONCRETE

The above section provides an overview of the formulation and background of Eurocode models. But shear failure mechanism of reinforced concrete beams is a complex process, there has been a lot of discussion about the mechanism of shear transfer in reinforced concrete members, particularly about the relevant variables to incorporate in shear prediction models. As stated in the textbook of Prestressed Concrete [35], this is a conservative model to predict the shear resistance but in reality the simple truss assumed here will not have this simple pattern with perfect hinges connections and thus it difficult to analyze this accurately.

According to ASCE-ACI Committee 426 [26], when a diagonal crack occurs, the shear force is transferred by several internal shear transfer mechanisms which are widely discussed in many researches about shear. These mechanisms are- Shear force transfer due uncracked concrete compression zone, aggregate interlock, dowel action (longitudinal reinforcement) as shown in the figure below. Experimental analysis by Walraven [1] suggest that, aggregate interlocking contributes towards a large amount of shear transfer which is influenced by the size of aggregate, compressive strength, etc. The contribution of dowel action, however in cracked beams without shear reinforcement can be small as it has to take the tensile strength of concrete cover as well.

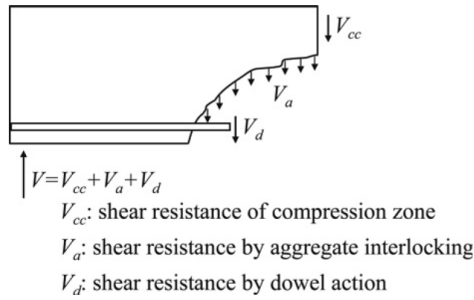


Figure 2.10: Shear transfer mechanisms
[7]

FACTORS INFLUENCING SHEAR BEHAVIOUR

Compressive strength:

According to the design equation, compressive strength directly affects the shear resistance for both beams with (resistance provided by strut) and without shear reinforcement. However, from Walraven's study (1978) [40] about concrete strength, the deviations in shear strength were less in concrete with lower strength and higher deviations with increase in concrete strength class [32].

Shear span-Depth Ratio (a_v/d):

For studies done for conventional concrete beams previously, it has been proved from experiments that it has a significant effect in the shear behavior of reinforced concrete beams. In a research done by Wu et al. [22][23], it was proved that a/d ratio has a notable

influence in shear strength provided by both concrete and reinforcement. Eurocode 6.2.2 clause (6) states the In an experimental observation done by Biao Hu et al.[20], it showed that values of $V_{Rd,s}$ and $V_{Rd,c}$ are significantly affected by a/d where $V_{Rd,c}$ decreases much as a/d increases, while $V_{Rd,s}$ has an opposite behavior.

EC clause 6.2.2 (6) states the need of multiplying shear force with a reduction factor ($\beta = a_v/2d$) if shear span ratio (a_v/d) is less than 2. And even when the shear span ratio is greater than 2 there is another check. So Eurocode does account the shear span ratio although not directly put in the shear resistance formula.

Amount of reinforcement in tensile zone:

Reinforcement ratio is another influencing factor that affects the shear capacity. In shear models by EC, the design equation takes into account the area of reinforcement.

2.2.4. CRACK WIDTH CONTROL

From the beginning of the loading phase, involved forces and induced stresses, the mechanism of how crack initiates, propagates, eventually leading to failure – everything related in this process has a significant effect to determine the crack pattern. The formula to calculate the crack width in EN 1992-1-1 (expression 7.8) is given as,

$$W_k = S_{r,max}(\epsilon_{sm} - \epsilon_{cm})$$

where,

$S_{r,max}$ is the maximum crack spacing

ϵ_{sm} is the mean strain in the reinforcement under the relevant combination of loads, including effect of imposed deformations and taking into account the effects of tension stiffening. Only the additional tensile strain beyond the state of zero strain of the concrete at the same level is considered.

ϵ_{cm} is the mean strain in the concrete between cracks

$$\epsilon_{sm} - \epsilon_{cm} = \frac{\sigma_s - k_t \frac{f_{ct,eff}}{\rho_{p,eff}} (1 + \alpha_e \rho_{p,eff})}{E_s} \geq 0.6 \frac{\sigma_s}{E_s}$$

where:

E_s is the modulus of elasticity of steel

k_t is a factor dependent on the duration of the load

σ_s is the stress in the tension reinforcement assuming a cracked section.

α_e is the ratio E_s/E_{cm}

$$\rho_{p,eff} = A_s/A_{c,eff}$$

$$A_{c,eff} = h_{c,eff} * b$$

$$h_{c,eff} = \text{Minimum of } (2.5(h - d), (h - x)/3 \text{ or } h/2)$$

The maximum spacing is given as,

$$S_{r,max} = k_3 c + k_1 k_2 k_4 \phi / \rho_{p,eff}$$

BACKGROUND AND MECHANISM BEHIND A CRACK IN CONCRETE

Cracks in concrete can occur due to various causes like shrinkage, imposed deformation (thermal loading), external loading etc. Shrinkage cracks can be controlled to some extent but not fully as there will always be temperature differences and relative humidity.

These cracks are small but might show big influence in the structural behaviour of concrete. However, if we have a look on to the micro structure level, certainly there are ways to reduce these kinds of cracks to some extent. But due to limited scope of the research, the main concern will be given to the cracks induced by external loading. The cracks caused due to shrinkage and thermal loading are out of scope of this research.

Concrete when cracks, cannot carry the tensile force anymore which is then carried by the reinforcement. It is well known that concrete is strong in compression and weak in tension. When reinforcement starts taking the tensile force of concrete, a bond stress is activated between concrete and steel which is assumed to be constant and two times the mean tensile strength f_{ctm} of the concrete i.e. bond stress (τ_{bm}) = $2f_{ctm}$.

The formulation of crack width and spacing was established relating to a reinforced concrete bar subjected to axial tensile force. This whole mechanism is distinguished into 4 stages- uncracked stage, crack formation stage, stabilized cracking stage, steel yielding stage. [35]

Phase 1- Uncracked phase:

Here, the concrete doesn't crack and behaves as linear elastic. In this phase the force required for concrete to crack is small. The tensile stress is less than the mean tensile strength $(\sigma_{ct} < f_{ctm})$ and thus the concrete can take all tensile stress. Both steel and concrete has same the strain and thus stiffness is constant too.

Phase 2- Crack formation stage:

Further when concrete strain increases, the concrete tensile stress reaches the mean tensile strength $(\sigma_{ct} = f_{ctm})$, thus now concrete cannot take the tensile stress anymore giving rise to the first crack from tension side of concrete. From this point, the reinforcement takes the tensile stress of the concrete. After crack initiates, force and stiffness decreases although the strain keeps increasing. Further increase in strain causes force increase. This force keeps increasing till another crack forms and this keeps repeating again and again-the series of appearance of new cracks- thus is called "Crack formation stage".

Phase 3- Stabilized cracking stage

Now, as the load increases, the concrete tensile stress starts exceeding the mean tensile stress and the yielding of steel also starts $(\sigma_s = f_{yd})$. This can also be know as the beginning of plastic phase.

Phase 4- Crushing of concrete:

In this phase, compressive stress reaches the maximum strength of concrete $(\sigma_c = f_{cd})$ in fibres of compression zone resulting in crushing of concrete and corresponding strain of concrete is 3.5‰.

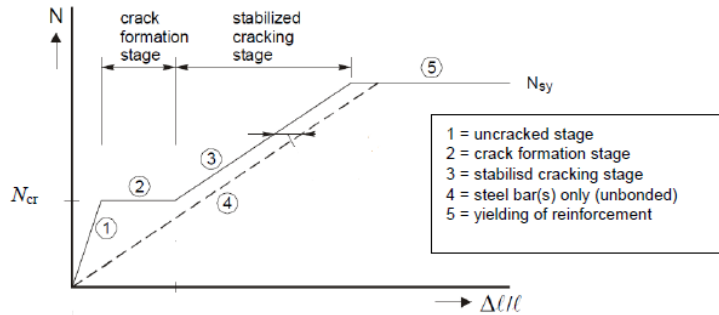


Figure 2.11: Different phases of crack of concrete

The assumption of stage 2 being horizontal is not true in reality; it is rather inclined. However, this assumption of horizontal line is considered to be accurate enough taking into account the influence of uncertainties like reinforcement position, actual tensile strength etc. [Beton1993CEBFIPMC]

FACTORS INFLUENCING CRACK BEHAVIOUR IN CONCRETE

Looking at the model to calculate crack width, multiple variables can be seen as influencing factors like **Concrete strength**, **Concrete cover**, **Reinforcement ratio**, **Bond strength between steel and concrete**, **shape of the bar**. Another important factor that influences the crack behaviour is bond between reinforcement and the concrete. In conventional RC application, efficient and reliable force transfer between reinforcement and concrete is required for optimal design for safety measure in structural components. To understand how the bond force transfers is important to determine the crack pattern. The part where concrete is cracked, all the tensile stress is taken by steel. On both sides of the crack, there is a gradual increase of concrete tensile stress up to a point where the concrete has its initial tensile stress back. From the crack to this point, which is called transfer length, there is a gradual process of re-introducing force into the concrete and here the bond strength comes into importance.

2.2.5. BENDING MOMENT

Bending moment of a concrete cross section with increasing load is calculated using equilibrium of forces and moment with an assumption that plane section remains plane (Bernoulli's law).

- **Cracking moment:** When the concrete on loading loses its tensile strength, it is not able to take the tensile stress anymore when the first crack appears; then the reinforcement in tension takes the tensile stress of concrete. This is the cracking moment of concrete and is calculated as a product of section modulus of cross section and mean axial tensile strength,

$$M_{cr,fl} = \frac{I * f_{ctm}}{e}$$

- Yielding moment: The height of compressive zone needed to resist the reinforcing steel force is estimated using compressive forces of steel and concrete and because of the equilibrium, all the horizontal forces are equated to get height of compressive zone (for rectangular cross section) as,

$$x_u = \frac{N_c}{b * \alpha * f_{cd}}$$

where,

$$N_c = A_s * f_{yd} \text{ (Horizontal equilibrium: } N_c = N_s \text{)}$$

where α can be obtained from the bi-linear stress-strain relationship. Further, steel strain is calculated using this calculated/assumed compression zone height. This calculated strain values are checked with yielding strain of given concrete and steel.

$$\epsilon_s = \left(\frac{d - x_u}{x_u} \right) \epsilon_c \text{ and}$$

$$M_y = N_s * \left(d - \frac{1}{3} x_u \right)$$

- Ultimate moment: When the concrete reaches its ultimate compressive strain, ultimate moment is calculated as

$$M_u = z * N_c$$

where,

$z = d - \beta * x_u$ (β again is obtained using the bi-linear stress-strain relationship of the concrete.)

M- κ diagram:

Further, M- κ diagram can be drawn to observe and study these moments at every step with increasing load until the failure. The respective stages in M - κ diagram are cracking moment (M_{cr}), yielding moment (M_e), plastic moment (M_{pl}) and ultimate moment (M_u),

FACTORS INFLUENCING BENDING BEHAVIOUR IN CONCRETE

From above expressions to calculate moments at different phases, clearly, the influencing factors are **mean axial tensile strength, compressive strength, section modulus, amount of reinforcement, compression zone height.**

2.3. EXPERIMENTS

To test the beams to study shear and bending, four point bending test can be done. In the 4 points bending test, there is a central zone with pure and constant flexure. In 4-point bending, the shear stress is zero in the region between the two loading points (region of pure bending) and has a non-zero value outside this central region (out of the two loading points). This helps study the behaviour in that region clearly as the moment is constant.

3

METHODOLOGY

This chapter provides all the information and step by step approach adopted for this research. This includes description of all the experiments carried out and a general overview about further step of analysing and studying.

3.1. RESEARCH PLAN

- **Preparation of the experiments:**

This research is an experimental study and analysis of structural behaviour of Geopolymer concrete to check the Eurocode applicability. Thus, the first step was to prepare for all the experiments that needs to be carried out to sufficiently answer the research questions. This includes collecting all the background information about the beams needed to be experimented, designing a setup according to the capacity of the testing machine in Stevin II Laboratory, deciding how to place the LVDTs, arranging and checking all the equipment and materials needed to be used during the experiment like ensuring proper functioning of machine, arranging rods for LVDTs, paint, glue, crack measuring ruler, etc.

- **Performing the experiments:**

The second step was to start the experiments according to the planning. The beams were transported from the company to TU Delft and after all the arrangements, experiment was started. The aim was to 2 to 3 beams per day initially. However, from placing the beams to drawing the lines to glue LVDTs, painting etc. all the preparation would take few hours and some days no beams were tested because of technical problems. A total of 1 month and 1 week was needed to test all the 24 beams. The beams tested with the respective date of testing is shown in table A.1. To perform the experiments, for each beam, LVDT positions were measures drawn in the beam and accordingly glued to the beam. The front side of beam was painted white to get the clarity of the cracks and to draw the crack pattern. This section also includes clicking pictures and collection of data obtained as per the beam, writing a log about observations. Details about LVDTs and beams are given in other sections followed in this chapter.

- **Analytical prediction of results:**

After the completion of experiments, analytical calculations were made as per EC2 regulations as it is directly related to the main topic of this research. The formulae used are shown in 3.3.1 section of this chapter and all the calculations are attached in the appendix from A.2.5. section of the report. These calculations were done to check and compare with the obtained experimental data.

- **Post processing:**

After getting all the data from the experiment and from the company (for mechanical properties), they were used to compare by means of tables and charts. Detailed look at parameters and their influence on the results and experiments were studied.

A detailed description of each step of the plan is done in coming sections.

3.2. EXPERIMENTAL PART

Although this research's main area of focus is to study the structural behaviour, a brief analysis of material behaviour in regard to EC has been done too. The first part of the experiments to obtain the mechanical properties results were done in the company laboratory and the data was used here to analyse the areas within the scope.

3.2.1. SAMPLES USED

Two types of concrete mix was prepared namely RAMAC 28/35 and RAMAC 33/43. The strength class for these samples was initially aimed for C 30/37 and C 50/60 but was not achieved and are C28/35 and C33/43 respectively. With an aim of making the bridge fully circular and sustainable, the concrete was produced without using any amount of ordinary portland cement (OPC) and using recycled aggregates. The type of recycled aggregate used is Thermally Recycled Asphalt Aggregate (TRI) instead of natural or recycled (common type of recycled aggregate from demolished buildings) aggregates. This type of aggregate hasn't been used much in practice.

3 cube specimens were prepared per sample mix each of dimension $150 \times 150 \times 150 \text{ mm}^3$ using EPS mold. Due to a low temperature at the time of casting, after pouring into the molds it was closed with lid and kept in heated container for hardening.



Figure 3.1: Cube specimen prepared (Jansen and Sqape laboratory)

3.2.2. TESTS FOR MECHANICAL PROPERTIES

The tests to check the mechanical properties were carried out at the company laboratory. The ones to be discussed in this research include compressive strength test, split tensile strength test and Elastic modulus test.

3.2.3. CASTING AND CURING OF BEAMS:

A total of 24 beams were casted using those 2 types of mixture RAMAC C28/35 and RAMAC C33/43. All the beams were casted in January and outdoors. Concrete was mixed at Jansen Beton BV (mixing plant) and from there transported to Valkenswaard which is approximately which is 35 kms from the mixing plant. The temperature then was around 4°C outside. The method of curing the beams were done by casting in temporary wooden formwork (18mm thickness) as shown in the figure below. During the start of casting, measures were taken for the formwork to be above 5°C. Right after casting some plastic foils were laid on top of the fresh concrete. Additionally, an extra layer of insulation foil was applied because of the cold weather conditions. For a period of at least a week, the temperature was kept under the insulation foil between 18 and 22 degrees Celsius as temperature is one of the important factors influencing the hydration process of concrete. While casting the beams, workability was observed to be harder than the normal concrete.



Figure 3.2: Casting of GPC beams at Valkenswaard (Boskalis)

3.2.4. CLASSIFICATION OF THE BEAMS:

Second and the major experiments in this research for beams were carried out in TU Delft Stevin II Laboratory. A total of 24 beams were tested. These tests were entirely done to study the structural behaviour of GPC. To study and achieve the goal of this research, 12 beams were designed to fail in shear and 12 beams were designed to fail in bending so

that it could be studied for the respective behaviour. Within these groups, height, layout of reinforcement and distance between support and the loads were variables.

Characterisation based on depth, reinforcement layout and strength class:

Table 3.1 below shows all the specimens according to layout of the reinforcement, depth of the beam in and their strength class.

beam 1-2-3 beam 13-14-15 $L \times B \times H = 2500 \times 300 \times 250\text{mm}^3$ Strength class C28/35 cover 60mm top reinf. 2 diameter 16mm bottom reinf. 3 diameter 20mm stirrups diameter 12-125		
beam 4-5-6 beam 16-17-18 $L \times B \times H = 2500 \times 300 \times 400\text{mm}^3$ Strength class C28/35 cover 60mm top reinf. 2 diameter 16mm bottom reinf. 2 diameter 16mm stirrups diameter 16-150		
beam 7-8-9 beam 19-20-21 $L \times B \times H = 2500 \times 300 \times 400\text{mm}^3$ Strength class C33/43 cover 60mm top reinf. 2 diameter 16mm bottom reinf. 3 diameter 16mm stirrups diameter 16-150		
beam 10-11-12 $L \times B \times H = 2500 \times 300 \times 400\text{mm}^3$ Strength class C33/43 cover 60mm top reinf. 2 diameter 16mm bottom reinf. 3 diameter 16mm stirrups diameter 16-150		
beam 22-23-24 $L \times B \times H = 2500 \times 300 \times 400\text{mm}^3$ Strength class C33/43 cover 60mm top reinf. 3 diameter 16mm bottom reinf. 2 diameter 16mm stirrups diameter 16-150		

Table 3.1: Classification of beams according to depth, reinforcement layout and strength class

All these beams shown above used for testing aren't of the actual dimension that would be used for construction of the bridge except for beams 1, 2, 3, 13, 14, 15 which would be used as approach slab in the bridge. And this modification in the beam dimensions for all other beams were done as per the capacity of testing in TU Delft Stevin Laboratory. Taking into account the maximum beam length that could be fitted and to maintain the required a/d ratio, beam dimensions were designed.

The first two set of beams (1, 2, 3, 4, 5, 6, 13, 14, 15, 16, 17, 18) were casted using C28/35

whereas the remaining 3 set of beams (7, 8, 9, 10, 11, 12, 19, 20, 21, 22, 23, 24) were casted using C33/43. Shear reinforcement in 12 of the beams are only placed in half of the member and this is because these were to be used as bridge deck (plate element) and in this case bridge deck according to design requirements for the bridge, didn't require shear reinforcement. Those are beams 7, 8, 9, 10, 11, 12, 19, 20, 21, 22, 23, 24. These beams were intended to be analysed for shear behaviour during the experiments. Other beams were designed for approach slab and abutments which has been classified and shown in table 3.2

Characterisation based on components/different parts of the bridge

Each beam casted for the experiments represented different components of the bridge structure. These have been listed in the table 3.2 along with the actual height that was designed for the bridge construction.

Beams	Representing the part	Actual height in the structure (mm)
1	Approach slab	250
2	Approach slab	250
3	Approach slab	250
4	abutment	700
5	abutment	700
6	abutment	700
7	Deck (plate element)	700
8	Deck (plate element)	700
9	Deck (plate element)	700
10	Deck (plate element)	700
11	Deck (plate element)	700
12	Deck (plate element)	700
13	Approach slab	250
14	Approach slab	250
15	Approach slab	250
16	abutment	700
17	abutment	700
18	abutment	700
19	Deck (plate element)	700
20	Deck (plate element)	700
21	Deck (plate element)	700
22	Deck (plate element)	700
23	Deck (plate element)	700
24	Deck (plate element)	700

Table 3.2: The components in the structure and respective beam representative

Reinforcement Details of all the beams:

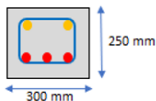
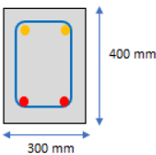
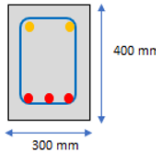
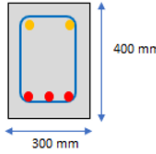
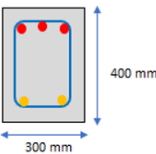
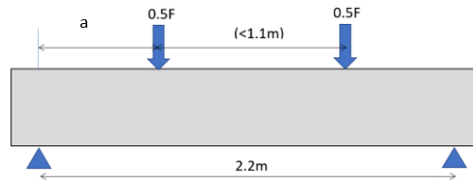
BEAMS	LAYOUT	Cover (mm)	REINFORCEMENT		Tensile Reinforcement ρ (%)
			Compression	Tension	
Beam 1-2-3 Beam 13-14-15		60	2 \varnothing 16mm	3 \varnothing 20mm	1.84
Beam 4-5-6 Beam 16-17-18		60	2 \varnothing 16mm	2 \varnothing 16mm	0.42
Beam 7-8-9 Beam 19-20-21		60	2 \varnothing 16mm	3 \varnothing 20mm	1
Beam 10-11-12		60	2 \varnothing 16mm	3 \varnothing 20mm	1
Beam 22-23-24		60	3 \varnothing 20mm	2 \varnothing 16mm	0.42

Table 3.3: Reinforcement layout in all the beams

Figure 3.3 shows the cross section of all the beams with respective longitudinal reinforcement (both in tension and compression zone). Reinforcement used in all the beams were designed to provide minimum yield strength of 500 MPa and were of ribbed type and grade B500B. Amount of reinforcement meets the minimum design reinforcement requirement. Beam group 22, 23, 24 had the same cross section as beam group 7, 8, 9 and later was decided to reverse upside down to decrease the amount of reinforcement in tensile zone to check the governing failure mode.

The design for cover was also done in accordance to EC 2 depending on the exposure class. The table of EC classification of Exposure class is attached in appendix A.3. The beams designed for this research falls under the exposure class XD3 as they are all components of a bridge which matches those environmental conditions (Cyclic wet and dry-Parts of bridges exposed to spray containing chlorides, pavements, car park slabs).

Characterisation based on application of load:

Beams number	Distance between load and the support (mm)	Effective depth (mm)	Shear span depth ratio (a/d)
1, 2, 3, 13, 14, 15	600	170	3.53
4, 5, 6, 22, 23, 24	950	316	3.01
7, 8, 9	950	314	3.03
10	750	314	2.39
11	850	314	2.72
12	950	314	3.03
16, 17, 18	850	316	2.69
19, 20, 21	1100	314	3.50

Table 3.4: Classification of beams according to the distance between loads and supports

Within the 12/12 beams designed to shear and bending, distance between loads and supports were changed to compare and study the varied behaviour according to varied a/d .

The first 3 beams tested were 10, 11, 12 beginning with beam 10 (750 mm) increasing 100 mm for beam 11 and again 100 mm for beam 12. This was done to check the load transfer of load to the support to decide distances for other beams.

3.2.5. EXPERIMENTAL SETUP AND INSTRUMENTATION

The main aim for the tests carried out in Stevin Lab was to analyse the structural behaviour of GPC beams intended to be used in the bridge construction (KW15). The main areas to be analysed were shear, flexure and cracks. Taking that into consideration, a setup was designed. Depending on the maximum test capacity, the beam depth was decided as 400 mm before the casting. The experiment was planned with some pre-decided conditions. All the beams had a span of 2.5 m (which again is the maximum length which could be fitted there) and the center-to-center distance between the supports was set to 2.2m for all the 24 experiments.

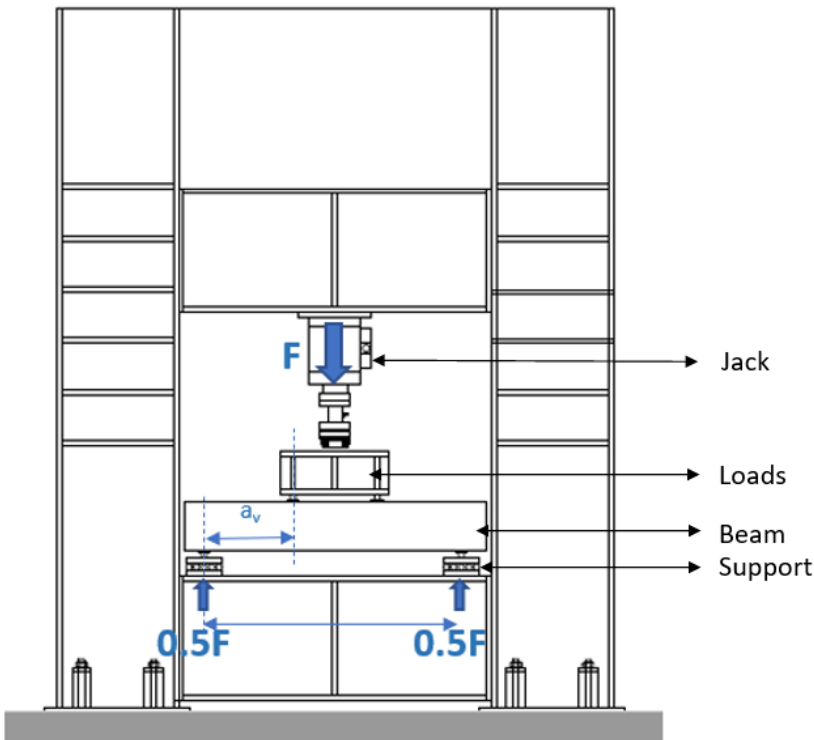


Figure 3.3: Designed test setup

4-point bending test was carried out for all the beams except beams 19, 20, 21 for which 3 point bending test was done. As 12 beams were planned to be tested for shear and 12 for bending, the distance between load and the support (a_v) was a variable in every beam depending on the required mode of failure which is distinguished in tables in the previous section. For that, the loads shown in figure 3.3 was adjusted accordingly. The loading was deformation controlled and was set to 0.01 mm/sec. All the specimens were painted white to facilitate marking of cracks. For the first experiment, load was applied at increment of 10 kN in every step to observe the behaviour in change of the beam. From second experiment it was realised that increment of 20 kN load per step was more efficient, less time taking and the deformation was also notable. After every load step of 20 kN, the machine was paused to stop loading and the beam was observed at the painted side to check appearance of cracks if any. Gradually when crack initiated and propagated, pictures were taken after every 20 kN load step and crack pattern was drawn along with measuring crack widths approximately at the bottom longitudinal reinforcement level. And eventually the governing failure mode was observed after the failure of the beam.



Figure 3.4: Actual test setup in the lab with a beam

Figure 3.3 shows the designed setup according to the requirement of the research. The machine was adjusted according to length of the beam. All the components are mentioned in the diagram. Figure 3.4 shows the actual picture of experimental setup of one beam right before the experiment.

3.2.6. LVDTs POSITIONING

The LVDTs were placed in such a way that the outcome of the results from these LVDTs would give displacement values of the required location, the critical points. As mentioned earlier, these beams were tested for both shear and flexure and thus two kinds of LVDT placement were done as shown in the figure 3.5. However, due to change in the distance between supports and the load points, distance between LVDTs were changed accordingly within the same type of positioning as well to cover the crack displacement effectively.

The distance between LVDTs were decided this way: Firstly, a line of 45° from both the loads and supports were drawn towards each other. Then three lines normal to those previously drawn lines were drawn equally distributed to cover those lines where the main shear crack is expected to occur. To measure the flexure crack widths, bottom LVDTs were placed at the bottom surface of the beam equally distributed.

Beams	<u>LVDT 1</u>	LVDT on front side of the beam (<u>LVDTs 2, 3, 4, 5, 6, 7</u>)	LVDT on the bottom side of the beam (<u>LVDTs 8, 9, 10</u>)
4, 5, 6, 7, 8, 9, 10, 11, 12, 16, 17, 18, 19, 20, 21, 22, 23, 24	To measure the vertical displacement of the beam	To measure the inclined shear cracks at the front surface of the beam	To measure the flexure cracks of the bottom fibre of the beams

Beams	<u>LVDT 1</u>	LVDT on the bottom side of the beam (<u>LVDTs 2, 3, 4, 5, 6</u>)
1, 2, 3, 13, 14, 15	To measure the vertical displacement of the beam	To measure the flexure cracks of the bottom fibre of the beams

Table 3.5: LVDTs used in each beam and their aim

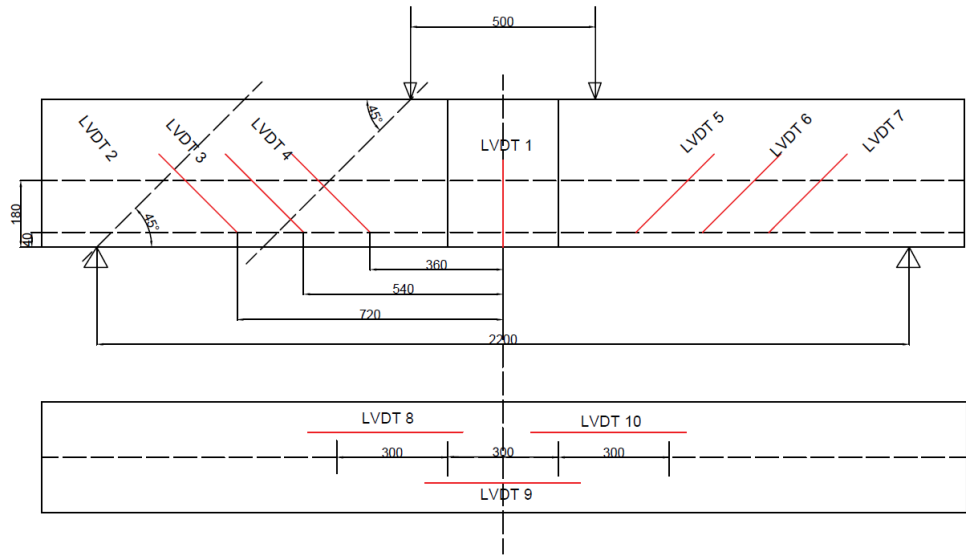


Figure 3.5: LVDTs positions and dimensions of beams 10, 11, 16, 17, 18 (all dimensions are in mm)

Figure 3.5 shows the LVDT placements that was taken for beams 10, 11, 16, 17 and 18. The LVDT positions and distances of rest all other beams are attached in appendix section A.1



Figure 3.6: Picture after placing the LVDTs in one of the beams (front part)



Figure 3.7: Picture after placing the LVDTs in one of the beams (bottom part)

While the crack was measured by LVDTs, an additional way of measuring cracks using concrete crack width ruler was done at the level of bottom longitudinal reinforcement at certain load steps. This can be seen in the figure 3.8. This additional way of measurement would provide a basis of comparison between LVDT and ruler measured cracks. This could give an indication of whether the LVDT can give an accurate measurement.

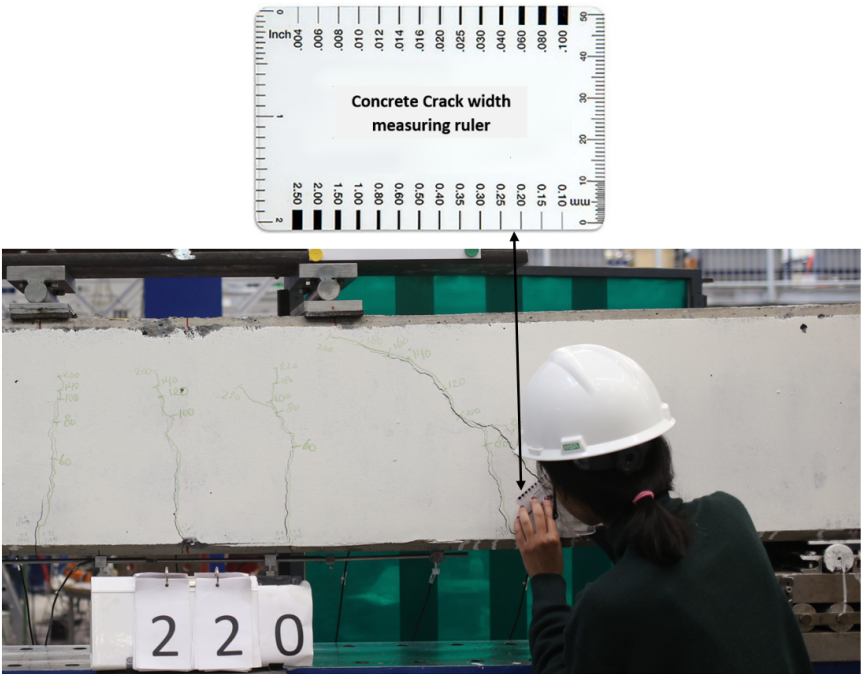


Figure 3.8: Measurement of cracks using concrete crack width ruler

3.3. POST EXPERIMENTAL PART

3.3.1. ANALYTICAL CALCULATIONS

Moment capacity and curvature		
Cracking Moment	$M_{cr} = \frac{I * f_{ctm}}{e}$	
	$\kappa = 2 * \epsilon_{cr} / h$	
Yeilding Moment	$M_y = N_s (d - \frac{1}{3} x)$ where,	
	$x = \frac{-2 * A_s * n \pm \sqrt{4 * n^2 * A_s^2 - 4 * b * (-2 * n * d * A_s)}}{2 * b}$	
	$\kappa = (\epsilon_c + \epsilon_s) / d$	
Bending Moment when $\epsilon_c = \epsilon_{c3}$	$M_y = N_s (d - \frac{1}{3} x_c)$, where $x_c = \frac{N_c}{b * \alpha * f_{cm}}$	
	$\kappa = \epsilon_s / (d - x)$	
Ultimate Bending Moment	$M_u = z * N_c$ where, $z = d - \beta * x_u$ and $x_u = \frac{N_c}{b * \alpha * f_{cm}}$	
	$\kappa = \epsilon_{cu3} / x_u$	
Shear capacity		
Shear capacity concrete	$V_{Rd,c} = \left[C_{Rm,c} k (100 \rho_l f_{cm})^{\frac{1}{3}} + k_1 \sigma_{cp} \right] b_w d$	EN 1992-1-1 (6.2.a)
Shear capacity stirrups	$V_{Rd,s} = \frac{A_{sw}}{S} z f_{yw} \cot \theta$	EN 1992-1-1 (6.8)
Ultimate capacity Compressive strut	$V_{Rd,max} = \alpha_{cw} b_w v_1 f_{cm} (\cot \theta + \tan \theta)$	EN 1992-1-1 (6.9)
Crack width control		
Maximum crack spacing	$S_{r,max} = k_3 c + k_1 k_2 k_4 \varphi / \rho_{p,eff}$	EN 1992-1-1 (7.11)
Crack width	$W_k = S_{r,max} (\epsilon_{sm} - \epsilon_{cm})$	EN 1992-1-1 (7.8)

Table 3.6: An overview of all the formulae used to make analytical predictions

Parameters:

In the formulae given in EC, design values for materials are used taking into account the partial safety factors. The parameters highlighted in the table are the mean values of materials and not the design values which were taken for calculations to compare with that of the experimental results to make it more comparable. This was done because using the mean values would give a more realistic prediction to compare with the experiments and considering the fact that EC is too conservative. The calculations made for all the beams using these models are shown in appendix A.2.5. Calculations using design values were done too in order to check the accuracy of EC models for GPC.

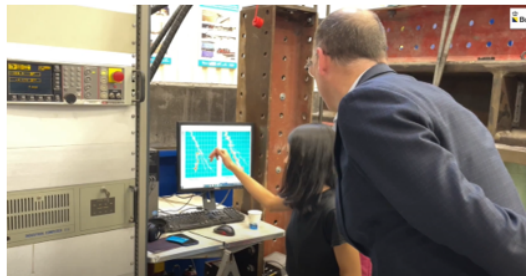
Assumptions:

- The main assumption made is that the models for designing and calculating capacities for a (normal cement) concrete structural element/beam can be used for Geopolymer concrete as well which is why the predictions were made using these models.
- The influence of mechanical properties of GPC are similar to that of normal concrete which is why all the calculations take material parameters the same way as taken in Eurocode models.

3.3.2. POST PROCESSING OF RESULTS

After completion of all the experiments and making required calculations, the collected data obtained from the experiments were used to draw graphs, charts characterizing the structural behaviour of Geopolymer concrete. These data were further used to compare with that of Eurocode predictions done after the experiments.

Literature study was done where a detailed study of Eurocode models and the influencing parameters for different behaviours like shear and bending were identified. From the obtained results, the influence of these parameters for GPC was known and compared accordingly.



4

RESULTS & DISCUSSIONS

Experimental results of all the tests performed are shown in this chapter.

A part of the research experiments were done in Ajansen and Sqape laboratories whose results are important for the research and the data will be taken for further analyzation and comparisons. Those include the results of compressive strength and splitting tensile strength. Besides those, are the results of experiments for beams carried out in Stevin II laboratory.

4.1. MATERIAL BEHAVIOUR

4.1.1. COMPRESSIVE STRENGTH

Compressive strength of the samples was measured according to NEN-EN 12390-3 standard. The strength of 1, 3, 5, 14, 28, 56, 91 days of the two mixes were checked which are presented below in table 4.1 and graph figure 4.1.

Table 4.1 gives an overview of measured cube compressive strength over time. 3 cubes were measured at every age and an average of those 3 cube samples were taken as the cube compressive strength for the respective number of days.

From the graph, strength development over time of the concrete can be studied. It is evident that there is an increase in the strength up to 28 days. And the rate of increase of the strength slows down till 56 days. However, a slight increase in rate of strength development can be seen after 56 days. RAMAC C28/35-2 and RAMAC C33/43 shows a similar trend of strength development. It can be seen in the graph that RAMAC C28/35-2 shows an increasing trend of strength development from day 1 to day 91. And for RAMAC C28/35-2 mix, there is less increase in strength between 5 and 15 days compared to that of RAMAC C33/43. But if the strength between 28 and 91 days are compared, RAMAC C28/35-2 shows a higher increase compared to that of C33/43.

Compressive strength (MPa)						
Age (Days)	RAMAC 28/35-2			RAMAC 33/43		
	Measured (N/mm ²)	Mean	Standard deviation	Measured (N/mm ²)	Mean	Standard deviation
1	11.1	9.7	1.35	23.2	23.7	1.45
	8.4			25.3		
	9.7			22.5		
3	27.9	27.5	0.4	35.0	33.5	2.12
	27.1			34.5		
	27.5			31.1		
5	35.4	33.0	2.26	36.8	36.6	0.81
	32.7			37.3		
	30.9			35.7		
14	36.6	35.5	1.02	45.4	46.9	1.55
	34.6			46.8		
	35.2			48.5		
28	43.1	42.3	0.85	50.3	50.4	1.20
	42.3			49.2		
	41.4			51.6		
56	43.4	43.1	0.7	49.6	51.5	1.69
	42.3			51.9		
	43.6			52.9		
91	51.7	48.7	3.05	54.3	54.0	1.61
	48.9			55.5		
	45.6			52.3		

Table 4.1: Overview of measured compressive strength values according to time (Tests done in Jansen and Sqaep laboratory)

Cube strengths corresponding to every age can be seen in the table 4.1. This gave the mean value of cube compressive strength which was further used to determine the characteristic cube strength using $f_{ck} = f_{cm} - 8$. This value further multiplied with a factor of 0.8 gave the characteristic cylinder strength of the concrete.

So at 28 days, for C28/35, the mean cube strength in table 4.1 is 42.3 N/mm^2 which gave, characteristic cube strength as $42.3 - 8 \approx 35 \text{ N/mm}^2$ and characteristic cylinder strength as $35 * 0.8 = 28 \text{ N/mm}^2$.

This is how the strength class was decided as C28/35 and same way for C33/43 as well.

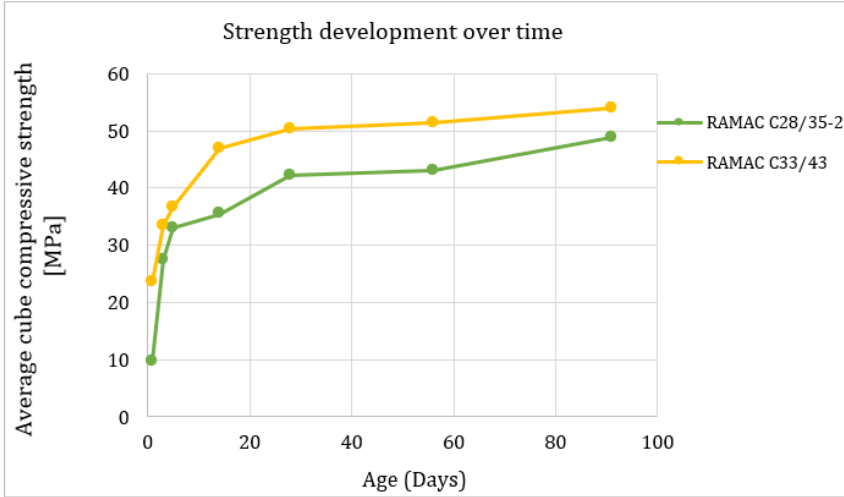


Figure 4.1: Development of compressive strength with time

Secondly, EC clause 3.1.2(6) expression:

$$f_{cm}(t) = \beta_{cc}(t) f_{cm}$$

is used to estimate the strength development according to time to further compare it to obtained trend of strength development of the mix used. This expression was formulated for normal cement concrete.

$$\beta_{cc}(t) = \exp \left\{ s \left[1 - \left(\frac{28}{t} \right)^{\frac{1}{2}} \right] \right\}$$

0.20 for Class R (rapid hardening); cement of strength classes CEM 42,5R, CEM 52,5N and CEM 52,5R

0.25 for Class N (normal hardening); cement of strength classes CEM 42,5N and CEM 32,5R

0.38 for Class S (slow hardening); cement of strength class CEM 32,5N.

Here, the factor "s" is initially taken as 0.20 assuming class R according to the observed

hardening behaviour (rapid) of this type of concrete. The comparison of estimated and experimental strength development can be seen in the figure 4.2 and 4.3 and the calculated table in the appendix A.2.2

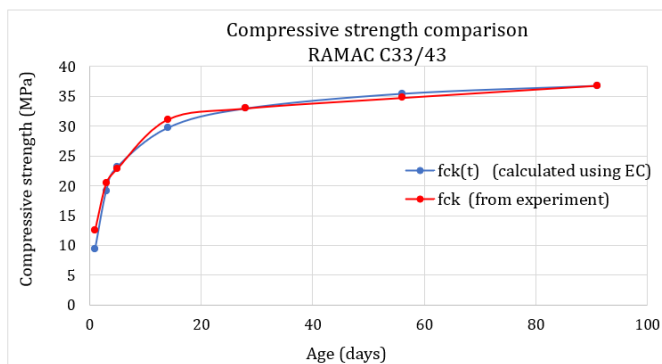


Figure 4.2: Strength development over time for RAMAC C33/43 taking "s"=0.2 (Eurocode 2 estimation vs measured)

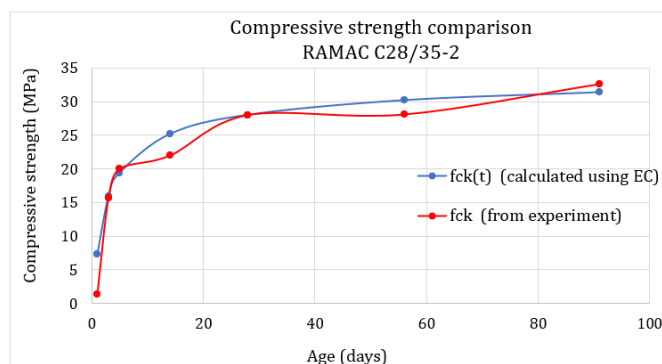


Figure 4.3: Strength development over time for RAMAC C28/35-2 taking "s"=0.2 (Eurocode 2 estimation vs measured)

Graphs shown in figures 4.2 and 4.3 show comparison between the strength development with age estimated using EC vs measured from the experiment. " $f_{ck}(t)$ (calculated using EC)" represents the curve drawn with the values obtained calculated using the expression for $f_{cm}(t)$. Then $f_{ck}(t)$ was calculated using determined $f_{cm}(t)$ and plotted along with the " $f_{ck}(\text{experiment})$ " which represents the cylinder compressive strength obtained from measuring in the lab. In figure 4.2, for RAMAC C33/43, both the lines align with each other quite closely. The ratio to observe the difference in both can be seen in table 4.2. However, at 5 and 56 days, the ratio between measured and estimated values come less than 1. This decrease of ratio is also seen at 3, 14, 28 and 56 days in RAMAC C28/35-2.

RAMAC C33/43				RAMAC C28/35-2		
Age (days)	f_{ck} (Mpa) (from experiment)	$f_{ck}(t)$ (MPa) (calculated using EC)	Measured-calculated ratio	f_{ck} (Mpa) (from experiment)	$f_{ck}(t)$ (MPa) (calculated using EC)	Measured-calculated ratio
1	12.53	9.38	1.34	1.39	7.26	0.19
3	20.43	19.18	1.06	15.60	15.87	0.98
7	22.88	23.20	0.99	20.00	19.39	1.03
14	31.12	29.74	1.05	21.97	25.14	0.87
28	33.00	33.00	1.00	28.00	28.00	1.00
56	34.77	35.47	0.98	28.08	30.17	0.93
91	36.83	36.82	1.00	32.59	31.35	1.04

Table 4.2: EC calculated vs measured (experimental) compressive strength over time for both RAMAC C33/43 and RAMAC C28/35-2

In the classification of "s" value, for class S, cement is of strength class CEM 32,5N. Here, one of the concrete mixes has the same strength (RAMAC C33/43). Then, the estimation was calculated taking "s" values as 0.25 (Class N) and 0.38 (Class S) as well for one mix to check and compare the variation. Values 0.25 and 0.38 has cement strength classes 32,5R and 32,5N respectively.

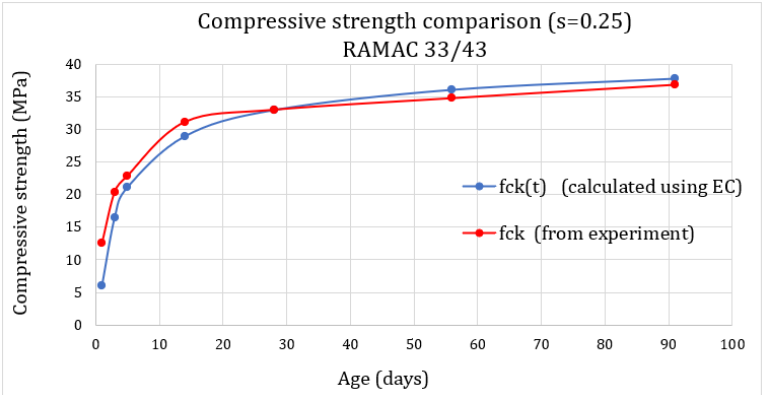


Figure 4.4: Strength development over time for RAMAC C33/43 taking "s"=0.25 (Eurocode 2 estimation vs measured)

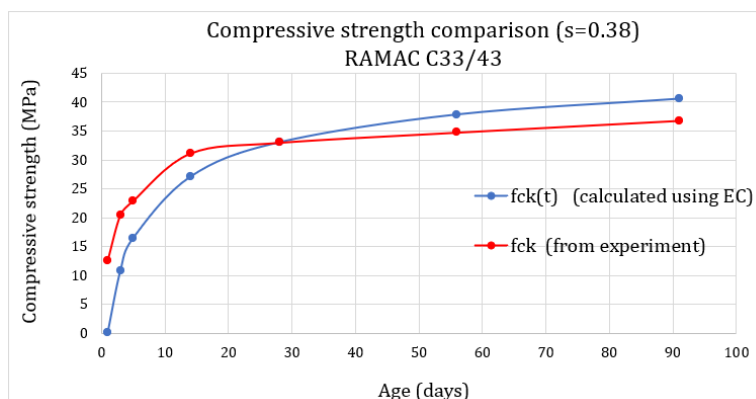


Figure 4.5: Strength development over time for RAMAC C33/43 taking "s"=0.38 (Eurocode 2 estimation vs measured)

Comparing all three (graphs) figures 4.2, 4.4 and 4.5 for RAMAC C33/43 with different values of "s", it is observed that the closest values between measured and estimated are obtained when $s = 0.20$ is taken which was initially assumed. So, the classification of factor "s" given in EC2 seems to be fine for the concrete mix RAMAC C33/43 as well given that the hardening of concrete observed is rapid. To check the accuracy of other "s" values given, samples of concrete with varying nature of hardening can be taken to estimate and further compared. Similarly, looking at the strength development of RAMAC C28/35-2, it can be observed that there is a significant difference in the strength development estimated vs measured. most of the measured strengths being less than the estimated ones. The non uniformity in this measured curve of RAMAC C28/35-2 could be due to the composition of concrete.

Additionally, from all these observations, it is can be inferred that the expression used to estimate mean compressive strength development in normal concrete cannot be entirely relied on for estimating that for GPC mainly looking at the measured-calculated ratio of RAMAC C28/35-2.

However, this can be said only for the geopolymer concrete mix used in this project and not for other mixes. Geopolymer concrete can vary in mix proportions. Compressive strength of concrete depends on factors like type of alkaline activator, curing conditions, aggregate binder ratio, etc [8]. Thus, a general conclusion for all GPC concrete cannot be given in this regard about Eurocode expression not being applicable for calculating strength over time.

4.1.2. SPLIT TENSILE STRENGTH

Table 4.3 below shows the values of splitting tensile strength that were measured in lab over time (1, 3, 5, 14, 28, 56, 91 days). 3 cubes were tested per mix at a time and the average of that 3 has been taken as the mean splitting tensile strength.

Splitting tensile strength (MPa)						
Age (Days)	RAMAC 28/35-2			RAMAC 33/43		
	Measured (N/mm ²)	Mean	Standard deviation	Measured (N/mm ²)	Mean	Standard deviation
1	1.46	1.06	0.35	2.31	2.72	0.58
	0.78			3.39		
	0.93			2.47		
3	2.67	2.91	0.22	2.66	2.67	0.32
	2.93			2.35		
	3.12			2.99		
5	4.16	4.06	0.17	4.16	3.68	0.45
	3.85			3.62		
	4.16			3.25		
14	3.75	3.68	0.21	4.47	4.48	0.35
	3.44			4.16		
	3.85			4.81		
28	3.61	4.22	0.53	4.24	3.91	0.29
	4.45			3.82		
	4.59			3.68		
56	4.02	3.98	0.06	3.43	3.44	0.01
	4.02			3.45		
	3.9			-		
91	4.19	4.22	0.13	4.61	5.07	0.40
	4.1			5.23		
	4.36			5.38		

Table 4.3: Overview of measure Splitting tensile strength according to age (Tests done in Jansen and Sqape laboratory)

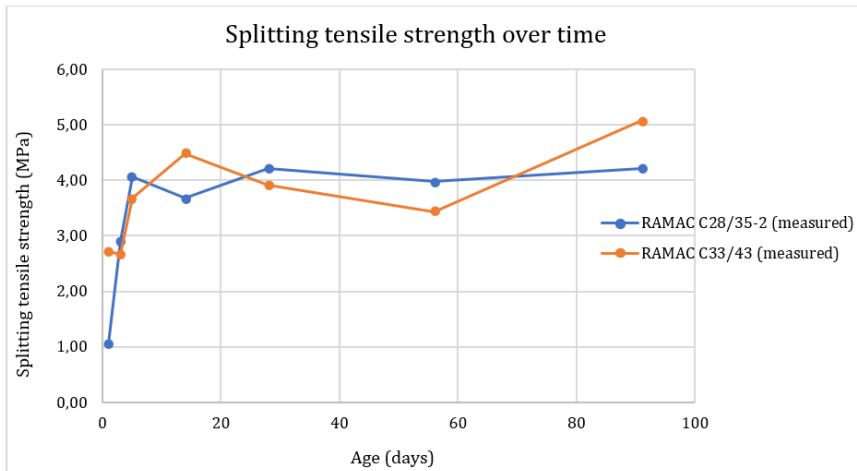


Figure 4.6: Development of split tensile strength with time

In the figure 4.6, the development of splitting tensile strength can be studied. It is clear that the development is not quite uniform throughout. For RAMAC C28/35-2, there is a drop in strength after 5 days till 14 days and then a rise and again a slight decrease giving an average split tensile strength value of 4.22 MPa at 91 days which is the same as 28 days. In case of RAMAC C33/43, a continuous decrease can be seen after 14 days till 56 days and then a rise eventually resulting an average split tensile strength value of 5.07 MPa at 91 days.

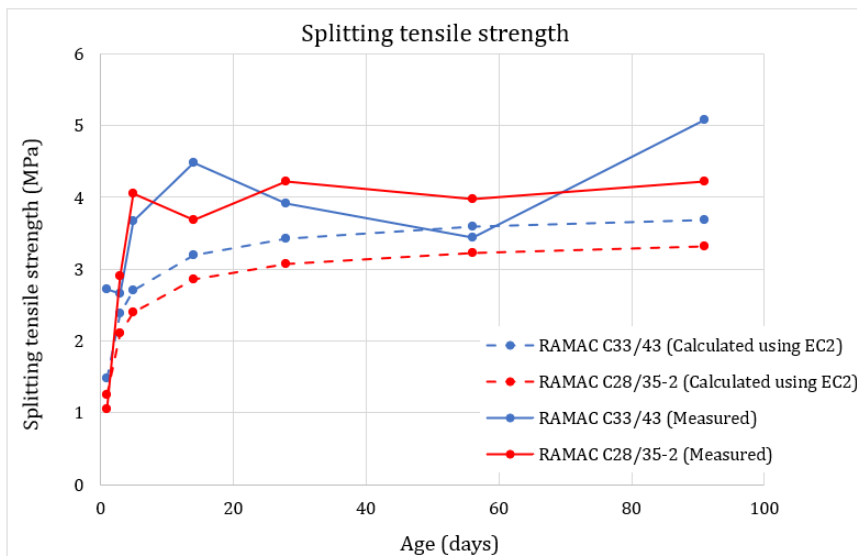


Figure 4.7: Comparison of split tensile strength over time (Calculated from cylinder compressive strength vs average split tensile strength measured in the lab)

Figure 4.7 shows a comparison of between split tensile strength over time calculated vs measured in lab for both the mixes. In the graph, "calculated using compressive strength" refers to the split tensile strength valued determined using the expression:

$$f_{ctm} = 0.3 * f_{ck}^{2/3}$$

where f_{ck} is the measured cylinder compressive strength and further using the relation:

$$f_{ct} = 0.9 * f_{ct,sp} \text{ to get the split tensile strength, } f_{ct,sp}.$$

It is then plotted to compare with the measured average split tensile strength of the mixes.

It can be seen in figure 4.7 that for RAMAC C28/35-2, the measured curve is higher than the one drawn calculating with measured f_{ck} using EC expression. For RAMAC C33/43, the curve drawn using measured values shows non uniform strength development at 56 days, the split tensile strength is lower than the calculated one.

RAMAC C33/43				RAMAC C28/35-2		
Age (days)	$f_{ct,sp}$ (Mpa) (measured)	$f_{ct,sp}$ (MPa) (calculated from f_{ck})	Measured-calculated ratio	$f_{ct,sp}$ (Mpa) (measured)	$f_{ct,sp}$ (MPa) (calculated from f_{ck})	Measured-calculated ratio
1	2.72	1.48	1.84	1.06	1.25	0.85
3	2.67	2.39	1.12	2.91	2.10	1.38
7	3.68	2.71	1.36	4.06	2.41	1.69
14	4.48	3.20	1.40	3.68	2.86	1.29
28	3.91	3.43	1.14	4.22	3.07	1.37
56	3.44	3.60	0.96	3.98	3.23	1.23
91	5.07	3.69	1.38	4.22	3.31	1.27

Table 4.4: calculated vs measured split tensile strength over time for both RAMAC C33/43 and RAMAC C28/35-2

Table 4.4 is the tabular representation of figure 4.7. For both the mixes all the values of measured-calculated ratio can be seen more than 1 except for RAMAC C33/43 at 56 days.

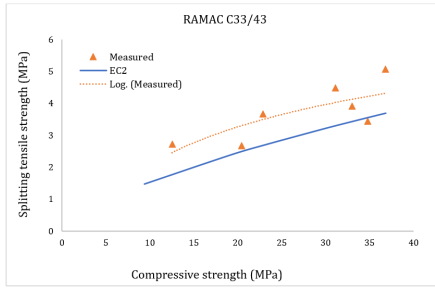


Figure 4.8: Ratio between splitting tensile strength and compressive strength (RAMAC C33/43)

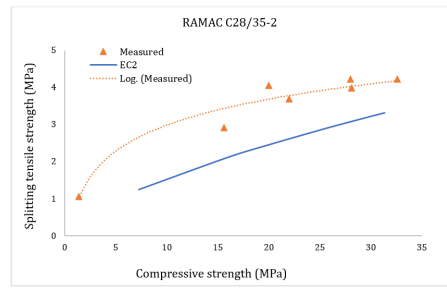


Figure 4.9: Ratio between splitting tensile strength and compressive strength (RAMAC C28/35-2)

Furthermore, the ratio between splitting tensile strength and compressive strength of these concrete mixes were compared with EC2 shown in figures 4.8 and 4.9. The 'measured' values shown in the graph refers to the observed splitting tensile strength and compressive strength during the test. 'EC2' refers to the calculated values of compressive strength and tensile strength using Eurocode 2 expressions for these. The calculated results has been presented in the appendix section A.2.3.

It can be seen that the ratio between between splitting tensile strength and compressive strength of both the mixes doesn't show a consistent trend. However, almost all of them have higher ratio that the one given by EC2. For RAMAC 33/43, the results are spread more than that of RAMAC C28/35-2.

While majority results can be observed to be higher than the EC2 line, the inconsistent trend of results does not give a clear indication of the overall idea of the relationship between splitting tensile strength and compressive strength of these concrete mixes.

4.2. BEAM RESULTS

This section comprises of all the obtained results done in Stevin Laboratory for analysing bending/shear/cracks. For comparison, predictions were made prior the experiment using Eurocode models. These predictive models for shear, bending and cracks all were done with following approaches and the results are used accordingly where needed:

1. **Using all mean values (to get the results closer to experimental values making it more comparable)**
2. **Using all design values (to compare and check the applicability of Eurocode)**

4.2.1. CRACK PATTERNS VISUALISATION & FAILURE MODES:

Table 4.5 showing groups of beams with observed respective failure modes according to shear span ratio and amount of tensile reinforcement is presented below.

Beams	Strength class	Effective depth, d (mm)	span to depth ratio [a/d]	Tensile reinforcement ratio [ρ (%)]	First cracking Load (kN)	Yielding Load (kN)	Maximum Failure Load (kN)	Observed Failure Modes*
1	C28/35	170	3.53	1.84	30	221.4	240.4	F
2		170	3.53	1.84	20	217.4	231.7	F
3		170	3.53	1.84	25	220.1	241.7	F
4		316	3.01	0.42	50	126.1	160	F
5		316	3.01	0.42	52	140.9	164.1	F
6		316	3.01	0.42	50	137.6	165.5	F
7	C33/43	314	3.03	1	50	188.9	234.3	SC
8		314	3.03	1	50	204.3	255.1	SC
9		314	3.03	1	40	183.4	232.8	SC
10		314	2.39	1	60	256.7	334.8	FS
11		314	2.72	1	50	217.5	270	FS
12		314	3.03	1	60	172.5	206.5	SC
13	C28/35	170	3.53	1.84	25	220.7	244	F
14		170	3.53	1.84	25	224.2	247.6	F
15		170	3.53	1.84	20	232.7	252	F
16		316	2.69	0.42	65	139.3	176.7	F
17		316	2.69	0.42	60	142.2	186.8	F
18		316	2.69	0.42	50	138.1	190.3	F
19	C33/43	314	3.50	1	60	-	195.3	SC
20		314	3.50	1	50	164.5	184.9	SC
21		314	3.50	1	40	-	178.1	SC
22		316	3.01	0.42	35	124.8	175.2	FS
23		316	3.01	0.42	35	120.8	148.02	FS
24		316	3.01	0.42	40	121.8	172.52	FS

*F = Flexure; SC = Shear Compression; FS = Flexure shear

Table 4.5: General overview of results of all the beams showing the loads at different stages and respective failure modes

Table 4.5 gives a general overview of all the beams distinguished according to different parameters with the resulting cracking load, yielding load and ultimate load observed from the experiment. First cracking load refers to the load that was noted during the experiment when first crack was seen. Yielding load was taken as the approximate value observing from the load-deflection graph and maximum failure load refers to the ultimate load before the beams failed; this data was recorded in the testing machine. These values can be seen in load deflection diagrams too. For beam 19 and 21, the yielding of reinforcement could not be observed in the load-deflection diagram. This could be an indication that the beam failed before yielding of reinforcement with a brittle failure.

The judgement of failure modes shown in the last column of table 4.5 for these beams were made using experimental observation, the resulting crack and deflection and from the literature study (elaboration in section 2.2.1) about failure modes in normal reinforced cement concrete beams. An overview of failed beams and respective load deflection curve for few groups of beam are shown as follows.

Here, the crack development of one beam per group is shown since each group has the same properties and loading conditions and respective failure type. However, remaining pictures of all other beams not shown here are attached in the appendix A.7.

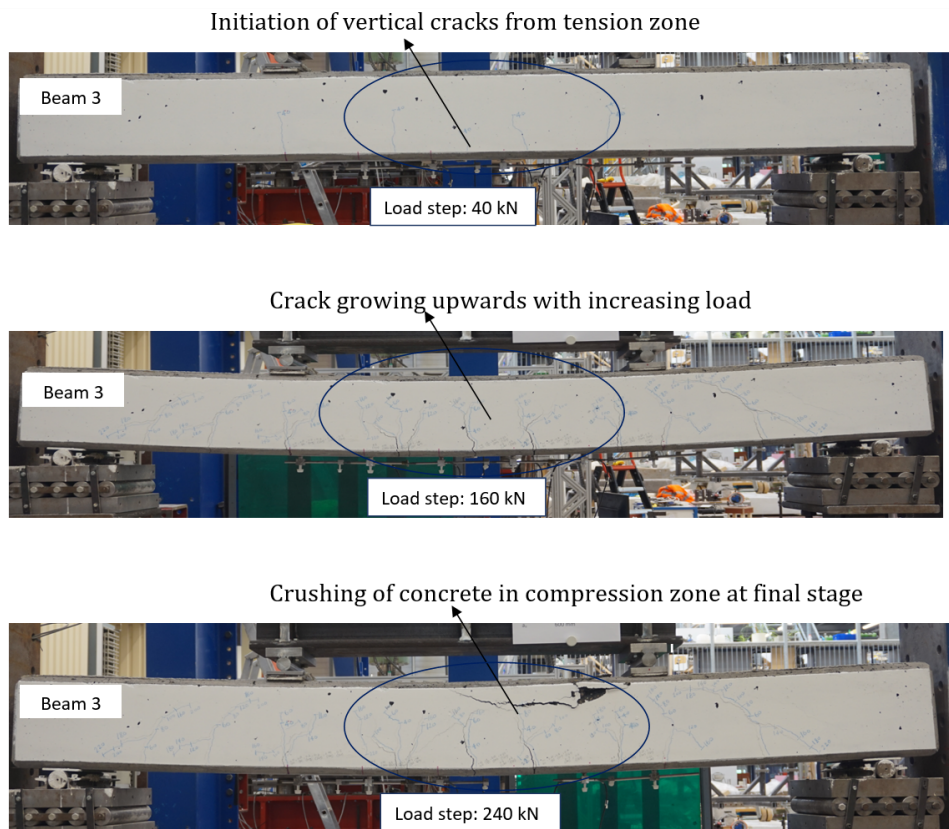


Figure 4.10: Crack propagation in beam 3

Figure 4.10 above shows how the cracks initiate as vertical flexure crack around mid section in the early stages. They slowly extends upwards resulting in crushing of concrete in the final stage for beam 3 which can be seen in the last picture of 4.10. The failure observed was ductile. The failure crack can be seen in precisely around the midspan at compression zone.

In figure 4.11, as shown, the first crack appeared at 25 kN force (noted during the experiment). This observation was made and noted during the experiment. Yielding of reinforcement can be noticed at 220 kN after which the concrete compressive zone crushed resulting in failure at 240 kN. This can also be seen in figure 4.10.

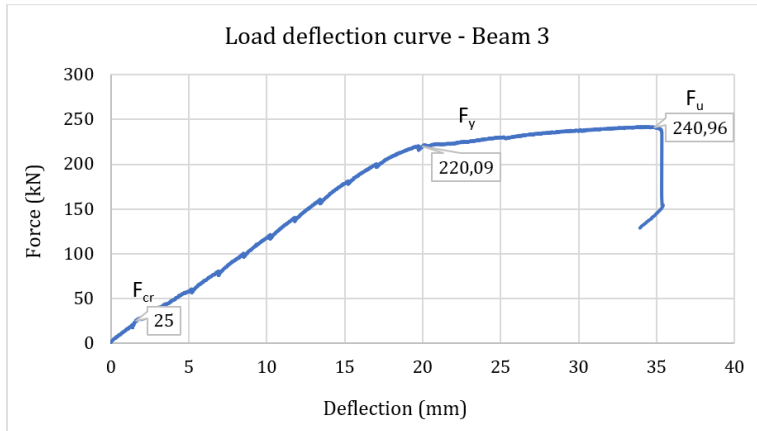


Figure 4.11: Load deflection curves of beam 3 showing the cracking (F_{cr}), yielding (F_y) and ultimate load (F_u)

Similar failure pattern was seen in beams 1, 2, 13, 14, 15 as well which can be clearly seen in the load-deflection diagram below 4.12 and the pictures of respective beams with respective loads at different steps are attached in appendix A.4 and A.7.

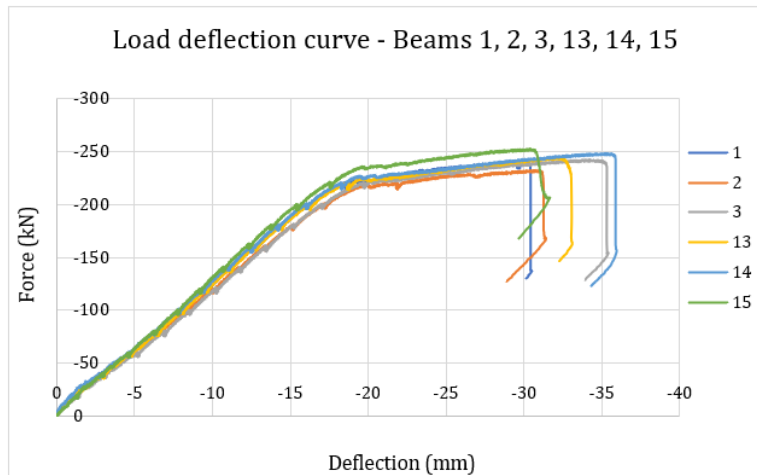


Figure 4.12: Load deflection curves of beam group 1-2-3-13-14-15

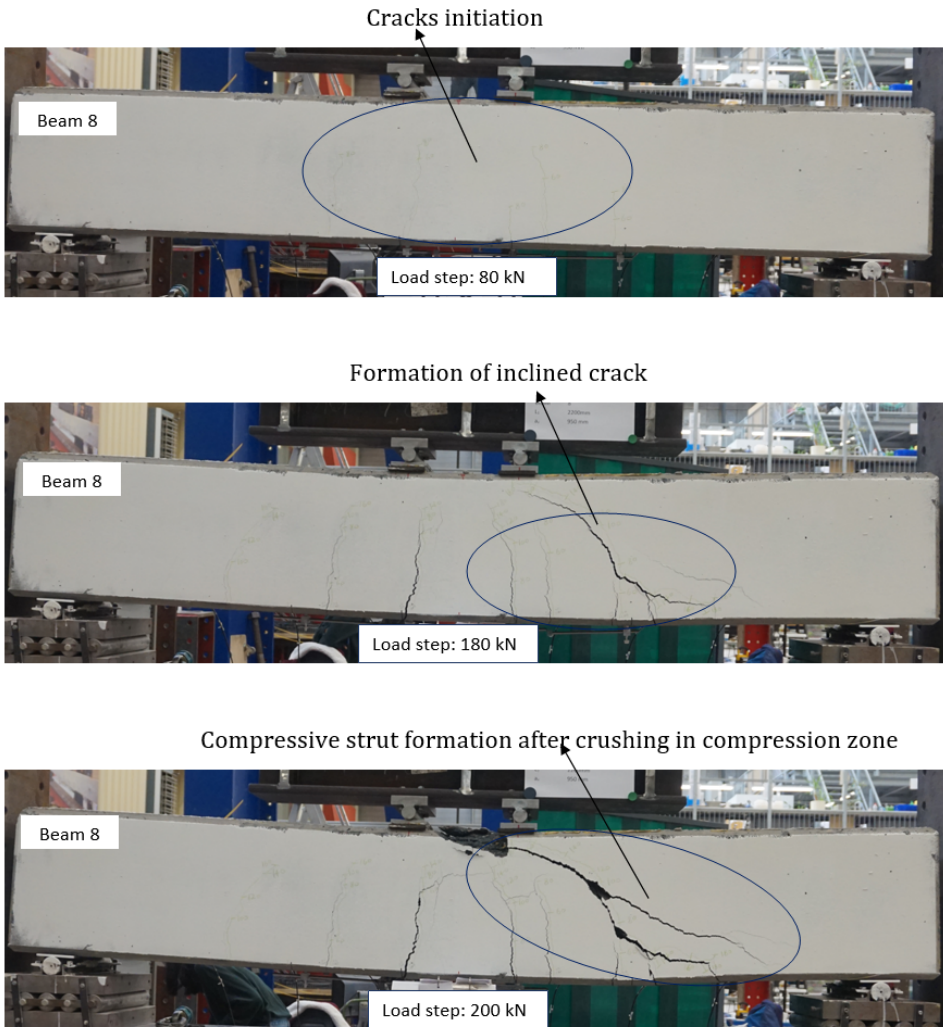


Figure 4.13: Crack propagation in beam 8

From figure 4.13, it can be observed that the cracks started from bottom as flexure cracks concentrated at center portion of the beam, gradually spreading towards the supports. The first crack started at 50 kN (figure 4.14). Formation of diagonal crack can be seen in further stages. The governing crack here is the same diagonal/shear crack which further gives rise to formation of a compressive strut after crushing of concrete in compression zone (third figure). The failure is brittle and can be pronounced as **shear compression failure** mode as discussed in the literature 2.2.1. In the ultimate stage, concrete spalling could be seen at the compression zone (figure 4.13). The failure crack can be seen under the point load within part the of beam without shear reinforcement

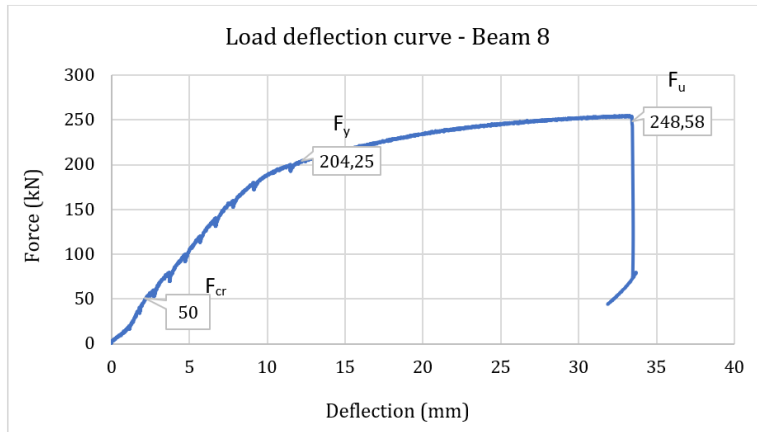


Figure 4.14: Load deflection curves of beam 8 showing the cracking (F_{cr}), yielding (F_y) and ultimate load (F_u)

Figure 4.14 shows the load deflection curve for beam 8 where it can be seen that the first crack was seen at 50 kN (noted during the experiment), yielding of reinforcement at 204.25 kN (approximate value taken from the graph) and finally failure at 248 kN. Beams 7, 9 showed a similar failure pattern as well. The load deflection diagrams of these beams can be seen in figure below. The loads at different of loading along with pictures for these beams can be found in A.4 and A.7.

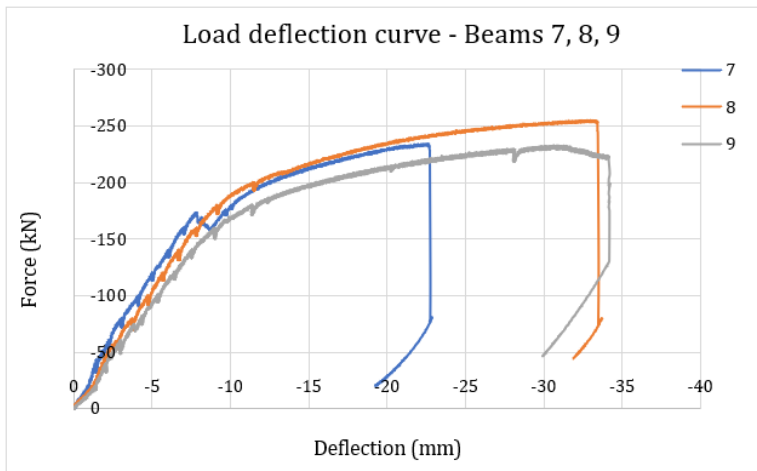


Figure 4.15: Load deflection curves of beam group 7-8-9

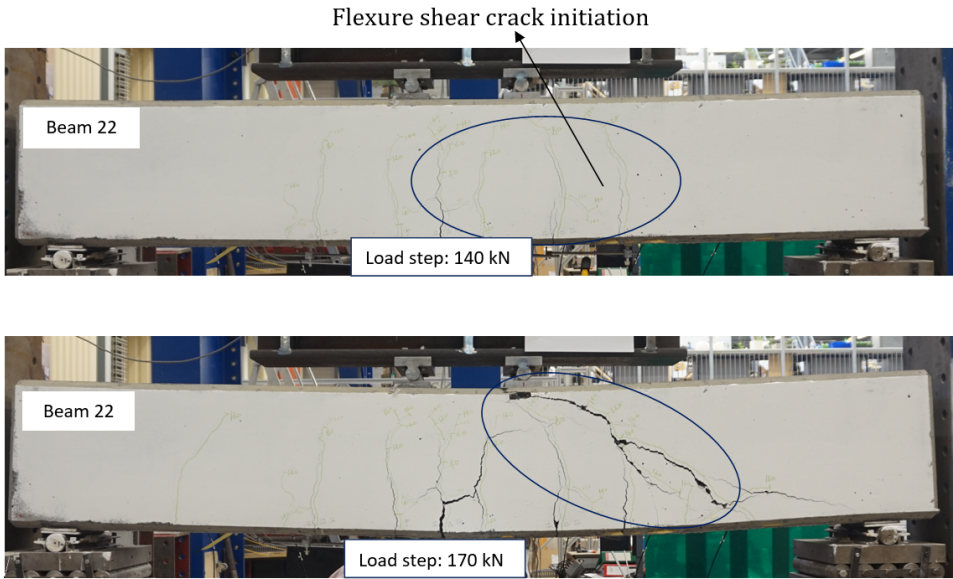


Figure 4.16: Crack propagation in beam 22

Similarly, in figure 4.16, failure type seen in beams 22 can be categorised under **flexure shear failure** as it grows from flexure shear cracks developing a critical inclined shear crack as a governing one. The failure was observed to be brittle. In early stages, the cracks started at 23 kN and which followed by formation of flexure-shear cracks near the supports. These cracks grew towards compression zone causing that flexure crack to become a critical inclined crack at ultimate loading (174 kN). The failure crack was seen under the point load within part of the beam without shear reinforcement.

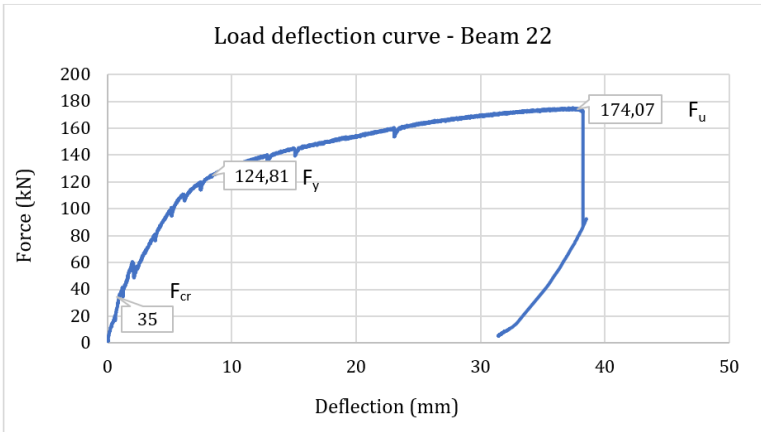


Figure 4.17: Load deflection curves of beam 22 showing the cracking (F_{cr}), yielding (F_y) and ultimate load (F_u)

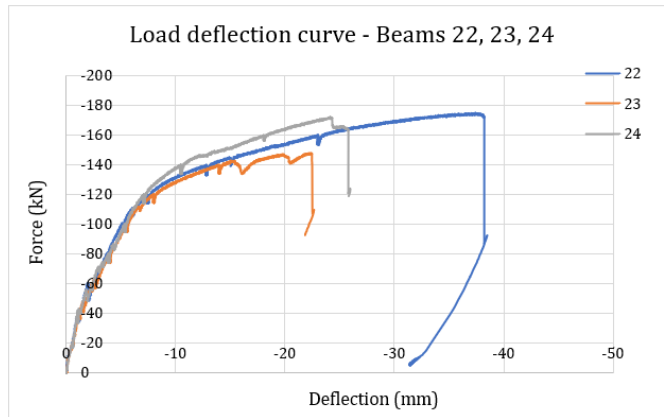


Figure 4.18: Load deflection curves of beams 22, 23, 24

Few obtained experimental results were further compared with few data obtained from past experiments for normal cement concrete of similar range parameters taken from shear database [4]. The closest possible values were taken to observe their failure modes and compare with similar GPC beams used in this research.

Beams (Geopolymer concrete)	f'_c (MPa)	a/d	d (mm)	ρ (%)	Failure mode observed
7	34.3	3.03	314	1	SC
8	34.4	3.03	314	1	SC
9	34.4	3.03	314	1	SC
22	35.2	3.01	316	0.42	FS
23	35.2	3.01	316	0.42	FS
24	35.3	3.01	316	0.42	FS
From database*					
(Normal cement concrete)					
Tariq & Newhook	34.1	3.54	325	1.54	S
	34.1	3.54	325	1.54	S
Sherwood et. al	37.5	3.38	307	0.93	S
	37.1	3.38	307	0.93	S

f'_c = concrete cylinder strength at the date of testing

a/d = shear span to depth ratio

d = effective depth

ρ = tensile reinforcement percentage

"S" = shear (which includes diagonal-tension, shear-compression, "shear proper" flexure-shear etc.)

"SC" = shear-compression

"FS" = Flexure-shear

Table 4.6: failure mode comparison with some past research database ([4])

For beams taken in table 4.6, the compressive strength at the day of testing are quite close in range. For all the samples taken, for both the normal concrete beam group and geopolymer concrete beam group, it shows a shear failure. However, some variation can be seen in values of a/d ratio and reinforcement percentage. But if beam group 7, 8, 9 is compared with Sherwood et al. samples, it is quite comparable and both the beam group show a shear failure.

This, however, is just a small number of data found within the range of tested beams.

The predictions about failure modes made before the experiment calculating the bending and shear capacity and checking the governing one, all the GPC beams tested complied with the predicted failure modes. Considering the comparison between past research and the experiments and the similarity of failure modes in predictions and outcome, it can be said that reinforced GPC beams behave the same way as reinforced OPC concrete beams in regard to the failure mode.

4.2.2. SHEAR CAPACITY

12 of the beams (the part of the bridge they would be used for did fulfil the requirement of having enough resistance without shear reinforcement) without shear reinforcement were designed to fail in shear to check the shear capacity and study this behaviour for GPC. Mostly those beams results will be used to analyse this section. The predicted values in table 4.7 were calculated using mean values. Values used and calculations are attached in appendix A.2.5

Mean values here refers to f_{cm} , f_{ym} , $C_{Rm,c}$ which was used instead of design values (f_{cd} , f_{yd} , $C_{Rd,c}$) in the formulae used assuming that the experimental results would be more comparable to the predicted results (Eurocode being more conservative with design values).

The model given by Eurocode 2 for calculating shear resistance without shear reinforcement is given as,

$$V_{Rd,c} = [C_{Rd,c}k(100\rho_l f_{ck})^{1/3} + k_1\sigma_{cp}]b_w d > (v_{min} + k_1\sigma_{cp})b_w d$$

In this model, σ_{cp} is stress due to axial loading/prestressing and is not taken here for calculations because although the bridge was prestressed, beams casted for testing were not and thus this component of prestressing was not taken into account.

Table 4.7 shows a comparison between predictive and experimental ultimate shear capacity for beams failed in shear. Results are shown in groups of beams with similar properties. The beam groups vary according to distance between load and support and reinforcement in tensile zone. The first experiment was done for beam 10 followed by 11 and 12 to identify the load transfer from load to support and to decide the distance between load and support for other beams.

Beam	$f_{ck}(t)$ (MPa)	Distance between load and support 'a' (mm)	a/d	Tensile reinforcement ρ (%)	Shear resistance, $V_{Rm,c}$ (kN)		Test to prediction ratio
					Predicted	Experimental	
7	42.3	950	3.03	3.38	88.61	117.18	1.34
8	42.4	950	3.03	3.38	88.61	127.57	1.46
9	42.4	950	3.03	3.38	88.61	116.39	1.33
10	42.2	750	2.39	3.38	88.47	167.44	1.91
11	42.3	850	2.71	3.38	88.54	135.00	1.54
12	42.3	950	3.03	3.38	88.54	103.29	1.18
22	43.2	950	3.01	1.28	67.31	87.63	1.32
23	43.2	950	3.01	1.28	67.31	74.01	1.12
24	43.3	950	3.01	1.28	67.37	86.26	1.30

*Beams 22, 23, 24 have the same cross section as beams 7, 8, 9 but during the experiment were inverted upside down decreasing the tensile reinforcement

Table 4.7: Summary of results of beams failed in shear (Predicted and Experimental)

Shear resistance in table 4.7 was calculated using compressive strength for that particular date the experiment was carried out. The dates and respective compressive strength approximated from the measured strengths has been shown in appendix A.1.

It can clearly be seen in table 4.7 that for all the beams failed in shear, the test prediction ratios for ultimate shear force are greater than 1 giving an indication that it would be fine to calculate shear resistance using EC models for Geopolymer concrete. However, a statistical evaluation needs to be done to reach to a concrete conclusion to prove that it is safe. The predictive results obtained in the table above were calculated using mean values which are higher than the design values since partial safety factors are not included and still the experimental results are higher giving a positive mark about using EC2.

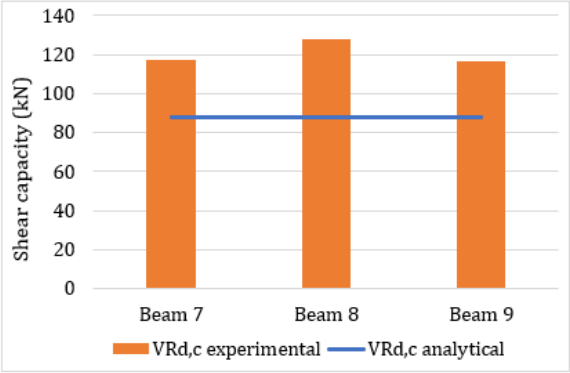


Figure 4.19: Shear capacity of Beam group 7, 8, 9 (experimental vs analytical)

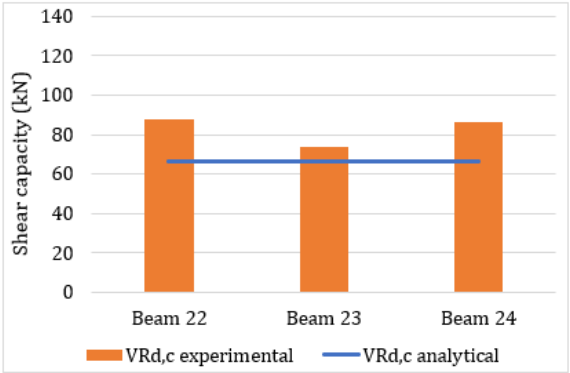


Figure 4.20: Shear capacity of Beam group 22, 23, 24 (experimental vs analytical)

Figures 4.19 and 4.20 show the comparison between analytical and experimental results for beam groups 7, 8, 9 and 22, 23, 24. Table 4.8 below shows a clear comparison between beams 7, 8, 9 and beams 22, 23, 24. The only difference between beam group 7, 8, 9 and 22, 23, 24 was that, beams 22, 23, 24 were reversed upside down which changed the number and diameter of reinforcement in the tensile region decreasing the overall amount of tensile reinforcement. Amount of decrease in shear resistance of concrete with decrease in reinforcement in tensile region can be seen.

Beams	7, 8, 9		22, 23, 24		Percentage decrease
Tensile reinforcement ρ (%)	3 \emptyset 20 mm		2 \emptyset 16 mm		
Area (A_{st})	942 mm ²		402.00 mm ²		57.32 %
$V_{Rd,c}$ (kN) [analytical]	175.25		132.30		24.50 %
$V_{Rd,c}$ (kN) [experimental]	234.36	240.76	175.25	165.26	31.36 %
	255.14		148.02		
	232.78		172.52		

Table 4.8: Comparison showing decrease in shear capacity due to decrease in reinforcement in tensile zone

There is a 24.5 % decrease in predicted shear capacity with 57.32 % decrease in reinforcement area which is expected because A_{st} (area of tensile reinforcement) in shear resistance design equation $V_{Rd,c}$ (6.2.a, EN-1992-1-1) takes into account the diameter and number of reinforcement. But a higher decrease (31.36%) in shear capacity can be seen from the experimental results (i.e, for GPC).

However, overall capacity is still greater than the calculated capacity which is a positive sign.

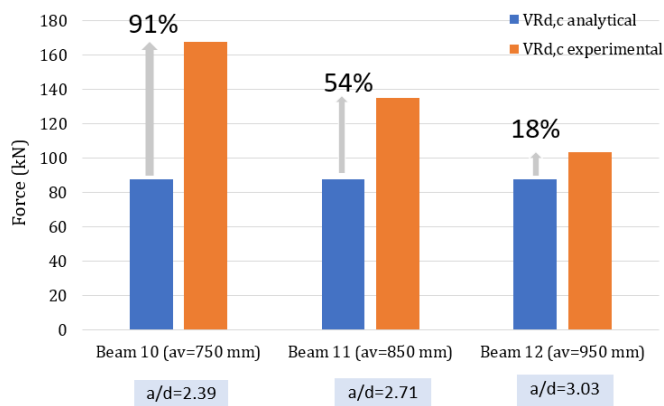


Figure 4.21: Shear resistance comparison (Experimental vs analytical) according to shear-span ratio

The bar chart above (figure 4.21) helps to understand the influence of span-depth ratio. The shear resistance of 3 other beams (10,11,12) which are similar to previously compared beams (7,8,9) but the a/d ratio are different. A distinct effect of a/d ratio can be noticed by the trend of decrease in shear capacity with increase in a/d ratio. Looking at the results of $V_{Rd,analytical}$ which is same for all the three beams gives an additional indication that shear resistance doesn't directly take into account the a/d ratio in the shear model (EC 6.2.a) as discussed earlier about factors influencing in section 2.2.3. This is still a matter of discussion in Eurocode for concrete structures. However, it can be said that clearly there is an influence of a/d ratio for shear capacity in GPC.

One of another important factors affecting the shear resistance is **compressive strength**. The formula to determine the shear resistance also takes strength factor (f_{ck})^{1/3}. The strength class of all the beams failed in shear was the same. So study the influence of this factor, beam groups 7, 8, 9 and 22, 23, 24 were considered taking the actual cylinder compressive strength at the day of testing which was approximated using measured compressive strengths for other days.

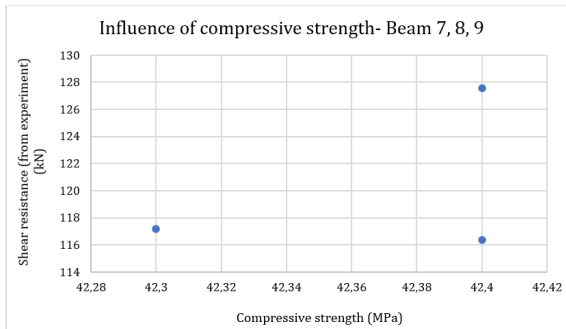


Figure 4.22: Influence of compressive strength on shear capacity- beams 7, 8, 9

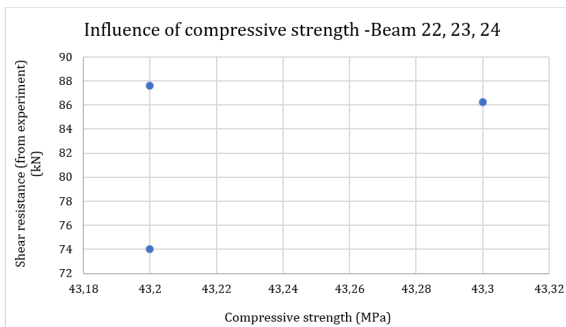


Figure 4.23: Influence of compressive strength on shear capacity- beams 22, 23, 24

Figures 4.22 and figure 4.23 shows the effect of compressive strength on shear capacity. For beam 7, 8, 9, there is an increase in shear capacity with increase in compressive strength for one beam but for another beam it slightly decreases. Looking at these figures, nothing concrete can be concluded because firstly, the compressive strength variation among these beams is very small and secondly, the compressive strength taken was approximated and it is not 100% accurate.

CHECKING THE ACCURACY OF EUROCODE FOR GPC:

Towards evaluating and supporting the predictive accuracy of shear model EC (eq. 6.2 a) given in the Eurocode for Geopolymer concrete, comparisons and analysis using calculations with actual design values (and not characteristic value) were done which includes safety factors as well. This was done to answer one of the research questions regarding how accurate would Eurocode be for GPC. Along with design values, the compressive strength was also taken as 28 days and not the one at actual day of testing.

The predictive calculations made in this whole section is done this way; using entirely as it is in the EC (using design values)

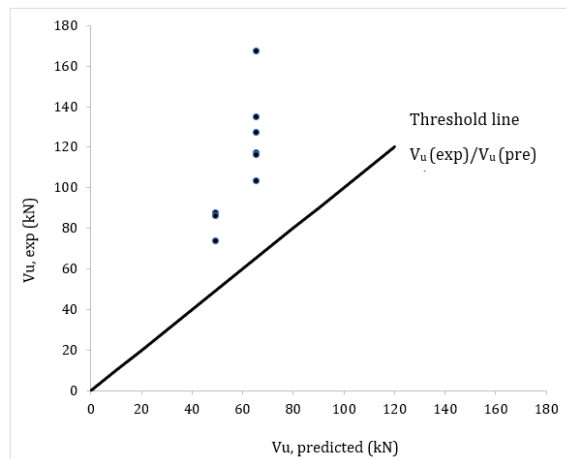


Figure 4.24: Graphical Comparison of prediction of EC2 with experimental results

The observations about test prediction ratios from these comparisons shown in figure 4.24 being more than 1 and also more than previously calculated test prediction ratios for the calculations made using mean values is pretty obvious because of the fact that design values in EC models make it more conservative.

Beams (Geopolymer concrete)	f'_c (MPa)	a/d	d (mm)	ρ (%)	Experimental Ultimate Shear force (kN)	Analytical Ultimate Shear force (EC2) (kN)	Test to prediction ratio (EC2)
7	34.3	3.03	314	1	117.18	65.21	1.80
8	34.4	3.03	314	1	127.57	65.21	1.96
9	34.4	3.03	314	1	116.39	65.21	1.79
22	35.2	3.01	316	0.42	87.63	49.23	1.78
23	35.2	3.01	316	0.42	74.01	49.23	1.50
24	35.3	3.01	316	0.42	86.26	49.23	1.75
From database* (Normal cement concrete)							
Tariq & Newhook	34.1	3.54	325	1.54	69.8	64.15	1.08
	34.1	3.54	325	1.54	70.5	64.15	1.09
Sherwood et. al	37.5	3.38	307	0.93	119.65	104.17	1.14
	37.1	3.38	307	0.93	125.1	105.21	1.18

Table 4.9: Comparison of ultimate shear force and test prediction ratios for GPC beams with that of normal cement concrete from past database [4]

Furthermore, some shear test data from past within the range of Geopolymer beams tested were taken to compare the ultimate shear force shown in table 4.9. All of these beams failed in shear. Taking the GPC beam group 7, 8, 9 and comparing it with Sherwood wide beams (normal cement concrete) which has similar parameters, the ultimate shear force is quite close. Additionally, the test results were compared to analytically calculated values using Eurocode 2. The test to prediction ratio can be seen less than the ones tested in this thesis for Geopolymer concrete using Eurocode 2. This clearly infers that EC2 is more conservative for GPC than normal cement concrete.

Behaviour of different parameters in shear resistance observed in experiment compared with EC2 calculations are shown as follows.

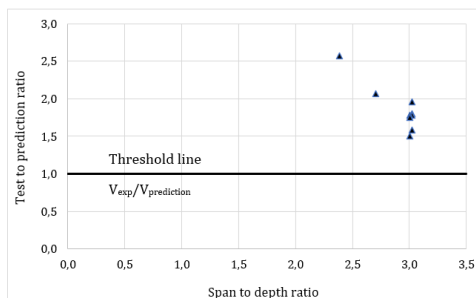


Figure 4.25: Influence of a/d on $\left(\frac{V_{exp}}{V_{pre}}\right)_{EC2}$

In figure 4.25, it can be seen that with a increase in span to depth ratio, the test to prediction ratio gradually decreases. From fig 4.21 and 4.25, it can be inferred that the shear resistance is underestimated this way for a lower a/d ratio if EC models are used to calculate the shear resistance and vice versa. However, due to lack of data for higher a/d ratio, the latter still remains to be discussed.

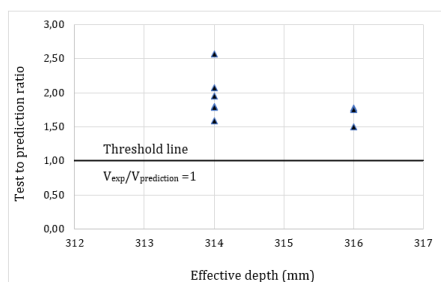


Figure 4.26: Influence of effective depth on $\left(\frac{V_{exp}}{V_{pre}}\right)_{EC2}$

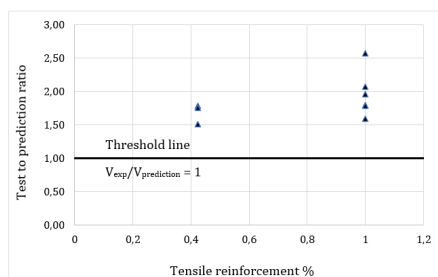


Figure 4.27: Influence of reinforcement on $\left(\frac{V_{exp}}{V_{pre}}\right)_{EC2}$

Similarly, the influence of effective depth and reinforcement ratio in shear resistance can be seen in figures 4.26 and 4.27. A decrease in test to prediction ratio can be seen with increase in effective depth of beam cross section. Secondly, higher test prediction ratio is observed with higher reinforcement ratio. This could indicate that EC underestimates the shear capacity for higher reinforcement ratio. However, it should be noted that out of these observations about influencing parameters, only the effect of a/d can be clearly pronounced. This is because within the beams tested and observed for effective depth and amount of reinforcement, other parameters vary too and not just those parameters alone.

4.2.3. BENDING CAPACITY

Out of the beams tested, 12 of them were designed to fail in flexure: 1, 2, 3, 4, 5, 6, 13, 14, 15, 16, 17, 18. These are the beams which had shear reinforcement throughout. Bending moment in table 4.10 was calculated using compressive strength for that particular date the experiment was carried out. The dates and respective compressive strength approximated from the measured strengths has been shown in appendix A.1.

Beams	$f_{ck}(t)$ (MPa)	Distance between load and support 'a' (mm)	a/d	Tensile reinforcement ρ (%)	Ultimate bending moment (kNm)		Test to prediction ratio
					$M_{u, analytical}$	$M_{u, experimental}$	
1	28.9	600	3.53	1.84	60.42	72.14	1.20
2	28.9	600			60.42	69.51	1.16
3	29	600			60.42	72.53	1.21
13	29.2	600			60.49	73.20	1.22
14	29.2	600			60.49	74.31	1.23
15	29.1	600			60.49	75.57	1.26
4	35.8	950	3.01	0.42	67.11	75.99	1.13
5	35.8	950			67.11	77.95	1.16
6	35.85	950			67.11	78.62	1.17
16	35.85	850	2.69	0.42	67.12	75.12	1.12
17	35.9	850			67.12	79.42	1.18
18	35.9	850			67.12	80.89	1.21

Table 4.10: Summary of results of beams failed in bending (Predicted and experimental)

Table 4.10 shows an overview of experimentally obtained ultimate moment along with analytically predicted ultimate moment for all the beams which failed in bending. The predicted values for ultimate bending moment presented in this table were calculated using mean values. Beams are categorised in groups depending on the variables the cross section dimensions, reinforcement ratios and concrete compressive strength. Although a/d ratio is varying too, it is not of importance in bending moment calculation as it is a cross section analysis. From the general overview of results, it can be seen that all the test results are more than that of the calculated ones. This can also be seen in bar charts presented below.

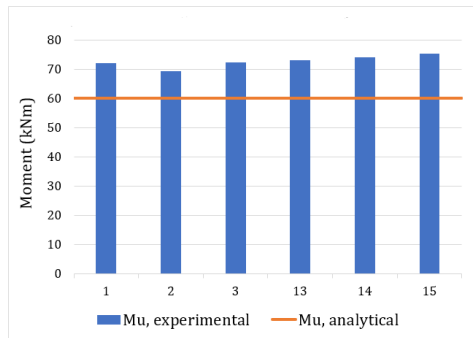


Figure 4.28: Ultimate moment - Experimental vs Analytical (beams 1, 2, 3, 13, 14, 15)

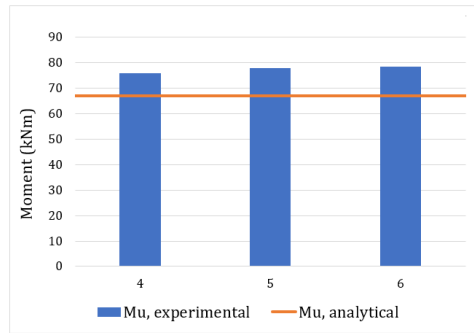


Figure 4.29: Ultimate moment comparison - Experimental vs Analytical (beams 4, 5, 6)

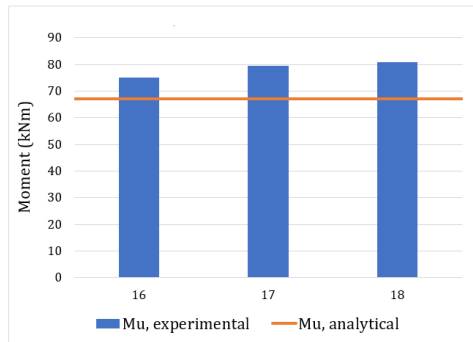


Figure 4.30: Ultimate moment comparison - Experimental vs Analytical (beams 16, 17, 18)

M-KAPPA DIAGRAMS:

In reinforced concrete beam, there are phases defined until it reaches failure as discussed in literature section 2.2.5. The experimental cracking moment (M_{cr}) in the experimentally obtained graph can be distinguished by observing an initial deviation of the linear slope in $M - \kappa$ diagram. Secondly, the experimental yielding moment (M_y), is when the curve starts deviating and showing a flat pattern. Lastly, the ultimate bending moment (M_u) is when the beams fails after reaching its ultimate load.

$M - \kappa$ diagrams according to beam groups are shown in figures below where these phases can be distinguished. The analytical calculation of $M - \kappa$ diagrams are attached in the appendix A.2.7 and all the experimental $M - \kappa$ for individual beams are attached in appendix A.5

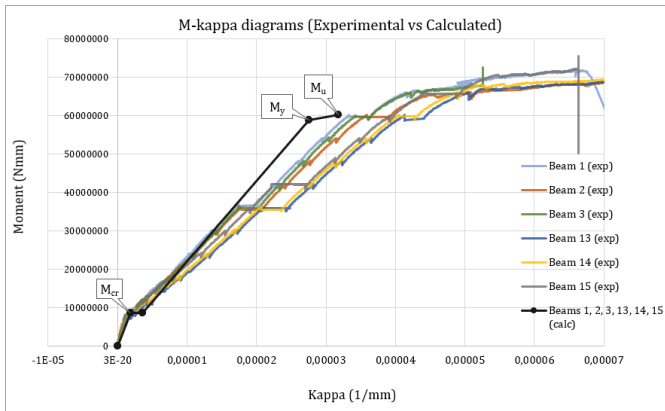


Figure 4.31: $M - \kappa$ diagram of beams 1, 2, 3, 13, 14, 15 (experimental vs calculated); distance between loads for these beams = 1000 mm

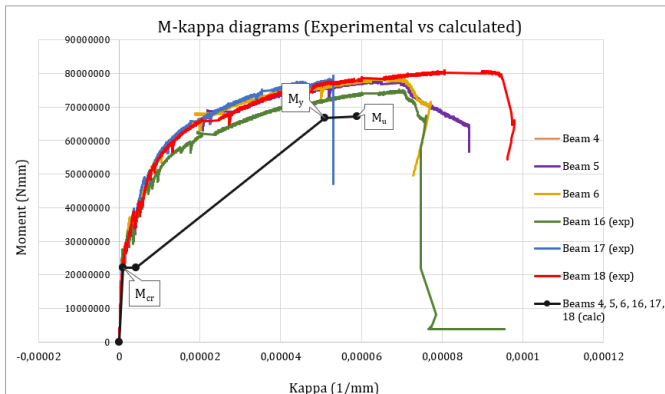


Figure 4.32: $M - \kappa$ diagram of beams 4, 5, 6, 16, 17, 18 (experimental vs calculated); distance between loads for beams 4, 5, 6 = 300 mm and for beams 16, 17, 18 = 500 mm

For beam group [1, 2, 3, 13, 14, 15], calculated vs obtained experimental doesn't show a large difference as beam group [4, 5, 6, 16, 17, 18]. The prediction for second group underestimates the moments after linear elastic phase. To evaluate kappa, experimental EI was calculated using four point deflection formula (appendix A.2.6). Following this approach, stiffness is assumed to be average throughout the beam while in reality the stiffness at the mid section (constant moment region or distance between the applied loads) is less than the stiffness near the end supports. This leads to higher experimental curvature for the given moment.

Beams	$M_{cr, exp}$ (kN-m)	$M_{cr, calculated}$ (kN-m)	$M_{y, exp}$ (kN-m)	$M_{y, calculated}$ (kN-m)	M_u, exp (kN-m)	$M_u, calculated$ (kN-m)
1	7.81	9.5	66.3	58.7	71.4	60.1
2	6.42	9.5	65.3	58.7	68.8	60.1
3	8.02	9.5	65.8	58.7	67.8	60.1
13	7.2	9.5	65.0	58.7	72.9	60.1
14	8.1	9.5	65.2	58.7	71.7	60.1
15	7.9	9.5	65.7	58.7	71.9	60.1
4	-	-	-	-	-	-
5	25.5	24.1	67.5	66.7	77.1	67.1
6	25.5	24.1	68.8	66.7	77.3	67.1
16	24.6	24.1	63.3	66.7	74.5	67.1
17	24.3	24.1	65.4	66.7	78.4	67.1
18	20.1	24.1	72.9	66.7	79.4	67.1

*Beam 4 graphs and values came a bit different than expected because of LVDT defect. So not included to analyse.

Table 4.11: Summary of predicted and experimental results for each phases

Table 4.11 shows experimentally obtained and the calculated cracking moment, yielding moment and ultimate moment. The experimental values shown in the table were taken from the $M - \kappa$ diagrams drawn for each beam which can be found in appendix A.5. As mentioned in previous section, it should be noted that after cracking of concrete, the stiffness is not constant in the beam and thus the calculated values of M_y (exp) and M_u (exp) is not 100% accurate. Comparing both the results, it is clear that the predicted moment at yielding and ultimate moment are lower than that of obtained from the experiment. However, observing the comparison of cracking moment of beam group [1, 2, 3, 13, 14, 15] and beam 18, cracking seems to have started before the prediction.

Effect of different parameters:

The factors influencing moment capacity of concrete are compressive strength, reinforcement ratio, stiffness, cross section dimensions, stress-strain relation of concrete etc. Results in regard to these areas are presented below.

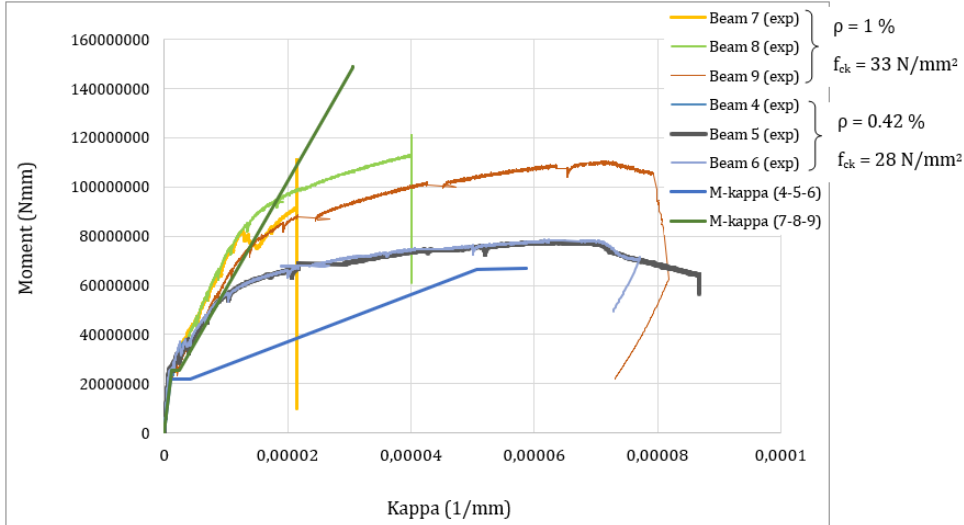


Figure 4.33: Flexure behaviour with varying compressive strength and reinforcement ratio

Graph 4.33 shows the experimental comparison of $M-\kappa$ between beam groups [4, 5, 6] and [7, 8, 9] which varies in compressive strength and the amount of tensile reinforcement. The cracking moment seems similar in both beam groups. To determine the cracking moment analytically, mean axial tensile strength is used which is dependent on compressive strength. But due to the similarity in cracking moment results in these two groups, it can be assumed that compressive strength doesn't have a major effect here. However, the yielding moment of beam group [4, 5, 6] is visibly lower than that of group [7, 8, 9]. This is possibly because reinforcement percentage is more in [7, 8, 9]. This shows that the reinforcement ratio has greater effect in bending than the compressive strength. The ultimate moment here cannot be compared as both beams had a different failure mode (Beam [7, 8, 9] failed in shear). In a normal reinforced cement concrete, before the occurrence of crack the tensile stress in concrete is taken by concrete tensile strength and in this phase, reinforcement does not have any role. The results suggest a similar behaviour for GPC in terms of dependency with compressive strength and the amount of reinforcement.

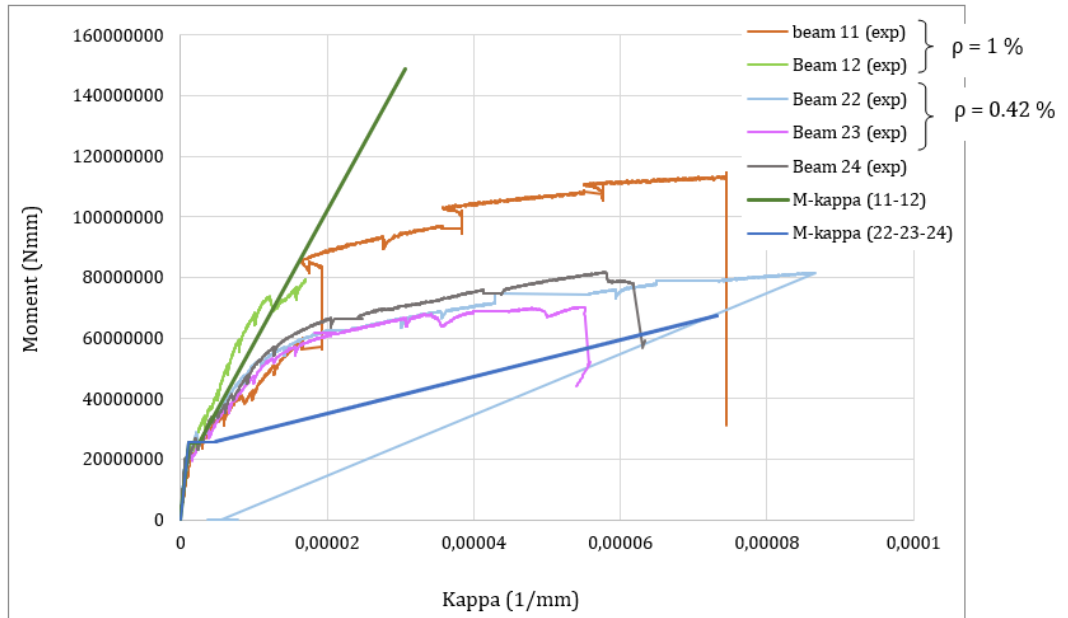


Figure 4.34: Behaviour with varying reinforcement ratio

Similarly, looking at figure 4.34, the effect of reinforcement ratio is realized as it is visibly clear, the difference in yielding moment between two groups [11, 12] and [22, 23, 24] which differs only by the amount of tensile reinforcement. To predict the yielding moment analytically, moment equilibrium is used and the force exerted by steel is dependent on the area of reinforcement. From this it can be said that the amount of reinforcement has an effect in bending.

CHECKING THE ACCURACY OF EUROCODE:

Towards evaluating and supporting the predictive accuracy of shear model EC (eq. 6.2 a) given in the Eurocode, comparisons and analysis using the calculations with actual design values (and not characteristic value) were done which includes safety factors as well. To prove the accuracy of certain model, sufficient number of tests should be carried out and here in this part, tested number (for shear) is 12.

Table 4.12 shows the comparison

Beams	a/d	Tensile reinforcement ρ (%)	Ultimate bending moment (kNm)		Test to prediction ratio
			$M_{u, analytical}$	$M_{u, experimental}$	
1	3.53	1.84	51.39	72.14	1.40
2			51.39	69.51	1.35
3			51.39	72.53	1.41
13			51.39	73.20	1.42
14			51.39	74.31	1.45
15			51.39	75.57	1.47
4	3.01	0.42	64.57	75.99	1.18
5			64.57	77.95	1.21
6			64.57	78.62	1.22
16	2.69	0.42	64.57	75.12	1.16
17			64.57	79.42	1.23
18			64.57	80.89	1.25

Mean = 1.31
Standard Deviation = 0.12
Coefficient of variation = 8.7 %

Table 4.12: Comparison between EC2 and calculated values

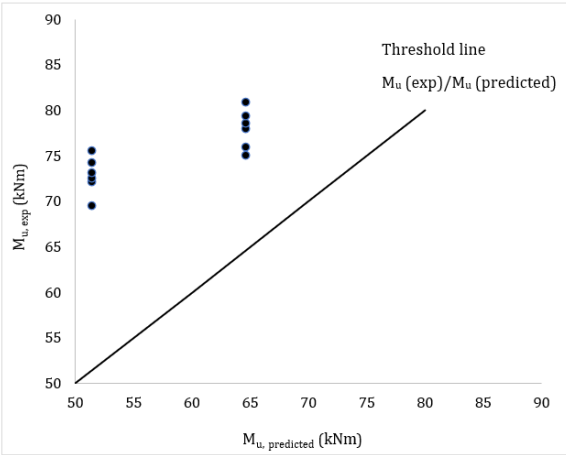
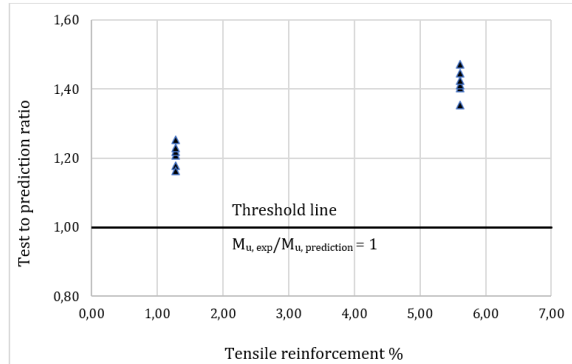


Figure 4.35: Comparison of prediction of EC2 with experimental results

From the table and graph above the experimental ultimate bending moment can be seen higher than that of calculated one. The mean of test to prediction ratios is 1.31 which clearly indicates that the analytically calculated ultimate capacities can be conservative to use for Geopolymer concrete.

Figure 4.36: Influence of amount of tensile reinforcement on $\left(\frac{M_{u,exp}}{M_{pre}}\right)_{EC2}$

It is observed in figure 4.36 that as the reinforcement in tension region increases, moment capacity increases as well. This effect has already been discussed earlier too. But looking at the figure above, it can be said that for a higher reinforcement value, analytically calculated values can be more conservative for calculating moment capacities for Geopolymer concrete.

4.2.4. CRACK BEHAVIOUR

CRACK SPACING

BEAM	Spacing between the cracks (mm)								Maximum measured Crack spacing (mm)	Maximum calculated crack spacing (mm)	Test to Prediction ratio
1	140.14	147.09	95.14	106.82	184.5	155.96	100.43	247.38	247.38	298.56	0.83
2	216.29	311.87	157.94	184.7	225.5				311.87	298.56	1.04
3	299.7	206.97	163.78	231.33	117.8				299.7	298.56	1.00
4	170.81	49.26	138.26						170.81	470.33	0.36
5	391.1								391.1	470.33	0.83
6	367.84	367.81							367.84	470.33	0.78
7	122.75	138.92	94.14						138.92	358.88	0.39
8	213.4	286.96	100.2						286.96	358.88	0.80
9	229.69	140.73							229.69	358.88	0.64
10	253.67	212.19	183.68	233.68					253.67	358.88	0.71
11	254.04	179.75							254.04	358.88	0.71
12	269.23	284.04							284.04	358.88	0.79
13	130.97	128.38	170.85	149.12	174.7	94.01	172.21	140.04	174.73	298.56	0.59
14	104.68	174.52	163.68	120.3	104.8	70.4	197.26	178.54	197.26	298.56	0.66
15	148.07	191.62	165.73	307.36	237.6				307.36	298.56	1.03
16	193.48	156.26	305.98						305.98	470.33	0.65
17	181.71	63.52	277.79						277.79	470.33	0.59
18	132.63	286.54	198.22	188.68					286.54	470.33	0.61
22	124.52	309.77							309.77	470.39	0.66
23	202.82	270.57							270.57	470.39	0.58
24	311.79								311.79	470.39	0.66

Table 4.13: Measured and calculated maximum crack spacing of all the beams

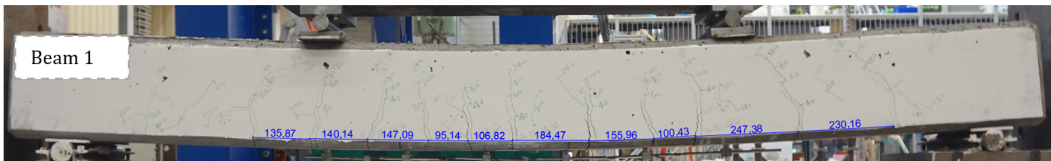


Figure 4.37: Crack spacing of beam 1 for reference

Table 4.13 shows the crack spacing values obtained from the experiment and the ones calculated for each beam. In each row, all the spacing measured are noted (like shown in fig 4.37) and the maximum of all the values are taken and then compared with the calculated maximum crack spacing using EC expression 7.11:

$$S_{r,max} = k_3 c + k_1 k_2 k_4 \phi / \rho_{p,eff}$$

Measured crack spacing refers to the ones obtained from the experiment and these measurement were done scaling the actual dimension of the beam to Autocad and measuring the spacing between the cracks of the beam after failure. Measured spacing for all the beams from experiment can be seen in appendix section A.6. The measured crack spacing however would not be 100% accurate because measuring in Autocad it was measured linearly and in reality there is a curvature while the beam bends.

Looking at the test prediction ratios, clearly, for almost all the beams, the (experimental) measured maximum spacing is less than that of the calculated one. From EC expression, crack width is directly proportional to maximum crack spacing. So, higher the crack spacing, larger will be the crack width. Here almost all the test-prediction ratios are less than 1. The actual crack spacing being less than the predicted ones is a positive mark towards using EC for calculating spacing for GPC as well. However, 3 of the beams had larger spacing than the predicted ones which still restricts from relying on EC entirely on this regard.

A clearer comparison chart of the same can be seen in the figure 4.38 as well. It can be seen that in almost all the beams, experimentally measured crack spacing is less than that of calculated ones.

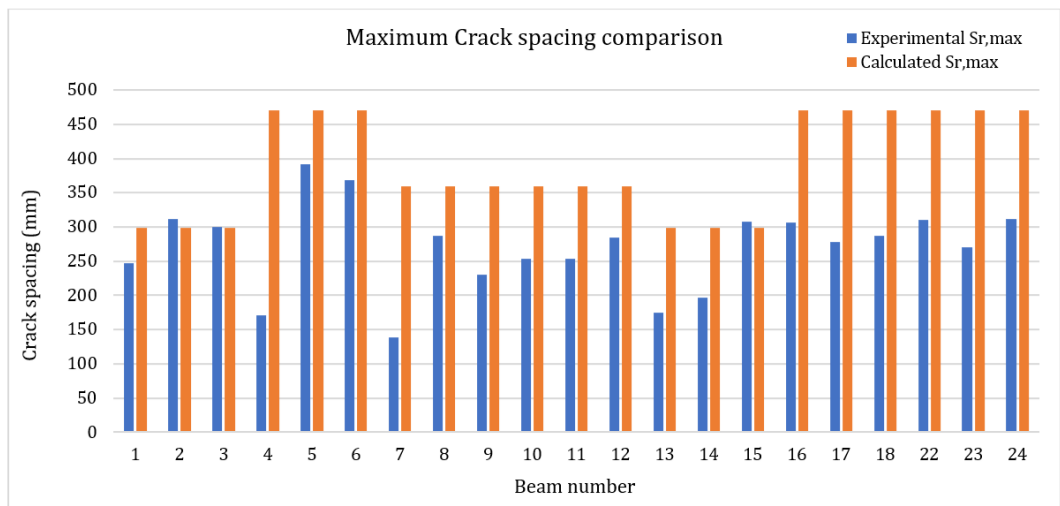


Figure 4.38: Crack spacing (Experimental vs prediction)

The expression for $S_{r,max}$ shows that crack spacing depends on bar diameter, effective reinforcement ratio, cover and "k" factors.

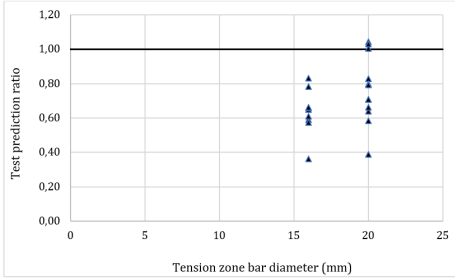


Figure 4.39: Influence of bar diameter of tension zone on $\left(\frac{S_{r,max}(exp)}{S_{r,max}(pre)}\right)_{EC2}$

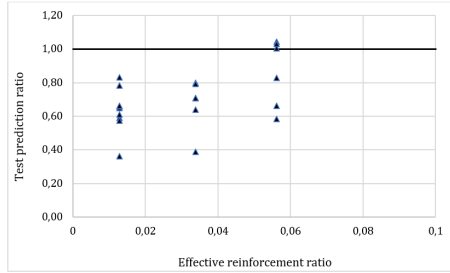


Figure 4.40: Influence of effective reinforcement on $\left(\frac{S_{r,max}(exp)}{S_{r,max}(pre)}\right)_{EC2}$

In figures 4.39 and 4.40, the effect of bar diameter and effective reinforcement ratio in the test prediction ratio have been shown. A clear effect of increasing either of the factors cannot be observed from this graph. From the formula, $S_{r,max}$ is directly proportional to the bar diameter and inversely proportional to effective reinforcement ratio. However, in figure 4.40, a slight increase in maximum spacing can be seen with increase in effective reinforcement ratio which is against the formula. A concrete conclusion about these influence couldn't be pronounced from observing these graph.

CRACK WIDTH

In order to analyse the crack openings in the beams, LVDTs were placed. The drawings of positions of LVDTs with dimensions for each beam are attached in appendix A.1. These LVDTs gave the measure of crack widths. Alternatively, crack widths were measured using crack measuring scale after certain load steps. All these manually measured crack widths can be found in appendix A.7 and tables where all these measurements are noted down. Calculations to determine crack width at yielding moment was done using EC expression 7.8:

$$W_k = S_{r,max}(\epsilon_{sm} - \epsilon_{cm}).$$

Using this expression, stresses at different moment were calculated to give crack widths at different phases. This has been further plotted in figure 4.41 to compare with experimentally obtained crack widths measured using LVDTs.

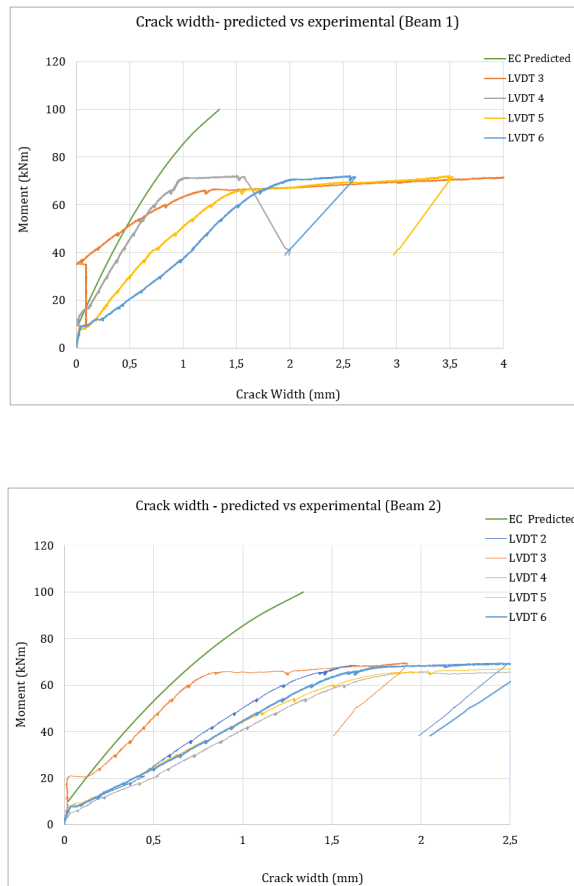


Figure 4.41: Comparison of calculated crack width and LVDT measured crack width- Beam 1 (top) and Beam 2 (bottom)

Figure 4.41 shows comparison of crack widths with increasing moment for beam 1 and beam 2. LVDT 2, 3, 4, 5, 6 were the bottom LVDTs in these beams. The green curve showing calculated crack width was determined for stage before yielding and all other experimental curves show the crack width even after yielding till the failure. Looking at both the curves, a clear distinction can be seen. Crack widths from the experiment are more than the calculated one for the corresponding moment in both the cases. It should be noted that the LVDTs being straight measure the exact horizontal cracks and doesn't take curvature into account. In reality, the beam has certain curvature after it starts deflecting. While taking these LVDT crack width values and plotting the graph, the curvature was neglected. Had it been considered and had approximate crack width been calculated then the crack widths plotted for LVDTs would be even larger. But the formula to calculate crack width only takes the steel strain and deducts the concrete strain, which in reality is present. The crack width value given by LVDT measures both concrete strain as well as steel strain. Calculations done for crack width can be found in appendix section A.2.5.

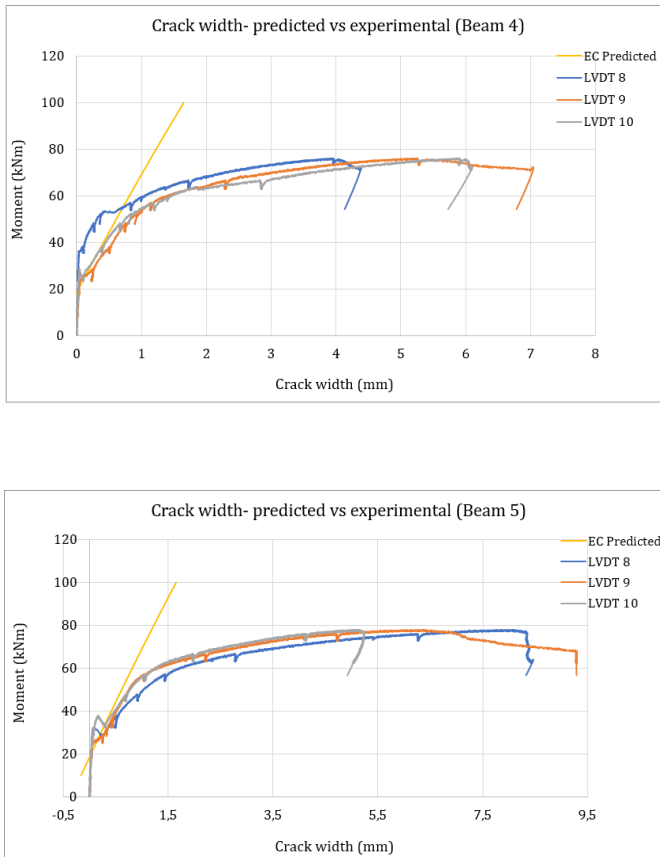


Figure 4.42: Comparison of calculated crack width and LVDT measured crack width- Beam 4 (top) and Beam 5 (bottom)

Similarly, the distinction of calculated and LVDT measured can be seen for beams 4 and 5 in figure 4.42.

The part of beam within which LVDTs were placed, values (from crack width card) from that part is only to be taken to maintain a basis of comparison.

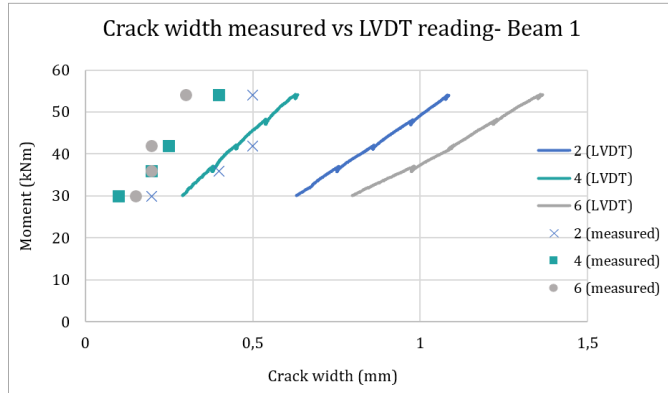


Figure 4.43: Crack width comparison for beam 1

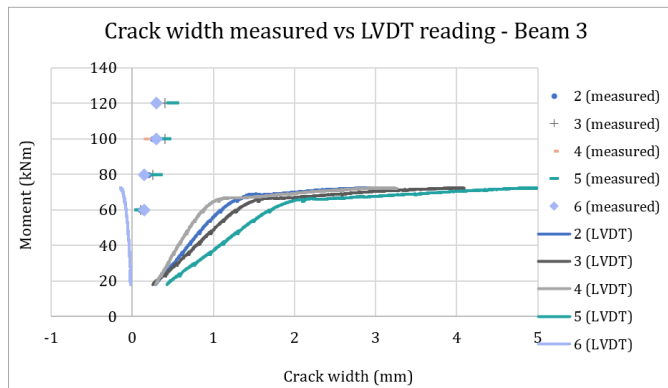


Figure 4.44: Crack width comparison for beam 3

In the graphs, 2,3,4,5,6 of the legend denotes the LVDT numbers. It is represented seeing the cracks between those LVDTs.

A difference in the graph of measured widths and widths from LVDT displacements can be seen. This could be because of the fact that LVDT readings give the value of extreme bottom fibre of the beam whereas manually measuring the cracks, no any strict rule was decided (was measured at approx 30 mm above the bottom fibre; sometimes more and sometimes less). There is a chance that sometimes it could have been measured at the level of reinforcement which would give a less value because of the concrete and steel bond at that point.

Similar difference could be observed in other beams whose results are attached in the appendix.

5

CONCLUSIONS AND RECOMMENDATIONS

This chapter consists of a summary of all the results obtained and conclusions derived from those results followed by a discussion to answer the research questions of this research. Furthermore, limitations and possible research recommendations for future has been suggested.

5.1. CONCLUSIONS

5.1.1. FAILURE MODES

The governing failure modes were observed as it was predicted using EC2 calculations i.e. either it will fail in shear or bending.

5.1.2. MATERIAL PROPERTIES

- Studying the compressive strength behaviour from tests and predictions 4.1.1, it can be concluded that the formula for predicting the compressive strength with age, given for normal cement concrete in EC (3.1.2(6)) can be a give a good estimation for that of GPC as well. However, it is still uncertain if this formula can be used to estimate the strength development of GPC.
- The split tensile strength values that were estimated using EC2 expression with the function of compressive strength were less than the measured values of split tensile strength except for RAMAC 33/43 at 56 days.
- The ratios between splitting tensile strength and compressive strength were observed to be higher than the relationship given by EC2 at all ages but one i.e. for RAMAC C33/43 at 56 days.

5.1.3. SHEAR

- Comparing the test results and predictions (using both mean and design values), it is observed that shear resistance using EC formula (6.2.a) seems to be conservative for calculating shear capacity of geopolymer concrete.
- Studying factors that influence the shear capacity from the obtained results, it was observed that amount of tensile reinforcement and a/d ratio has similar effect on shear resistance to that of reinforced normal concrete.
- When the obtained shear capacities for GPC was compared with the shear database of OPC with similar configurations, similar shear capacity was observed for both the type of concrete.

5.1.4. BENDING

- For beams failed in bending, the experimentally obtained yielding and ultimate moment were observed to be higher than predicted analytically. But the cracking moment for a beam group showed a lower experimental value.
- Comparing the cracking moment between beams with different strengths, it was seen that compressive strength did not show a major effect in the bending behaviour.
Further, to study the influence of different parameters on ultimate moment, both concrete beam groups with varying compressive strength and tensile reinforcement ratio showed that ultimate moment is directly proportional to the compressive strength and reinforcement ratio.

5.1.5. CRACK

- The predicted load at which first crack would occur was close to the actual crack that was observed in the experiment. This can be seen in table 4.11. Cracking moment calculated using the experimental results was observed to be close to the predicted cracking moment.
- The maximum crack spacing observed in the experiments for almost all the beams were less than that of analytically calculated ones. However, 3 of the beams had larger maximum spacing than the predicted maximum crack spacing.
- In case of crack width, the calculated crack widths before yielding at various moments were less than the actual crack widths measured for corresponding moments obtained from the experiment (LVDT).

5.2. DISCUSSION REGARDING RESEARCH QUESTIONS

1. **What are the observed mechanical behaviour like tensile and compressive strength of the concrete mix used here? Can EC2 estimations for predicting these behaviour according to time formulated for normal cement concrete be used for GPC as well?**

5

The compressive strength development (at ages 1, 3, 5, 14, 28, 56, 91 days) although the values in the graphs plotted for estimated and experimental measured values were close and most of the test prediction ratios were more than 1, some were still less than 1. Due to this reason, it still remains uncertain that EC2 expression can be used to estimate compressive strength over time. However, this can be only said for the GPC mix used here. Some research done in the past for GPC also show higher compressive strength than that of OPC concrete but GPC in itself can vary in mix proportions, curing conditions etc. which can influence the results.

To study the β factor, initial assumption made for the factor 's' ($=0.20$) to predict the strength at given age, which in EC2 is taken based on the nature of hardening of concrete showed to be the best fit for the concrete mix RAMAC C33/43. To check the accuracy of other 's' values, samples with normal and slow hardening concrete mix can be tested in the future. The same value of 's' however for RAMAC C28/35-2 did not show very close comparison. A possible way to deal with this would be to modify 's' factor to make it safe for all types of GPC. But due to the non uniformity observed in the rate of strength development of RAMAC C28/35-2, a better approach could also be to first study factors influencing the strength development in concrete composition of this type of concrete.

For splitting tensile strength, almost all the measured values were higher than the ones calculated using EC2 but the splitting tensile strength development over time for these two mixes were not uniform and a clear indication from the measured values could not be inferred. Additionally, the relationship between compressive strength and tensile strength of these mixes with respect to relationship given by

EC2 was checked and it was seen that the ratios of both the mixes from measured values did not show a consistent trend. Thus, proper implication could not be drawn about the behaviour of the mixes. However, almost all the obtained ratios were higher than the EC2 ratio (except for RAMAC C33/43) and seemed to be conservative for the mixes used here.

The inconsistency in the tensile strength development could be due to number of other factors influencing the material behavior of these mixes.

2. How do the failure modes look like? Is the crack initiation, crack propagation, crack pattern any different from that of normal concrete? If yes, in what way?

Different beam groups showed different failure modes depending on varying parameters. The resulting failure modes were observed to be as predicted from the calculations i.e., bending or shear failure. However, to compare it with normal cement concrete on this matter, normal cement concrete specimen with similar specifications were not casted. But additionally, data of a few normal cement concrete samples from past research was taken whose parameters were close to some of the GPC beams used (table 4.6). Both GPC beam group and normal cement concrete reinforced beams (of similar parameters taken from past research) showed the same failure mode.

The initial cracking force predicted before the experiment was close to the actual force noted during the experiment while first crack was seen. This can be seen in table 4.34 where a comparison between predicted cracking moment and experimentally observed cracking moment has been shown. Both the values were pretty close, in most cases experimental being more than the calculated ones.

3. How accurately does the Eurocode analytical model predict the experimental results?

From the obtained results, for bending and shear, it was experimentally observed that the ultimate capacity was more than the EC2 predicted capacity. EC2 was found to be conservative for GPC concrete.

Additionally, when a few reinforced normal cement concrete with similar configuration were compared to the GPC beams tested here, a similar shear capacity was observed for both OPC and GPC beams. Comparing the test prediction ratios of both the concrete types, EC2 model seemed to be more conservative for GPC than OPC.

4. What are the critical parameters that play major role behind the occurring mechanisms of normal cement concrete? Are those parameters equally influential for GPC as well? Can it be proved?

From literature study, factors like compressive strength, tensile reinforcement ratio, etc. affecting the structural behaviour of normal cement concrete

was studied and further from the experimental results, these factors showed an influence on behaviour of GPC beams as well.

In case of shear, amount of reinforcement, rebar diameter, effective depth and shear span to depth ratio were seen as an influencing factor to the overall shear behavior of GPC. Analysing compressive strength, it couldn't give a clear indication about its influence. More experiments with varying compressive strength would be needed to study this parameter.

For the bending capacity, reinforcement ratio showed a significant effect. However to compare the extent of influence with that of normal cement concrete, more database with varying parameters is needed.

5. Is it safe to use GPC over normal cement concrete for similar application? Is there a way to prove the overall safety? How?

While just looking at the results, it could be said that it would be fine to use these models for GPC as well, however, it cannot be said with confidence due to lack of validation of these models for GPC. A statistical evaluation needs to be done further to prove that EC2 models are 'safe' to determine capacities of the type of GPC used here. Only 2 mixes of GPC are used for the experiments and Geopolymer concrete can vary in proportions which could influence in the overall behaviour. Thus, determining design value from the obtained experimental data following a probabilistic approach using Eurocode 1990:2002 which covers all the model uncertainties can be a wise way to prove the safety of GPC in regard to using EC models.

5.3. LIMITATIONS

While checking Eurocode models for the GPC, although for Shear and Bending, EC seems conservative for GPC but this conclusion can be inferred only from the tested beams and they are 12 for shear and 12 for bending. Thus, for other type of mixes of GPC concrete, nothing can be said on that regard. Mix design might have other influencing factors on material level too and GPC can vary in mix proportions.

Although the beams tested showed a higher capacity than that of predicted values, it cannot still be concluded safe which is why it doesn't entirely give a freedom to use GPC over normal cement concrete yet.

5.4. SCOPE FOR FUTURE RESEARCH

- 24 beams tested here had different parameters and was divided into small groups. Study of the same mixes can be done again using EC2 expanding the database which will help draw conclusions for GPC in general.
- Material Behaviour after 91 days wasn't studied. EC estimation over 91 days can be made to compare the experimental values to check if the ratio between test and prediction shows a similar behavior after 91 days of casting.

- The aggregate used (Thermally recycled asphalt aggregate) here is not common in practice and a detail study about it's behaviour would be helpful to know the extent of influence it would have in the concrete mechanical and structural properties.
- The time dependent behaviour like creep and shrinkage could not be studied for this research. It would be helpful to know the influence of these behaviour to analyse how it could affect the overall structural behaviour.
- The prestressing component has not been taken in shear resistance formula (because the experimental beam was not prestressed although the actual beam was). However, this is an important area to study and would be of interest to know how prestressing can behave in Geopolymer concrete.
- A probabilistic study can be done using all these obtained results to validate the EC models for shear, bending and cracks. This will give more freedom to use GPC over normal cement concrete.

BIBLIOGRAPHY

- [1] J.C. Walraven. *AGGREGATE INTERLOCK: A theoretical and experimental analysis*. Tech. rep. 1980. URL: <https://repository.tudelft.nl/islandora/object/uuid%3Ac33a2890-f9c1-4176-929e-6988f0f23640>.
- [2] A. W. Beeby and R. S. Narayanan. "Designers' guide to EN 1992-1-1 and EN 1992-1-2. Eurocode 2: design of concrete structures : general rules and rules for buildings and structural fire design ". In: (2005).
- [3] R. K. Dhira, M. J. McCarthy, and K. A. Paine. "Engineering property and structural design relationships for new and developing concretes". In: *Materials and Structures* 38:1 38.1 (Jan. 2005), pp. 1–9. ISSN: 1871-6873. DOI: [10.1007/BF02480568](https://doi.org/10.1007/BF02480568). URL: <https://link.springer.com/article/10.1007/BF02480568>.
- [4] Edward Sherwood and Evan Bentz. "Where is shear reinforcement required? Review of research results and design procedures." In: *ACI Structural Journal* 108 (Aug. 2008).
- [5] Ee Hui Chang. "Department of Civil Engineering Shear and Bond Behaviour of Reinforced Fly Ash-Based Geopolymer Concrete Beams". In: (2009).
- [6] Rami A. Hawileh, Faris A. Malhas, and Adeeb Rahman. "Comparison between ACI 318-05 and Eurocode 2 (EC2-94) in flexural concrete design". In: *Structural Engineering and Mechanics* 32.6 (2009), pp. 705–724. DOI: [10.12989/SEM.2009.32.6.705](https://doi.org/10.12989/SEM.2009.32.6.705).
- [7] R. Sarkhosh et al. "Shear Capacity of Concrete Beams without Shear Reinforcement under Sustained Loads: Literature Survey". In: *Stevin Laboratory Report* 25.5.10-16 (2010). URL: <https://repository.tudelft.nl/islandora/object/uuid%3A45476ff2-450d-46cd-84ba-9f4b1aafb4bc>.
- [8] M. C.G. Juenger et al. *Advances in alternative cementitious binders*. Dec. 2011. DOI: [10.1016/j.cemconres.2010.11.012](https://doi.org/10.1016/j.cemconres.2010.11.012).
- [9] Zhu Pan, Jay G. Sanjayan, and B. Vijay Rangan. "Fracture properties of geopolymer paste and concrete". In: *Magazine of Concrete Research* 63.10 (Oct. 2011), pp. 763–771. DOI: [10.1680/MACR.2011.63.10.763](https://doi.org/10.1680/MACR.2011.63.10.763).
- [10] A. M. Mustafa Al Bakri et al. "Comparison of geopolymer fly ash and ordinary portland cement to the strength of concrete". In: *Advanced Science Letters* 19.12 (Dec. 2013), pp. 3592–3595. DOI: [10.1166/ASL.2013.5187](https://doi.org/10.1166/ASL.2013.5187).

- [11] Yuguang Yang. "Shear Behaviour of Reinforced Concrete Members without Shear Reinforcement: A New Look at an Old Problem". In: (2014). DOI: [10.4233/UUID:AC776CF0-4412-4079-968F-9EACB67E8846](https://doi.org/10.4233/UUID:AC776CF0-4412-4079-968F-9EACB67E8846). URL: <https://repository.tudelft.nl/islandora/object/uuid%3Aac776cf0-4412-4079-968f-9eacb67e8846>.
- [12] Tom Glasby et al. "EFC Geopolymer Concrete Aircraft Pavements at Brisbane West Wellcamp Airport". In: (2015).
- [13] P K Sarker. "Structural Behaviour and Design of Geopolymer Concrete Members". In: *Civil Engineering Dimension* 17.3 (2015). ISSN: 1410-9530. DOI: [10.9744/CED](https://doi.org/10.9744/CED).
- [14] M. F. Nuruddin et al. "Evolution of geopolymer binders: A review". In: *IOP Conference Series: Materials Science and Engineering* 133.1 (June 2016). DOI: [10.1088/1757-899X/133/1/012052](https://doi.org/10.1088/1757-899X/133/1/012052).
- [15] M. F. Nuruddin et al. "Geopolymer concrete for structural use: Recent findings and limitations". In: *IOP Conference Series: Materials Science and Engineering*. Vol. 133. 1. Institute of Physics Publishing, June 2016. DOI: [10.1088/1757-899X/133/1/012021](https://doi.org/10.1088/1757-899X/133/1/012021).
- [16] Faiz Uddin and Ahmed Shaikh. "Mechanical and durability properties of fly ash geopolymer concrete containing recycled coarse aggregates". In: *International Journal of Sustainable Built Environment* 5 (2016), pp. 277–287. DOI: [10.1016/j.ijjsbe.2016.05.009](https://doi.org/10.1016/j.ijjsbe.2016.05.009). URL: <http://dx.doi.org/10.1016/j.ijjsbe.2016.05.009>.
- [17] Silke Prinsse. *Alkali-activated concrete: development of material properties (strength and stiffness) and flexural behaviour of reinforced beams over time*. 2017. URL: <https://repository.tudelft.nl/islandora/object/uuid%3A975bf22e-4884-4ea2-8862-0bee8e7c1121>.
- [18] S. Samad and A. Shah. "Role of binary cement including Supplementary Cementitious Material (SCM), in production of environmentally sustainable concrete: A critical review". In: *International Journal of Sustainable Built Environment* 6.2 (Dec. 2017), pp. 663–674. ISSN: 2212-6090. DOI: [10.1016/J.IJSBE.2017.07.003](https://doi.org/10.1016/J.IJSBE.2017.07.003).
- [19] M Torres-Carrasco and F Puertas. "Alkaline activation of different aluminosilicates as an alternative to Portland cement: alkali activated cements or geopolymers La activación alcalina de diferentes aluminosilicatos como una alternativa al Cemento Portland: cementos activados alcalinamente o geopolímeros". In: (2017). URL: www.ricuc.cl.
- [20] Biao Hu and Yu Fei Wu. "Effect of shear span-to-depth ratio on shear strength components of RC beams". In: *Engineering Structures* 168 (Aug. 2018), pp. 770–783. ISSN: 0141-0296. DOI: [10.1016/J.ENGSTRUCT.2018.05.017](https://doi.org/10.1016/J.ENGSTRUCT.2018.05.017).
- [21] Amer Hassan, Mohammed Arif, and M. Shariq. *Use of geopolymer concrete for a cleaner and sustainable environment – A review of mechanical properties and microstructure*. June 2019. DOI: [10.1016/j.jclepro.2019.03.051](https://doi.org/10.1016/j.jclepro.2019.03.051).

- [22] Y. F. Wu and B. Hu. "Variation of Shear Strength Components of RC Beams". In: *Lecture Notes in Civil Engineering* 37 (2020), pp. 793–803. DOI: [10.1007/978-981-13-7603-0_{_}76](https://doi.org/10.1007/978-981-13-7603-0_{_}76).
- [23] Olaniyi Arowojolu et al. "Influence of Shear Span-to-Effective Depth Ratio on Behavior of High-Strength Reinforced Concrete Beams". In: *International Journal of Concrete Structures and Materials* 2021 15:1 15.1 (Feb. 2021), pp. 1–12. ISSN: 2234-1315. DOI: [10.1186/S40069-020-00444-7](https://doi.org/10.1186/S40069-020-00444-7). URL: <https://link.springer.com/articles/10.1186/s40069-020-00444-7> %20https://link.springer.com/article/10.1186/s40069-020-00444-7.
- [24] Azad A. Mohammed, Hemn Unis Ahmed, and Amir Mosavi. "Survey of Mechanical Properties of Geopolymer Concrete: A Comprehensive Review and Data Analysis". In: *Materials* 2021, Vol. 14, Page 4690 14.16 (Aug. 2021), p. 4690. DOI: [10.3390/MA14164690](https://doi.org/10.3390/MA14164690). URL: <https://www.mdpi.com/1996-1944/14/16/4690/htm%20https://www.mdpi.com/1996-1944/14/16/4690>.
- [25] S. V. Srinidhi and T. Srinivas. "Flexural behavior of RC structural elements made by geopolymer concrete". In: *AIP Conference Proceedings* 2358 (July 2021), p. 20011. ISSN: 15517616. DOI: [10.1063/5.0058496/FORMAT/PDF](https://doi.org/10.1063/5.0058496/FORMAT/PDF). URL: <https://doi.org/10.1063/5.0058496>.
- [26] *ACI-ASCE Committee-426 The shear Strength for Reinforced Concrete Members.pdf* | TOAZ.INFO. URL: <https://toaz.info/doc-viewer>.
- [27] James Aldred and John Day. *IS GEOPOLYMER CONCRETE A SUITABLE ALTERNATIVE TO TRADITIONAL CONCRETE?* Tech. rep.
- [28] *Beam Deflection Tables* | MechaniCalc. URL: <https://mechanicalc.com/reference/beam-deflection-tables>.
- [29] Rod Bligh and Tom Glasby. "Development of Geopolymer Precast Floor panels for the Global Change Institute at University of Queensland". In: ().
- [30] *Climate change: The massive CO2 emitter you may not know about - BBC News*. URL: <https://www.bbc.com/news/science-environment-46455844>.
- [31] *Difference between Characteristic Compressive Strength and Target Mean Strength*. URL: <https://www.prodyogi.com/2019/09/difference-between-characteristic.html>.
- [32] "Eurocode 2 Commentary (rev A 31-03-2017) Latest version EUROCODE 2 COMMENTARY". In: ().
- [33] *Failure Modes in Concrete Beams: Flexural and Shear Failure - The Constructor*. URL: <https://theconstructor.org/structural-engg/failure-modes-concrete-beams-flexural-shear/37752/>.
- [34] *FLEXURAL AND SHEAR BEHAVIOR OF REINFORCED CONCRETE BEAMS STRENGTHENED WITH CARBON TEXTILE REINFORCED CONCRETE - PDF Free Download*. URL: <https://docplayer.net/203759180-Flexural-and-shear-behavior-of-reinforced-concrete-beams-strengthened-with-carbon-textile-reinforced-concrete.html>.

- [35] dr.ir.drs. C.R. Braam prof.dr.ir. J.C. Walraven. "Prestressed concrete Textbook". In: ().
- [36] D M J Sumajouw et al. "Behaviour and Strength of Reinforced Fly Ash-Based Geopolymer Concrete Beams". In: ().
- [37] M D J Sumajouw and B V Rangan. "LOW-CALCIUM FLY ASH-BASED GEOPOLYMER CONCRETE: REINFORCED BEAMS AND COLUMNS". In: ().
- [38] *The concrete conundrum*. Tech. rep. URL: www.chemistryworld.org.
- [39] *Uses, Benefits, and Drawbacks of Fly Ash in Construction*. URL: <https://www.thespruce.com/fly-ash-applications-844761>.
- [40] Joost Wairaven, Jerome Frenay, and Research Engineer. "Influence of Concrete Strength and Load History on the Shear Friction Capacity of Concrete Members Arjan Pruijssers". In: ().
- [41] *What is Fly Ash?* | Concrete Construction Magazine. URL: https://www.concreteconstruction.net/how-to/materials/what-is-fly-ash_o.
- [42] *World's first public building with structural Geopolymer Concrete – Geopolymer Institute*. URL: <https://www.geopolymer.org/news/worlds-first-public-building-with-structural-geopolymer-concrete/>.
- [43] Joseph Robert Yost et al. "Structural behavior of alkali activated fly ash concrete. Part 2: structural testing and experimental findings". In: (). DOI: [10.1617/s11527-012-9985-0](https://doi.org/10.1617/s11527-012-9985-0).
- [44] Prodromos D Zararis. "Shear Compression Failure in Reinforced Concrete Deep Beams". In: (). DOI: [10.1061/ASCE0733-94452003129:4544](https://doi.org/10.1061/ASCE0733-94452003129:4544).

A

APPENDIX

A.1. EXPERIMENTS

LVDT POSITIONS

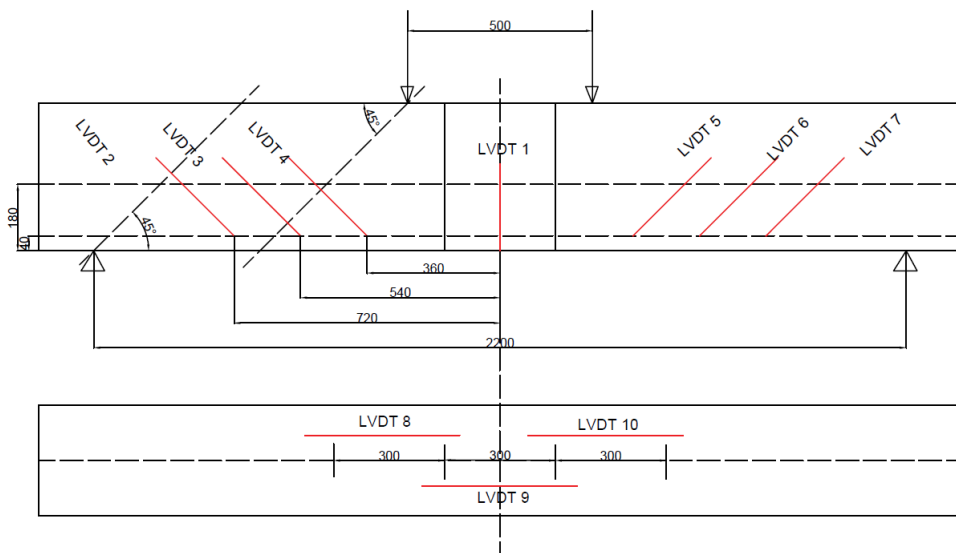


Figure A.1: LVDTs positions and dimensions of beams 10, 11, 16, 17, 18

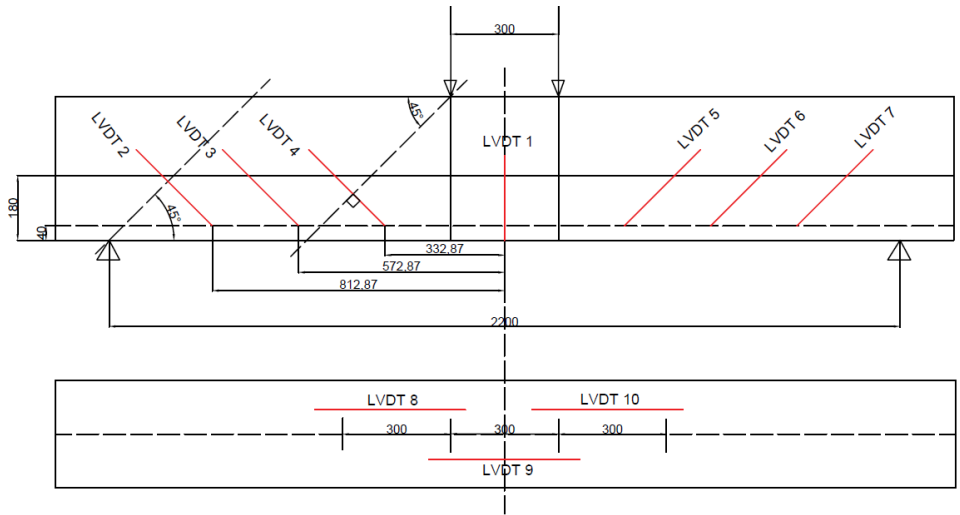


Figure A.2: LVDTs positions and dimensions of beams 4, 5, 6, 7, 8, 9, 12, 22, 23, 24

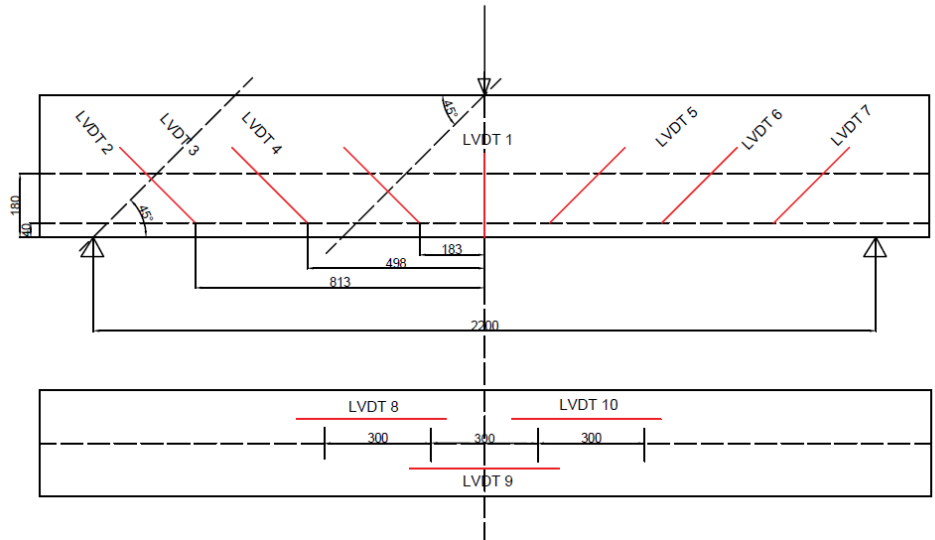


Figure A.3: LVDTs positions and dimensions of beam 19 (3-point loading)

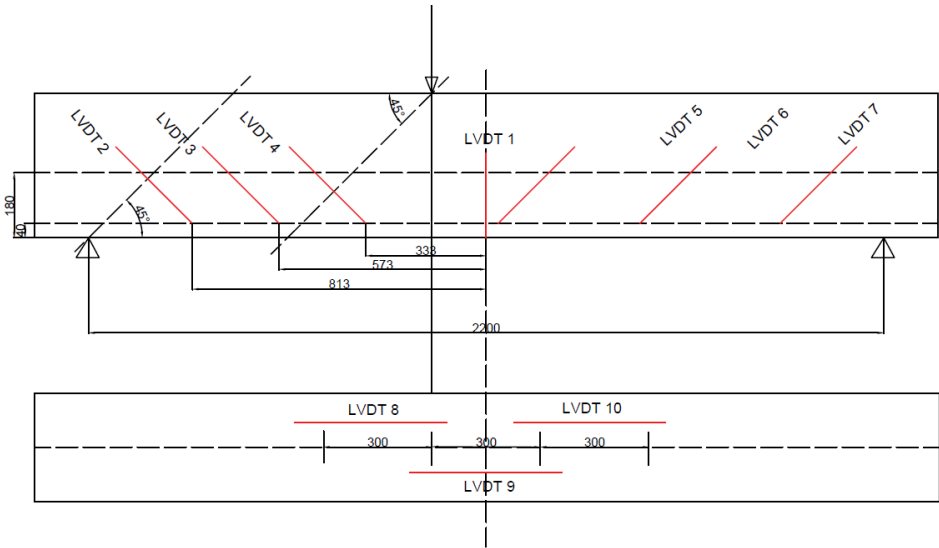


Figure A.4: LVDTs positions and dimensions of beam 20, 21 (3-point loading)

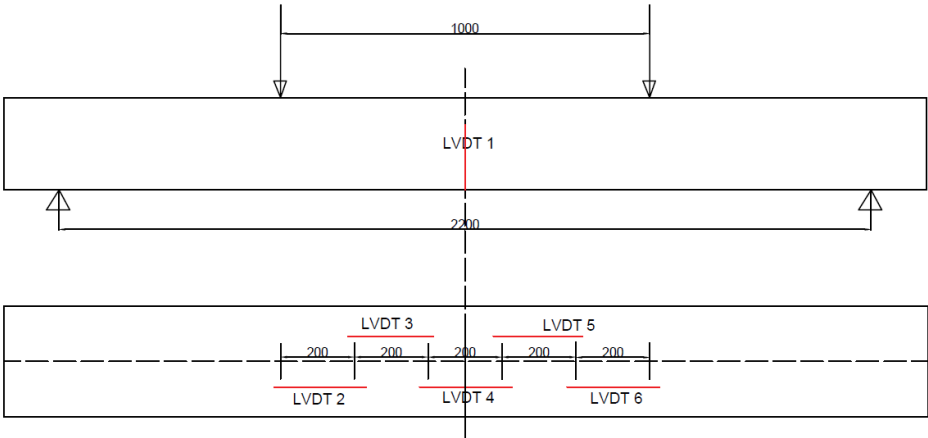


Figure A.5: LVDTs positions and dimensions of beam 1, 2, 3, 13, 14, 15

DATE OF EACH EXPERIMENT

Table A.1 provides the dates on which tests were carried out for respective beams.

Beam no.	strength class	Date of casting	Date of beam experiment	Number of days (t)	f_{ck} (t) N/mm ²	f_{cm} (t) N/mm ²
1	C 28/35	01/02/2021	06/04/2021	64	28.9	36.9
2	C 28/35	01/02/2021	06/04/2021	64	28.9	36.9
3	C 28/35	01/02/2021	07/04/2021	65	29	37
4	C 28/35	01/02/2021	19/03/2021	46	27.8	35.8
5	C 28/35	01/02/2021	22/03/2021	49	27.8	35.8
6	C 28/35	01/02/2021	23/03/2021	50	27.85	35.85
7	C 33/43	25/01/2021	05/03/2021	39	34.3	42.3
8	C 33/43	25/01/2021	08/03/2021	42	34.4	42.4
9	C 33/43	25/01/2021	11/03/2021	45	34.4	42.4
10	C 33/43	25/01/2021	02/03/2021	36	34.2	42.2
11	C 33/43	25/01/2021	03/03/2021	37	34.3	42.3
12	C 33/43	25/01/2021	04/03/2021	38	34.3	42.3
13	C 28/35	01/02/2021	08/04/2021	66	29.2	37.2
14	C 28/35	01/02/2021	08/04/2021	66	29.2	37.2
15	C 28/35	01/02/2021	07/04/2021	65	29	37
16	C 28/35	01/02/2021	24/03/2021	51	27.85	35.85
17	C 28/35	01/02/2021	25/03/2021	52	27.9	35.9
18	C 28/35	01/02/2021	26/03/2021	53	27.99	35.99
19	C 33/43	25/01/2021	12/03/2021	46	34.5	42.5
20	C 33/43	25/01/2021	18/03/2021	52	34.6	42.6
21	C 33/43	25/01/2021	18/03/2021	52	34.6	42.6
22	C 33/43	25/01/2021	30/03/2021	64	35.2	43.2
23	C 33/43	25/01/2021	30/03/2021	64	35.2	43.2
24	C 33/43	25/01/2021	31/03/2021	65	35.3	43.3

Table A.1: Dates of when the beams were casted and tested

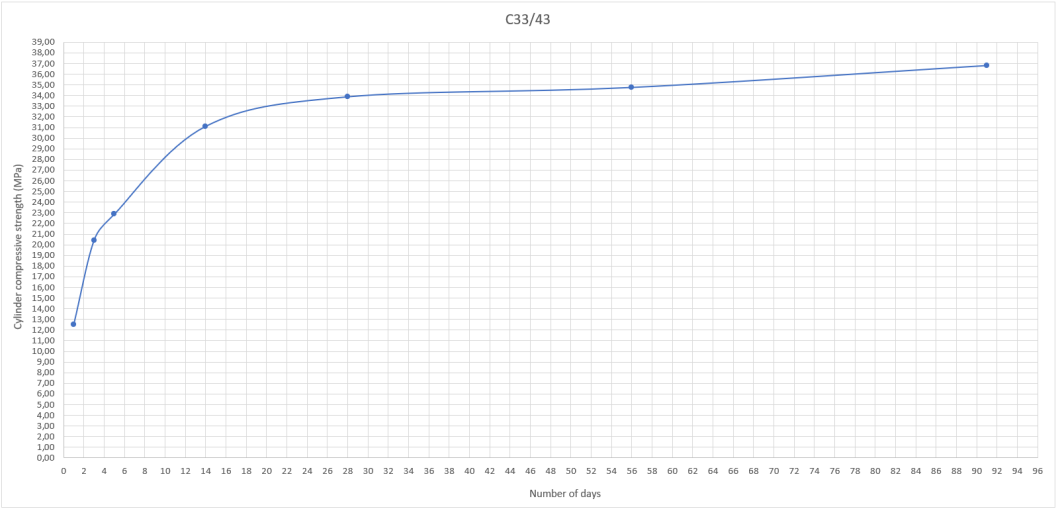


Figure A.6: Strength development with time curve for RAMAC C33/43 used to approximate the compressive strength value according to the experiment date

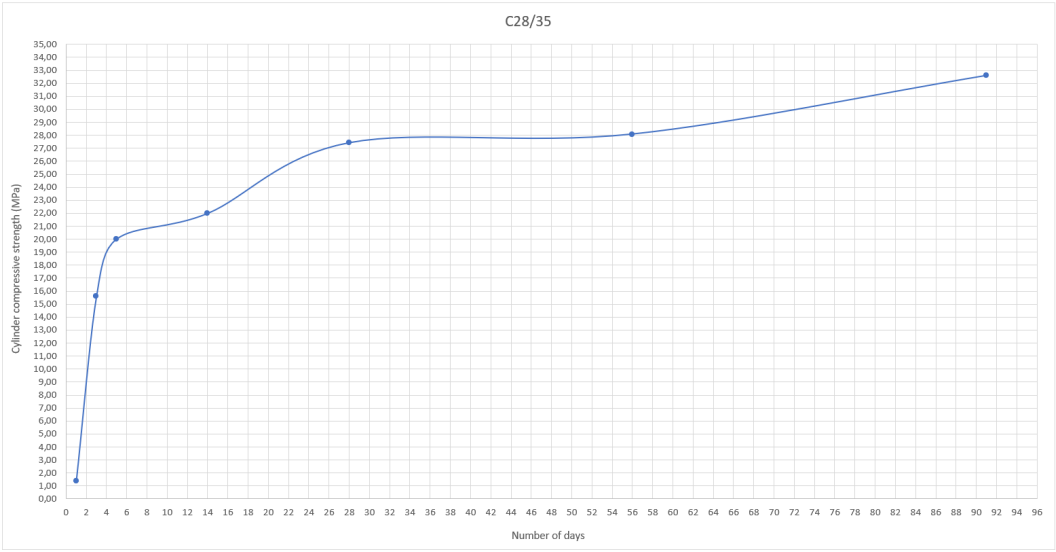


Figure A.7: Strength development with time curve for RAMAC C28/35 used to approximate the compressive strength value according to the experiment date

A.2. ANALYTICAL CALCULATIONS

General parameters used in the formulae

c	<i>cover on outer reinforcement</i>
ϕ_{hw}	<i>diameter of main reinforcement</i>
n_{hw}	<i>number of bars of main reinforcement</i>
ϕ_{bgl}	<i>diameter of stirrups</i>
b_w	<i>width of the cross section in the tensile area</i>
d	<i>effective depth of the beam</i>
h	<i>height of the beam</i>
A_c	<i>area of concrete cross section</i>
A_{sl}	<i>area of tensile reinforcement</i>
l	<i>length of the beam</i>
a_v	<i>distance between load and support</i>
f_{ck}	<i>Characteristic strength of concrete</i>
f_{cm}	<i>Mean cylinder compressive strength</i>
f_{ctm}	<i>Mean tensile strength</i>
$f_{ctm,fl}$	<i>flexural tensile strength</i>
f_{yk}	<i>Yield strength of steel</i>
f_{yd}	<i>Design yield strength of steel</i>
γ	<i>factor of safety</i>
α	<i>surface factor</i>
β	<i>distance factor</i>
ϵ_{cs}	<i>Crushing strain of concrete</i>
ϵ_{cu3}	<i>Ultimate strain of concrete</i>
E_{cm}	<i>Secant modulus of elasticity of concrete (for short-term loading)</i>
ϵ_{sy}	<i>Ultimate strain of reinforcement</i>
E_s	<i>Elastic modulus of reinforcing steel</i>
n	<i>Modular ratio of steel and concrete (E_s/E_c)</i>

A.2.1. COMPRESSIVE STRENGTH AND TENSILE STRENGTH MEASURED VALUES

25-1-2021 casting	C33/43	No. of cubes												
			Age (days)		Cube no.	volume	N/mm ²		Cube no.	volume	N/mm ²		Cube no.	volume
26/Jan	1	3	Compressive strength	1	2257	23,2		2	2266	25,3		3	2245	22,5
		3	Splitting tensile	1		2,31		2		3,39		3		2,47
28/Jan	3	3	Compressive strength	4	2274	35,0		5	2278	34,5		6	2228	31,1
		3	Splitting tensile	4		2,66		5		2,35		6		2,99
01/Feb	5	3	Compressive strength	7	2334	36,8		8	2266	37,3		9	2231	35,7
		3	Splitting tensile	7		4,16		8		3,62		9		3,25
08/Feb	14	3	Compressive strength	10	2260	45,4		11	2251	46,8		12	2258	48,5
		3	Splitting tensile	10		4,47		11		4,16		12		4,81
22/Feb	28	3	Compressive strength	13	2238	50,3		14	2226	49,2		15	2234	51,6
		3	Splitting tensile	15		4,24		15		3,82		15		3,68
22/Mar	56	3	Compressive strength	16	2323	49,6		17	2224	51,9		18	2263	52,9
		3	Splitting tensile	16		3,43		17		3,45				
26/Apr	91	3	Compressive strength	19	2280	54,3		20	2273	55,5		21	2279	52,3
		3	Splitting tensile	19		4,61		20		5,23		21		5,38

1-2-2021 casting	C28/35	No. of cubes												
			Age (days)		Cube no.	volume	N/mm ²		Cube no.	volume	N/mm ²		Cube no.	volume
02/Feb	1	3	Compressive strength	1	2335	11,1		2	2310	8,4		3	2297	9,7
		3	Splitting tensile	1		1,46		2		0,78		3		0,93
04/Feb	3	3	Compressive strength	4	2287	27,9		5	2302	27,1		6	2306	27,5
		3	Splitting tensile	4		2,67		5		2,93		6		3,12
08/Feb	5	3	Compressive strength	7	2305	35,4		8	2260	32,7		9	2290	30,9
		3	Splitting tensile	7		4,16		8		3,85		9		4,16
15/Feb	14	3	Compressive strength	10	2320	36,6		11	2340	34,6		12	2264	35,2
		3	Splitting tensile	10		3,75		11		3,44		12		3,85
1.Mar	28	3	Compressive strength	13	2359	43,1		14	2315	42,3		15	2317	41,4
		3	Splitting tensile	13		3,61		14		4,45		15		4,59
29/Mar	56	3	Compressive strength	16	2290	43,4		17	2305	42,3		18	2375	43,6
		3	Splitting tensile	16		4,02		17		4,02		18		3,9
03/May	91	3	Compressive strength	19	2257	51,7		20	2323	48,9		21	2315	45,6
		3	Splitting tensile	19		4,19		20		4,1		21		4,36

A.2.2. COMPRESSIVE STRENGTH ESTIMATION USING EC CLAUSE 3.1.2 (6)**RAMAC C33/43**

C 33/43	$f_{ck} = 33$	$f_{cm} (f_{ck}+8) = 41$
---------	---------------	--------------------------

$$f_{cm}(t) = \beta_{cc}(t) * f_{cm}$$

$$\beta_{cc}(t) = \exp\{s[1 - (28/t)^{1/2}]\}$$

$$s \quad 0,2$$

Age (days)	$\beta_{cc}(t)$	$f_{cm}(t)$ (MPa)	$f_{ck}(t)$ (calculated using EC)	f_{ck} (from experiment)
1	0,423881847	17,37915574	9,38	12,53
3	0,66298024	27,18218985	19,18	20,43
5	0,760874855	31,19586906	23,20	22,88
14	0,920495918	37,74033265	29,74	31,12
28	1	41	33,00	33,89
56	1,060328371	43,4734632	35,47	34,77
91	1,0931462	44,81899421	36,82	36,83

RAMAC C28/35

C 28/35	$f_{ck} = 28$	$f_{cm} (f_{ck}+8) = 36$
---------	---------------	--------------------------

$$f_{cm}(t) = \beta_{cc}(t) * f_{cm}$$

$$\beta_{cc}(t) = \exp\{s[1 - (28/t)^{1/2}]\}$$

$$s \quad 0,2$$

Age (days)	$\beta_{cc}(t)$	$f_{cm}(t)$ (MPa)	$f_{ck}(t)$ (calculated using EC)	f_{ck} (from experiment)
1	0,423881847	15,25974651	7,26	1,39
3	0,66298024	23,86728865	15,87	15,60
5	0,760874855	27,39149478	19,39	20,00
14	0,920495918	33,13785306	25,14	21,97
28	1	36	28,00	27,41
56	1,060328371	38,17182134	30,17	28,08
91	1,0931462	39,35326321	31,35	32,59

A.2.3. RELATION BETWEEN COMPRESSIVE STRENGTH AND SPLITTING TENSILE STRENGTH

RAMAC C33/43

$f_{cm}(t) = \beta_{cc}(t) * f_{cm}$	$f_{ct} = 0.9 * f_{ct,sp}$
$f_{ck}(t) = f_{cm}(t) - 8$	$f_{ctm} = 0.3 * (f_{ck})^{2/3}$
	$f_{ct,sp} = [0.3 * (f_{ck})^{2/3}] / 0.9$

Age (days)	$f_{ck}(t)$ (EC2)	$f_{ct,sp}$ (EC2)	f_{ck} (measured)	$f_{ct,sp}$ (measured)
1	9,38	1,48	12,53	2,72
3	19,18	2,39	20,43	2,67
5	23,20	2,71	22,88	3,68
14	29,74	3,20	31,12	4,48
28	33,00	3,43	33,00	3,91
56	35,47	3,60	34,77	3,44
91	36,82	3,69	36,83	5,07

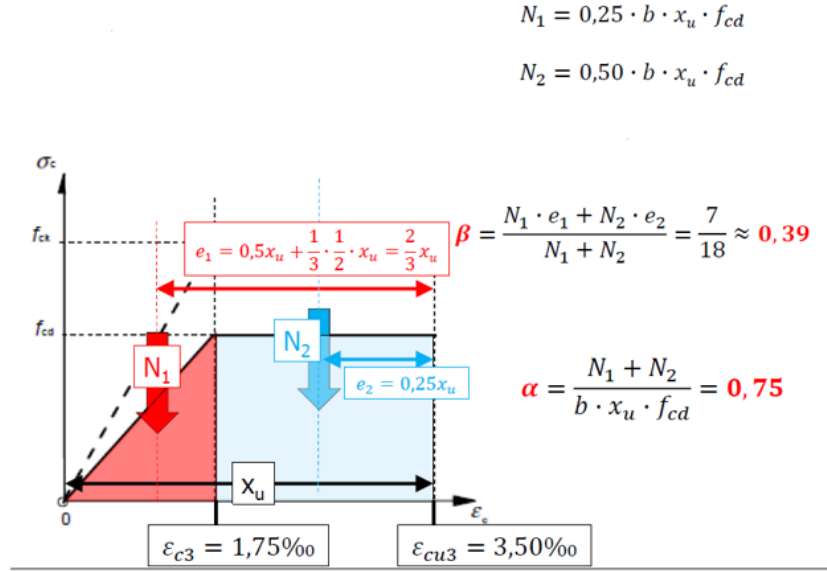
RAMAC C28/35-2

$f_{cm}(t) = \beta_{cc}(t) * f_{cm}$	$f_{ct} = 0.9 * f_{ct,sp}$
$f_{ck}(t) = f_{cm}(t) - 8$	$f_{ctm} = 0.3 * (f_{ck})^{2/3}$
	$f_{ct,sp} = [0.3 * (f_{ck})^{2/3}] / 0.9$

Age (days)	$f_{ck}(t)$ (EC2)	$f_{ct,sp}$ (EC2)	f_{ck} (measured)	$f_{ct,sp}$ (measured)
1	7,26	1,25	1,39	1,06
3	15,87	2,10	15,60	2,91
5	19,39	2,41	20,00	4,06
14	25,14	2,86	21,97	3,68
28	28,00	3,07	28,00	4,22
56	30,17	3,23	28,08	3,98
91	31,35	3,31	32,59	4,22

A.2.4. CALCULATION OF SURFACE FACTOR (α) AND DISTANCE FACTOR (β)

To calculate values of surface factor (α) and distance factor (β) for the concrete used in this research using the obtained stress-strain graph of the concrete, the approach below is used.



Using this, the calculated values were:

For RAMAC 28/35: [$\epsilon_{c3}=2.2 \text{ ‰}$ and $\epsilon_{c3}=2.3 \text{ ‰}$]

α (yielding)=**0.475** α (ultimate)= **0.525**

β (yielding)=**0.36** β (yielding)=**0.32**

For RAMAC 28/35: [$\epsilon_{c3}=2.5 \text{ ‰}$ and $\epsilon_{c3}=2.5 \text{ ‰}$]

α (yielding)=**0.5** α (ultimate)= **0.5**

β (yielding)=**0.33** β (yielding)=**0.33**

A.2.5. SHEAR AND CRACK CALCULATIONS:

BEAMS 1, 2, 3, 13, 14, 15

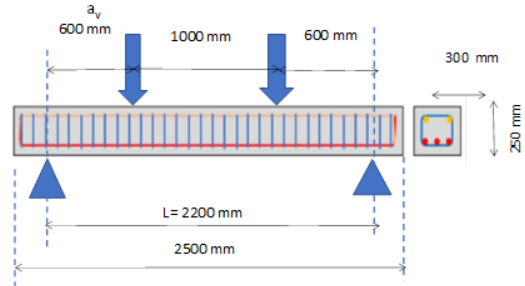
Using Mean values

Using Design Values

Dimensions	
b	300 mm
h	250 mm
d (d = h - c - ϕ_{top} - 0.5 * ϕ_{hw})	170 mm
ϕ_{hw} (Diameter of upper reinforcement)	20 mm
n_{hw} (number of reinforcement at top)	3
ϕ_{st} (diameter of stirrups)	12 mm
Other variables	
L	2200 mm
a_y	600 mm
c	60 mm
f_{ck}	28 N/mm ²
f_{cm} ($f_{\text{cm}} = f_{\text{ck}} + 8$)	36 N/mm ²
f_{cd} ($f_{\text{cd}} = f_{\text{ck}} / \gamma_c$)	18.67
f_{ctm} ($f_{\text{ctm}} = 0.3 * f_{\text{ck}} (2/3)$)	2.77 N/mm ²
$f_{\text{ctm},s}$ ($f_{\text{ctm},s} = (1.6-h) * f_{\text{ctm}}$)	3.73 N/mm ²
f_{yk}	500 N/mm ²
f_{ym} ($f_{\text{ym}} = 1.1 * f_{\text{ym}}$)	550 N/mm ²
f_{yd}	434.78 N/mm ²
A_{sl}	942.48 mm ²
E_{cm}	16363.636 N/mm ²

Shear Capacity of Concrete	
$C_{\text{Rm},c}$	0.15
$C_{\text{Rk},c}$	0.12
$k = \text{MIN}(1 + (200/d)^{1/4}, 2)$	2
$\rho_1 = \text{MIN}(A_{\text{sl}} / (b * d), 0.02)$	0.0185
$V_{\text{Rd},c} = [C_{\text{Rk},c} k (100 \rho_1 f_{\text{cm}})^{1/3} + k_1 \sigma_{cp}] b_w d$ > ($v_{\text{min}} + k_1 \sigma_{cp}) b_w d$	
$V_{\text{Rm},c}$	61995 N
$V_{\text{Rd},c}$	45611 N

Shear capacity of stirrups	
$A_{\text{sw}} = 2 * 1/4 \text{ PI } \phi_{\text{st}}^2$ (2-bracket)	157 mm ²
θ , angle optimised if necessary $V_{\text{Rd},s} = V_{\text{Rd},\text{max}}$	45.0 degrees
θ	0.38 rad
$V_{\text{Rd},s} = A_{\text{sw}} / s * z * \cot(\theta) * f_{yk}$	
$V_{\text{Rm},s}$	115837 N
$V_{\text{Rd},s}$	79062 N



crackwidth at yielding moment

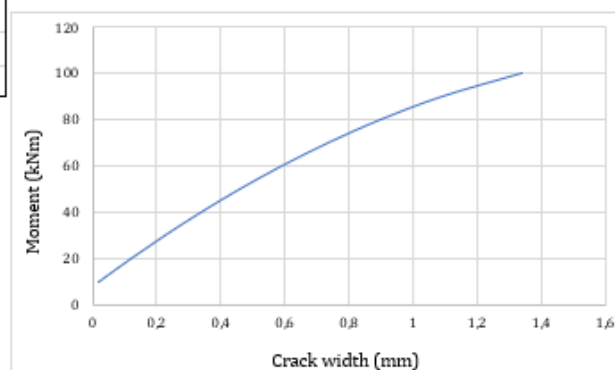
k_1 (EC 7.3.4: Ribbed steel $k_1 = 0.8$)	0.8
k_2 (EC 7.3.4: pure bending $k_2 = 0.8$)	0.5
k_3 (EC 7.3.4)	3.4
k_4 (EC 7.3.4)	0.425
$h_{\text{c,eff}} = \text{MIN}(2.5(h-d), (h-x)/3, h/2)$	56
$A_{\text{c,eff}} = h_{\text{c,eff}} * b$	16786
$\rho_{\text{p,eff}} = A_s / A_{\text{c,eff}}$	0.0561
$s_{\text{r,max}} = k_3 * c + k_1 * k_2 * k_4 * \phi_{\text{hw}} / \rho_{\text{p,eff}}$	299 mm
$\sigma_s = f_{\text{ym}}$	550 N/mm ²
$\sigma_s = f_{\text{yd}}$	500 N/mm ²
k_t	0.6
$\epsilon_{\text{sm}} - \epsilon_{\text{cm}} =$	0.00226
$\sigma_s - k_t \frac{f_{\text{ct,eff}}}{\rho_{\text{p,eff}}} (1 + a_e \rho_{\text{p,eff}}) \geq 0.6 \frac{\sigma_s}{E_s}$	
$w_k = s_{\text{r,max}} * (\epsilon_{\text{sm}} - \epsilon_{\text{cm}})$	
$w_{k,m} (\sigma_s = 200)$	0.22
$w_{k,m} (\sigma_s = 300)$	0.37
$w_{k,m} (\sigma_s = 550)$	0.75 mm
$w_{k,d} ((\sigma_s = 500))$	0.58 mm

Ultimate capacity compressive strut

θ , angle optimised if necessary $V_{\text{Rd},s} = V_{\text{Rd},\text{max}}$	21.8 degrees
θ	0.38 rad
v_1	0.6
$V_{\text{Rd},\text{max}} = b * z * \sin \theta * \cos \theta * v_1 * \alpha_{\text{cw}} * f_{\text{cm}}$	374480 N
	167650 N

Crack width and steel stress calculation according to moment

c_{nw}	70	kt	0,6
k_1	0,800	$f_{ct,eff}$	2,77
k_2	0,500	α_e	12,22
k_3	3,400	E_s	200000
k_4	0,425		
ϕ_{nw}	20		
$h_{c,eff}$	56		
$A_{c,eff}$	16786		
$\rho_{p,eff}$	0,056		
$s_{r,max}$	299		



My	a	b	c	σ_s	$\epsilon_{sm} - \epsilon_{cm}$		W_k	My
10000000	0,0612	-170	10610,33	63,8839	7E-05		0,021	10
20000000	0,0612	-170	21220,66	131,01	0,00041		0,121	20
30000000	0,0612	-170	31830,99	201,93	0,00076		0,227	30
40000000	0,0612	-170	42441,32	277,369	0,00114		0,34	40
50000000	0,0612	-170	53051,65	358,32	0,00154		0,46	50
60000000	0,0612	-170	63661,98	446,204	0,00198		0,592	60
70000000	0,0612	-170	74272,31	543,181	0,00247		0,736	70
80000000	0,0612	-170	84882,64	652,842	0,00301		0,9	80
90000000	0,0612	-170	95492,97	782,033	0,00366		1,093	90
1E+08	0,0612	-170	106103,3	947,621	0,00449		1,34	100

BEAMS 4,5,6

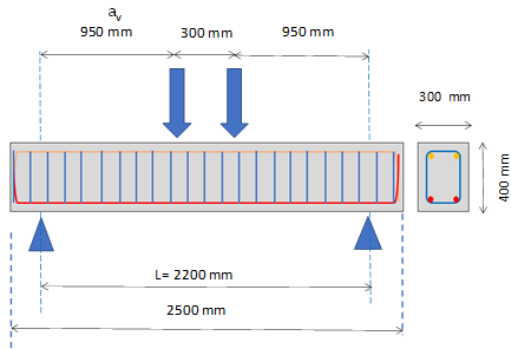
Using Mean values

Using Design Values

Dimensions	
b	300 mm
h	400 mm
d (d = h - c - ϕ_{bgl} - 0.5 * ϕ_{inv})	316 mm
ϕ_{inv} (Diameter of upper reinforcement)	16 mm
n _{inv} (number of reinforcement at top)	2
ϕ_{bgl} (diameter of stirrups)	12 mm
Other variables	
L	2200 mm
a _v	950 mm
c	60 mm
f _{ck}	28 N/mm ²
f _{cm} (f _{cm} = f _{ck} + 8)	36 N/mm ²
f _{cd} (f _{cd} = f _{ck} / γ_c)	18,67
f _{ctm} (f _{ctm} = 0.3 * f _{ck} (2/3))	2,77 N/mm ²
f _{ctm,fl} (f _{ctm,fl} = (1.6-h) * f _{ctm})	3,32 N/mm ²
f _{yk}	500 N/mm ²
f _{ym} (f _{ym} = 1.1 * f _{ym})	550 N/mm ²
f _{yd}	434,78 N/mm ²
A _{sl}	402,12 mm ²
E _{cm}	

Shear Capacity of Concrete	
C _{Rm,c}	0,15
C _{Rk,c}	0,12
k = MIN (1 + (200/d) ² , 2)	2
$\rho_l = \text{MIN} (A_{sl} / (b * d), 0.02)$	0,0185
V _{Rd,c} =	
$[C_{Rk,c} k (100 \rho_l f_{cm})^{1/3} + k_1 \sigma_{cp}] b_w d$	
$> (v_{\min} + k_1 \sigma_{cp}) b_w d$	
V _{Rm,c}	63346 N
V _{Rdc}	46604 N

Shear capacity of stirrups	
A _{sw} = 2 * $\frac{1}{4} \pi \phi_{\text{bgl}}^2$ (2-bracket)	157 mm ²
θ , angle optimised if necessary V _{Rds} = V _{Rd,max}	45,0 degrees
θ	0,38 rad
V _{Rds} = A _{sw} /s * z * cot(θ) * f _{yk}	
V _{Rm,s}	464418 N
V _{Rds}	355743 N



crackwidth at yielding moment

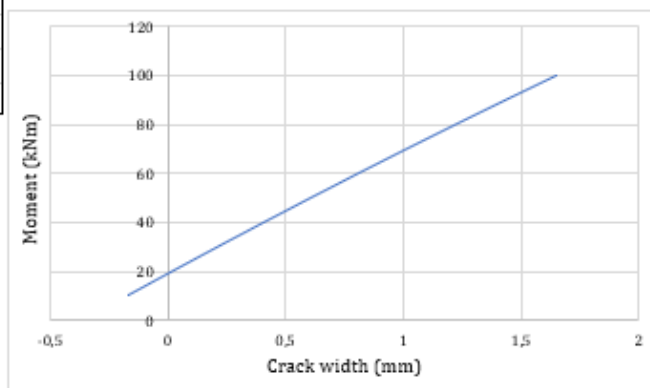
k ₁ (EC 7.3.4: Ribbed steel k ₁ = 0.8)	0.8
k ₂ (EC 7.3.4: pure bending k ₂ = 0.8)	0.5
k ₃ (EC 7.3.4)	3.4
k ₄ (EC 7.3.4)	0.425
h _{ceff} = MIN(2.5(h - d), (h - x) / 3, h / 2)	104
A _{ceff} = h _{ceff} * b	31332
$\rho_{p,eff} = A_s / A_{ceff}$	0,0128
S _{p,max} = k ₃ * c + k ₁ * k ₂ * k ₄ * ϕ_{inv} / $\rho_{p,eff}$	470
$\sigma_s = f_{ym}$	550 N/mm ²
$\sigma_s = f_{yd}$	500 N/mm ²
k _t	0.6
$\epsilon_{sm} - \epsilon_{cm} =$	0.00226
$\frac{\sigma_s - k_t \frac{f_{ct,eff}}{\rho_{p,eff}} (1 + \alpha_e \rho_{p,eff})}{E_s} \geq 0.6 \frac{\sigma_s}{E_s}$	
W _k = S _{r,max} * ($\epsilon_{sm} - \epsilon_{cm}$)	
W _{k,m} ($\sigma_s=200$)	0,28
W _{k,m} ($\sigma_s=300$)	0,42
W _{k,m} ($\sigma_s=550$)	0,94 mm
W _{k,d} ($\sigma_s=500$)	0,68 mm

Ultimate capacity compressive strut

θ , angle optimised if necessary V _{Rds} = V _{Rd,max}	21,8 degrees
θ	0,38 rad
v ₁	0,60
V _{Rd,max} = b * z * sin θ * cos θ * v ₁ * α_{cw} * f _{cm}	850015 N
	427079 N

Crack width and steel stress calculation according to moment

c_{hw}	76	kt	0,6
k_1	0,800	$f_{ct,eff}$	2,77
k_2	0,500	α_e	12,22
k_3	3,400	E_s	200000
k_4	0,425		
ϕ_{hw}	16		
$h_{c,eff}$	104		
$A_{c,eff}$	31332		
$\rho_{p,eff}$	0,013		
$s_{r,max}$	470		



My	a	b	c	σ_s	$\epsilon_{sm} - \epsilon_{cm}$	W_k	My
10000000	#####	-314	24867,96	79,72625	-0,00035	-0,164	10
20000000	#####	-314	49735,92	160,5393	5,47E-05	0,0257	20
30000000	#####	-314	74603,88	242,4848	0,000464	0,2184	30
40000000	#####	-314	99471,84	325,6118	0,00088	0,4139	40
50000000	#####	-314	124339,8	409,9729	0,001302	0,6123	50
60000000	#####	-314	149207,8	495,6247	0,00173	0,8137	60
70000000	#####	-314	174075,7	582,6284	0,002165	1,0183	70
80000000	#####	-314	198943,7	671,0501	0,002607	1,2263	80
90000000	#####	-314	223811,6	760,9615	0,003057	1,4377	90
1E+08	#####	-314	248679,6	852,4404	0,003514	1,6528	100

BEAMS 7, 8, 9

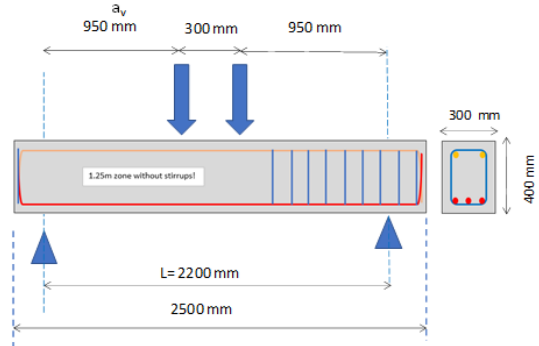
Using Mean values

Using Design Values

Dimensions	
b	300 mm
h	400 mm
d ($d = h - c - \phi_{\text{gl}} - 0.5 * \phi_{\text{nw}}$)	314 mm
ϕ_{nw} (Diameter of upper reinforcement)	20 mm
n_{nw} (number of reinforcement at top)	3
ϕ_{gl} (diameter of stirrups)	12 mm
Other variables	
L	2200 mm
a_v	950 mm
c	60 mm
f_{ck}	33 N/mm ²
f_{cm} ($f_{cm} = f_{ck} + 8$)	41 N/mm ²
f_{cd} ($f_{cd} = f_{ck} / \gamma_c$)	22,00
f_{ctm} ($f_{ctm} = 0.3 * f_{ck} (2/3)$)	3,09 N/mm ²
$f_{ctm,d}$ ($f_{ctm,d} = (1.6-h) * f_{ctm}$)	3,70 N/mm ²
f_{yk}	500 N/mm ²
f_{ym} ($f_{ym} = 1.1 * f_{ym}$)	550 N/mm ²
f_{yd}	434,78 N/mm ²
A_{sl}	402,12 mm ²
E_{cm}	

Shear Capacity of Concrete	
$C_{Rm,c}$	0.15
$C_{Rk,c}$	0.12
$k = \text{MIN} (1 + (200/d)^{2/3}, 2)$	2
$\rho_l = \text{MIN} (A_{sl} / (b * d), 0.02)$	0,0185
$V_{Rd,c} =$ $[C_{Rk,c} k (100 \rho_l f_{cm})^{1/3} + k_1 \sigma_{cp}] b_w d$ $> (v_{min} + k_1 \sigma_{cp}) b_w d$	
$V_{Rm,c}$	87624 N
$V_{Rd,c}$	65206 N

Shear capacity of stirrups	
$A_{sw} = 2 * \pi / 4 * \rho_l \phi_{\text{gl}}^2$ (2-bracket)	157 mm ²
θ , angle optimised if necessary $V_{Rd,s} = V_{Rd,max}$	45,0 degrees
θ	0,38 rad
$V_{Rd,s} = A_{sw} / s * z * \cot(\theta) * f_{ym}$	
$V_{Rm,s}$	0 N
$V_{Rd,s}$	0 N



crackwidth at yielding moment

k_1 (EC 7.3.4: Ribbed steel $k_1 = 0.8$)	0.8
k_2 (EC 7.3.4: pure bending $k_2 = 0.8$)	0.5
k_3 (EC 7.3.4)	3.4
k_4 (EC 7.3.4)	0.425
$h_{c,eff} = \text{MIN}(2.5(h-d), (h-x)/3, h/2)$	93
$A_{c,eff} = h_{c,eff} * b$	27854
$\rho_{p,eff} = A_s / A_{c,eff}$	0,0338
$s_{r,max} = k_3 * c + k_1 * k_2 * k_4 * \phi_{nw} / \rho_{p,eff}$	359
$\sigma_s = f_{ym}$	550 N/mm ²
$\sigma_s = f_{yd}$	500 N/mm ²
k_t	0.6
$\epsilon_{sm} - \epsilon_{cm} =$	0.00226
$\frac{-\sigma_s - k_t \frac{f_{ct,eff}}{\rho_{p,eff}} (1 + \alpha_e \rho_{p,eff})}{E_s} \geq 0.6 \frac{\sigma_s}{E_s}$	
$W_k = s_{r,max} * (\epsilon_{sm} - \epsilon_{cm})$	
$W_{k,m} (\sigma_s = 200)$	0,22
$W_{k,m} (\sigma_s = 300)$	0,40
$W_{k,m} (\sigma_s = 550)$	0,85 mm
$W_{k,d} ((\sigma_s = 500))$	0,66 mm

Ultimate capacity compressive strut

θ , angle optimised if necessary $V_{Rd,s} = V_{Rd,max}$	21,8 degrees
θ	0,38 rad
v_1	0,60
$V_{Rd,max} = b * z * \sin \theta * \cos \theta * v_1 * \alpha_{cw} * f_{cm}$	0 N

BEAMS 16, 17, 18

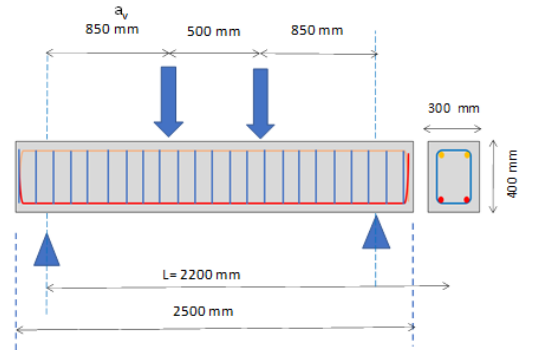
Using Mean values

Using Design Values

Dimensions	
b	300 mm
h	400 mm
d ($d = h - c - \phi_{bgl} - 0.5 * \phi_{inv}$)	316 mm
ϕ_{inv} (Diameter of upper reinforcement)	16 mm
n_{inv} (number of reinforcement at top)	2
ϕ_{bgl} (diameter of stirrups)	12 mm
Other variables	
L	2200 mm
a_v	850 mm
c	60 mm
f_{ck}	28 N/mm ²
f_{cm} ($f_{cm} = f_{ck} + 8$)	36 N/mm ²
f_{cd} ($f_{cd} = f_{ck} / \gamma_c$)	18.67
f_{ctm} ($f_{ctm} = 0.3 * f_{ck} (2/3)$)	2.77 N/mm ²
$f_{ctm,d}$ ($f_{ctm,d} = (1.6-h) * f_{ctm}$)	3.32 N/mm ²
f_{yk}	500 N/mm ²
f_{ym} ($f_{ym} = 1.1 * f_{ym}$)	550 N/mm ²
f_{yd}	434.78 N/mm ²
A_{sl}	402.12 mm ²
E_{cm}	

Shear Capacity of Concrete	
$C_{Rm,c}$	0.15
$C_{Rk,c}$	0.12
$k = \text{MIN} (1 + (200/d)^{2/3}, 2)$	2
$\rho_l = \text{MIN} (A_{sl} / (b * d), 0.02)$	0.0185
$V_{Rd,c} =$ $[C_{Rk,c} k (100 \rho_l f_{cm})^{1/3} + k_1 \sigma_{cp}] b_w d$ $> (v_{min} + k_1 \sigma_{cp}) b_w d$	
$V_{Rm,c}$	63346 N
$V_{Rd,c}$	46604 N

Shear capacity of stirrups	
$A_{inv} = 2 * 1/4 \text{ Pl } \phi_{bgl}^2 (2\text{-bracket})$	157 mm ²
θ , angle optimised if necessary $V_{Rd,s} = V_{Rd,max}$	45.0 degrees
θ	0.38 rad
$V_{Rd,s} = A_{inv} / s * z * \cot(\theta) * f_{yk}$	
$V_{Rm,s}$	464418 N
$V_{Rd,s}$	355743 N



crackwidth at yielding moment

k_1 (EC 7.3.4: Ribbed steel $k_1 = 0.8$)	0.8
k_2 (EC 7.3.4: pure bending $k_2 = 0.8$)	0.5
k_3 (EC 7.3.4)	3.4
k_4 (EC 7.3.4)	0.425
$h_{c,eff} = \text{MIN}(2.5(h-d), (h-x)/3, h/2)$	104
$A_{c,eff} = h_{c,eff} * b$	31332
$\rho_{p,eff} = A_s / A_{c,eff}$	0.0128
$s_{r,max} = k_3 * c + k_1 * k_2 * k_4 * \phi_{inv} / \rho_{p,eff}$	470
$\sigma_s = f_{ym}$	550 N/mm ²
$\sigma_s = f_{yd}$	500 N/mm ²
k_t	0.6
$\epsilon_{sm} - \epsilon_{cm} =$	0.00226
$\frac{\sigma_s - k_t \frac{f_{ct,eff}}{\rho_{p,eff}} (1 + \alpha_e \rho_{p,eff})}{E_s} \geq 0.6 \frac{\sigma_s}{E_s}$	
$w_k = s_{r,max} * (\epsilon_{sm} - \epsilon_{cm})$	
$w_{k,m} (\sigma_s = 200)$	0.28
$w_{k,m} (\sigma_s = 300)$	0.42
$w_{k,m} (\sigma_s = 550)$	0.94 mm
$w_{k,d} ((\sigma_s = 500))$	0.68 mm

Ultimate capacity compressive strut

θ , angle optimised if necessary $V_{Rd,s} = V_{Rd,max}$	21.8 degrees
θ	0.38 rad
v_1	0.60
$V_{Rd,max} = b * z * \sin \theta * \cos \theta * v_1 * \alpha_{cw} * f_{cm}$	850015 N
	427079 N

BEAMS 10, 11, 12

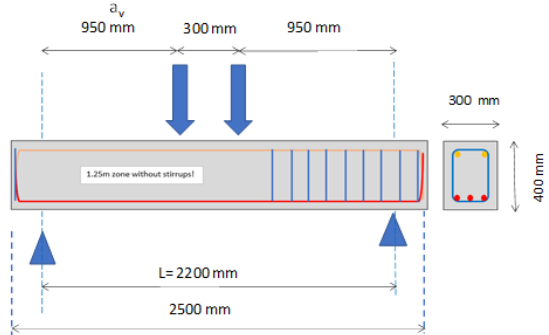
Using Mean values

Using Design Values

Dimensions	
b	300 mm
h	400 mm
d ($d = h - c - \phi_{sgl} - 0.5 * \phi_{nw}$)	314 mm
ϕ_{nw} (Diameter of upper reinforcement)	20 mm
n_{nw} (number of reinforcement at top)	3
ϕ_{sgl} (diameter of stirrups)	12 mm
Other variables	
L	2200 mm
a_v	950 mm
c	60 mm
f_{ck}	33 N/mm ²
f_{cm} ($f_{cm} = f_{ck} + 8$)	41 N/mm ²
f_{cd} ($f_{cd} = f_{ck} / \gamma_c$)	22,00
f_{ctm} ($f_{ctm} = 0.3 * f_{ck} (2/3)$)	3,09 N/mm ²
$f_{ctm,d}$ ($f_{ctm,d} = (1.6-h) * f_{ctm}$)	3,70 N/mm ²
f_{yk}	500 N/mm ²
f_{ym} ($f_{ym} = 1.1 * f_{yk}$)	550 N/mm ²
f_{yd}	434,78 N/mm ²
A_{sl}	402,12 mm ²
E_{cm}	

Shear Capacity of Concrete	
$C_{Rm,c}$	0,15
$C_{Rk,c}$	0,12
$k = \text{MIN} (1 + (200/d)^2, 2)$	2
$\rho_l = \text{MIN} (A_{sl} / (b * d), 0.02)$	0,0185
$V_{Rd,c} =$ $[C_{Rk,c} k (100 \rho_l f_{cm})^{1/3} + k_1 \sigma_{cp}] b_w d$ $> (v_{min} + k_1 \sigma_{cp}) b_w d$	
$V_{Rm,c}$	87624 N
$V_{Rd,c}$	65206 N

Shear capacity of stirrups	
$A_{sw} = 2 * \frac{1}{4} \pi \phi_{sgl}^2$ (2-bracket)	157 mm ²
θ , angle optimised if necessary $V_{Rd,s} = V_{Rd,max}$	45,0 degrees
θ	0,38 rad
$V_{Rd,s} = A_{sw} / s * z * \cot(\theta) * f_{ym}$	
$V_{Rm,s}$	0 N
$V_{Rd,s}$	0 N



crackwidth at yielding moment

k_1 (EC 7.3.4: Ribbed steel $k_1 = 0.8$)	0.8
k_2 (EC 7.3.4: pure bending $k_2 = 0.8$)	0.5
k_3 (EC 7.3.4)	3.4
k_4 (EC 7.3.4)	0.425
$h_{c,eff} = \text{MIN}(2.5(h-d), (h-x)/3, h/2)$	93
$A_{c,eff} = h_{c,eff} * b$	27854
$\rho_{p,eff} = A_s / A_{c,eff}$	0,0338
$s_{r,max} = k_3 * c + k_1 * k_2 * k_4 * \phi_{nw} / \rho_{p,eff}$	359
$\sigma_s = f_{ym}$	550 N/mm ²
$\sigma_s = f_{yd}$	500 N/mm ²
k_t	0.6
$\epsilon_{sm} - \epsilon_{cm} =$	0.00226
$\frac{\sigma_s - k_1 \frac{f_{ct,eff}}{\rho_{p,eff}} (1 + \alpha_e \rho_{p,eff})}{E_s} \geq 0.6 \frac{\sigma_s}{E_s}$	
$w_k = s_{r,max} * (\epsilon_{sm} - \epsilon_{cm})$	
$w_{k,m} (\sigma_s=200)$	0,22
$w_{k,m} (\sigma_s=300)$	0,40
$w_{k,m} (\sigma_s=550)$	0,85 mm
$w_{k,d} ((\sigma_s=500))$	0,66 mm

Ultimate capacity compressive strut

θ , angle optimised if necessary $V_{Rd,s} = V_{Rd,max}$	21,8 degrees
θ	0,38 rad
v_1	0,60
$V_{Rd,max} = b * z * \sin \theta * \cos \theta * v_1 * \alpha_{cw} * f_{cm}$	0 N

BEAMS 22, 23, 24

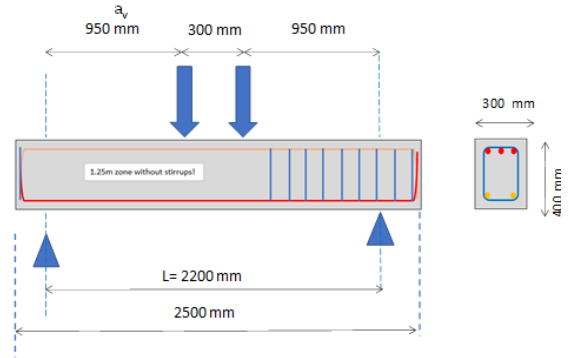
Using Mean values

Using Design Values

Dimensions	
b	300 mm
h	400 mm
d (d = h - c - ϕ_{stl} - 0.5 * ϕ_{tw})	316 mm
ϕ_{tw} (Diameter of upper reinforcement)	16 mm
n_{tw} (number of reinforcement at top)	2
ϕ_{stl} (diameter of stirrups)	12 mm
Other variables	
L	2200 mm
a_v	950 mm
c	60 mm
f_{ck}	33 N/mm ²
f_{cm} ($f_{\text{cm}} = f_{\text{ck}} + 8$)	41 N/mm ²
f_{cd} ($f_{\text{cd}} = f_{\text{ck}} / \gamma_c$)	22,00
f_{ctm} ($f_{\text{ctm}} = 0.3 * f_{\text{ck}}(2/3)$)	2.77 N/mm ²
$f_{\text{ctm},s}$ ($f_{\text{ctm},s} = (1.6-h) * f_{\text{ctm}}$)	3.73 N/mm ²
f_{yk}	500 N/mm ²
f_{ym} ($f_{\text{ym}} = 1.1 * f_{\text{ym}}$)	550 N/mm ²
f_{yd}	434,78 N/mm ²
A_{sl}	942,48 mm ²
E_{cm}	

Shear Capacity of Concrete	
$C_{Rk,c}$	0,15
$C_{Rk,c}$	0,12
$k = \text{MIN}(1 + (200/d)^{2/3}, 2)$	2
$\rho_1 = \text{MIN}(A_{\text{sl}} / (b * d), 0.02)$	0,0185
$V_{Rd,c} =$ $[C_{Rk,c} k (100 \rho_1 f_{\text{cm}})^{1/3} + k_1 \sigma_{cp}] b_w d$ $> (v_{\text{min}} + k_1 \sigma_{cp}) b_w d$	
$V_{Rm,c}$	66152 N
$V_{Rd,c}$	49228 N

Shear capacity of stirrups	
$A_{\text{sw}} = 2 * \frac{1}{4} \text{PI } \phi_{\text{stl}}^2$ (2-bracket)	157 mm ²
θ , angle optimised if necessary $V_{Rd,s} = V_{Rd,\text{max}}$	45,0 degrees
θ	0,38 rad
$V_{Rd,s} = A_{\text{sw}} / s * z * \cot(\theta) * f_{\text{yk}}$	
$V_{Rm,s}$	0 N
$V_{Rd,s}$	0 N



crackwidth at yielding moment	
k_1 (EC 7.3.4: Ribbed steel $k_1 = 0.8$)	0.8
k_2 (EC 7.3.4: pure bending $k_2 = 0.8$)	0.5
k_3 (EC 7.3.4)	3.4
k_4 (EC 7.3.4)	0.425
$h_{\text{ceff}} = \text{MIN}(2.5(h - d), (h - x) / 3, h / 2)$	104
$A_{\text{ceff}} = h_{\text{ceff}} * b$	31340
$\rho_{p,\text{eff}} = A_s / A_{\text{ceff}}$	0.0128
$s_{r,\text{max}} = k_3 * c + k_1 * k_2 * k_4 * \phi_{\text{tw}} / \rho_{p,\text{eff}}$	470
$\sigma_s = f_{\text{ym}}$	550 N/mm ²
$\sigma_s = f_{\text{yd}}$	500 N/mm ²
k_t	0.6
$\epsilon_{sm} - \epsilon_{cm} =$	0.00226
$\frac{\sigma_s - k_t \frac{f_{\text{ct},\text{eff}}}{\rho_{p,\text{eff}}} (1 + a_e \rho_{p,\text{eff}})}{E_s} \geq 0.6 \frac{\sigma_s}{E_s}$	
$w_k = s_{r,\text{max}} * (\epsilon_{sm} - \epsilon_{cm})$	
$w_{k,m} (\sigma_s = 200)$	0,28
$w_{k,m} (\sigma_s = 300)$	0,42
$w_{k,m} (\sigma_s = 550)$	0,90 mm
$w_{k,d} ((\sigma_s = 500))$	0,64 mm

Ultimate capacity compressive strut	
θ , angle optimised if necessary $V_{Rd,s} = V_{Rd,\text{m}}$	21,8 degrees
θ	0,38 rad
v_1	0,60
$V_{Rd,\text{max}} = b * z * \sin \theta * \cos \theta * v_1 * \alpha_{\text{cw}} * f_{\text{cm}}$	0 N

A.2.6. BENDING MOMENT AND $M - \kappa$ DIAGRAMS:

All the theoretical predictions for calculating capacities were made using Eurocode models as the main research focuses on analysing EC for Geopolymer concrete. In following pages, tables with calculations have been shown. Similarly, to calculate moment and curvature for different stages, standard formulae used are shown in tables.

Additionally, for drawing $M - \kappa$ diagrams from experimental data, a standard deflection formula for four point bending is used and equated to calculate the stiffness followed by moment and kappa calculations.

From structural mechanics, total deflection of a beam at midspan is given by

$$W = \frac{M}{24EI} (3L^2 - 4a^2)$$

where,

W is the deflection and

M is the moment given by $F * a$

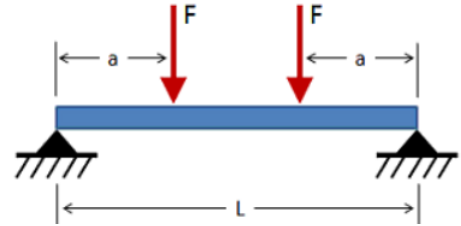


Figure A.8: Four point beam [28]

Equating the stiffness, EI from this deflection formula using the step wise force obtained from the experiment, $\kappa(\kappa)$ was calculated as M/EI and $M - \kappa$ diagrams for respective beams were plotted. However, it should be noted that the EI obtained this way is the average stiffness while in reality it is not constant throughout the cross section. This can be very well distinguished from the plotted graph for theoretical vs experimental.

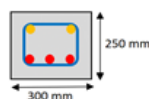
A.2.7. BENDING MOMENT CALCULATIONS:

BEAMS 1, 2, 3, 13, 14, 15

A

Using Mean values

Using Design Values



Dimensions	
b	300 mm
h	250 mm
d ($d = h - c - \phi_{bg} - 0.5 \cdot \phi_b$)	170 mm
ϕ_t (Diameter of upper reinforcement)	16 mm
n_u (number of reinforcement at top)	2
ϕ_b (Diameter of lower reinforcement)	20 mm
n_b (number of reinforcement at bottom)	3
ϕ_{bg} (diameter of stirrups)	12 mm
Other variables	
L	2200 mm
c	60 mm
f_{ck}	28 N/mm ²
f_{cm} ($f_{cm} = f_{ck} + 8$)	36 N/mm ²
f_{ctd} ($f_{ctd} = f_{ctk} / \gamma_c$)	18.67
f_{ctm} ($f_{ctm} = 0.3 \cdot f_{ck}^{2/3}$)	2.77 N/mm ²
$f_{ctm,fl}$ ($f_{ctm,fl} = (1.6 \cdot h) \cdot f_{ctm}$)	3.73 N/mm ²
f_{yk}	500 N/mm ²
f_{ym} ($f_{ym} = 1.1 \cdot f_{yk}$)	550 N/mm ²
f_{yd}	434.78 N/mm ²
A_{st}	942.48 mm ²
ϵ_{cs}	2.20 ‰
ϵ_{cs3}	2.30 ‰
α (yielding)	0.48
β (yielding)	0.36
α (ultimate)	0.525
β (ultimate)	0.320
E_s	200000.00 N/mm ²
E_{cm}	16363.64 N/mm ²

Centroid and moment of inertia	
z1 (concrete)	125 mm
Z2 (upper reinforcement)	170 mm
Z3 (lower reinforcement)	82 mm
A1	75000 mm ²
A2	402.12 mm ²
A3	942.48 mm ²
n	12.2
centroid d, e	122.00 mm
x1 (distance from n. a and center of concrete)	3.00 mm
x2 (distance between top reinf and n.a)	46
x3 (distance between bottom reinf and n.a)	42
I	422019742 mm ⁴

For M-kappa diagram:	
1 Cracking moment	8644568 Nmm
Kappa	1.8257E-06
2 Yielding moment	8644568 Nmm
Kappa	3.6599E-06
3 Steel yielding	58750819 Nmm
Kappa	2.7542E-05
4 Ultimate moment	60184782 Nmm
Kappa	3.1825E-05

Cracking Moment without reinforcement	
$W = 1/6 \cdot b \cdot h^2$	3125000 mm ³
$M_{cr,fl} = W \cdot f_{ctm}$	8644568 Nmm
$\epsilon_{cr} = f_{ctm,fl} / E_{cm}$	0.0002282
$\kappa = 2 \cdot \epsilon_{cr} / h$	1.8257E-06 1/mm

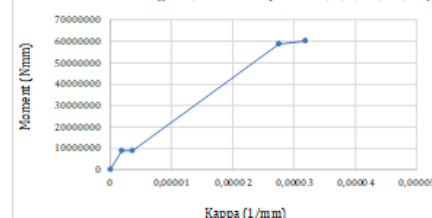
Cracking Moment with reinforcement	
I	422019742 mm ⁴
$M_{cr,fl} = I \cdot f_{ctm} / e$	9581798 Nmm

Yielding Moment	
$N_k = A_s \cdot f_{ym}$	518363 N
$N_c = N_k$	518363 N
$x = \frac{-2 \cdot A_s \cdot n \pm \sqrt{4 \cdot n^2 \cdot A_s^2 - 4 \cdot b \cdot (-2 \cdot n \cdot d \cdot A_s)}}{2 \cdot b}$	82 mm
$\epsilon_c = x / (d - x) \cdot \epsilon_s$	2.033 ‰
check $\epsilon_c < 2.2$ promille	agree
$M_y = N_k \cdot (d - 1/3 x)$	73928769
$M_y = N_k \cdot (d - 1/3 x)$	58441715 Nmm
$\kappa = (\epsilon_c + \epsilon_{cs}) / d$	3.6599E-06

Bending Moment at $\epsilon_c = \epsilon_{cs3}$	
$N_k = A_s \cdot f_{yd}$ (did not agree with f_{ym})	409773 N
$N_c = N_k$	409773 N
$\epsilon_c = \epsilon_{cs3}$	2.20 ‰
$xc = N_c / (b \cdot \alpha \cdot f_{cm})$	80 mm
$\epsilon_s = (d - xc) / xc \cdot \epsilon_c$	2.48 ‰
check $\epsilon_s > 2.175$ promille	agree
$M_y = N_k \cdot (d - 1/3 xc)$	58750819
$M_y = N_k \cdot (d - 1/3 xc)$	48619563 Nmm
$\kappa = \epsilon_s / (d - x)$	2.7542E-05

Ultimate bending moment	
$N_k = A_s \cdot f_{td}$ (did not agree with f_{ym})	409773 N
$N_c = N_k$	409773 N
$x_u = N_c / (\alpha \cdot b \cdot f_{cm})$	72 mm
$z = d - \beta \cdot x_u$	147 mm
$M_u = z \cdot N_c$	60184782
$M_u = z \cdot N_c$	51385062 Nmm
$\kappa = \epsilon_{cu} / x_u$	3.1825E-05

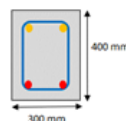
M-k diagram, calculated (Beams 1, 2, 3, 13, 14, 15)



BEAMS 4, 5, 6, 16, 17, 18

Using Mean values

Using Design Values



Dimensions	
b	300 mm
h	400 mm
d (d = h - c - ϕ_{top} - 0.5 * ϕ_{bot})	314 mm
ϕ_t (Diameter of upper reinforcement)	16 mm
n_t (number of reinforcement at top)	2
ϕ_b (Diameter of lower reinforcement)	16 mm
n_b (number of reinforcement at bottom)	2
ϕ_{ngl} (diameter of stirrups)	12 mm
Other variables	
L	2200 mm
c	60 mm
ξ_k	28 N/mm ²
ξ_{cm} ($\xi_{cm} = \xi_k + 8$)	36 N/mm ²
ξ_{cd} ($\xi_{cd} = \xi_k / \gamma_c$)	18.67
ξ_{cm} ($\xi_{cm} = 0.3 * \xi_k$)	2.77 N/mm ²
$\xi_{cm,fl}$ ($\xi_{cm,fl} = (1.6-h) * \xi_{cm}$)	3.32 N/mm ²
ξ_k	500 N/mm ²
ξ_{jm} ($\xi_{jm} = 1.1 * \xi_k$)	550 N/mm ²
ξ_{jd}	434.78 N/mm ²
A_{st}	402.12 mm ²
ϵ_{c3}	2.20 ‰
ϵ_{c3}	2.30 ‰
α (yielding)	0.48
β (yielding)	0.36
α (ultimate)	0.525
β (ultimate)	0.320
E_s	200000.00 N/mm ²
E_{cm}	16363.64 N/mm ²

Centroid and moment of inertia	
z1 (concrete)	200 mm
Z2 (upper reinforcement)	320 mm
Z3 (lower reinforcement)	80 mm
A1	120000 mm ²
A2	402.12 mm ²
A3	402.12 mm ²
n	12.2
centroid, e	200.00 mm
x1 (distance from n. a and center of concrete)	0.00 mm
x2 (distance between top reinf and n.a)	120
x3 (distance between bottom reinf and n.a)	120
I	1741547599 mm ⁴

For M-kappa diagram:	
1 Cracking moment	22130094 Nmm
Kappa	1.0143E-06
2 Yielding moment	22130094 Nmm
Kappa	4.1794E-06
3 Steel yielding	66710742 Nmm
Kappa	5.1029E-05
4 Ultimate moment	67128473 Nmm
Kappa	5.8964E-05

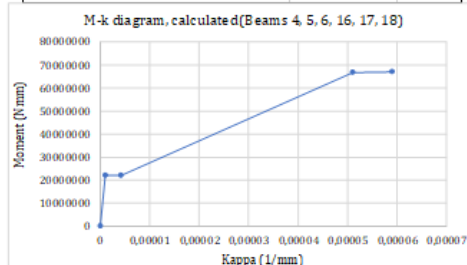
Cracking Moment without reinforcement	
$W = 1/6 * b * h^2$	800000 mm ³
$M_{cr,fl} = W * \xi_{cm}$	22130094 Nmm
$\epsilon_{cr} = \xi_{cm,fl} / E_{cm}$	0.0002029
$\kappa = 2 * \epsilon_{cr} / h$	1.0143E-06 1/mm

Cracking Moment with reinforcement	
I	1741547599 mm ⁴
$M_{cr,fl} = I * \xi_{cm} / e$	24087883 Nmm

Yielding Moment	
$N_s = A_s * f_{ym}$	221168 N
$N_c = N_s$	221168 N
$x = \frac{-2 * A_s * n \pm \sqrt{4 * n^2 * A_s^2 - 4 * b * (-2 * n * d * A_s)}}{2 * b}$	87 mm
$\epsilon_c = x / (d-x) * \epsilon_s$	0.822 ‰
check $\epsilon_c < 2.2$ promille	agree
$M_y = N_s * (d - 1/3 x)$	63498701
$M_y = N_c * (d - 1/3 x)$	50196601 Nmm
$\kappa = (\epsilon_s + \epsilon_c) / (d-x)$	4.1794E-06

Bending Moment at $\epsilon_c = \epsilon_{c3}$	
$N_s = A_s * f_{ym}$	221168 N
$N_c = N_s$	221168 N
$\epsilon_c = \epsilon_{c3}$	2.20 ‰
$xc = N_c / (b * \alpha * \xi_{cm})$	43 mm
$\epsilon_s = (d - xc) / xc * \epsilon_c$	13.93 ‰
check $\epsilon_s > 2.175$ promille	agree
$M_y = N_s * (d - 1/3 xc)$	66710742
$M_y = N_c * (d - 1/3 xc)$	51417772 Nmm
$\kappa = \epsilon_s / (d-x)$	5.1029E-05

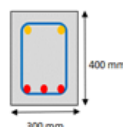
Ultimate bending moment	
$N_c = A_s * f_{yd}$ (did not agree with ξ_{jm})	221168 N
$N_c = N_s$	221168 N
$x_u = N_c / (\alpha * b * \xi_{cm})$	39 mm
$z = d - \beta * x_u$	304 mm
$M_u = z * N_c$	67128473
$M_u = z * N_s$	64565008 Nmm
$\kappa = \epsilon_{c3} / x_u$	5.8964E-05



BEAMS 7, 8, 9

Using Mean values

Using Design Values



Dimensions	
b	300 mm
h	400 mm
d (d = h - c - ϕ_{top} - 0.5 * ϕ_{top})	314 mm
ϕ_c (Diameter of upper reinforcement)	16 mm
n_c (number of reinforcement at top)	2
ϕ_b (Diameter of lower reinforcement)	20 mm
n_b (number of reinforcement at bottom)	3
ϕ_{top} (diameter of stirrups)	12 mm
Other variables	
L	2200 mm
c	60 mm
$\bar{\epsilon}_{ck}$	33 N/mm ²
$\bar{\epsilon}_{cm}$ ($\bar{\epsilon}_{cm} = \bar{\epsilon}_{ck} + 8$)	41 N/mm ²
$\bar{\epsilon}_{cd}$ ($\bar{\epsilon}_{cd} = \bar{\epsilon}_{ck} / \gamma_c$)	22.00
$\bar{\epsilon}_{cm}$ ($\bar{\epsilon}_{cm} = 0.3 * \bar{\epsilon}_{ck}^{2/3}$)	3.09 N/mm ²
$\bar{\epsilon}_{cm,fl}$ ($\bar{\epsilon}_{cm,fl} = (1.6 \cdot h) * \bar{\epsilon}_{cm}$)	3.70 N/mm ²
$\bar{\epsilon}_{ck}$	500 N/mm ²
$\bar{\epsilon}_{ym}$ ($\bar{\epsilon}_{ym} = 1.1 * \bar{\epsilon}_{yk}$)	550 N/mm ²
$\bar{\epsilon}_{yd}$	434.78 N/mm ²
A_{s1}	942.48 mm ²
ϵ_{c3}	2.50 ‰
ϵ_{cu3}	2.50 ‰
α (yielding)	0.50
β (yielding)	0.33
α (ultimate)	0.5
β (ultimate)	0.330
E_s	200000.00 N/mm ²
E_{cm}	16400.00 N/mm ²

Centroid and moment of inertia

z1 (concrete)	200 mm
Z2 (upper reinforcement)	320 mm
Z3 (lower reinforcement)	82 mm
A1	120000 mm ²
A2	402.12 mm ²
A3	942.48 mm ²
n	12.2
centroid, e	194.37 mm
x1 (distance from n. a and center of concrete)	5.63 mm
x2 (distance between top reinf and n.a)	124
x3 (distance between bottom reinf and n.a)	114
I	1829099923 mm ⁴

For M-kappa diagram:

1 Cracking moment	24691864 Nmm
Kappa	1.1292E-06
2 Yielding moment	24691864 Nmm
Kappa	2.4875E-06
3 Steel yielding	148202231 Nmm
Kappa	2.9661E-05
4 Ultimate moment	148347868 Nmm
Kappa	2.9661E-05

Cracking Moment without reinforcement

$W = 1/6 * b * h^2$	8000000 mm ³
$M_{cr,fl} = W * \bar{\epsilon}_{cm}$	24691864 Nmm
$\epsilon_{cr} = \bar{\epsilon}_{cm,fl} / E_{cm}$	0.0002258
$\kappa = 2 * \epsilon_{cr} / h$	1.1292E-06 1/mm

Cracking Moment with reinforcement

I	1829099923 mm ⁴
$M_{cr,fl} = I * \bar{\epsilon}_{cm} / e$	29044889 Nmm

Yielding Moment

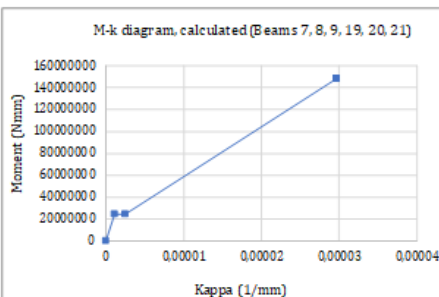
$N_s = A_s * f_{ym}$	518363 N
$N_c = N_s$	518363 N
$x_c = \frac{-2 * A_s * n \pm \sqrt{4 * n^2 * A_s^2 - 4 * b * (-2 * n * d * A_s)}}{2 * b}$	121 mm
$\epsilon_c = x / (d - x) * \epsilon_s$	1.372 ‰
check $\epsilon_c < 2.2$ promille	agree
$M_y = N_s * (d - 1/3 x)$	141778759
$M_y = N_s * (d - 1/3 x)$	112078070 Nmm
$\kappa = (\epsilon_s + \epsilon_c) / d$	2.4875E-06

Bending Moment at $\epsilon_c = \epsilon_{c3}$

$N_s = A_s * f_{ym}$	518363 N
$N_c = N_s$	518363 N
$\epsilon_c = \epsilon_{c3}$	2.50 ‰
$x_c = N_c / (b * \alpha * f_{cm})$	84 mm
$\epsilon_s = (d - x_c) / x_c * \epsilon_c$	6.81 ‰
check $\epsilon_s > 2.175$ promille	agree
$M_y = N_s * (d - 1/3 x_c)$	148202231
$M_y = N_s * (d - 1/3 x_c)$	111707710 Nmm
$\kappa = \epsilon_s / (d - x_c)$	2.9661E-05

Ultimate bending moment

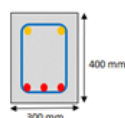
$N_s = A_s * f_{yd}$ (d did not agree with f_{ym})	518363 N
$N_c = N_s$	518363 N
$x_u = N_c / (\alpha * b * f_{cm})$	84 mm
$z = d - \beta * x_u$	286 mm
$M_u = z * N_c$	148347868
$M_u = z * N_c$	135895917 Nmm
$\kappa = \epsilon_{cu} / x_u$	2.9661E-05



BEAMS 10, 11, 12

Using Mean values

Using Design Values



Dimensions	
b	300 mm
h	400 mm
d (d = h - c - ϕ_{bg} - 0.5 * ϕ_{hw})	314 mm
ϕ_s (Diameter of upper reinforcement)	16 mm
n_d (number of reinforcement at top)	2
ϕ_b (Diameter of lower reinforcement)	20 mm
n_b (number of reinforcement at bottom)	3
ϕ_{bg} (diameter of stirrups)	12 mm
Other variables	
L	2200 mm
c	60 mm
f_{ck}	33 N/mm ²
f_{cm} ($f_{cm} = f_{ck} + 8$)	36 N/mm ²
f_{ctd} ($f_{ctd} = f_{ctk} / \gamma_c$)	22,00
f_{ctm} ($f_{ctm} = 0.3 * f_{ck}^{2/3}$)	3,09 N/mm ²
$f_{ctm,fl}$ ($f_{ctm,fl} = (1.6-h) * f_{ctm}$)	3,70 N/mm ²
f_{yk}	500 N/mm ²
f_{ym} ($f_{ym} = 1.1 * f_{yk}$)	550 N/mm ²
f_{yd}	434,78 N/mm ²
A_{s1}	942,48 mm ²
ϵ_{c3}	2,50 ‰
ϵ_{cu3}	2,50 ‰
α (yielding)	0,50
β (yielding)	0,33
α (ultimate)	0,5
β (ultimate)	0,330
E_s	200000,00 N/mm ²
E_{cm}	16400,00 N/mm ²

Centroid and moment of inertia	
z1 (concrete)	200 mm
Z2 (upper reinforcement)	320 mm
Z3 (lower reinforcement)	82 mm
A1	120000 mm ²
A2	402,12 mm ²
A3	942,48 mm ²
n	12,2
centroid, e	194,37 mm
x1 (distance from n. a and center of concrete)	5,63 mm
x2 (distance between top reinf and n.a)	124
x3 (distance between bottom reinf and n.a)	114
I	1829099923 mm ⁴

For M-kappa diagram:

1 Cracking moment	24691864 Nmm
Kappa	1,1292E-06
2 Yielding moment	24691864 Nmm
Kappa	2,4875E-06
3 Steel yielding	148202231 Nmm
Kappa	2,9661E-05
4 Ultimate moment	148347868 Nmm
Kappa	2,9661E-05

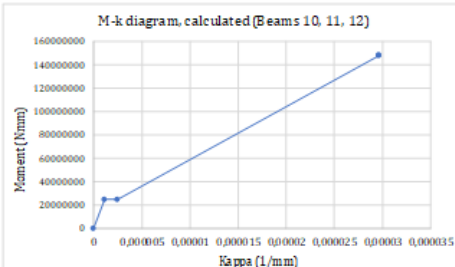
Cracking Moment without reinforcement	
$W = 1/6 * b * h^2$	8000000 mm ³
$M_{cr,fl} = W * f_{ctm}$	24691864 Nmm
$\epsilon_{cr} = f_{ctm,fl} / E_{cm}$	0,0002258
$\kappa = 2 * \epsilon_{cr} / h$	1,1292E-06 1/mm

Cracking Moment with reinforcement	
I	1829099923 mm ⁴
$M_{cr,fl} = I * \kappa_{cr} / e$	29044889 Nmm

Yielding Moment	
$N_s = A_s * f_{ym}$	518363 N
$N_c = N_s$	518363 N
$x =$	
$\frac{-2 * A_s * n \pm \sqrt{4 * n^2 * A_s^2 - 4 * b * (-2 * n * d * A_s)}}{2 * b}$	121 mm
$\epsilon_c = x / (d - x) * \epsilon_s$	1,372 ‰
check $\epsilon_c < 2.2$ promille	agree
$M_y = N_s * (d - 1/3 x)$	141778759
$M_y = N_s * (d - 1/3 x)$	112078070 Nmm
$\kappa = (\epsilon_s + \epsilon_c) / d$	2,4875E-06

Bending Moment at $\epsilon_c = \epsilon_{c3}$	
$N_s = A_s * f_{ym}$	518363 N
$N_c = N_s$	518363 N
$\epsilon_c = \epsilon_{c3}$	2,50 ‰
$xc = N_c / (b * \alpha * f_{cm})$	84 mm
$\epsilon_s = (d - xc) / xc * \epsilon_c$	6,81 ‰
check $\epsilon_s > 2.175$ promille	agree
$M_y = N_s * (d - 1/3 xc)$	148202231
$M_y = N_s * (d - 1/3 xc)$	111707710 Nmm
$\kappa = \epsilon_s / (d - x)$	2,9661E-05

Ultimate bending moment	
$N_s = A_s * f_{yd}$ (did not agree with f_{ym})	518363 N
$N_c = N_s$	518363 N
$x_u = N_c / (\alpha * b * f_{cm})$	84 mm
$z = d - \beta * x_u$	304 mm
$M_u = z * N_c$	148347868
$M_u = z * N_c$	135895917 Nmm
$\kappa = \epsilon_{cu3} / x_u$	2,9661E-05

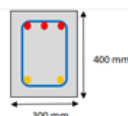


BEAMS 22, 23, 24

A

Using Mean values

Using Design Values



Dimensions	
b	300 mm
h	400 mm
d ($d = h - c - \phi_{\text{stg}} - 0.5 \cdot \phi_{\text{hw}}$)	316 mm
ϕ_c (Diameter of upper reinforcement)	20 mm
n_u (number of reinforcement at top)	3
ϕ_s (Diameter of lower reinforcement)	16 mm
n_b (number of reinforcement at bottom)	2
ϕ_{stg} (diameter of stirrups)	12 mm
Other variables	
L	2200 mm
c	60 mm
f_{dk}	33 N/mm ²
f_{cm} ($f_{\text{cm}} = f_{\text{ck}} + 8$)	41 N/mm ²
f_{ctd} ($f_{\text{ctd}} = f_{\text{ctk}} / \gamma_c$)	18,67
f_{ctm} ($f_{\text{ctm}} = 0.3 \cdot f_{\text{ck}}^{2/3}$)	3,09 N/mm ²
$f_{\text{ctm,8}}$ ($f_{\text{ctm,8}} = (1.6 \cdot h) \cdot f_{\text{ctm}}$)	3,70 N/mm ²
f_{yk}	500 N/mm ²
f_{ym} ($f_{\text{ym}} = 1.1 \cdot f_{\text{yk}}$)	550 N/mm ²
f_{yd}	434,78 N/mm ²
A_{sl}	402,12 mm ²
ϵ_{c3}	2,50 ‰
ϵ_{cu3}	2,50 ‰
α (yielding)	0,50
β (yielding)	0,33
α (ultimate)	0,5
β (ultimate)	0,330
E_s	200000,00 N/mm ²
E_{cm}	16400,00 N/mm ²

Centroid and moment of inertia	
z1 (concrete)	200 mm
z2 (upper reinforcement)	318 mm
z3 (lower reinforcement)	80 mm
A1	120000 mm ²
A2	942,48 mm ²
A3	402,12 mm ²
n	12,2
centroid, e	205,63 mm
x1 (distance from n. a and center of concrete)	-5,63 mm
x2 (distance between top reinf and n.a)	114
x3 (distance between bottom reinf and n.a)	124
I	1829099923 mm ⁴

For M-kappa diagram:	
1 Cracking moment	24691864 Nmm
Kappa	1,1292E-06
2 Yielding moment	24691864 Nmm
Kappa	4,6611E-06
3 Steel yielding	67237889 Nmm
Kappa	6,9517E-05
4 Ultimate moment	67264401 Nmm
Kappa	6,9517E-05

Cracking Moment without reinforcement	
$W = 1/6 \cdot b \cdot h^2$	8000000 mm ³
$M_{\text{cr,8}} = W \cdot f_{\text{ctm}}$	24691864 Nmm
$\epsilon_{\text{cr,8}} = f_{\text{ctm,8}} / E_{\text{cm}}$	0,0002258
$\kappa = 2 \cdot \epsilon_{\text{cr,8}} / h$	1,1292E-06 1/mm

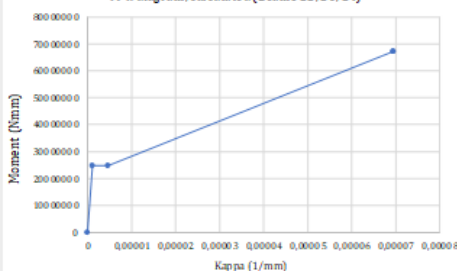
Cracking Moment with reinforcement	
I	1829099923 mm ⁴
$M_{\text{cr,8}} = I \cdot \epsilon_{\text{ctm}} / e$	27454723 Nmm

Yielding Moment	
$N_s = A_s \cdot f_{\text{ym}}$	221168 N
$N_c = N_s$	221168 N
$x = \frac{-2 \cdot A_s \cdot n \pm \sqrt{4 \cdot n^2 \cdot A_s^2 - 4 \cdot b \cdot (-2 \cdot n \cdot d \cdot A_s)}}{2 \cdot b}$	87 mm
$\epsilon_c = x / (d - x) \cdot \epsilon_s$	0,821 ‰
check $\epsilon_c < 2.2$ promille	agree
$M_y = N_s \cdot (d - 1/3 x)$	63504664
$M_y = N_s \cdot (d - 1/3 x)$	50201315 Nmm
$\kappa = (\epsilon_s + \epsilon_c) / d$	4,6611E-06

Bending Moment at $\epsilon_c = \epsilon_{\text{c3}}$	
$N_s = A_s \cdot f_{\text{ym}}$	221168 N
$N_c = N_s$	221168 N
$\epsilon_c = \epsilon_{\text{c3}}$	2,50 ‰
$x_c = N_c / (b \cdot \alpha \cdot f_{\text{cm}})$	36 mm
$\epsilon_s = (d - x_c) / x_c \cdot \epsilon_c$	19,47 ‰
check $\epsilon_s > 2.175$ promille	agree
$M_y = N_s \cdot (d - 1/3 x_c)$	67237889
$M_y = N_c \cdot (d - 1/3 x_c)$	52160666 Nmm
$\kappa = \epsilon_c / (d - x)$	6,9517E-05

Ultimate bending moment	
$N_s = A_s \cdot f_{\text{yd}}$ (did not agree with f_{ym})	221168 N
$N_c = N_s$	221168 N
$x_u = N_c / (\alpha \cdot b \cdot f_{\text{cm}})$	36 mm
$z = d - \beta \cdot x_u$	304 mm
$M_u = z \cdot N_c$	67264401
$M_u = z \cdot N_c$	64997593 Nmm
$\kappa = \epsilon_{\text{cu3}} / x_u$	6,9517E-05

M-k diagram, calculated (Beams 22, 23, 24)



A.3. EUROCODE TABLES

Table 2.1N: Partial factors for materials for ultimate limit states

Design situations	γ_c for concrete	γ_s for reinforcing steel	γ_s for prestressing steel
Persistent & Transient	1,5	1,15	1,15
Accidental	1,2	1,0	1,0

Strength classes for concrete															Analytical relation / Explanation
f_{ck} (MPa)	12	16	20	25	30	35	40	45	50	55	60	70	80	90	
$f_{ck, cube}$ (MPa)	15	20	25	30	37	45	50	55	60	67	75	85	95	105	2,8
f_{cm} (MPa)	20	24	28	33	38	43	48	53	58	63	68	78	88	98	$f_{cm} = f_{ck} + 8$ (MPa)
f_{ctm} (MPa)	1,6	1,9	2,2	2,6	2,9	3,2	3,5	3,8	4,1	4,2	4,4	4,6	4,8	5,0	$f_{ctm} = 0,30 \times f_{cm}^{2/3}$ < C50/60 $f_{ctm} = 2,12 \cdot \ln(1 + (f_{cm}/10))$ > C50/60
$f_{ck, 0.05}$ (MPa)	1,1	1,3	1,5	1,8	2,0	2,2	2,5	2,7	2,9	3,0	3,1	3,2	3,4	3,5	$f_{ck, 0.05} = 0,7 \times f_{cm}$ 5% fractile
$f_{ck, 0.95}$ (MPa)	2,0	2,5	2,9	3,3	3,8	4,2	4,6	4,9	5,3	5,5	5,7	6,0	6,3	6,6	$f_{ck, 0.95} = 1,3 \times f_{cm}$ 95% fractile
E_{cm} (GPa)	27	29	30	31	33	34	35	36	37	38	39	41	42	44	$E_{cm} = 22 \times (f_{cm}/10)^{1/3}$ (f_{cm} in MPa)
ε_{cu1} (‰)	1,8	1,9	2,0	2,1	2,2	2,25	2,3	2,4	2,45	2,5	2,6	2,7	2,8	2,8	see Figure 3.2 $\varepsilon_{cu1}^{(f_{cu})} = 0,7 \cdot f_{cm}^{0.33} \leq 2,8$ ‰
ε_{cu1} (‰)	3,5									3,2	3,0	2,8	2,8	2,8	see Figure 3.2 for $f_{ck} \geq 50$ Mpa $\varepsilon_{cu1}^{(f_{cu})} \geq 2,8 + 27 \cdot (98 - f_{cm}) / 100$ ‰
ε_{cu2} (‰)	2,0									2,2	2,3	2,4	2,5	2,6	see Figure 3.3 for $f_{ck} \geq 50$ Mpa $\varepsilon_{cu2}^{(f_{cu})} = 2,0 + 0,085 \cdot (f_{ck} - 50)^{0.83}$
ε_{cu2} (‰)	3,5									3,1	2,9	2,7	2,6	2,6	see Figure 3.3 for $f_{ck} \geq 50$ Mpa $\varepsilon_{cu2}^{(f_{cu})} = 2,6 + 35 \cdot (90 - f_{ck}) / 100$ ‰
n	2,0									1,75	1,6	1,45	1,4	1,4	for $f_{ck} \geq 50$ Mpa $n = 1,4 + 23,4 \cdot [(90 - f_{ck}) / 100]^4$
ε_{cu3} (‰)	1,75									1,8	1,9	2,0	2,2	2,3	see Figure 3.4 for $f_{ck} \geq 50$ Mpa $\varepsilon_{cu3}^{(f_{cu})} = 1,75 + 0,55 \cdot [(f_{ck} - 50) / 40]$
ε_{cu3} (‰)	3,5									3,1	2,9	2,7	2,6	2,6	see Figure 3.4 for $f_{ck} \geq 50$ Mpa $\varepsilon_{cu3}^{(f_{cu})} = 2,6 + 35 \cdot [(90 - f_{ck}) / 100]^4$

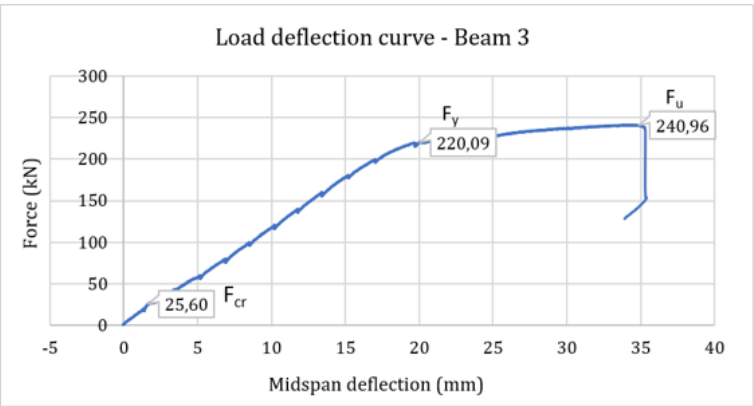
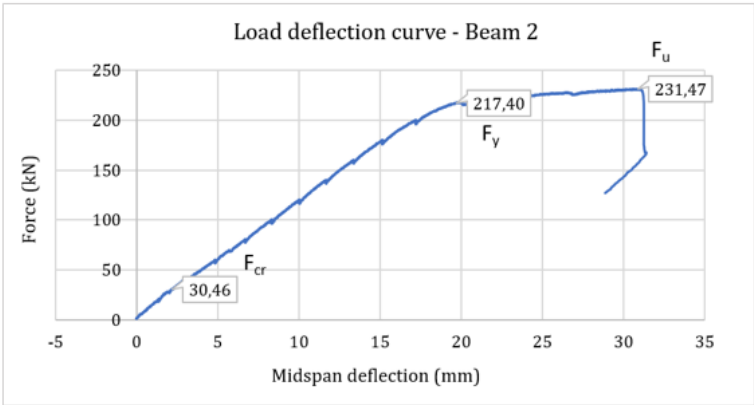
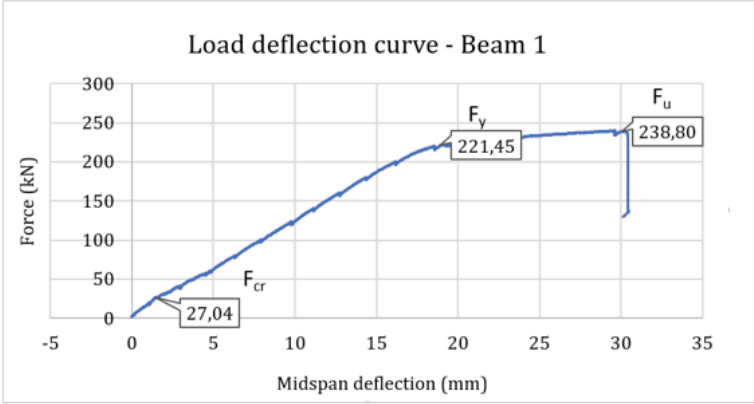
Table 3.1 Strength and deformation characteristics for concrete

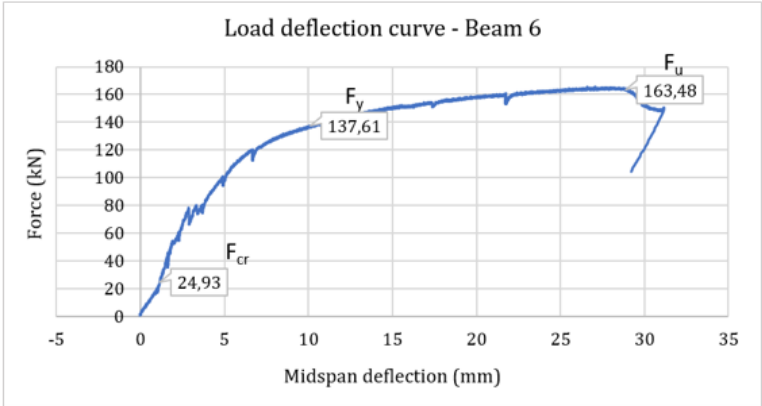
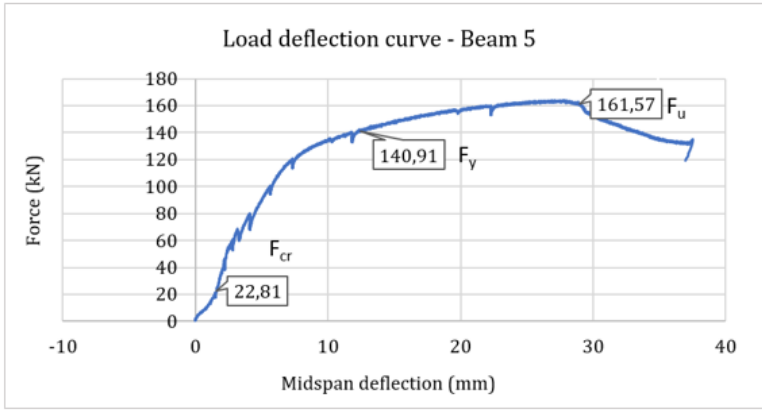
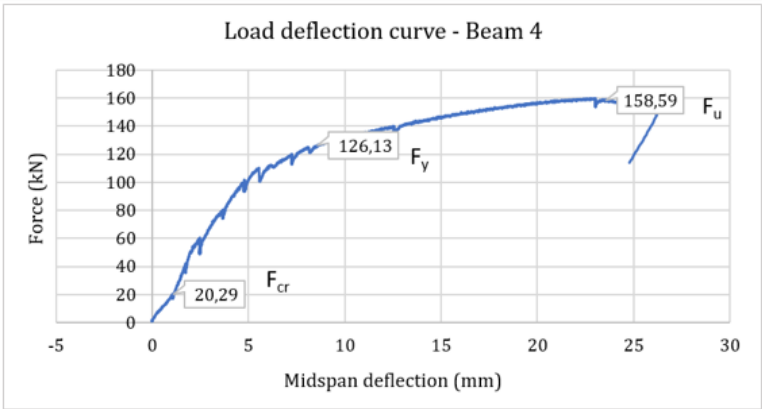
Table 4.1: Exposure classes related to environmental conditions in accordance with EN 206-1

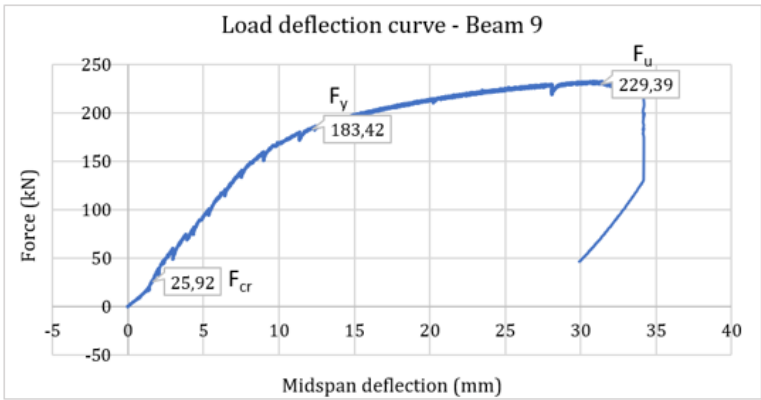
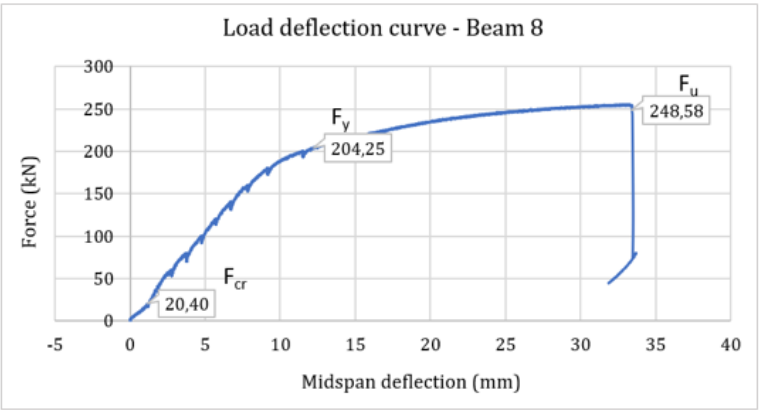
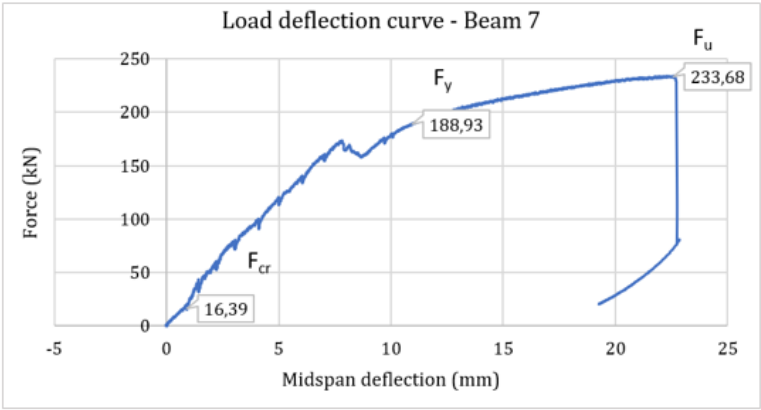
Class designation	Description of the environment	Informative examples where exposure classes may occur
1 No risk of corrosion or attack		
X0	For concrete without reinforcement or embedded metal: all exposures except where there is freeze/thaw, abrasion or chemical attack For concrete with reinforcement or embedded metal: very dry	Concrete inside buildings with very low air humidity
2 Corrosion induced by carbonation		
XC1	Dry or permanently wet	Concrete inside buildings with low air humidity Concrete permanently submerged in water
XC2	Wet, rarely dry	Concrete surfaces subject to long-term water contact Many foundations
XC3	Moderate humidity	Concrete inside buildings with moderate or high air humidity External concrete sheltered from rain
XC4	Cyclic wet and dry	Concrete surfaces subject to water contact, not within exposure class XC2
3 Corrosion induced by chlorides		
XD1	Moderate humidity	Concrete surfaces exposed to airborne chlorides
XD2	Wet, rarely dry	Swimming pools Concrete components exposed to industrial waters containing chlorides
XD3	Cyclic wet and dry	Parts of bridges exposed to spray containing chlorides Pavements Car park slabs
4 Corrosion induced by chlorides from sea water		
XS1	Exposed to airborne salt but not in direct contact with sea water	Structures near to or on the coast
XS2	Permanently submerged	Parts of marine structures
XS3	Tidal, splash and spray zones	Parts of marine structures
5. Freeze/Thaw Attack		
XF1	Moderate water saturation, without de-icing agent	Vertical concrete surfaces exposed to rain and freezing
XF2	Moderate water saturation, with de-icing agent	Vertical concrete surfaces of road structures exposed to freezing and airborne de-icing agents
XF3	High water saturation, without de-icing agents	Horizontal concrete surfaces exposed to rain and freezing
XF4	High water saturation with de-icing agents or sea water	Road and bridge decks exposed to de-icing agents Concrete surfaces exposed to direct spray containing de-icing agents and freezing Splash zone of marine structures exposed to freezing
6. Chemical attack		
XA1	Slightly aggressive chemical environment according to EN 206-1, Table 2	Natural soils and ground water
XA2	Moderately aggressive chemical environment according to EN 206-1, Table 2	Natural soils and ground water
XA3	Highly aggressive chemical environment according to EN 206-1, Table 2	Natural soils and ground water

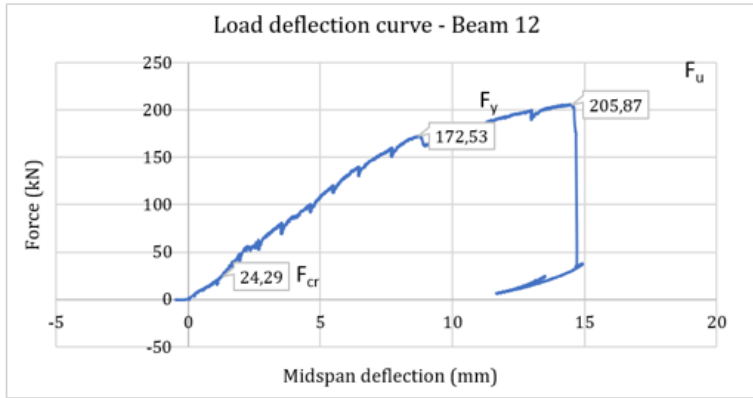
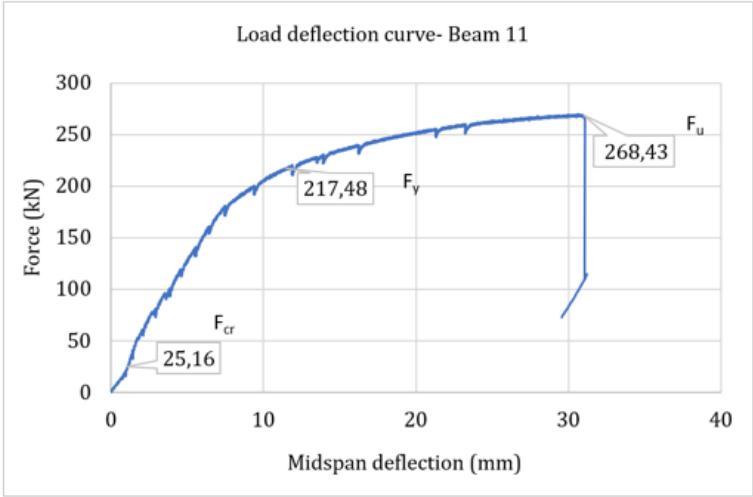
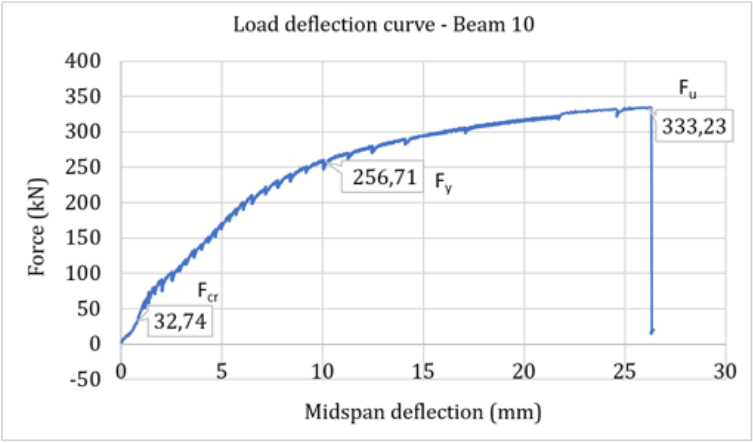
A.4. LOAD-DEFLECTION DIAGRAMS OF ALL BEAMS

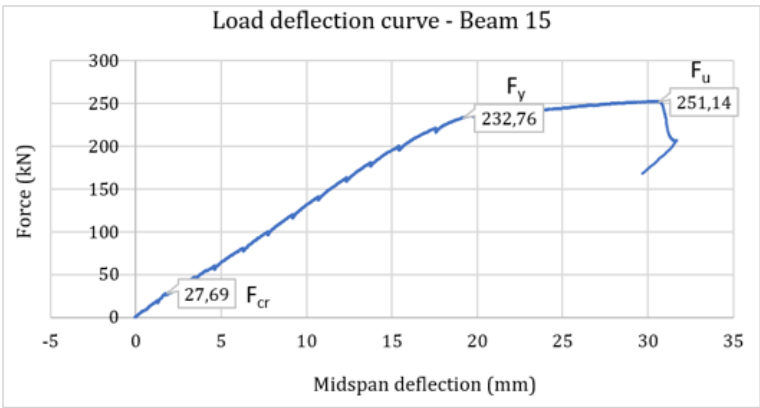
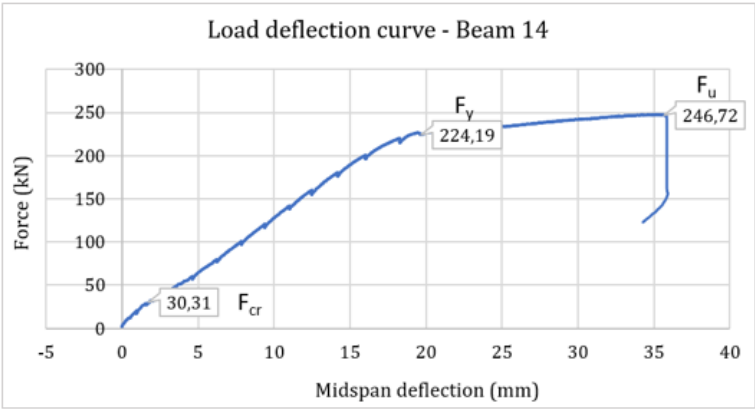
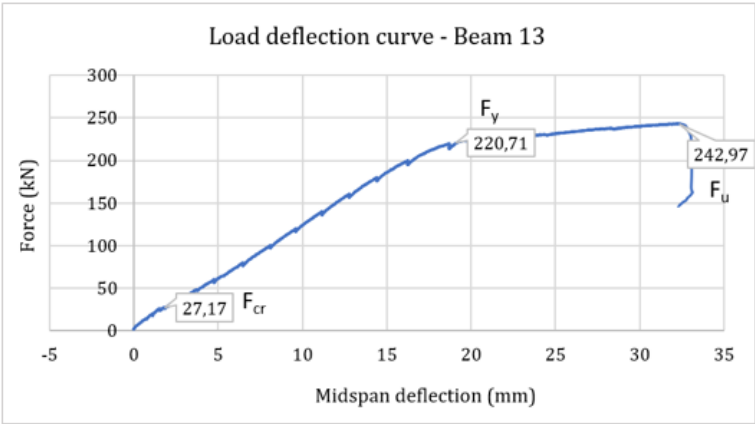
F_{cr} = Force at first crack; F_y = Force at yielding; F_u = Force at failure

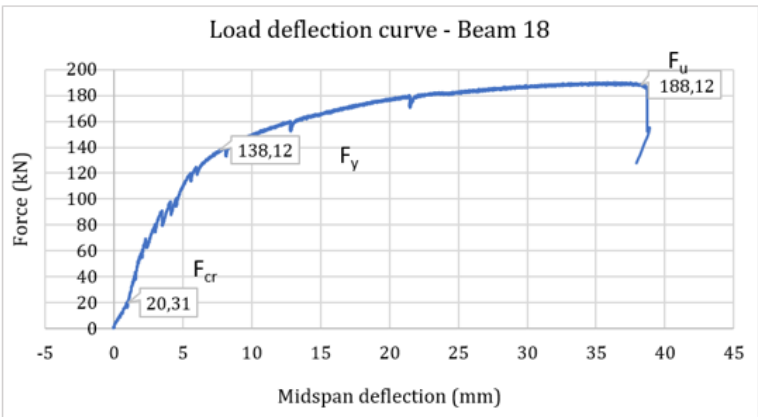
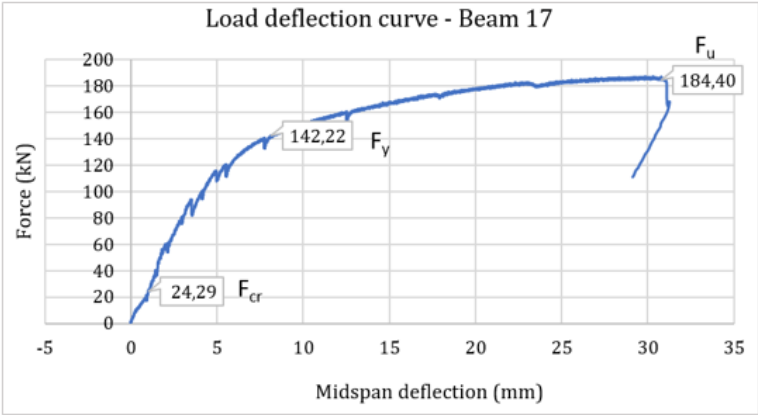
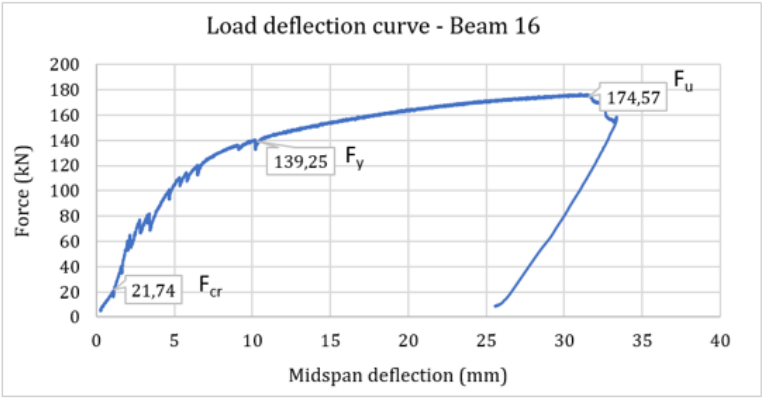


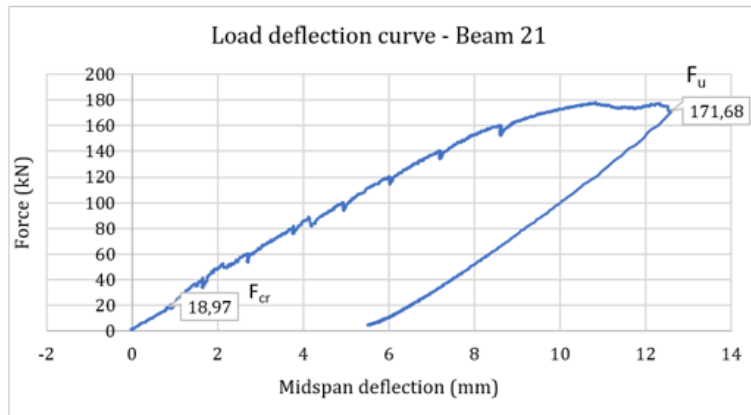
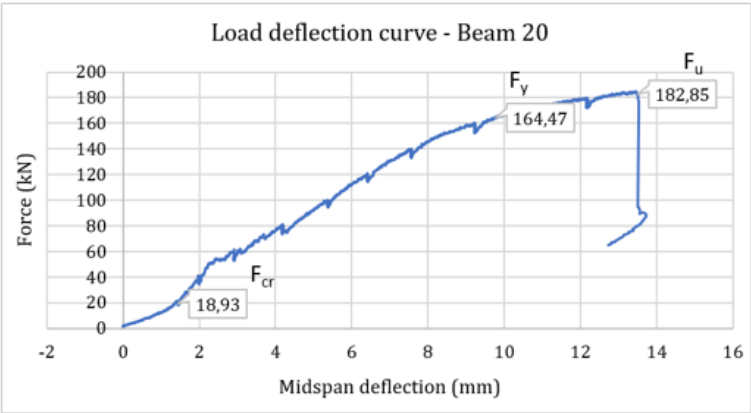
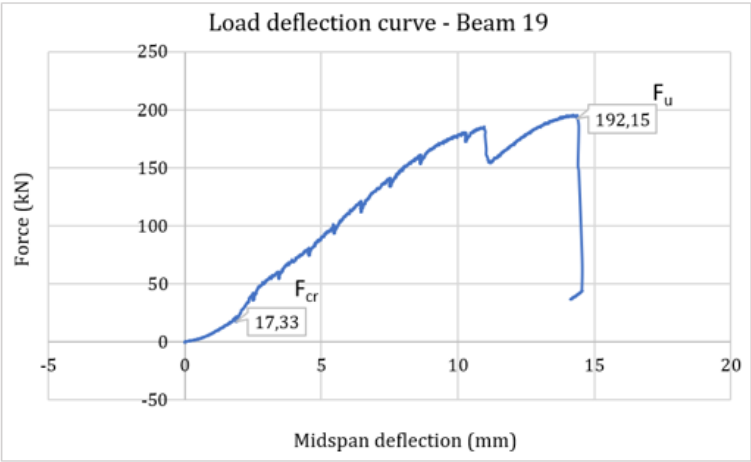


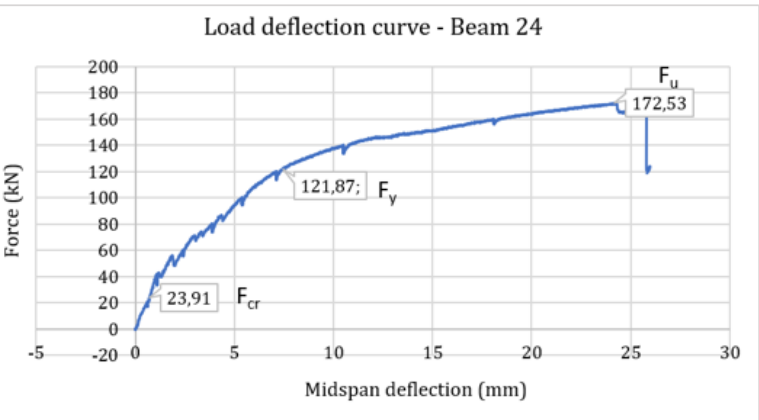
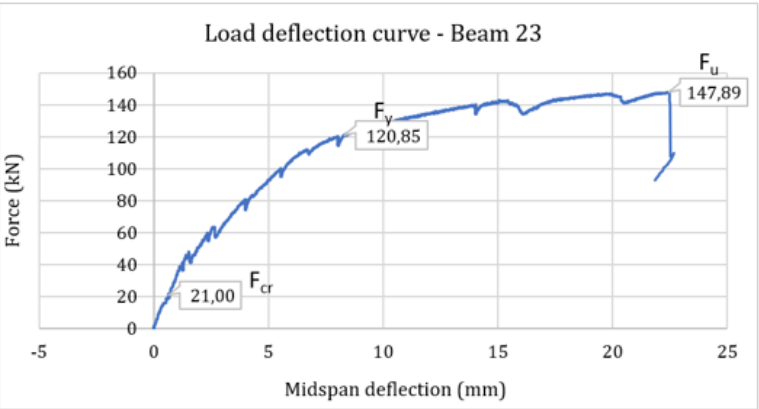
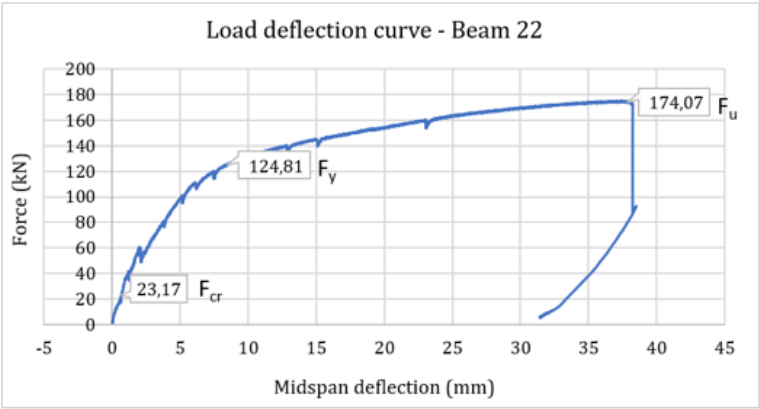




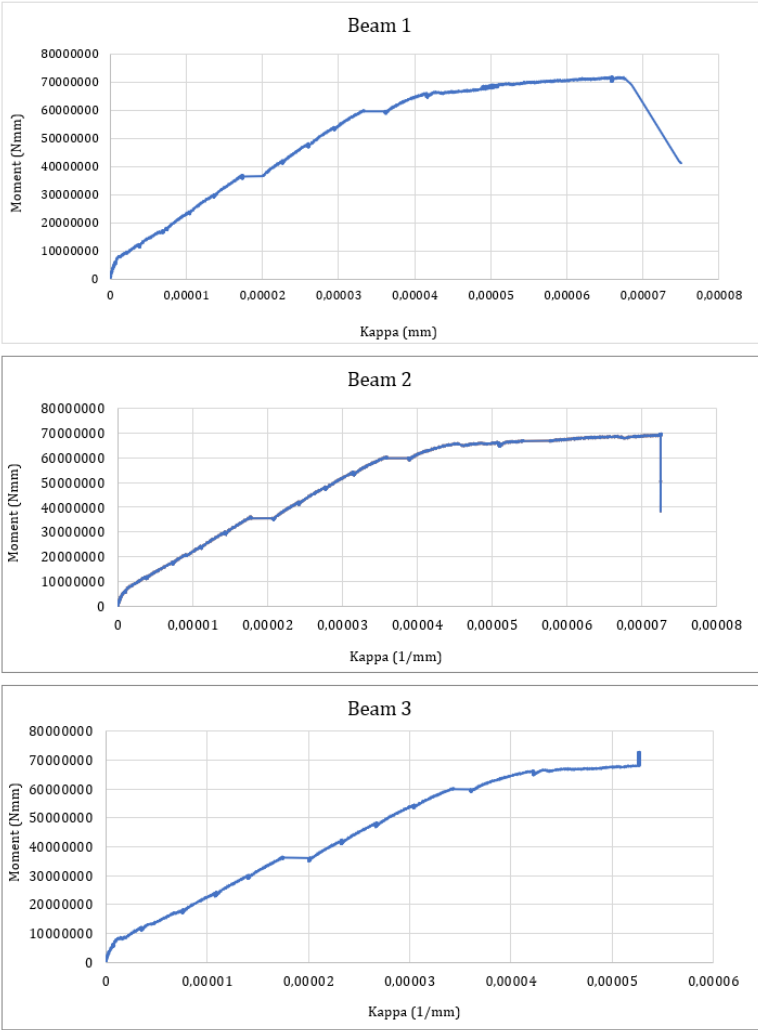


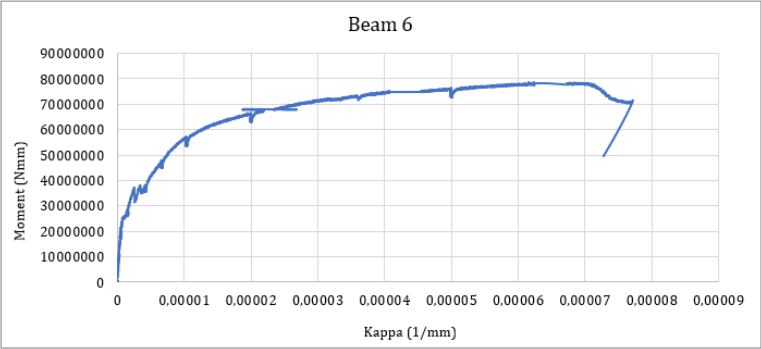
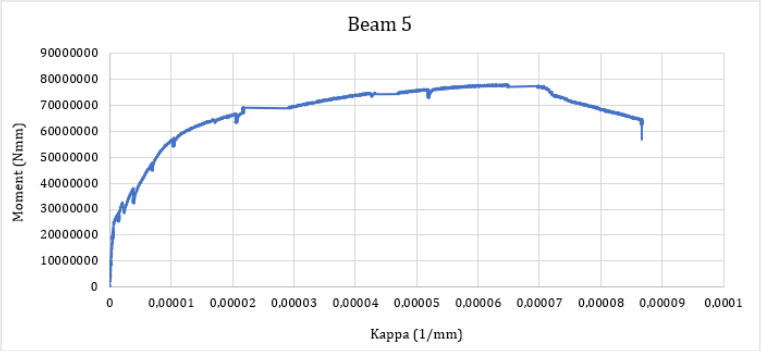
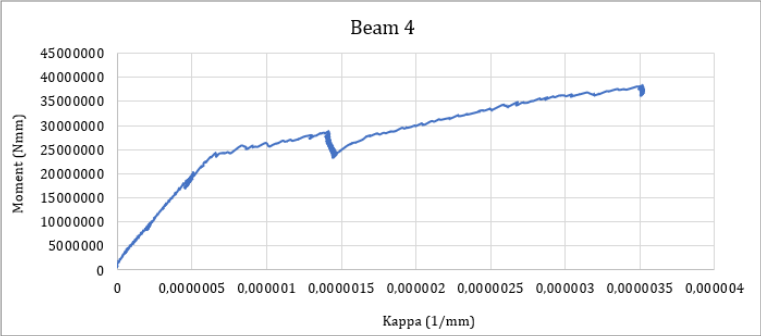


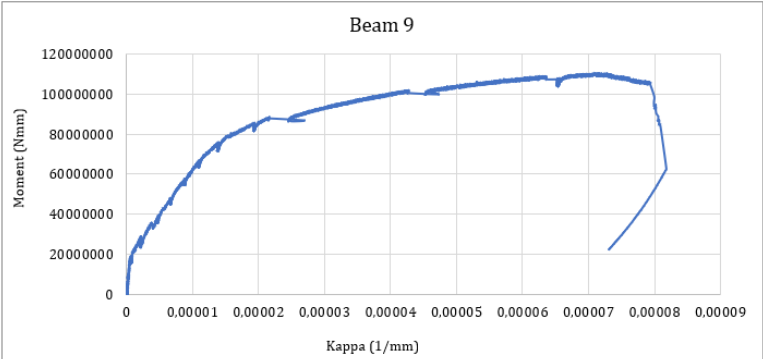
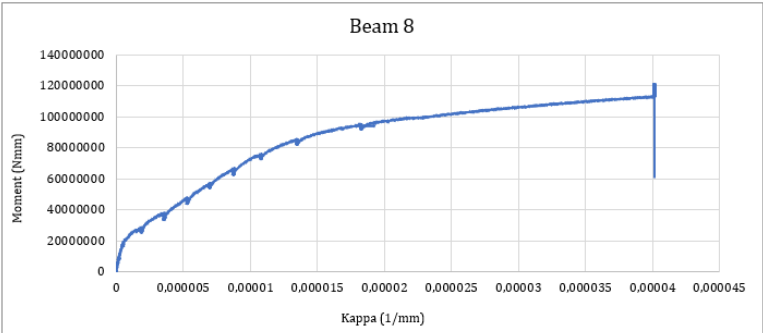
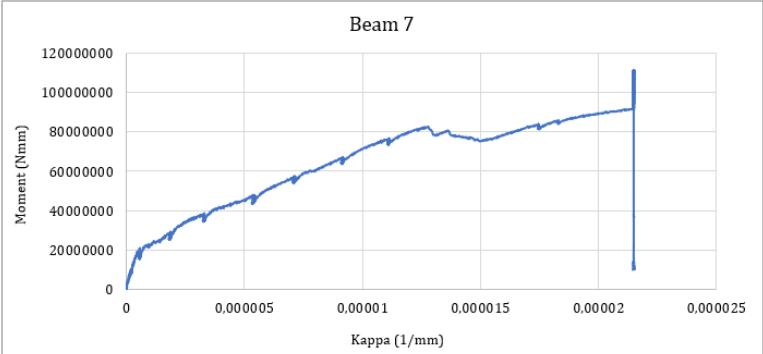


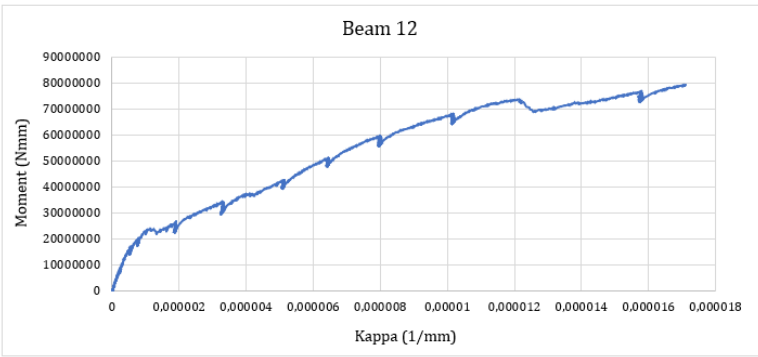
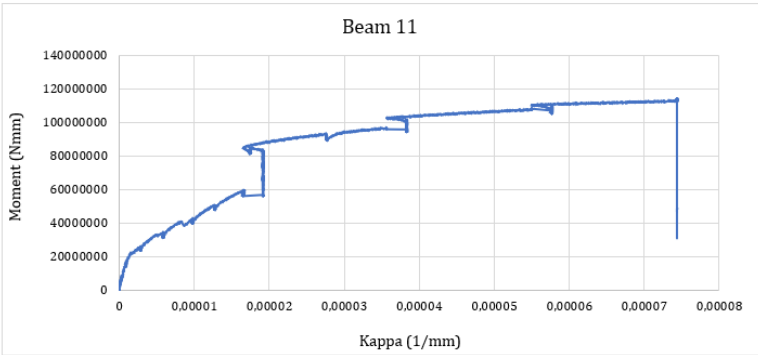
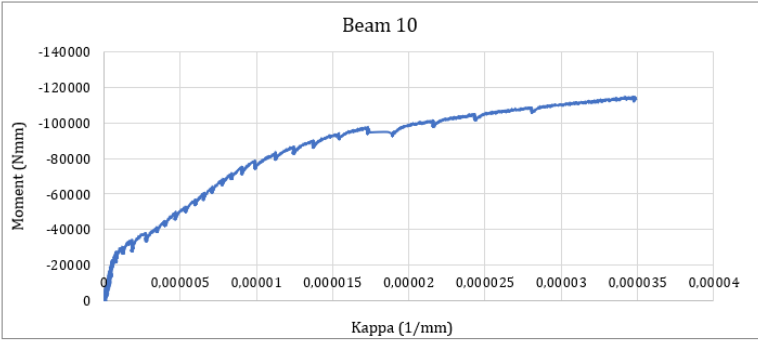


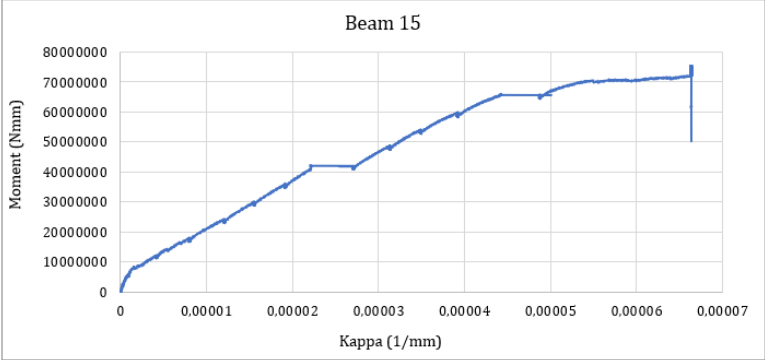
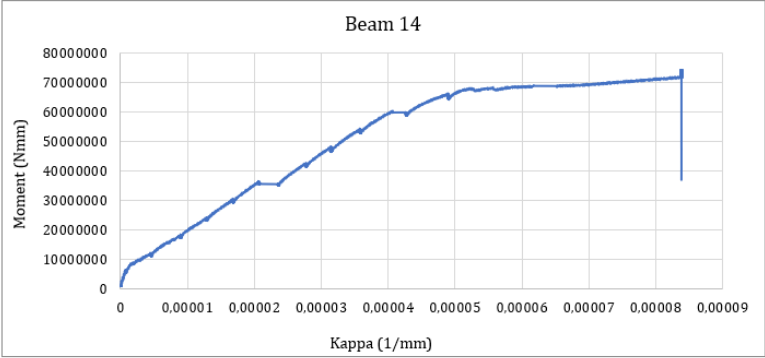
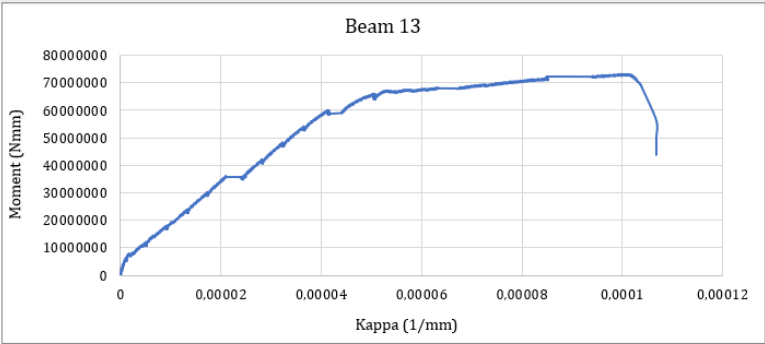
A.5. EXPERIMENTAL M- κ DIAGRAMS

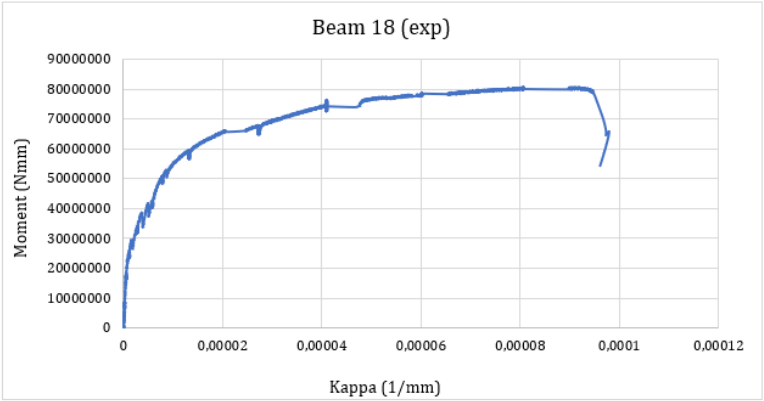
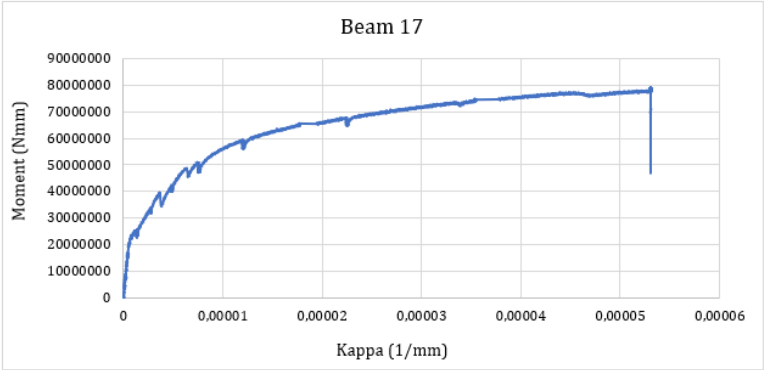
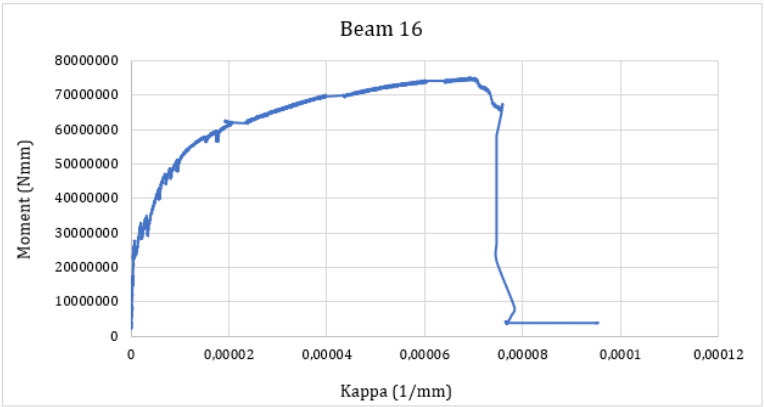


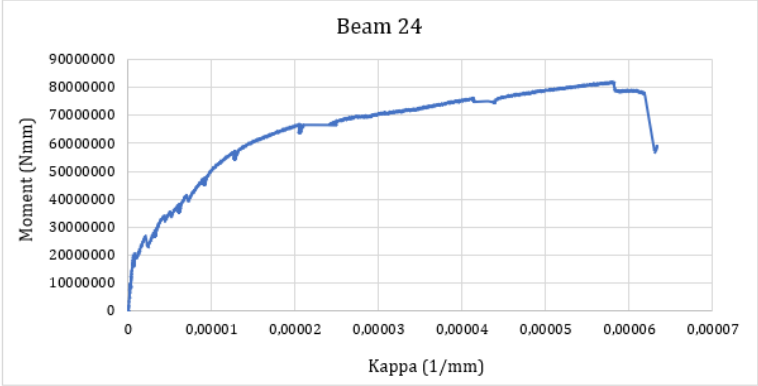
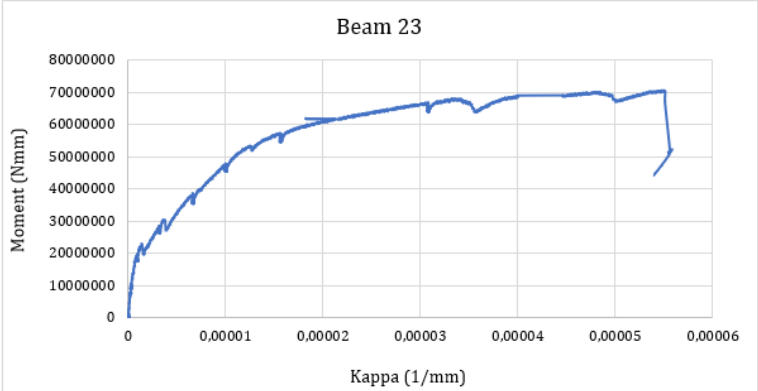
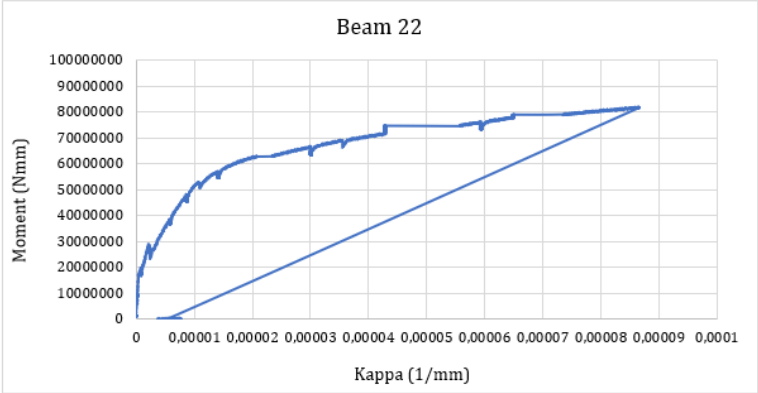




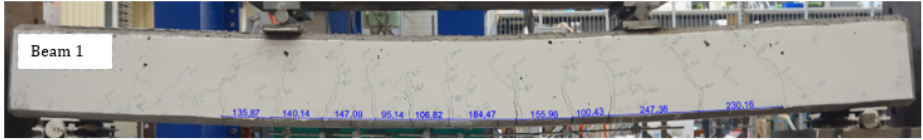






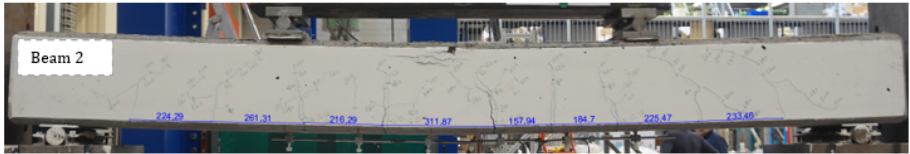


A.6. BEAM PICTURES AT FAILURE



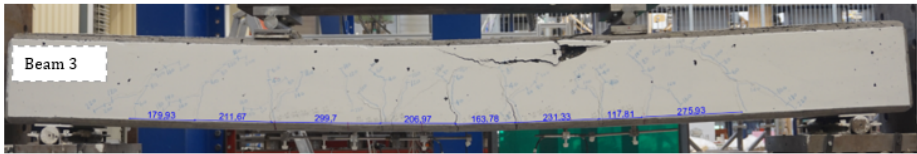
a = 600 mm
a/d = 3.53
tensile reinforcement = 5.41 %

Failure mode: Flexure
Predicted failure load: 200.6 kN
Experimental failure load: 240.4 kN



a = 600 mm
a/d = 3.53
tensile reinforcement = 5.41 %

Failure mode: Flexure
Predicted failure load: 200.6 kN
Experimental failure load: 231.7 kN



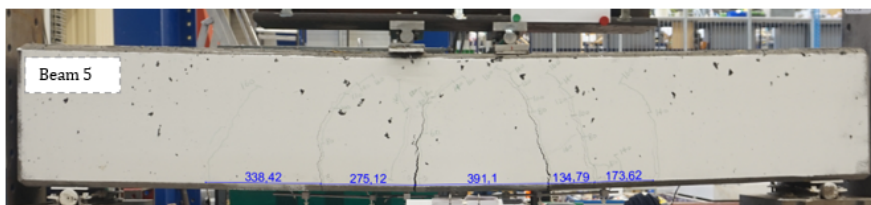
a = 600 mm
a/d = 3.53
tensile reinforcement = 5.41 %

Failure mode: Flexure
Predicted failure load: 200.6 kN
Experimental failure load: 241.7 kN

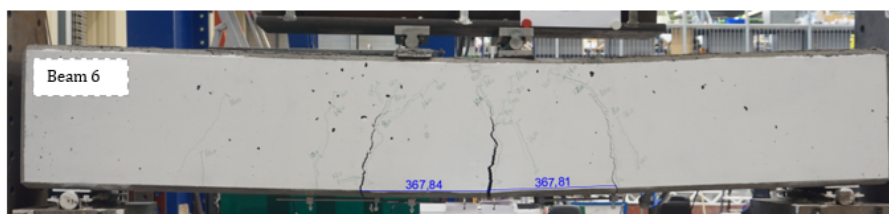


a = 950 mm
a/d = 3.01
tensile reinforcement = 1.25 %

Failure mode: Flexure
Predicted failure load: 141.3 kN
Experimental failure load: 160 kN



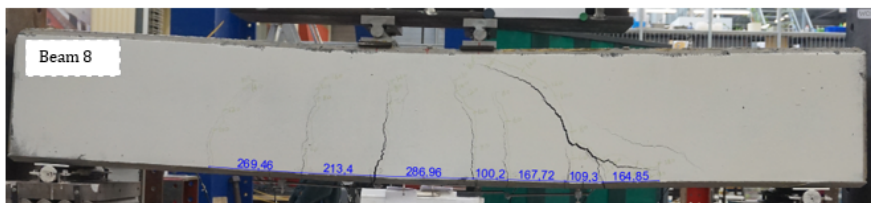
a = 950 mm	Failure mode:	Flexure
a/d = 3.01	Predicted failure load:	141.3 kN
tensile reinforcement = 1.25 %	Experimental failure load:	164.1 kN



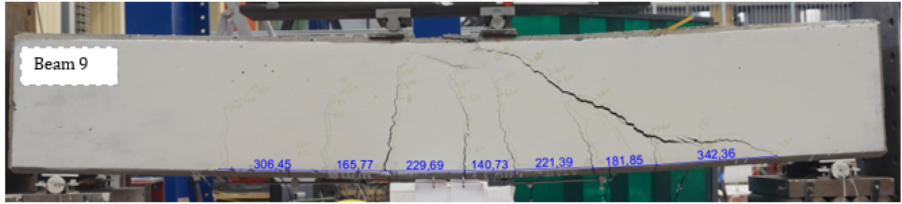
a = 950 mm	Failure mode:	Flexure
a/d = 3.01	Predicted failure load:	141.3 kN
tensile reinforcement = 1.25 %	Experimental failure load:	165.5 kN



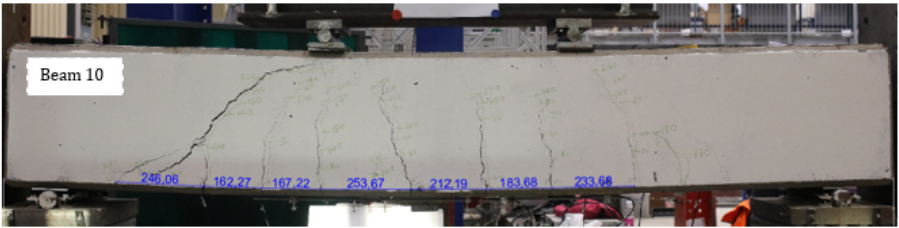
a = 950 mm	Failure mode:	Shear Compression
a/d = 3.03	Predicted failure load:	87.6 kN
tensile reinforcement = 3.2 %	Experimental failure load:	117.1 kN



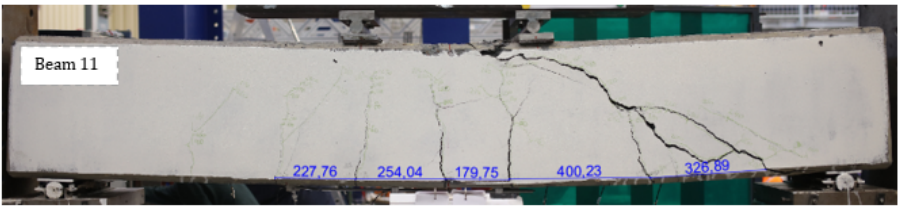
a = 950 mm	Failure mode:	Shear compression
a/d = 3.03	Predicted failure load:	87.6 kN
tensile reinforcement = 3.2 %	Experimental failure load:	127.57 kN



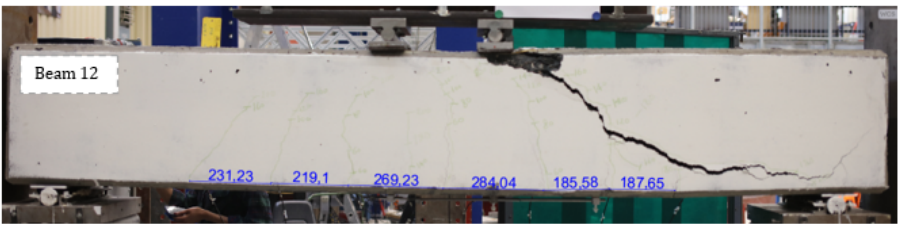
a = 950 mm	Failure mode:	Shear compression
a/d = 3.03	Predicted failure load:	87.6 kN
tensile reinforcement = 3.2 %	Experimental failure load:	116.3 kN



a = 750 mm	Failure mode:	Flexure shear
a/d = 2.39	Predicted failure load:	87.6 kN
tensile reinforcement = 3.2 %	Experimental failure load:	167.4 kN



a = 850 mm	Failure mode:	Flexure shear
a/d = 2.71	Predicted failure load:	87.6 kN
tensile reinforcement = 3.2 %	Experimental failure load:	135 kN



a = 950 mm	Failure mode:	Shear compression
a/d = 3.03	Predicted failure load:	87.6 kN
tensile reinforcement = 3.2 %	Experimental failure load:	



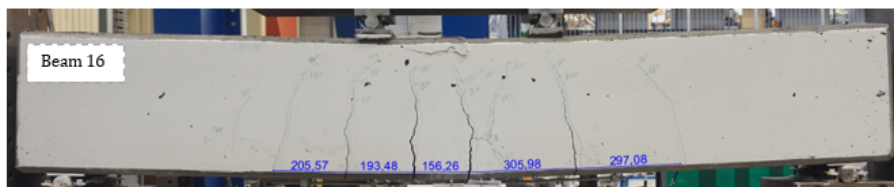
a = 600 mm	Failure mode:	Flexure
a/d = 3.53	Predicted failure load:	200.6 kN
tensile reinforcement = 5.41 %	Experimental failure load:	244 kN



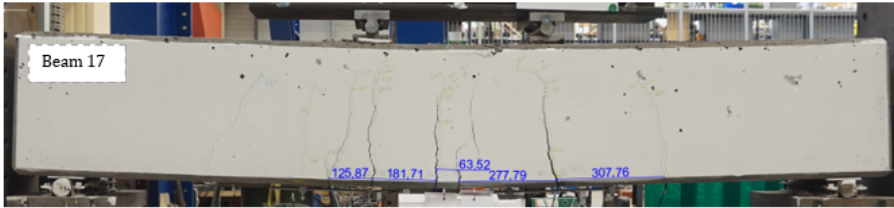
a = 600 mm	Failure mode:	Flexure
a/d = 3.53	Predicted failure load:	200.6 kN
tensile reinforcement = 5.41 %	Experimental failure load:	247.6 kN



a = 600 mm	Failure mode:	Flexure
a/d = 3.53	Predicted failure load:	200.6 kN
tensile reinforcement = 5.41 %	Experimental failure load:	252 kN

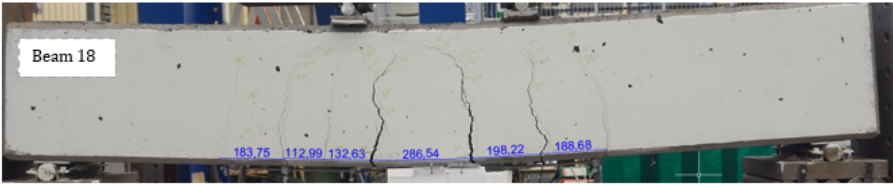


a = 850 mm	Failure mode:	Flexure
a/d = 2.69	Predicted failure load:	158 kN
tensile reinforcement = 1.25 %	Experimental failure load:	176.7 kN



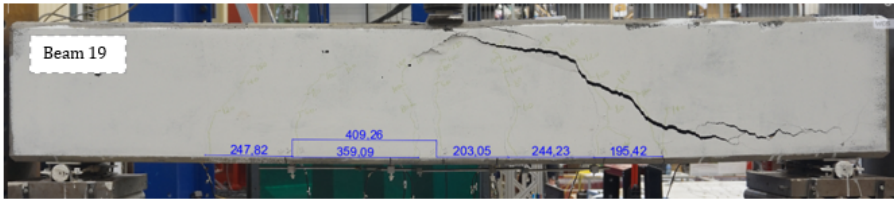
a = 850 mm
a/d = 2.69
tensile reinforcement = 1.25 %

Failure mode: Flexure
Predicted failure load: 158 kN
Experimental failure load: 186.8 kN



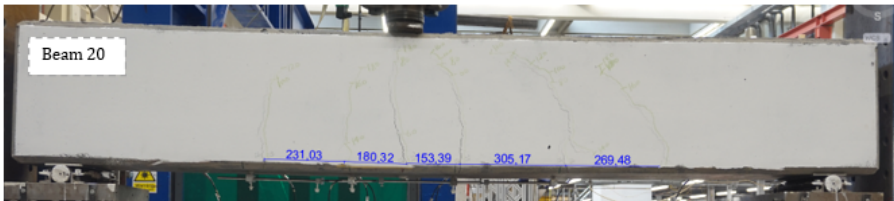
a = 850 mm
a/d = 2.69
tensile reinforcement = 1.25 %

Failure mode: Flexure
Predicted failure load: 158 kN
Experimental failure load: 190.3 kN



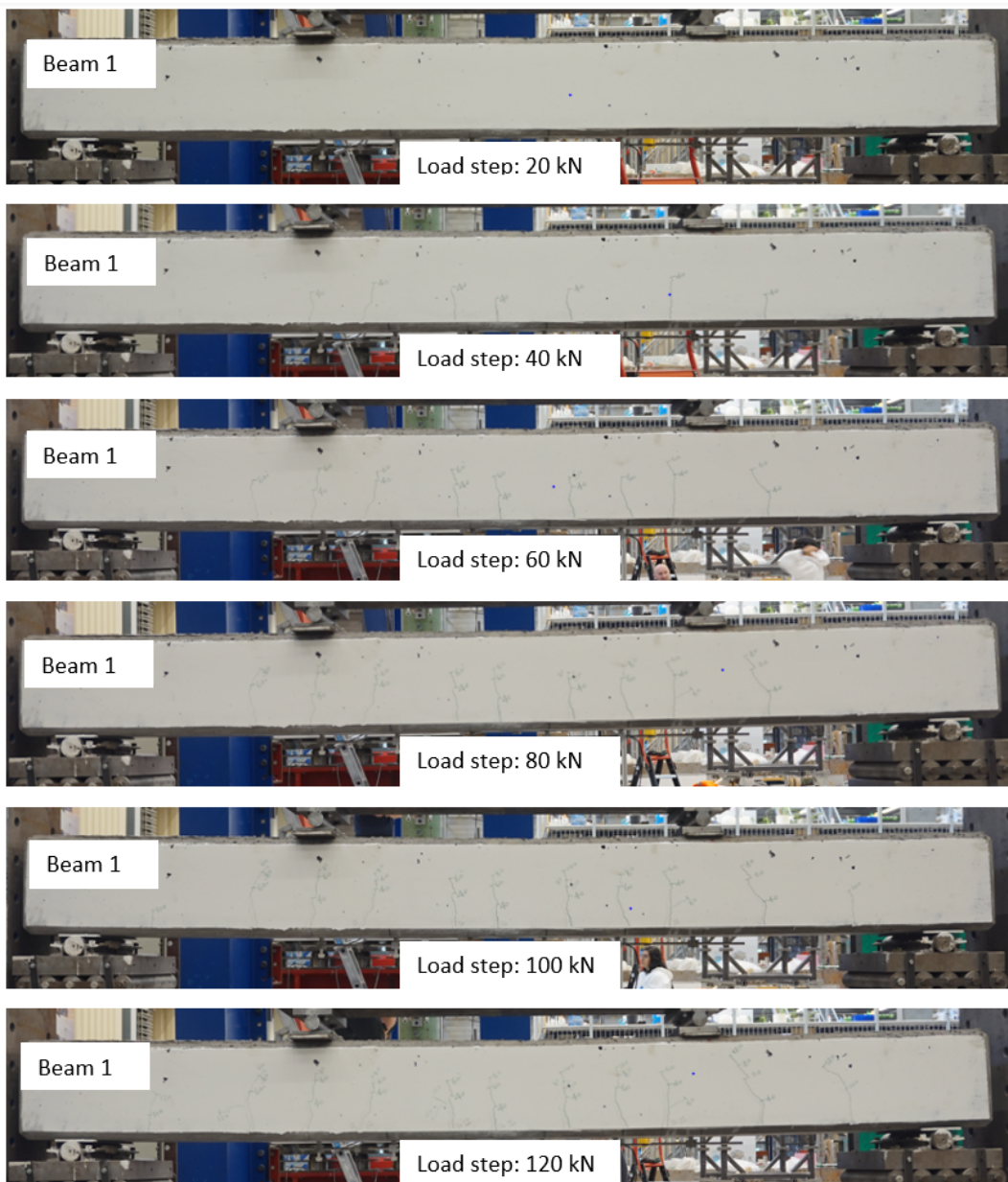
a = 1100 mm
a/d = 3.5
tensile reinforcement = 3.2 %

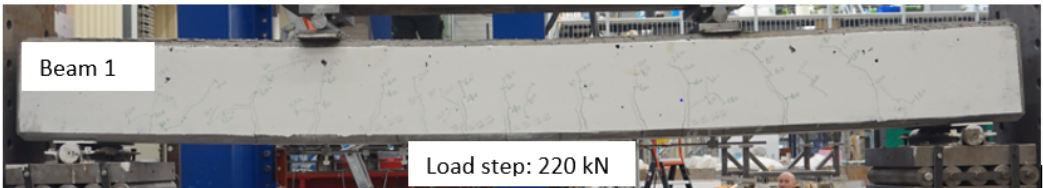
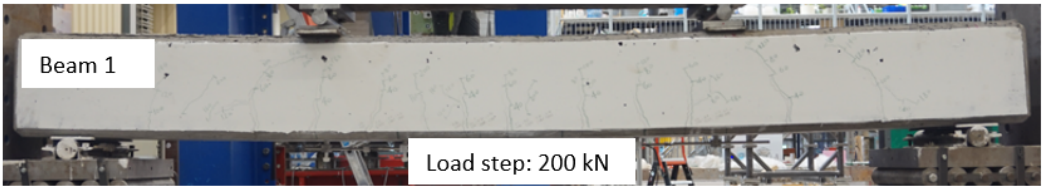
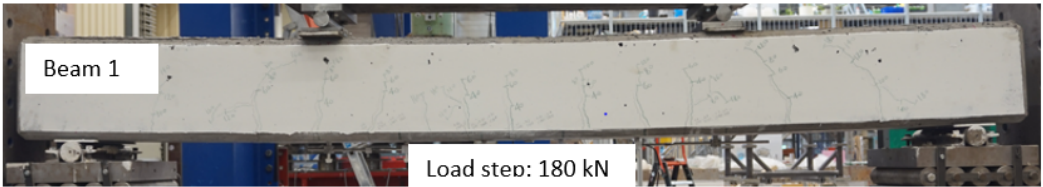
Failure mode: Shear compression
Predicted failure load:
Experimental failure load: 195.3 kN



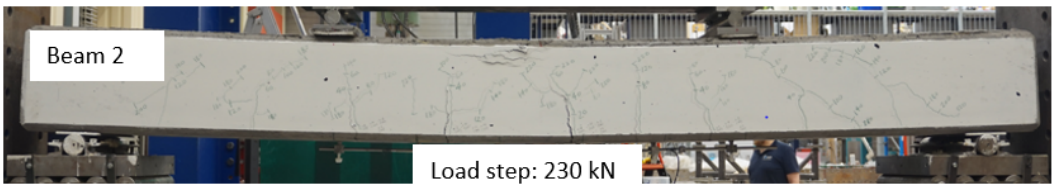
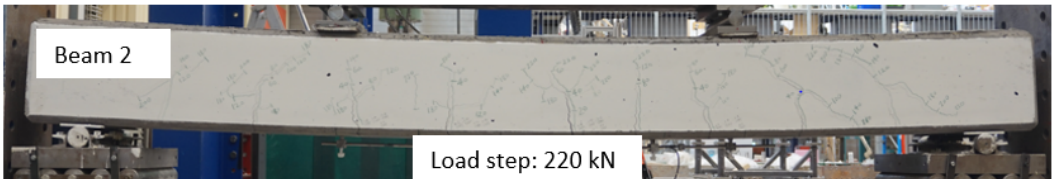
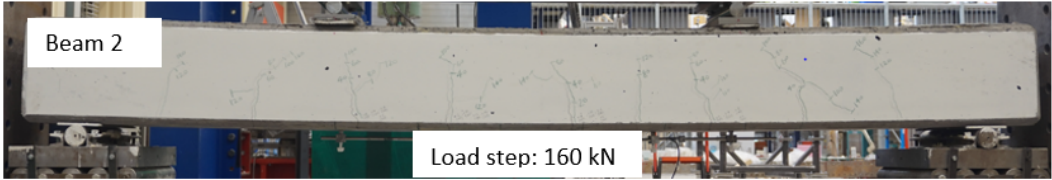
a = 950 mm
a/d = 3.5
tensile reinforcement = 3.2 %

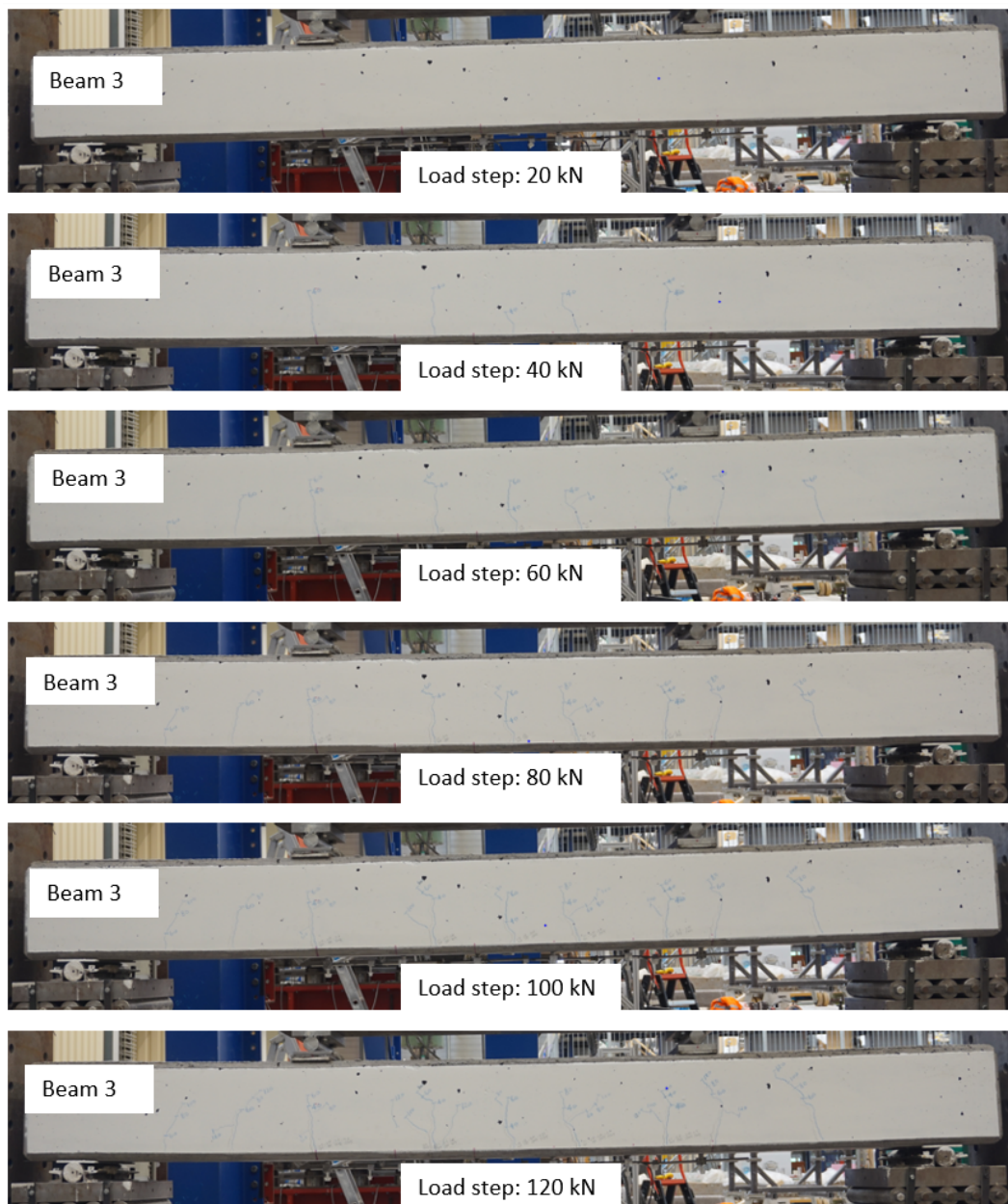
Failure mode: Shear compression
Predicted failure load:
Experimental failure load: 184.9 kN

A.7. INDIVIDUAL BEAM PICTURES AT EVERY LOAD STEP

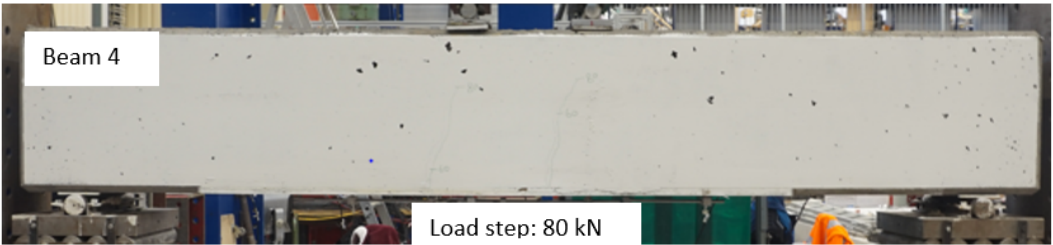
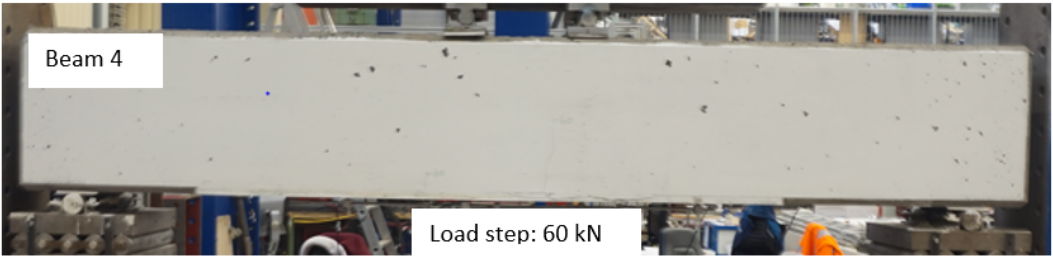
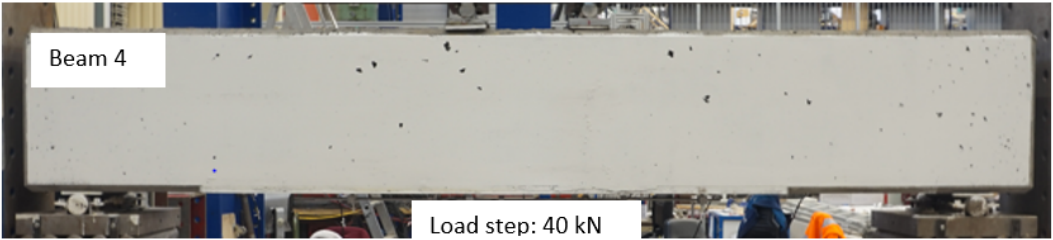
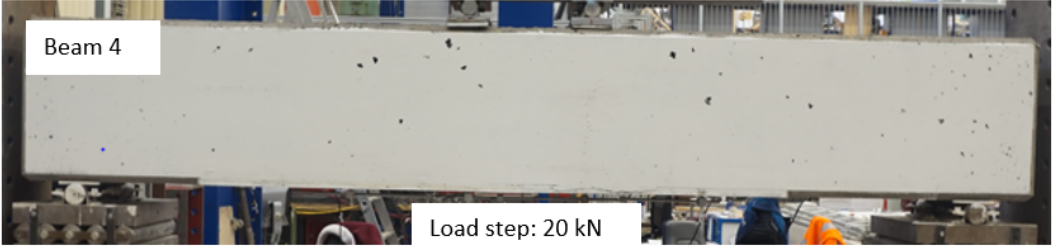


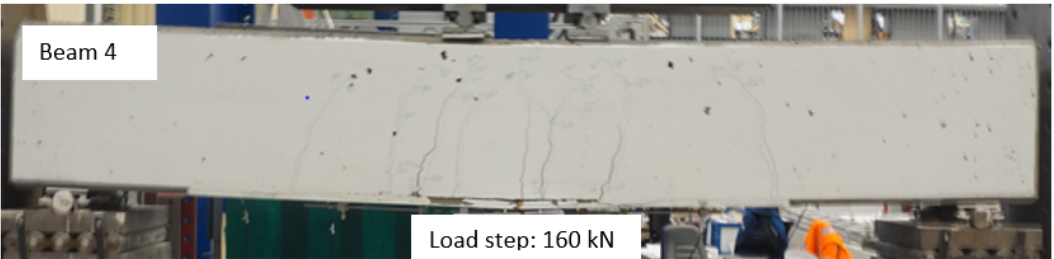
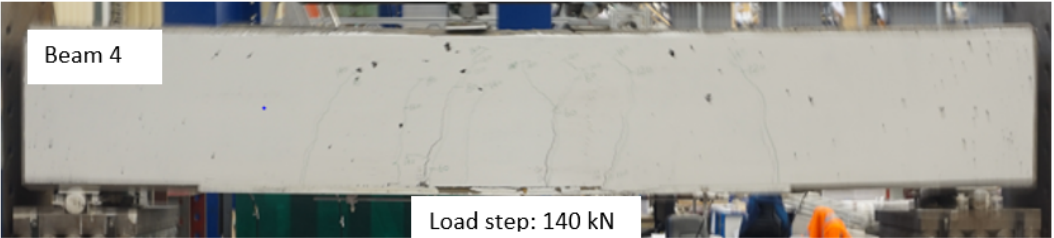
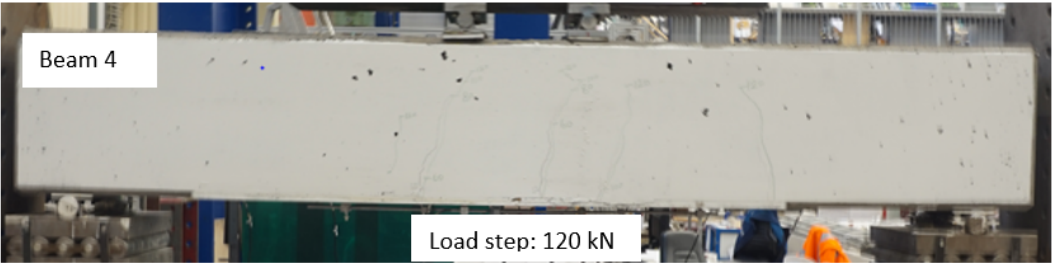
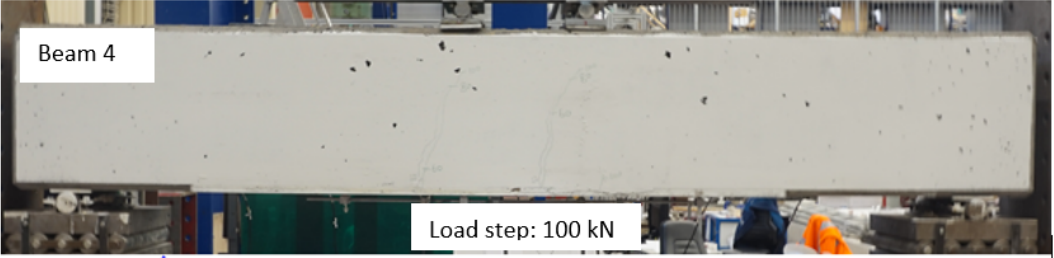


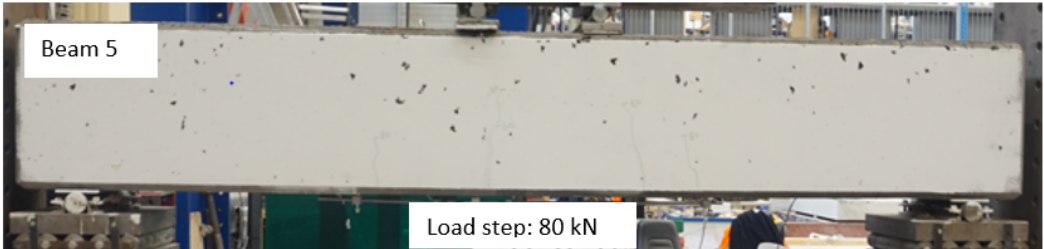
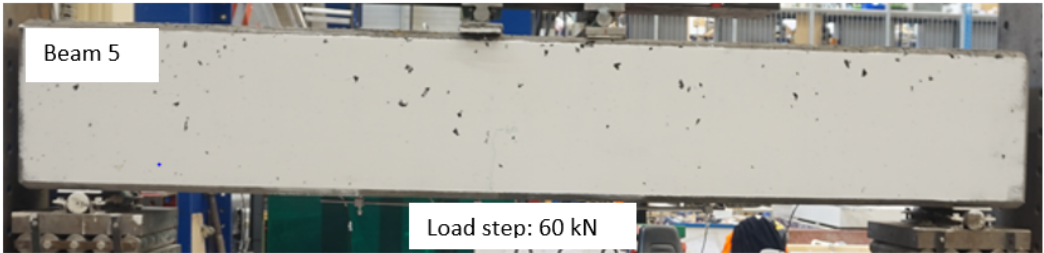
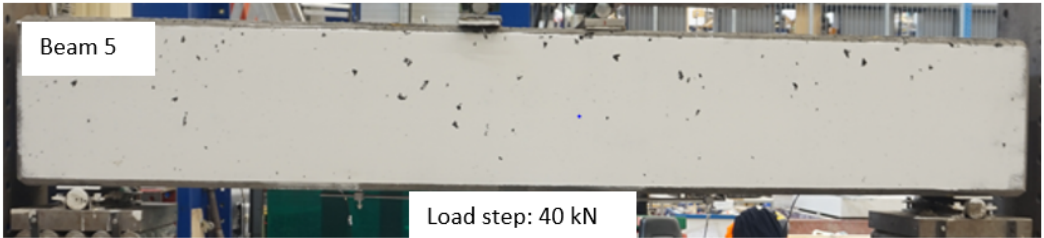


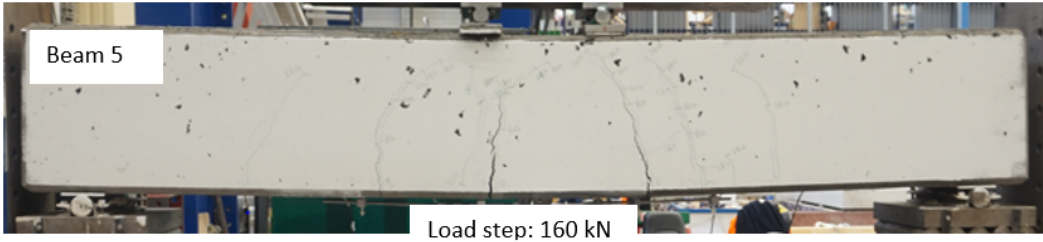
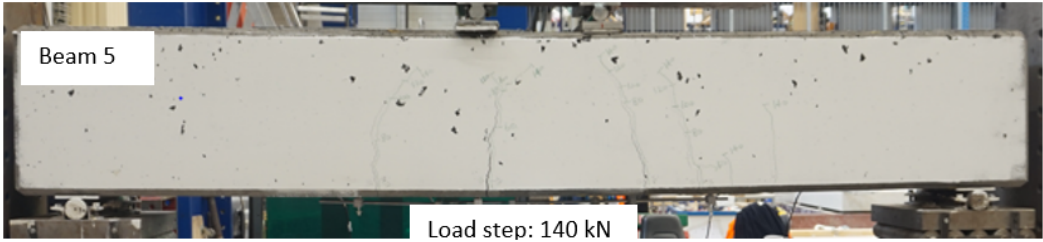
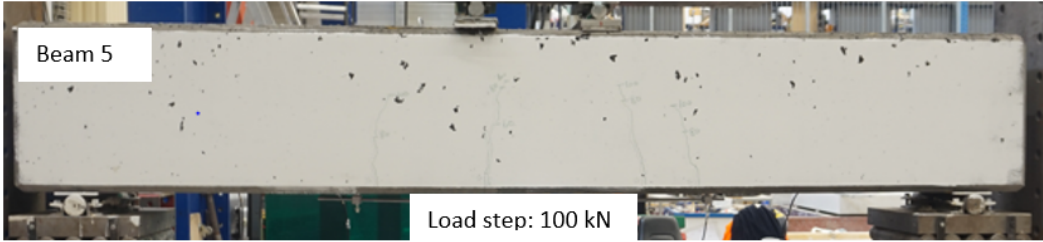






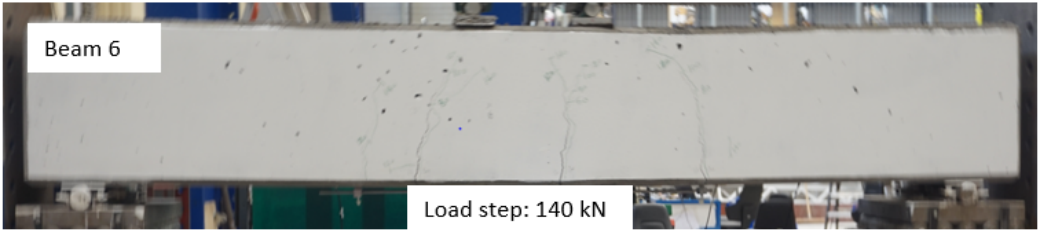
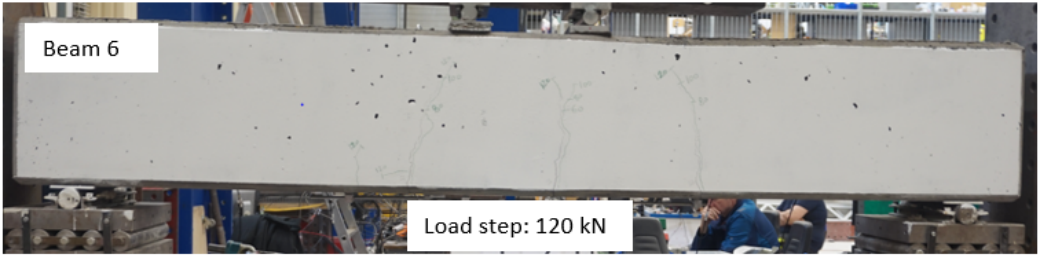


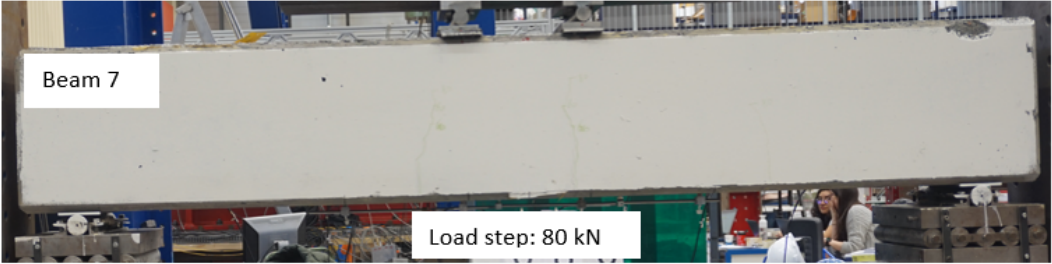
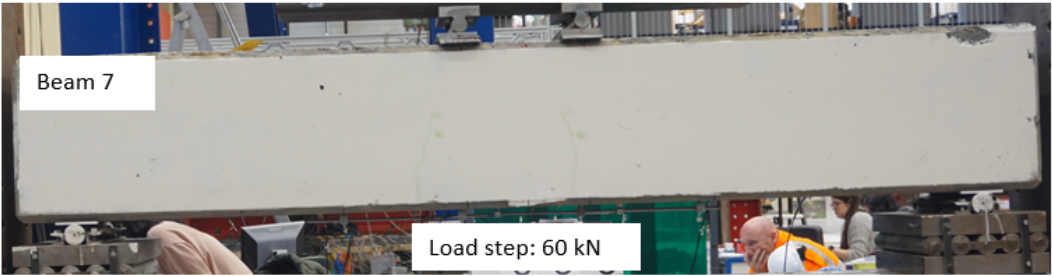
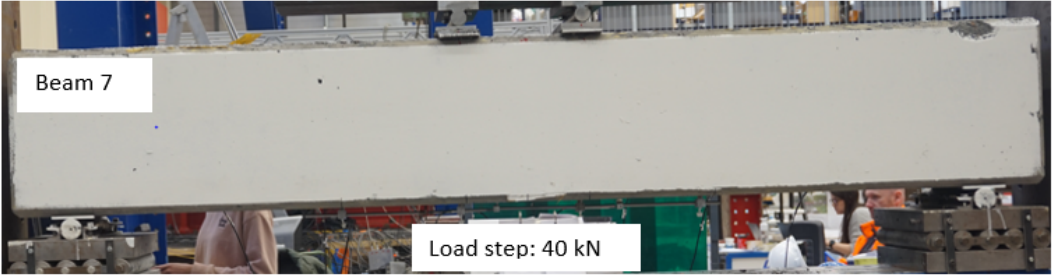


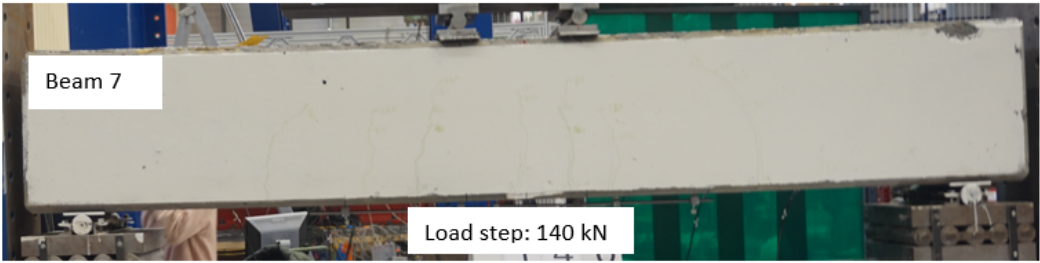
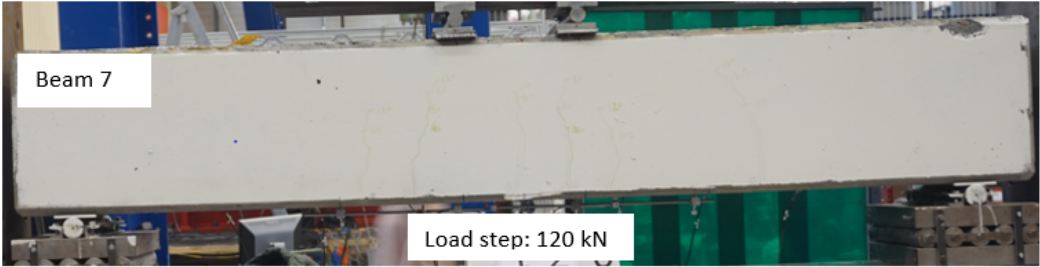
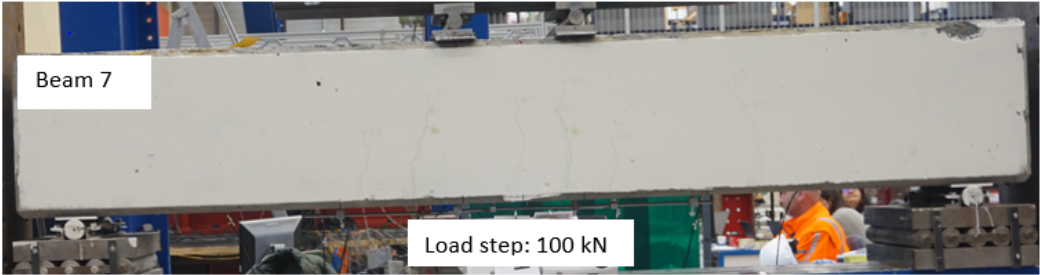


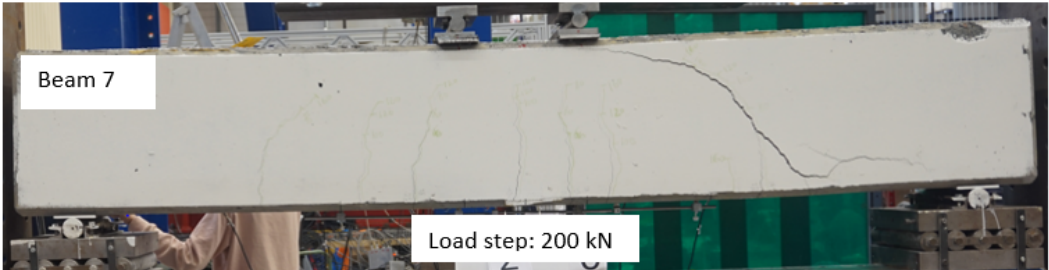
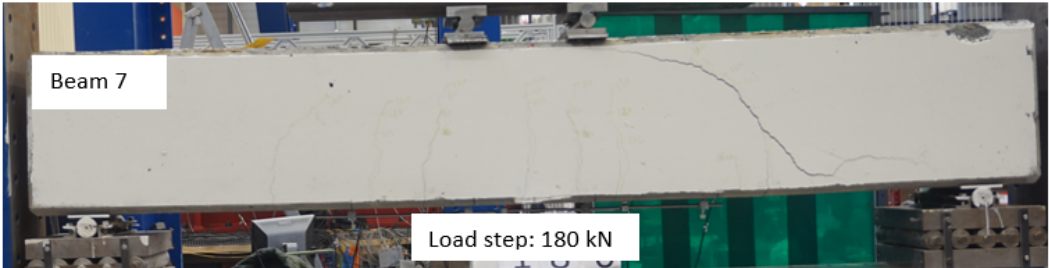


A

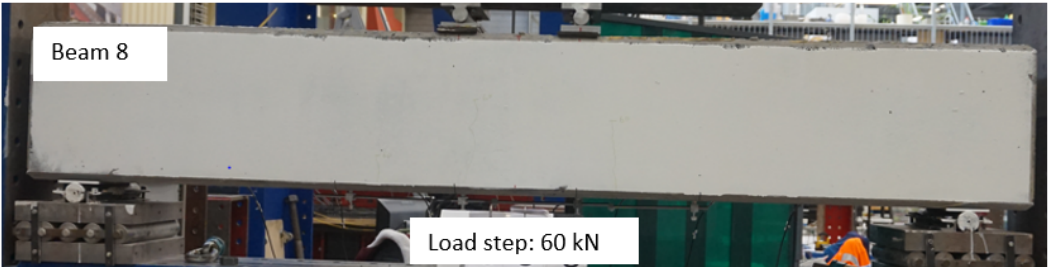


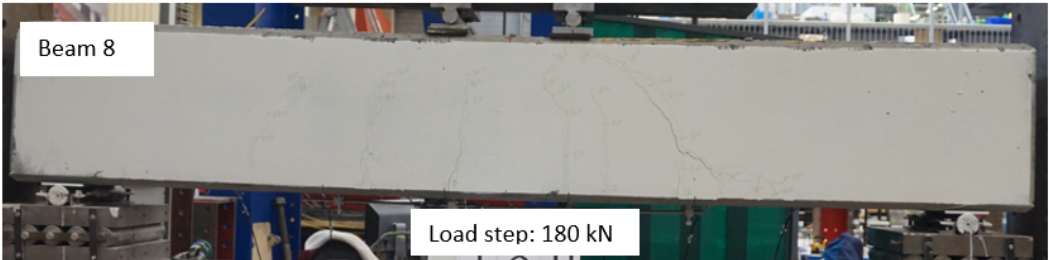
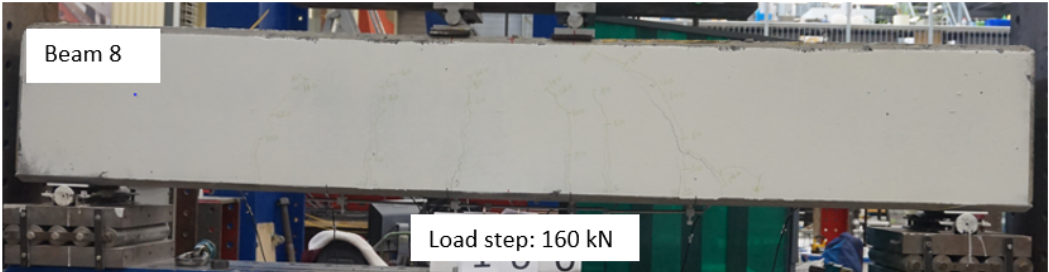
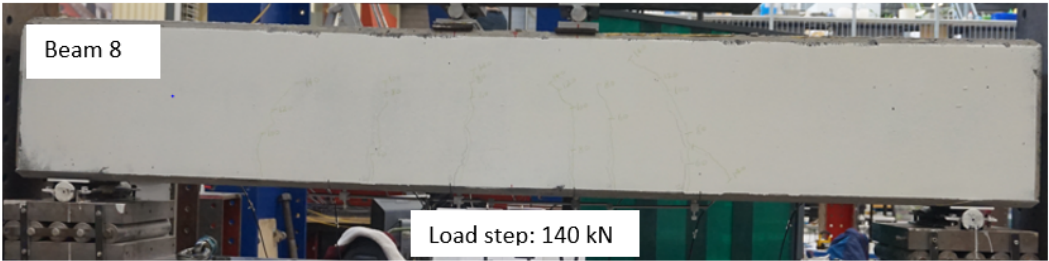
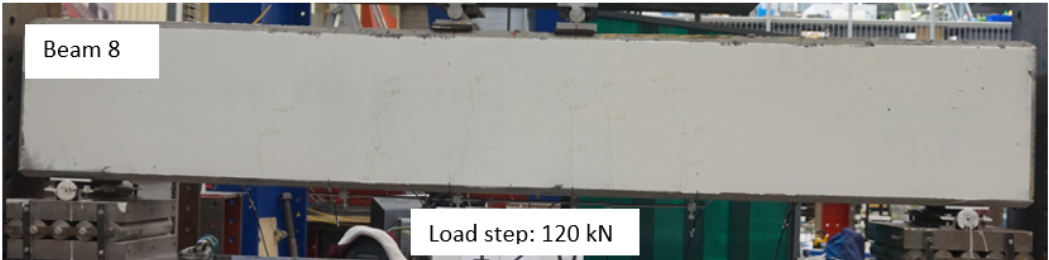


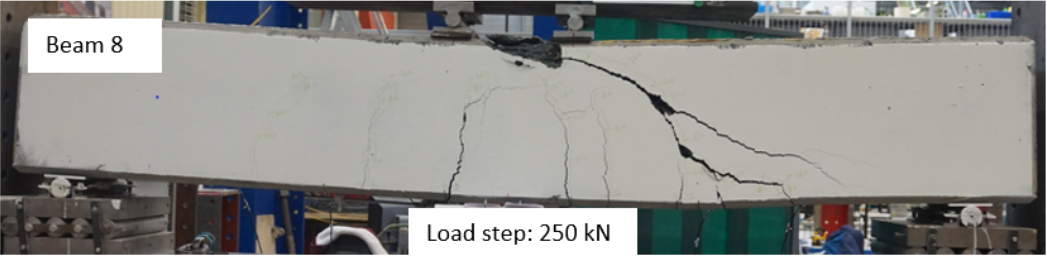
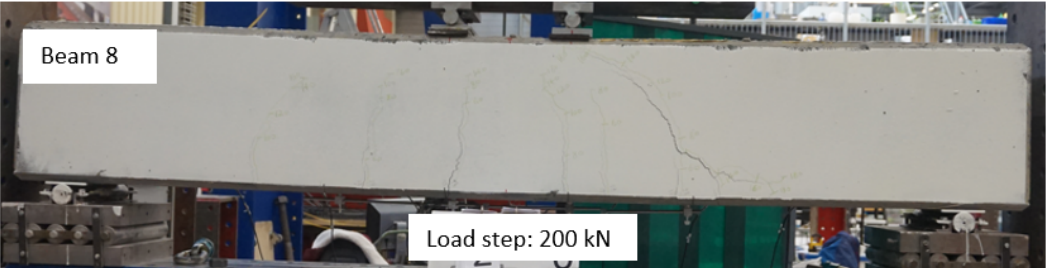


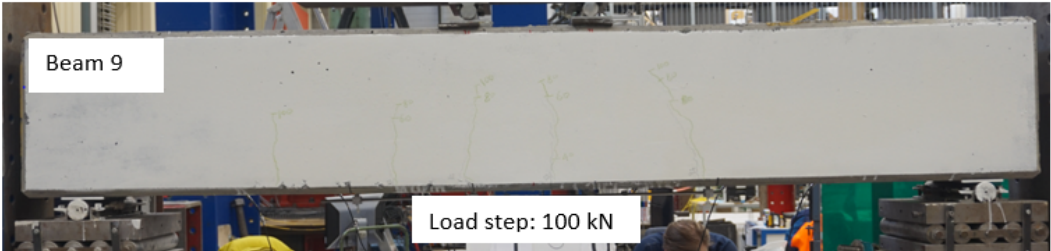
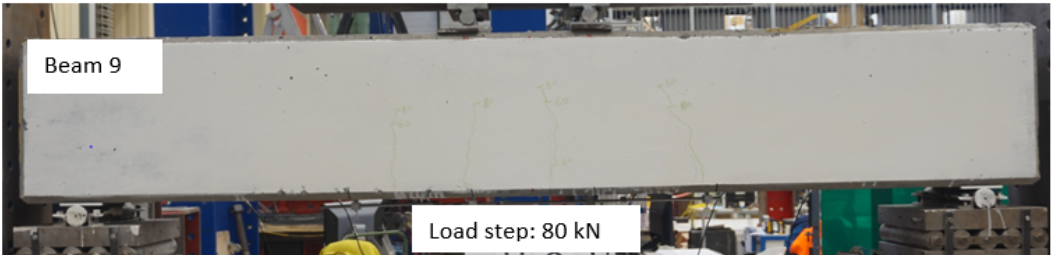
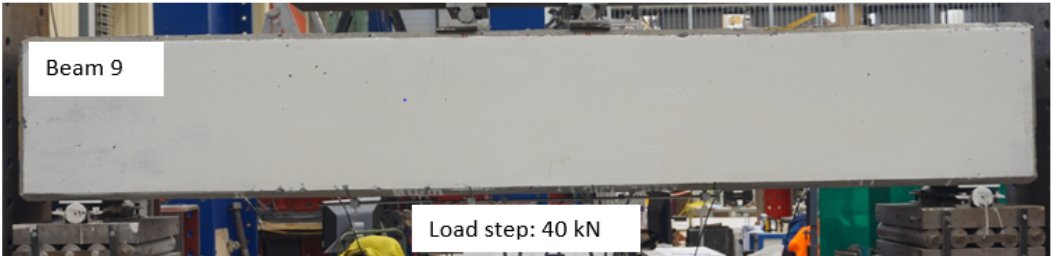


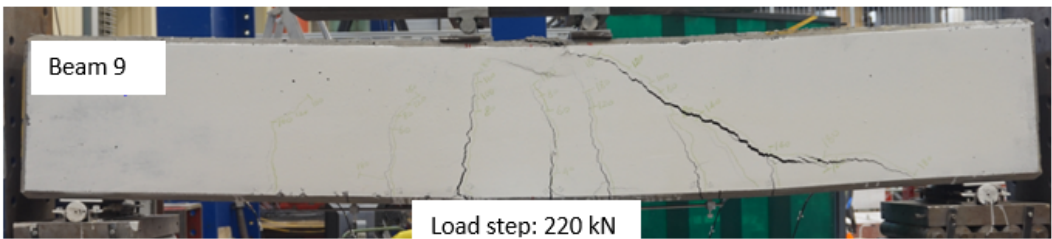
A

















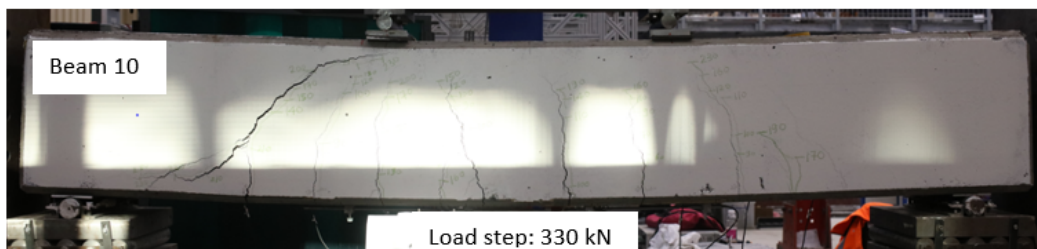
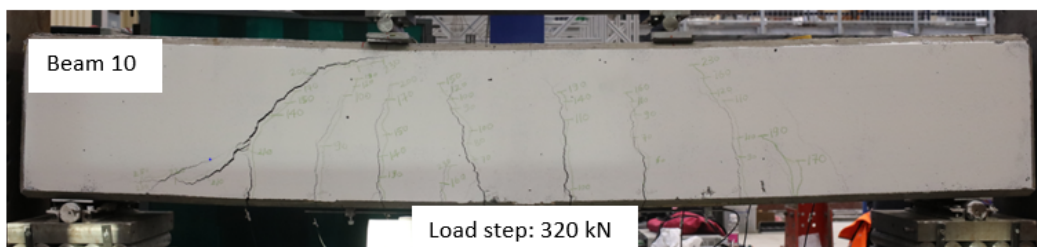
A

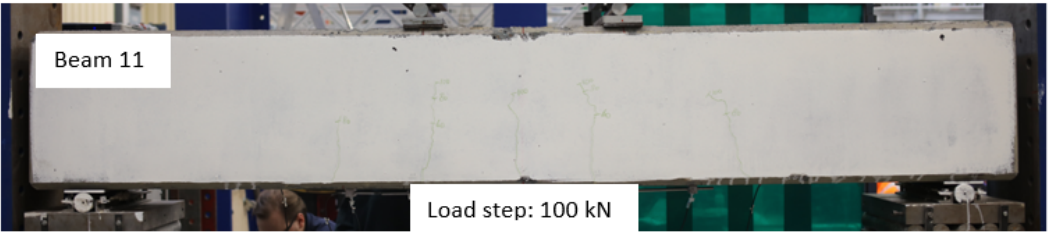
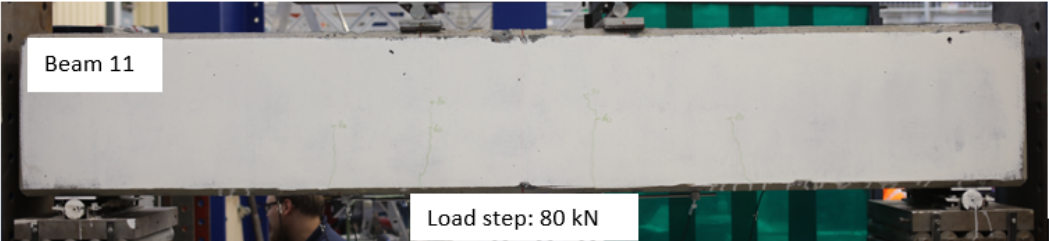
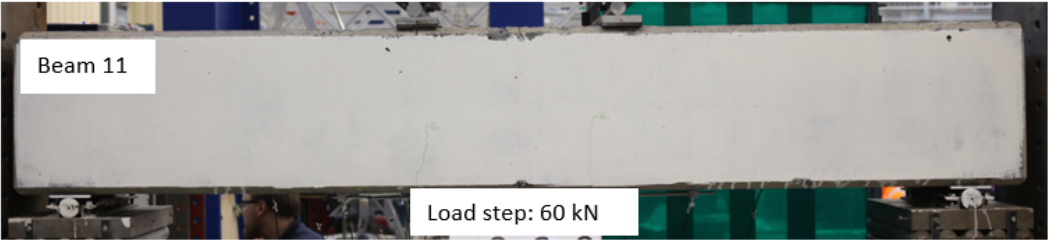




A

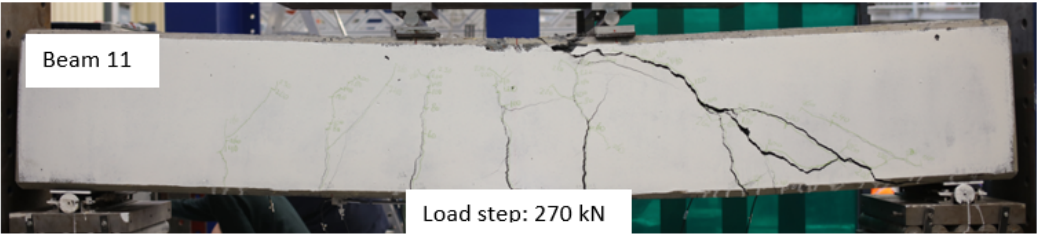
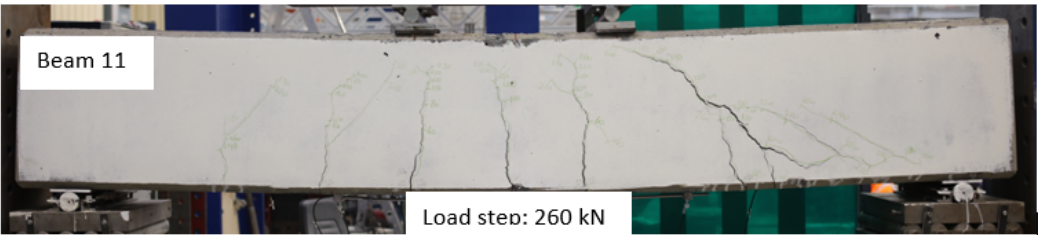
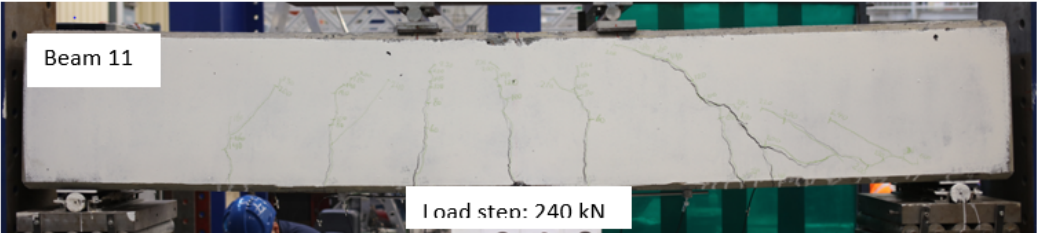
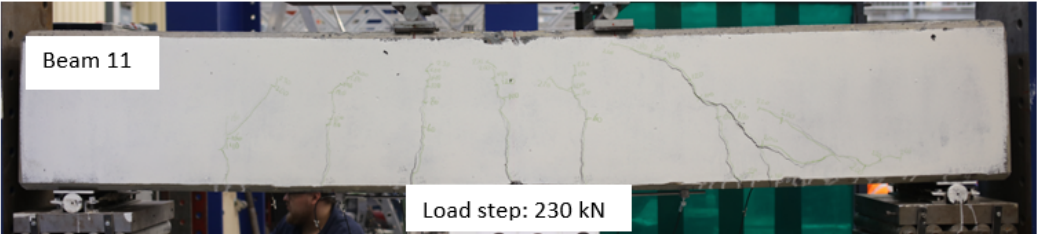
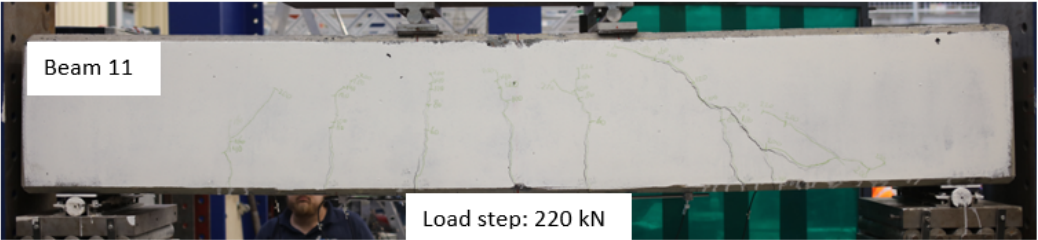


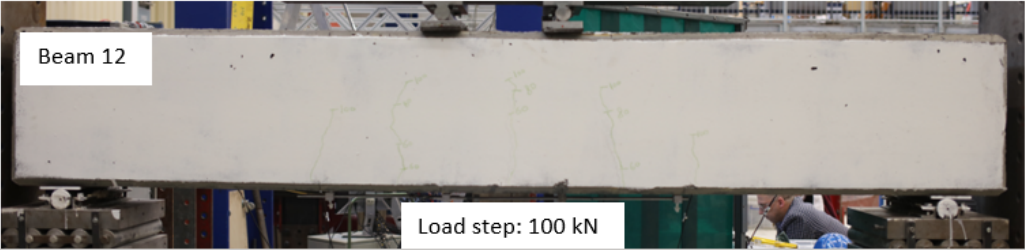
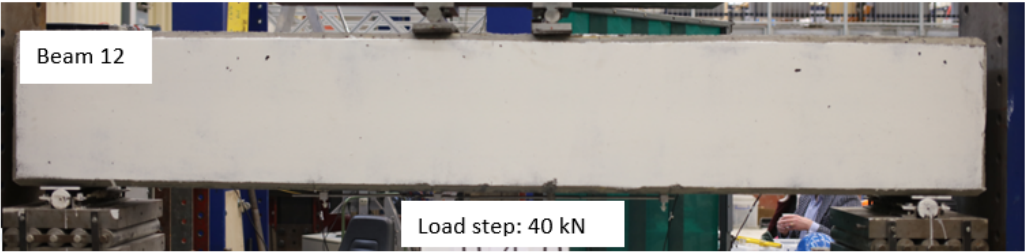




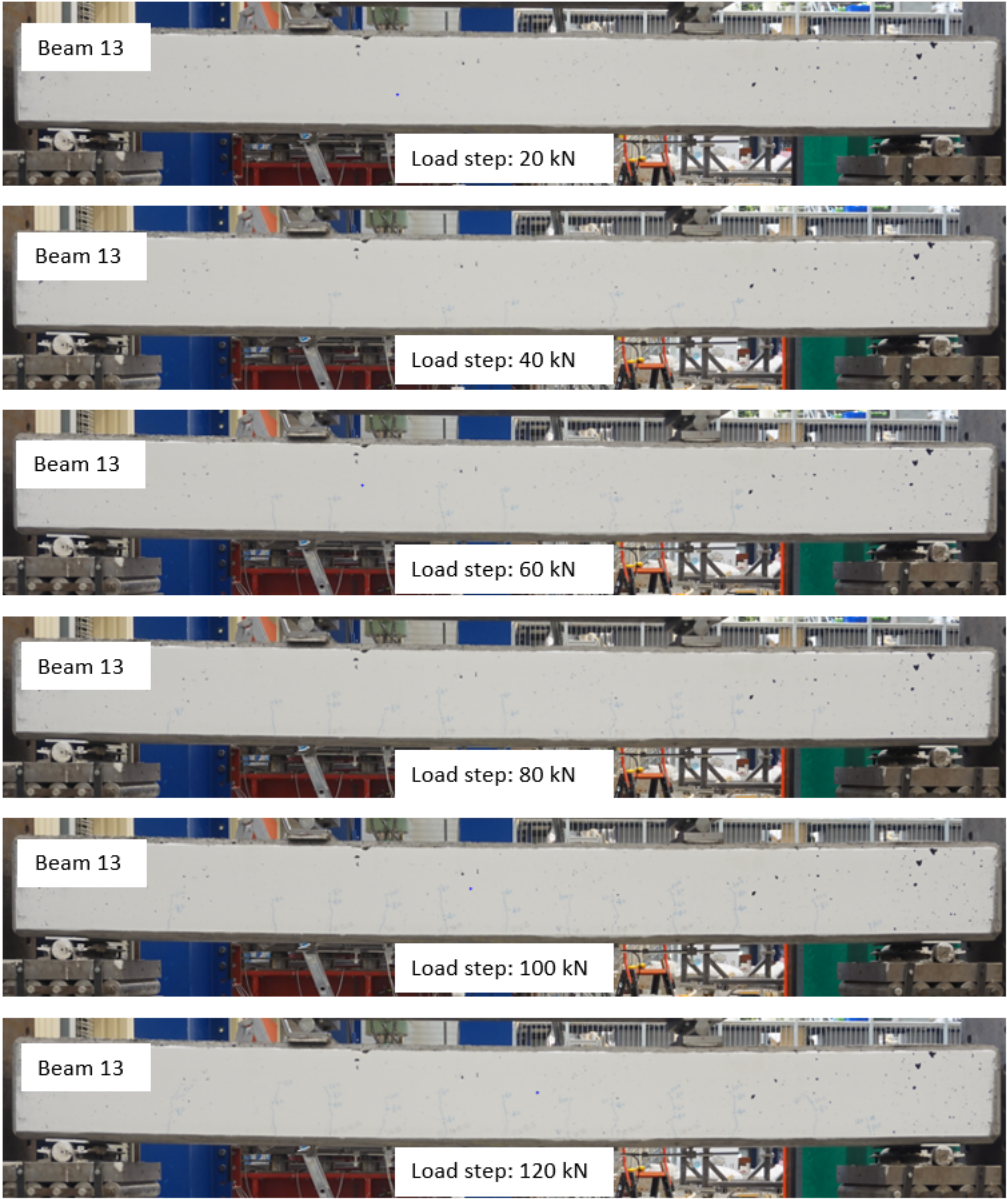


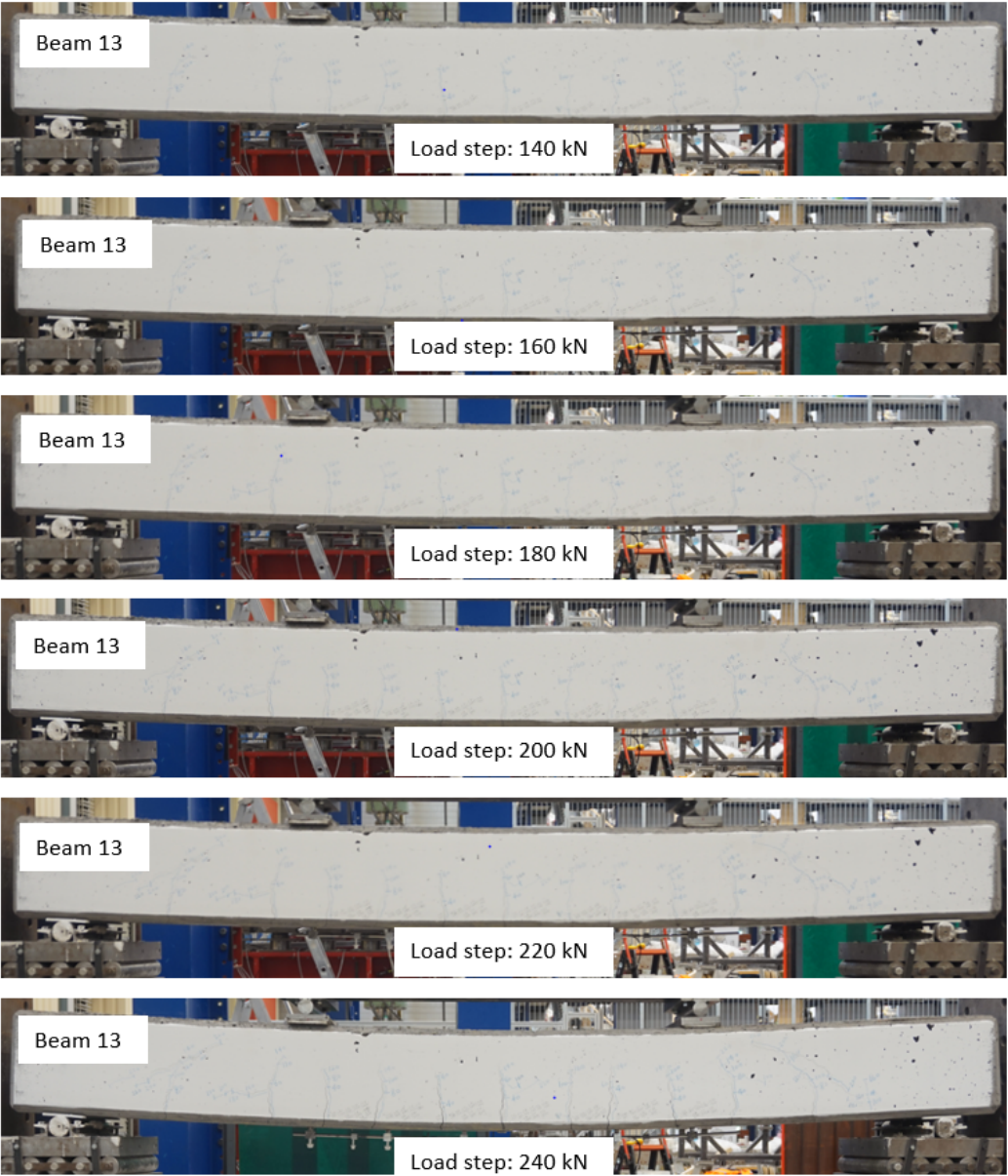
A

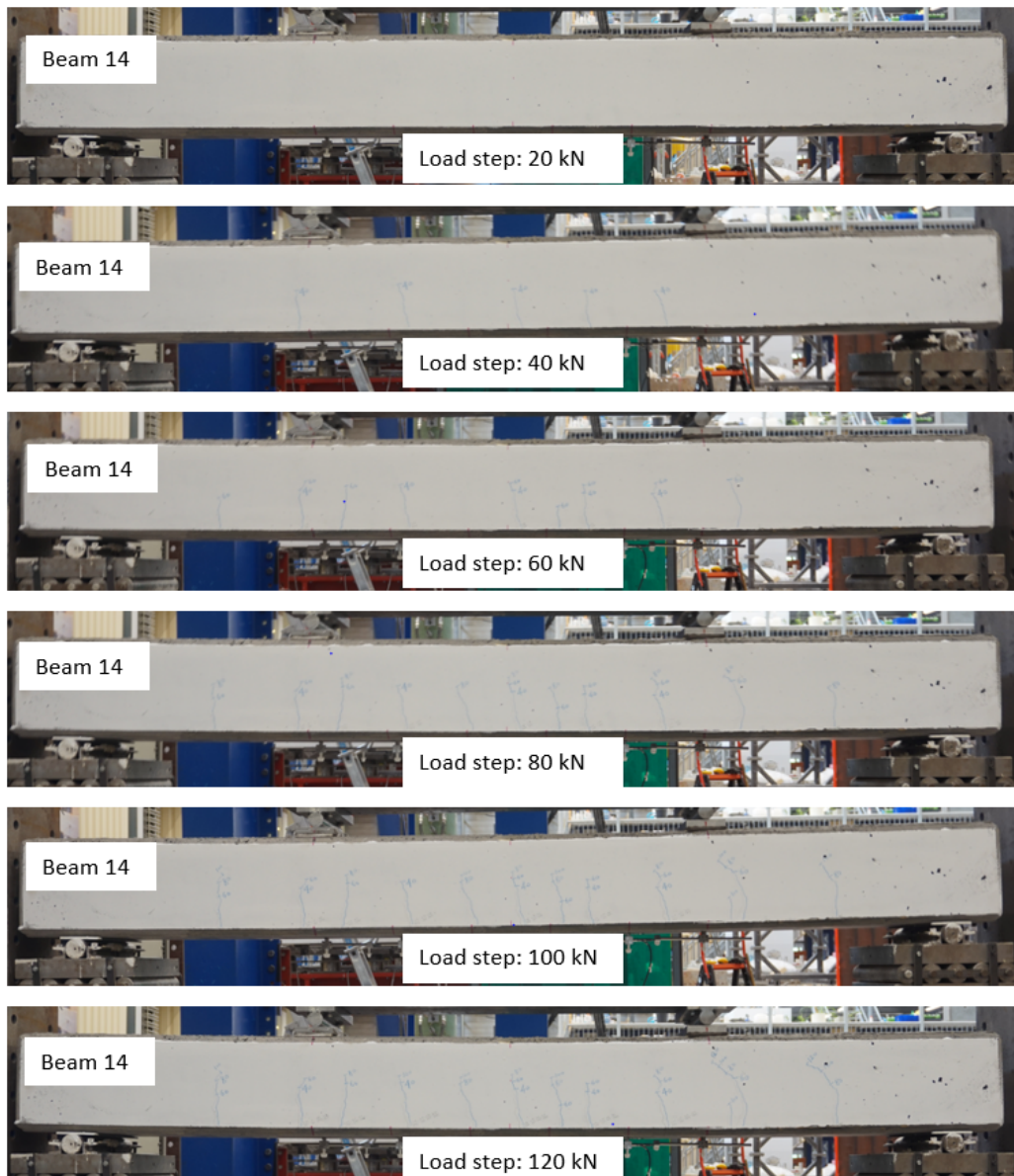






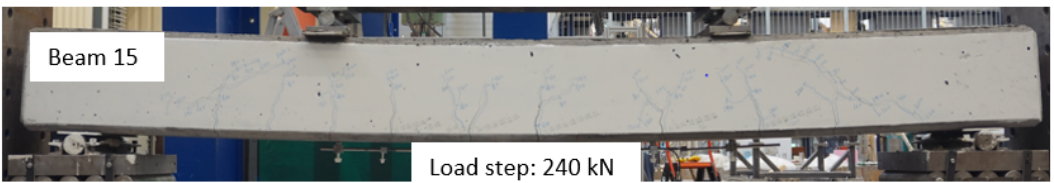
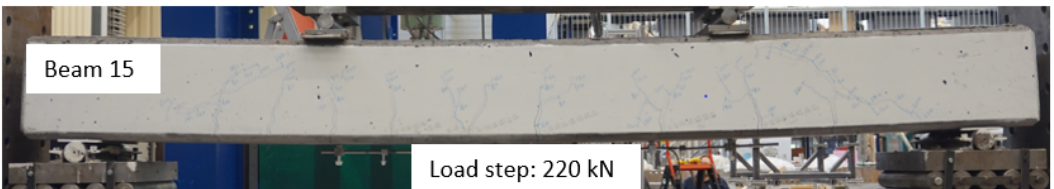
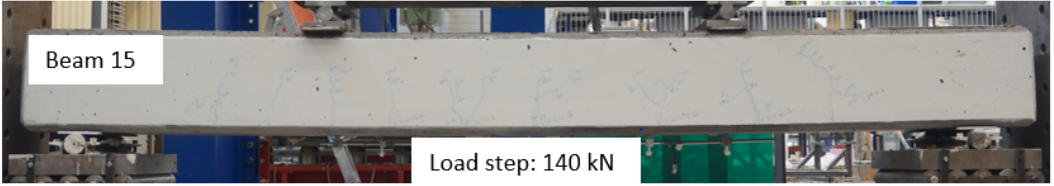




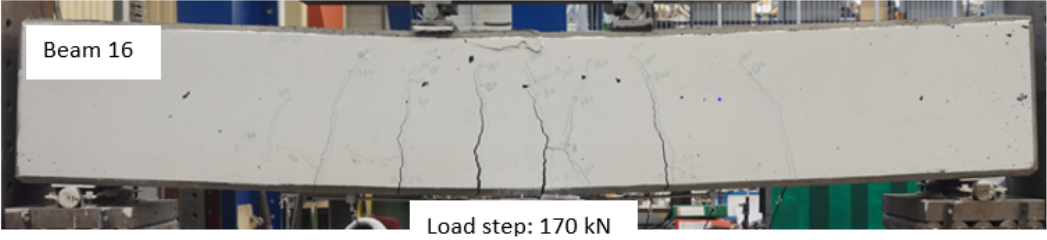
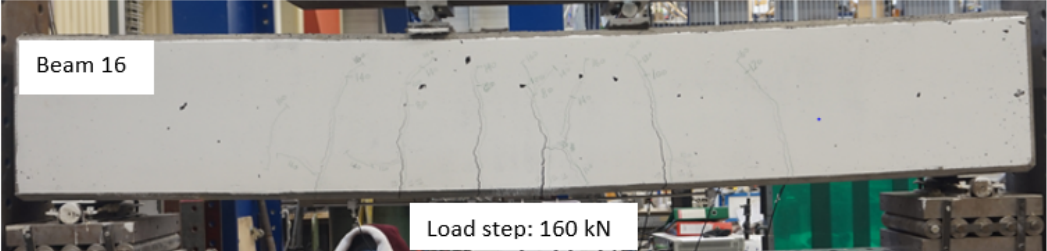
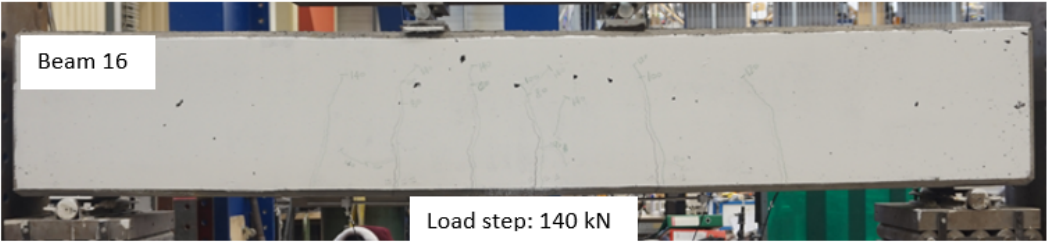
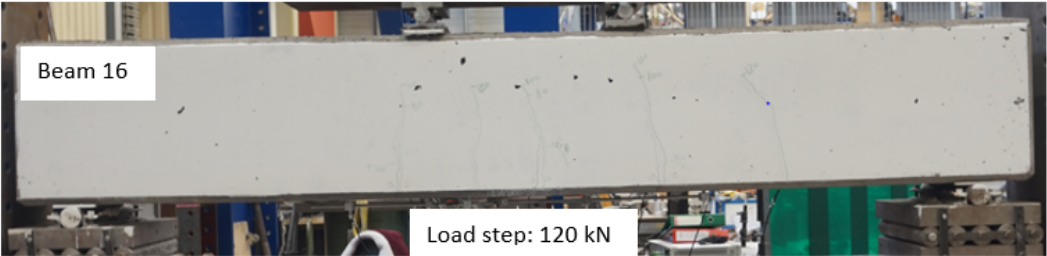




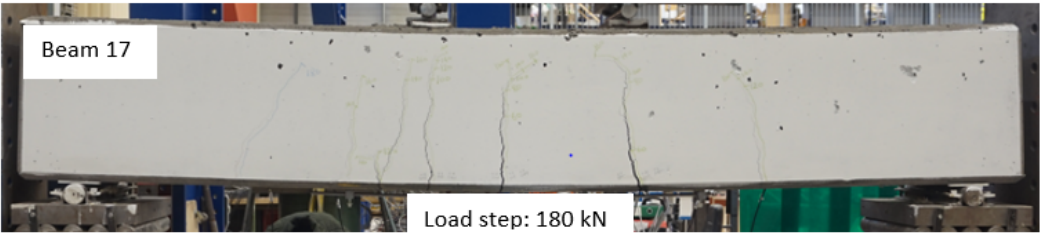
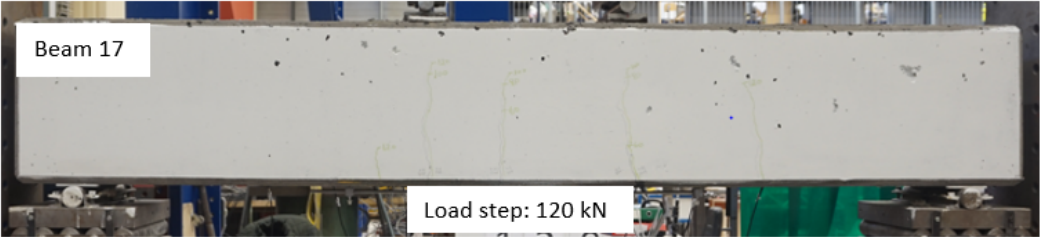




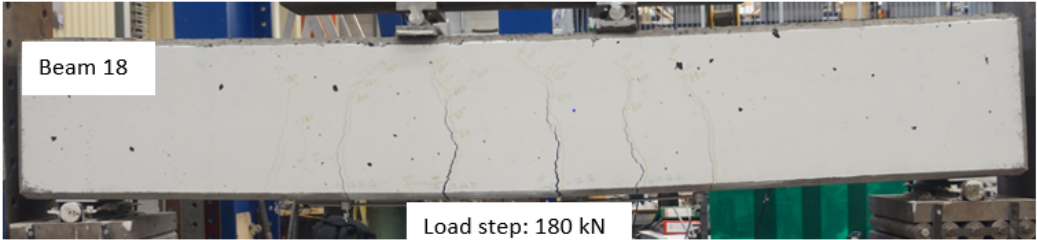
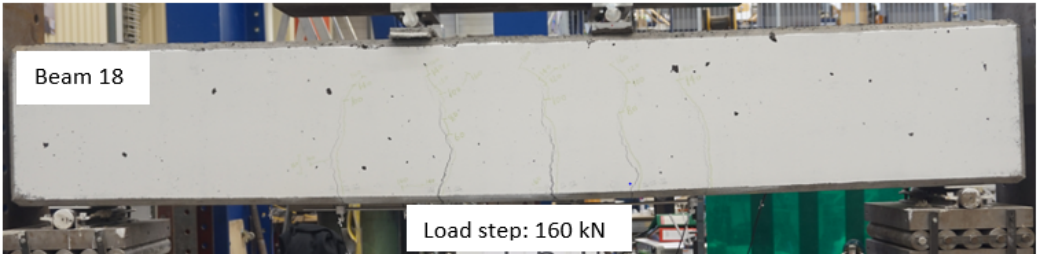
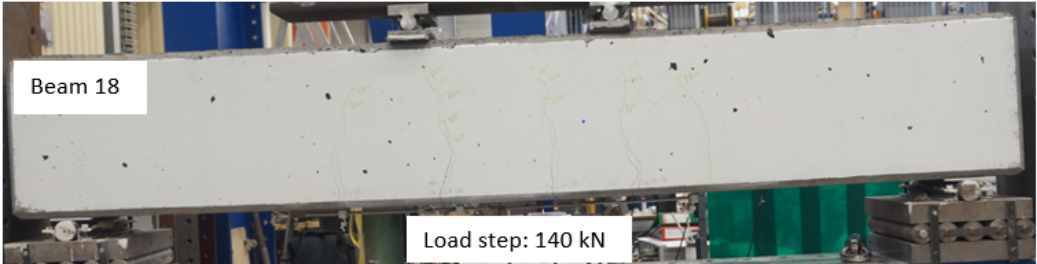
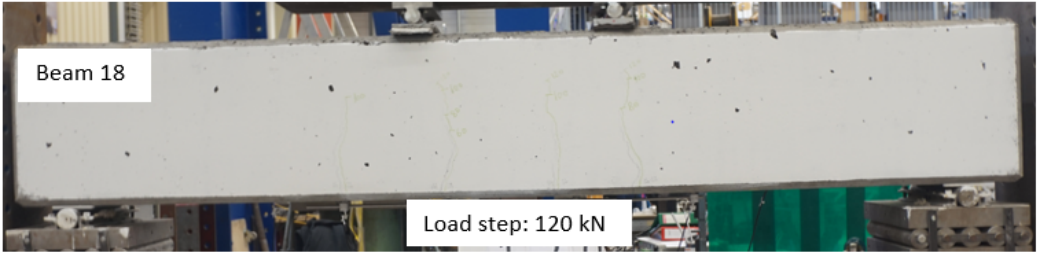


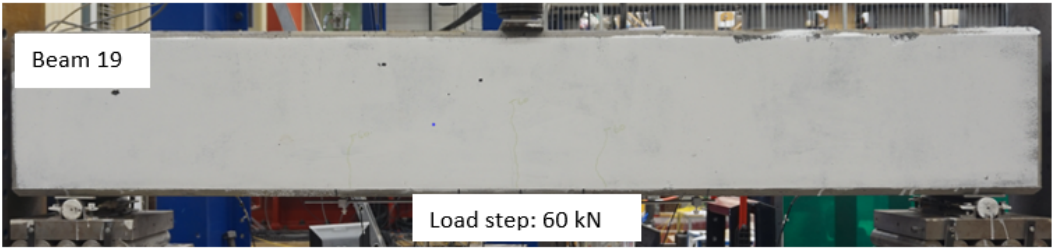
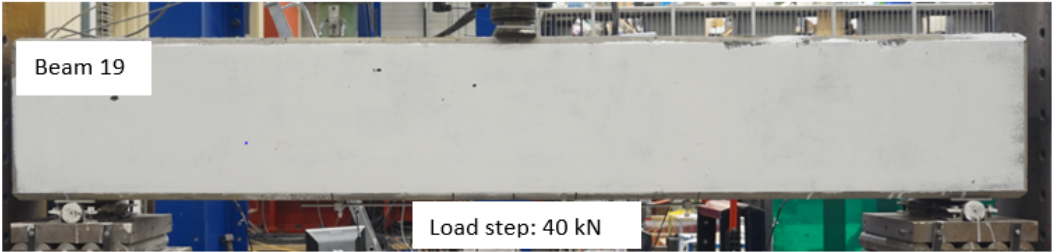












A

